On-The-Fly Generation of Differential Resonance Scattering Probability Distribution Functions for Monte Carlo Codes

by

Eva Elizabeth Sunny

A dissertation submitted in partial fulfillment
of the requirements for the degree of
Doctor of Philosophy
(Nuclear Engineering and Radiological Sciences)
in the University of Michigan
2013

Doctoral Committee:

Professor William R. Martin, Chair
Adjunct Professor Forrest B. Brown
Professor Thomas J. Downar
Professor James P. Holloway
Professor Divakar Viswanath

Dedication

To my parents, Annie Sunny and Sunny Mathew,
and my sister, Steffi Sunny.

Acknowledgements

Being able to pursue my graduate studies at the University of Michigan has been one of the biggest privileges of my life and it has been a wonderful experience. I would like to thank my advisor, Professor William Martin, for his immense patience, support, and guidance over the last five and a half years. Words cannot express the gratitude I have for all his mentoring, especially his calm composure after any research setback that I experienced. I would like to thank all my committee members, Dr. Forrest Brown, Professor Thomas Downar, Professor James Holloway, and Professor Divakar Viswanath, for taking time out of their busy schedules to be on my thesis committee. I would like to thank Dr. Forrest Brown, and Dr. Brian Kiedrowski for their mentoring at LANL over the summer of 2011 without which many aspects of this thesis would not have come together. I would also like to acknowledge Dr. Mark Williams for pointing my advisor and I to the journal paper by Blackshaw, Professor Ron Dagan for the discussions we had on this thesis topic during his visit to Michigan, and Professor Fleming for providing me with numerous references on resonances. The funding provided by NEUP grants and the Post Graduate Scholarship from the Natural Sciences and Engineering Research Council of Canada enabled me to pursue this research and degree.

My graduate life at Michigan would not have been enjoyable had it not been for my wonderful colleagues and the staff at NERS. Peggy Jo Gramer took on the role of mentor, friend, therapist, graduate coordinator; you name it, she wore all the different hats. I sincerely appreciate her support during my graduate studies, and all the work that she does, and the care she has for the graduate students. I would like to thank all my friends at NERS for the laughs, and even the pranks, without which my graduate studies would have been incomplete. I appreciate the friendship, and guidance of Dr. Gokhan Yesilyurt, Dr. Kaushik Banerjee, Benjamin Betzler, and Andrew Pavlou, during the FSV/VHTR projects, and my thesis research. I would also like to thank Eric Baker,

Dr. Troy Becker, Efrain Hernandez-Rivera, Maria Morell Gonzalez, Dr. Seth Johnson, Sonal Joshi-Kaye, William Morgan, Suzanne Nowicki, Crystal Thrall, Dr. Nick Touran, Mitchell Young, and Dr. Peng Zhang, for their friendship, and encouragement during my graduate studies. Over the last five and a half years, I was fortunate to sit in Office 2940. On a daily basis, I never knew if I would be coming into the office to hear uplifting or deriding comments, and would like to acknowledge my office mates for keeping my workplace entertaining.

I was always encouraged by the support of Cassarah Brown, who took it upon herself to ensure that I kept a well-balanced lifestyle during my last two years at NERS. I am also grateful to her for volunteering to edit this dissertation. I partly credit my success in graduate school due to the encouragement, and friendship of Dr. Jinan Yang, and am indebted to her for always willing to answer any of my questions at anytime of the day. Dr. Emily Wolters has been an amazing friend, and words cannot express my gratitude for her unwavering faith in me, and advice for all spheres of my life. The Wolters family has been like an extended family of mine in Ann Arbor, and I would like to thank them for always welcoming me into their home. Farina Baig has been my faithful cheerleader for the past decade, and I am always thankful for her assuring words. I would not be in graduate school had it not been for the encouragement of Dr. Bill Muirhead and Dr. Ellen Vogel at UOIT, where I pursued my undergraduate studies. My visits with them, and their routine emails kept me focused; I cannot thank them enough for their mentoring, and friendship over the past decade.

Work-life balance in my final year would have been non-existent had it not been for Dr. Greg Davidson. I thank him for his patience, faith, and reassurance, which made the final stretch of my student life vastly more enjoyable. Finally, I would like to thank my extended family members, especially, Dr. Cherian Idicheria, and his family, and my grandmother, Esther George, for their good wishes and prayers. I am grateful for the steadfast encouragement of my parents, Sunny Mathew and Annie Sunny, and sister, Steffi Sunny. I would not be in this position had it not been for the strong emphasis placed on education by my parents. I acknowledge them for the personal sacrifices they made to provide my sister and I with a good upbringing, and for always supporting my decisions.

Table of Contents

List of Figures

List of Tables

List of Appendices

CHAPTER 1

Introduction To Monte Carlo For Reactor Analysis

1.1 Introduction

Particle transport involving neutrons, photons, and electrons is modeled and analyzed in many fields including, but not limited to, radiation shielding applications, medical physics, radiation protection and dosimetry, fission and fusion reactor design and analysis, radiation detector analysis, and analysis of supernovae behavior. Particle transport is a broad field and many different methods are utilized to simulate movement of these particles in various media. Neutron transport in various media is modeled using the Boltzmann transport equation, initially developed by L. Boltzmann to study the kinetic theory of gases [1]. The Boltzmann transport equation describes the behavior of neutrons distributed in space, angle, and energy for steady state conditions in a nuclear reactor. This equation can also represent the distribution of neutrons as a function of time for time-dependent, transient analysis of reactors.

For steady state conditions in a nuclear reactor, the neutron transport equation is,

$$\begin{aligned}
&\mathbf{\Omega}\cdot\nabla\psi(\mathbf{x},\mathbf{\Omega},E)+\Sigma_t(\mathbf{x},E)\psi(\mathbf{x},\mathbf{\Omega},E)= \\
&\qquad\int_0^\infty\int_{4\pi}\Sigma_s(\mathbf{x},\mathbf{\Omega}'\cdot\mathbf{\Omega},E'\to E)\psi(\mathbf{x},\mathbf{\Omega}',E')\,d\mathbf{\Omega}'\,dE'+S(\mathbf{x},\mathbf{\Omega},E). \\
&\qquad\qquad \mathbf{x}\in R,\ \mathbf{\Omega}\in 4\pi,\ 0<E<\infty
\end{aligned} \tag{1.1}$$

The angular neutron flux, $\psi(\mathbf{x},\mathbf{\Omega},E)$, is represented here in six-dimensional phase-space: space (x, y, z), angle (polar and azimuthal) and energy. If time is considered, $\psi(\mathbf{x},\mathbf{\Omega},E,t)$ is represented in seven-dimensional phase-space.

On the left hand side of Eq. (1.1), the first term represents the net neutron leakage from a system, and the second term represents the total collision rate of neutrons. On the right hand side, the first term represents the in-scattering source and the second term represents the neutron source. The angular neutron flux, $\psi(\mathbf{x},\mathbf{\Omega},E)$, is proportional to the angular neutron density, $n(\mathbf{x},\mathbf{\Omega},E)$,

$$\psi(\mathbf{x},\mathbf{\Omega},E) = v\,n(\mathbf{x},\mathbf{\Omega},E)\,,$$

where v is the neutron speed [1]. The neutron speed, v, is calculated from $v = \sqrt{\frac{2E}{m}}$. Eq. (1.1) can be solved to determine quantities such as neutron scalar flux, neutron current, or k-eigenvalue of the system [1].

The spatial vector, $\mathbf{x}$, is represented in 3-D Cartesian coordinates by $\mathbf{x} = u\mathbf{i} + v\mathbf{j} + w\mathbf{k}$. The angular unit vector, $\mathbf{\Omega}$, consists of the polar angle, θ, and the azimuthal angle, γ. Figure 1.1 defines the components of $\mathbf{\Omega}$,

$$\begin{aligned} \Omega_u &= \sin\theta\cos\gamma, \\ \Omega_v &= \sin\theta\sin\gamma, \\ \Omega_w &= \cos\theta. \end{aligned} \tag{1.2}$$

If μ is the cosine of polar angle where $\mu = \cos\theta$, we can rewrite Eq. (1.2) as,

$$\begin{aligned} \Omega_u &= \sqrt{1-\mu^2}\cos\gamma, \\ \Omega_v &= \sqrt{1-\mu^2}\sin\gamma, \\ \Omega_w &= \mu. \end{aligned} \tag{1.3}$$

The polar angle, θ, is within the range $[0,\pi]$ and the azimuthal angle, γ, is within the range $[0,2\pi]$. Figure 1.1 shows the position, direction and energy of a neutron [1].

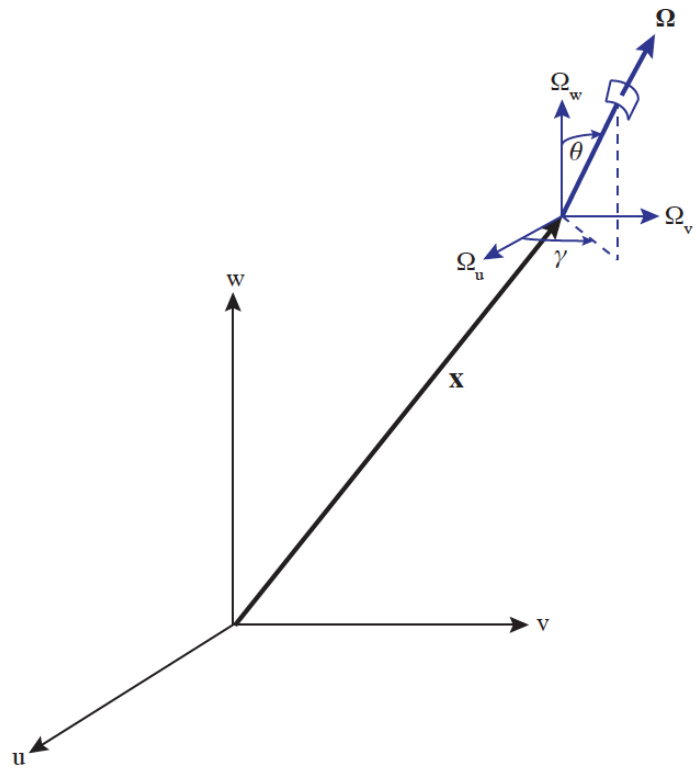

Figure 1.1: Position and direction of a neutron [1]

For isotropic fixed source problems, the source term can be written as $S(\mathbf{x},\mathbf{\Omega},E)=\frac{Q(\mathbf{x},E)}{4\pi}$, where $Q(\mathbf{x},E)$ is an isotropic source of neutrons distributed in energy and space. For regions with fissile material, the neutron source is distributed as a function of the neutron flux within the specified region of interest in a reactor core,

$$S(\mathbf{x},\mathbf{\Omega},E)=\frac{\chi(E)}{4\pi k}\int_0^\infty\int_{4\pi}\nu\Sigma_f(E')\psi(\mathbf{x},\mathbf{\Omega}',E')d\mathbf{\Omega}'dE'. \tag{1.4}$$

Reactor calculations that solve the k-eigenvalue of the system are usually referred to as criticality calculations. The largest eigenvalue, k, is determined for a unique, positive and nonzero solution for the eigenfunction, ψ [2], i.e, the angular flux. A nuclear reactor is considered to be critical when k is equal to one, subcritical when k is

less than one and supercritical when k is greater than one. In reactor analysis, the largest eigenvalue, k, can be physically interpreted as the neutron multiplication factor. When k is equal to one, the rate of neutron production in the reactor is equal to the rate of neutron loss through absorption or leakage. When k is less than one, neutron production is less than neutron loss in the reactor, and vice versa when k is greater than one.

Criticality calculations performed for reactors in steady state conditions solve the Boltzmann transport equation using different boundary conditions, e.g. reflecting, and vacuum boundary conditions [1], [2], [3]. Analytical solutions for Eq. (1.1) exist only for simplified problems. Numerical approximations must be made to solve the problem deterministically for complicated neutron transport problems. These numerical approximations reduce computational run times and produce solutions with reasonable accuracy. However, deterministic methods might not always produce the most accurate answers. These methods are usually benchmarked against Monte Carlo methods, which rely on modeling a neutron's path through a system in a stochastic manner. Neutron transport in a nuclear reactor can be modeled using deterministic or Monte Carlo methods, or a hybrid of the two methods.

With deterministic methods, the Boltzmann transport equation is discretized in space, angle and energy. Numerical errors in these methods arise from errors in the experimental data of the cross sections and also from the discretization of space, angle and energy phase [3]. It is also very difficult to represent complex 3-D geometries in deterministic codes. Recent research efforts have been focused on the development of efficient 3-D deterministic neutron transport codes.

In Monte Carlo methods, neutron transport is stochastically modeled using the probabilities of neutron interactions. Each neutron path in a random walk is considered unique until the neutron is lost from the system. Errors that arise from this method include experimental errors in the cross section data, and stochastic uncertainties that arise from neutron random walks. Unlike deterministic methods, errors associated with spatial, angular and energy discretizations are avoided in Monte Carlo codes, and stochastic processes can be modeled in complex geometries. However, Monte Carlo codes can require very long computational times to predict neutron behavior in a reactor with a high degree of accuracy.

Advances in hybrid deterministic-Monte Carlo methods are ongoing, where deterministic methods are used to accelerate Monte Carlo methods. Errors associated with these hybrid methods may arise from both deterministic and Monte Carlo methods, depending on the specific hybrid approach that is used.

1.2 The Monte Carlo method

This thesis focuses on the acceleration of the current elastic scattering model used in Monte Carlo methods. Discussions throughout the remainder of this thesis will be focused on these methods. Chapter 2 will address details regarding elastic scattering.

Monte Carlo methods use neutron cross sections to determine probabilities of neutron interactions, and random numbers to sample from these probability distributions to stochastically simulate the random path of a neutron in the reactor until the neutron history is terminated through neutron capture or leakage from the system. The stochastic simulation of a neutron path through a system from birth to death is called a *random walk*. Figure 1.2 illustrates neutron random walk.

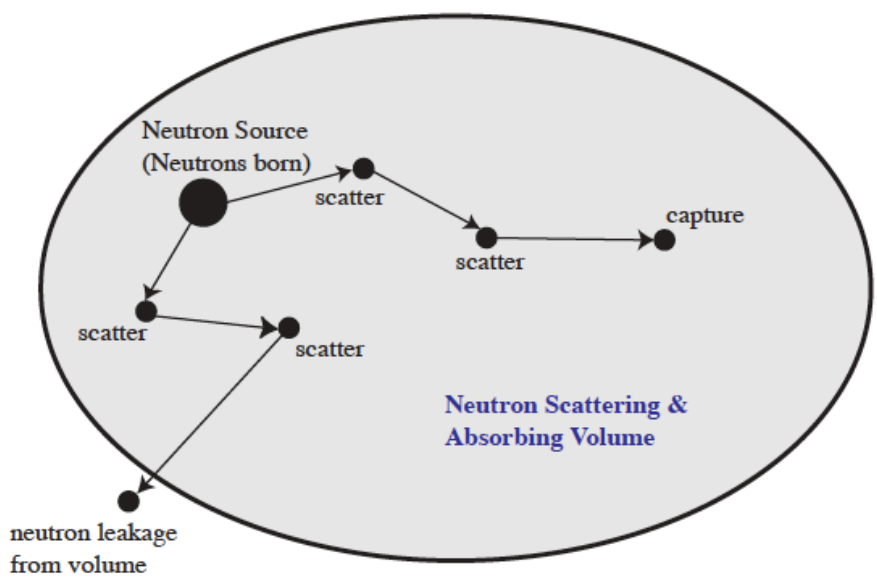

Figure 1.2: Random walk

The following subsections will discuss the details regarding the simulation of a random walk.

1.2.1 Source neutrons

Neutron sources introduce neutrons into a volume of interest and are the starting point for a neutron history in a stochastic process. These sources can depend on space, angle, and energy. $S(\mathbf{x},\mathbf{\Omega},E)d\mathbf{x}\,d\mathbf{\Omega}\,dE$ represents the total number of source neutrons produced per unit time in spatial region $d\mathbf{x}$ about $\mathbf{x}$, in angular region $d\mathbf{\Omega}$ about $\mathbf{\Omega}$ and energy range dE about E. The source neutrons can be produced within a system (volumetric source) or can leak into the system from the boundaries that define the volume (surface source).

1.2.2 Calculating distance to collision

Once the neutron has been introduced into the system, the next step is to determine the distance to collision with a target nuclide. The distance to collision, d, before the next neutron interaction, is determined using a random number, ξ, selected uniformly between 0 and 1, shown in Eq. (1.5),

$$d = -\frac{1}{\Sigma_t}\ln\xi, \tag{1.5}$$

where Σ_t is the total cross section. Eq. (1.5) is determined from the PDF for a collision given by $p(x) = \Sigma_t e^{-\Sigma_t x}$. Integrating the PDF, $p(x) = \Sigma_t e^{-\Sigma_t x}$, over the range [0, d] will yield the cumulative distribution function (CDF), $\int_o^d p(x)dx = P[d]$. Setting the CDF equal to a random number, ξ, and solving for d will provide us with Eq. (1.5). Once the distance to the collision site has been calculated, the particle is moved to the new location. If the distance to the boundary of the system is less than the distance to collision, the particle is moved to the boundary. If the boundary is an external boundary, then the particle will leak out of the system and the history is terminated. Otherwise, a new distance to collision is calculated using the properties of the new region and the neutron trajectory is continued.

1.2.3 Determining interaction type

After the particle is moved to a new collision site, it can undergo fission, capture, elastic scattering or inelastic scattering. The relationships between these cross sections are given by:

$$\begin{aligned} \Sigma_t(E) &= \Sigma_a(E) + \Sigma_s(E), \\ \Sigma_a(E) &= \Sigma_f(E) + \Sigma_\gamma(E), \\ \Sigma_s(E) &= \Sigma_e(E) + \Sigma_{ie}(E), \end{aligned} \tag{1.6}$$

where $\Sigma_a(E)$ is the total neutron absorption cross section, $\Sigma_s(E)$, is the total neutron scattering cross section, $\Sigma_f(E)$, is the fission cross section, $\Sigma_\gamma(E)$, is the capture cross section, $\Sigma_e(E)$, is the elastic scattering cross section, and $\Sigma_{ie}(E)$, is the inelastic scattering cross section. In elastic scattering, the neutron energy and momentum are preserved before and after the collision with the target nuclide. In inelastic scattering, the neutron energy and momentum are not preserved. Details regarding elastic scattering will be presented in greater detail in Chapter 2.

These cross sections are divided by the total cross section, $\Sigma_t(E)$, into different intervals, as shown in Eq. (1.7). A random number, ξ, is selected uniformly between 0 and 1 to determine the interaction type:

$$1 = \frac{\Sigma_a(E)}{\Sigma_t(E)} + \frac{\Sigma_s(E)}{\Sigma_t(E)}, \tag{1.7}$$

where $\frac{\Sigma_a(E)}{\Sigma_t(E)} = \frac{\Sigma_f(E)}{\Sigma_t(E)} + \frac{\Sigma_\gamma(E)}{\Sigma_t(E)}$, and $\frac{\Sigma_s(E)}{\Sigma_t(E)} = \frac{\Sigma_e(E)}{\Sigma_t(E)} + \frac{\Sigma_{ie}(E)}{\Sigma_t(E)}$.

For example, if $\xi < \frac{\Sigma_a(E)}{\Sigma_t(E)}$, then the neutron is absorbed, otherwise, it has scattered. Modeling neutrons in this manner is referred to as analog Monte Carlo.

1.2.4 Exiting direction of neutron after elastic collisions

If a neutron scatters at the collision site, then, given its initial direction $\left(\Omega_u, \Omega_v, \Omega_w\right)$ shown in Eq. (1.3), its new direction $\left(\Omega'_u, \Omega'_v, \Omega'_w\right)$ is determined in the following manner [8]:

$$\Omega'_u = \mu u + \frac{\sqrt{1-\mu^2}\left(uw\cos\gamma - v\sin\gamma\right)}{\sqrt{1-w^2}},$$

$$\Omega'_v = \mu v + \frac{\sqrt{1-\mu^2}\left(vw\cos\gamma + u\sin\gamma\right)}{\sqrt{1-w^2}}, \tag{1.8}$$

$$\Omega'_w = \mu w - \cos\gamma\sqrt{1-\mu^2}\sqrt{1-w^2}.$$

The azimuthal angle, γ, is sampled uniformly from $[0, 2\pi]$ and is determined by $\gamma = 2\pi\xi$ where ξ is the random number. If the scattering is isotropic, the cosine of polar angle, μ, can be sampled from a uniform distribution of $[-1, 1]$ by setting $\mu = 2\xi - 1$.

1.2.5 Tracking quantities of interest

While the neutron is tracked during a random walk, quantities such as neutron flux or current are estimated using the mean value for all the tallies or scores from each neutron history. These tallies, for example, may represent the track length in a given region or the net number of neutrons that cross a given boundary, providing estimates of scalar flux or net current, respectively. Eq. (1.9) shows how these estimators are tabulated:

$$\hat{x} = \frac{1}{N}\sum_{n=1}^{N} x_n. \tag{1.9}$$

N represents total number of neutron histories, and x_n represents the contribution from the nth neutron history for the tally.

1.2.6 Error estimation

Monte Carlo results can only be interpreted properly when accompanied by the uncertainty in the results represented in the form of standard deviation or variance. If x is a random variable and $f(x)$ is the PDF, then the expectation of x, $E[x]$, is represented by [3],

$$E[x] = \int_0^\infty x f(x) dx = \bar{x}. \tag{1.10}$$

The expectation value, $E[x]$, is equal to the mean value of x, $\bar{x}$. $\hat{x}$ from Eq. (1.10) is considered to be an unbiased estimator of the mean, $\bar{x}$ because [3],

$$E[\hat{x}] = E\left[\frac{1}{N}\sum_{n=1}^{N} x_n\right] = \frac{1}{N}\sum_{n=1}^{N} E[x_n] = E[x] = \bar{x}.$$

The variance quantifies the spread in the values of x about the mean, $\bar{x}$. It is calculated from Eq. (1.11),

$$\sigma^2(x) = \int_0^\infty (x-\bar{x})^2 f(x) dx = \overline{x^2} - \bar{x}^2. \tag{1.11}$$

The standard deviation is just $\sigma(x)$. The variance of the average can be expressed as [3],

$$\sigma^2(\hat{x}) = \frac{\sigma^2(x)}{N}, \tag{1.12}$$

and the standard deviation of the estimate of the mean is $\sigma(\hat{x})$. $\sigma(x)$ is a measure of the spread of values for each x_n about $\bar{x}$ drawn from a PDF; $\sigma(\hat{x})$ is a measure of the spread in values of $\hat{x}$ about $\bar{x}$ from N number of histories. Eq. (1.12) suggests that if N is

increased, the variance of the average will be reduced by a factor of N. The sample variance, S^2, shown here is an unbiased estimate of $\sigma^2(x)$,

$$S^2 = \frac{N}{N-1}\left(\frac{1}{N}\sum_{n=1}^{N} x_n^2 - \hat{x}^2\right), \tag{1.13}$$

where S^2 is the sample variance and, S, is the sample standard deviation. These quantities are tracked during a neutron history to provide unbiased estimates of tallies and the estimated error in these values after running N histories in a Monte Carlo simulation.

1.2.7 Typical reactor physics calculations using Monte Carlo

In fixed source problems, a neutron history begins at a point within a particular spatial region or on the boundary of the spatial mesh with a specified neutron angular direction and energy. This neutron is followed through the region(s) of interest until it is killed. The sample variance in tallies is calculated by accounting for the tally contribution from each history, which is then averaged over all histories, as shown in Eq. (1.13).

In criticality calculations, several neutron cycles are run with a specified number of neutron histories per cycle. The Monte Carlo calculation begins with a user-specified number of inactive cycles where the neutron fission source distribution is allowed to converge. Following the inactive cycles, the active cycles are invoked, during which, the quantities of interest are tallied in user-specified regions. The variance in quantities obtained from criticality calculations are averaged twice, once over each active cycle, and then over all the active cycles.

Monte Carlo codes take a very long time to produce answers with a high degree of accuracy for problems that are divided into very small spatial regions, in thick shields, or in media with high absorption cross sections. The number of neutron histories must be increased to ensure sufficient neutron transport through all the regions of interest to decrease the uncertainty of the quantity being tabulated in each region.

1.2.8 Variance reduction techniques

A number of variance reduction methods have been developed to reduce run times, since the number of histories N can be decreased to achieve a given error. Some of the more popular variance reduction methods are described below.

1.2.8.1 Implicit capture

With implicit capture, it is assumed that the neutron scatters at every collision site. Neutrons are assigned weights, and during each history, the neutron weight is reduced in proportion to the absorption probability. A history begins with a neutron weight of one and with each scatter the neutron weight is multiplied by the ratio in Eq. (1.14),

$$w_{i+1} = w_i \left(1 - \frac{\sigma_a}{\sigma_t}\right). \tag{1.14}$$

The user specifies a minimum neutron weight where it is considered for termination. When a neutron weight falls below the user-specified weight, it undergoes a Russian roulette process, which results in increased particle weight or particle termination. The use of implicit capture is an example of non-analog Monte Carlo.

1.2.8.2 Banking fission neutrons

The expected number of fission neutrons to be produced during the ith collision is calculated from [9],

$$f_i = w_i \nu \frac{\sigma_f}{\sigma_t}. \tag{1.15}$$

The mean number of neutrons produced per fission is represented by ν. At least n_i fission neutrons are banked during the ith collision, where n_i is equivalent to the rounded-down integer value of f_i, $n_i = \text{integer}\left[f_i\right]$. However, an additional fission neutron is banked with a probability of $(f_i - n_i)$ [9]. Therefore, for every i^{th} collision, the number of banked fission neutrons is determined by the following test:

If $\left(\xi < \left[f_i - n_i\right]\right)$ then produce $n_i + 1$ neutrons, else produce n_i neutrons.

These banked fission neutrons are used in the next cycle and subsequently followed through in the Monte Carlo simulation.

1.2.8.3 Termination of neutron history with Russian Roulette

A bias is introduced into the Monte Carlo process if a neutron history is terminated after its weight falls below a specified weight minimum. The steps outlined below have to be followed for unbiased termination of a neutron with a weight below the user-specified minimum [3].

1. Check to see if the neutron weight has fallen below user specified weight minimum.
2. Generate a random number, ξ, and compare to a user input value, T, which typically may range between 2 and 10 [3].
    a. If $\xi > 1/T$, terminate the history.
    b. Else, multiply neutron weight by T and continue with the neutron history and repeat until 2a. is achieved.

1.2.8.4 Figure of Merit

Figure of Merit (FOM) is a metric that measures the relative efficiency of a Monte Carlo calculation. A larger FOM results in a faster and more accurate Monte Carlo calculation. It is represented by,

$$FOM = \frac{1}{\sigma^2(x)t}, \tag{1.16}$$

where, t, is the mean time it takes to run a neutron history [3].

This shows that as the variance reduces, the FOM increases, which is why non-analog Monte Carlo is preferred over analog Monte Carlo.

1.2.8.5 Error estimation in variance reduction methods

The unbiased sample estimator must now include the neutron weights along with the quantity of interest that is tallied [3],

$$\widehat{wx} = \frac{1}{N}\sum_{n=0}^{N} w(x_n)x_n \,. \tag{1.17}$$

The sample variance now becomes,

$$S^2 = \frac{N}{N-1}\left(\widehat{wx^2} - \widehat{wx}^2\right). \tag{1.18}$$

The purpose of introducing variance reduction methods is to ensure higher confidence in tabulated values with increased computational efficiency. The goal is to achieve higher FOM by implementing these methods.

1.2.9 Rejection method

Computationally intensive sampling methods involved in determining various types of interactions and quantities contribute to long computational times for neutron simulation in Monte Carlo codes. An alternative method is rejection sampling. Rejection methods are typically used when an analytical solution does not exist for the CDF or it is computationally less expensive to use the rejection technique than a direct sampling method [4].

For a test based on the rejection method, a trial value, x_o, is selected between [0,1] for a complicated PDF, $f(x)$, which also lies in the range [0,1] as shown in Figure 1.3 [4].

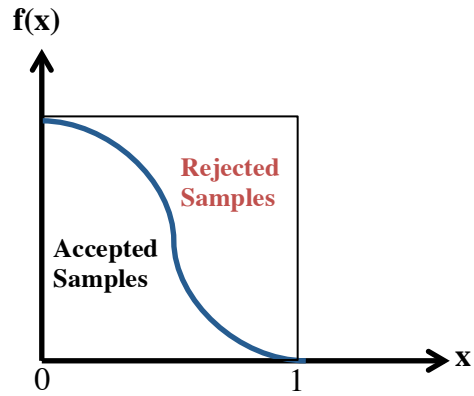

Figure 1.3: PDF to be sampled by rejection technique

The selected trial value must undergo tests to ensure that most values for $f(x_o)$ are accepted as x_o approaches zero and most values are rejected for $f(x_o)$ as x_o approaches one [4]. This means that the trial value, x_o, is selected with probabilities proportional to $f(x_o)$. For values that we select along the x axis, $f(x)$ will always be less than or equal to $f(0)$, since the largest value for $f(x)$ occurs when x is equal to zero [4]. If we select a second random number, ξ_2, between [0,1], we can test it against the trial value where we accept x_o if $\xi_2 \leq \frac{f(x_o)}{f(0)}$ [4]. By following this method, we are choosing values within a rectangle around the curve $f(x)$, where trial values that lie above the curve are rejected and values that lie below the curve are accepted. Here, the rectangle is picked for simplicity to explain the rejection method, however, these test functions can represent any type of general function that surrounds the original PDF to be sampled.

Rejection methods can be faster than direct sampling if chosen for appropriate functions. In most cases, rejection sampling is slower than direct sampling. It can be exceptionally slow if $\frac{f(x_o)}{f(0)} << 1$ because it leads to an increase in the number of random numbers that are required for the rejection test to pass.

Rejection methods are implemented to determine various outcomes in current Monte Carlo codes. For example, the bivariate scattering PDF used to sample the target nuclide speed and the cosine of polar angle of approach between the neutron and target nuclide during elastic scattering is a very complicated PDF. The quantities, target

nuclide speed and cosine of polar angle, are sampled using a rejection scheme based on the bivariate scattering PDF. The sampling algorithm is referred to as the free gas scattering algorithm, and it was first proposed by H. Kahn and presented in [5]. An overview of this PDF is presented in the next section.

1.3 Free gas scattering

Free gas scattering is implemented in Monte Carlo codes to simulate the elastic scattering process and this scattering model is based on three assumptions. The first is that the moderating and absorbing nuclei are unbound so that any molecular and crystalline effects are ignored. Second, the unbound nuclei are in a Maxwell-Boltzmann distribution in energy. Third, the scattering cross section (proportional to the probability of neutron scatter) is held constant for all nuclides.

The starting point for the derivation of the bivariate PDF begins with the effective scattering cross section,

$$\sigma_{eff,s}(v) = \int_{4\pi}\int_{0}^{\infty} \frac{|\mathbf{v}-\mathbf{V}|}{v}\sigma_s\left(|\mathbf{v}-\mathbf{V}|\right)P(\mathbf{V})\,d\mathbf{V}\,d\Omega, \tag{1.19}$$

where $P(\mathbf{V}) = \left(\frac{M}{2\pi kT}\right)^{\frac{3}{2}} e^{-\left(M/2kT\right)\mathbf{v}^2}$ represents the Maxwell-Boltzmann distribution in energy of the target nuclides. $\mathbf{v}$ is the neutron velocity, $\mathbf{V}$ is the target nuclide velocity, $|\mathbf{v}-\mathbf{V}|$ is the relative neutron velocity and $\sigma_s(|\mathbf{v}-\mathbf{V}|)$ is the scattering cross section as a function of the relative neutron velocity. M is the target nuclide mass, k is the Boltzmann constant and T is the temperature of the system. In Eq. (1.20), the double integral represents the integration of the probability of neutron collision per second over all polar and azimuthal angles, and target speeds. If σ_s is assumed to be constant, Eq. (1.20) can be derived for the effective scattering cross section of a neutron in free gas after performing several manipulations to Eq. (1.19) [5],

$$\sigma_{eff,s}(v) = \sigma_s \left[\frac{e^{-\alpha v^2}}{v\sqrt{\pi\alpha}} + \left(1 + \frac{1}{2\alpha v^2}\right) erf\left(v\sqrt{\alpha}\right) \right], \tag{1.20}$$

where $\alpha = \dfrac{M}{2kT}$.

The bivariate PDF can then be rewritten in the following form assuming σ_s is constant:

$$P(V,\mu \mid v)\, dV\, d\mu = \frac{\left(\dfrac{\alpha}{\pi}\right)^{3/2} \sigma_s \,|\, \mathbf{v} - \mathbf{V} \,|\, V^2 e^{-\alpha V^2} 2\pi\, dV\, d\mu}{\sigma_{eff,s}\left(v\right)} \tag{1.21}$$

Directly sampling from the bivariate PDF for target nuclide speed and angle is complicated due to the presence of relative speed, |**v**–**V**|. H. Kahn [5] recommended a rejection test to overcome the direct sampling problem in order to determine the target speed and the cosine of polar angle. This bivariate scattering PDF is an example of a complex PDF used in Monte Carlo codes today. The three assumptions used to form the bivariate PDF will be the topic of discussion for the remainder of this dissertation work.

1.3.1 Drawbacks of current method

There are several drawbacks to the free gas scattering method. These shortcomings are a result of assuming constant scattering cross sections in the epithermal range (1 eV to 0.1 MeV) for all nuclides. Figure 1.4 shows the scattering cross section for ^{1}H, a light nuclide in the lower epithermal region. The scattering cross section is constant for this selected energy range, but for this same energy range, Figure 1.5 shows that the scattering cross section for ^{238}U has extreme peaks and is far from constant. These sharp peaks are referred to as resonances, which will be discussed in greater detail in Chapter 2.

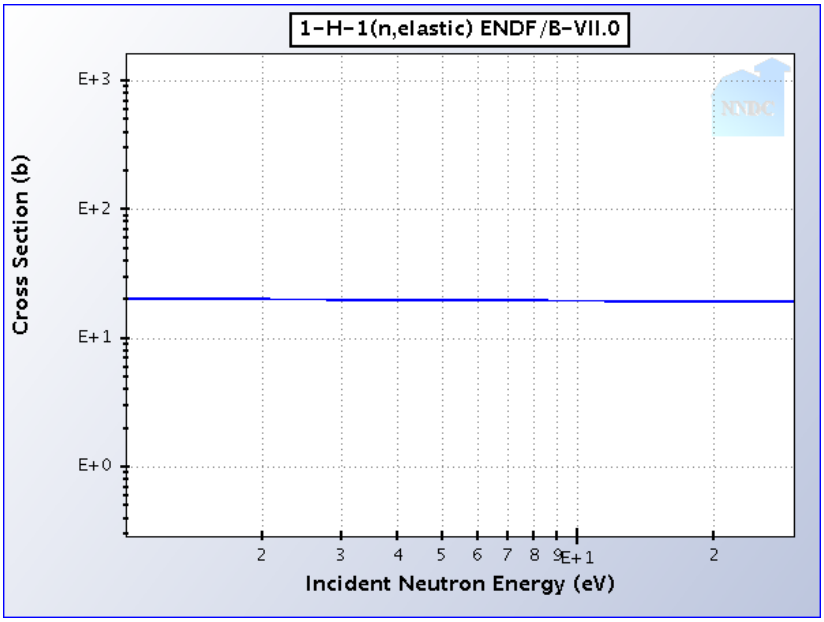

Figure 1.4: ^{1}H Elastic scattering cross section at 300 K [7]

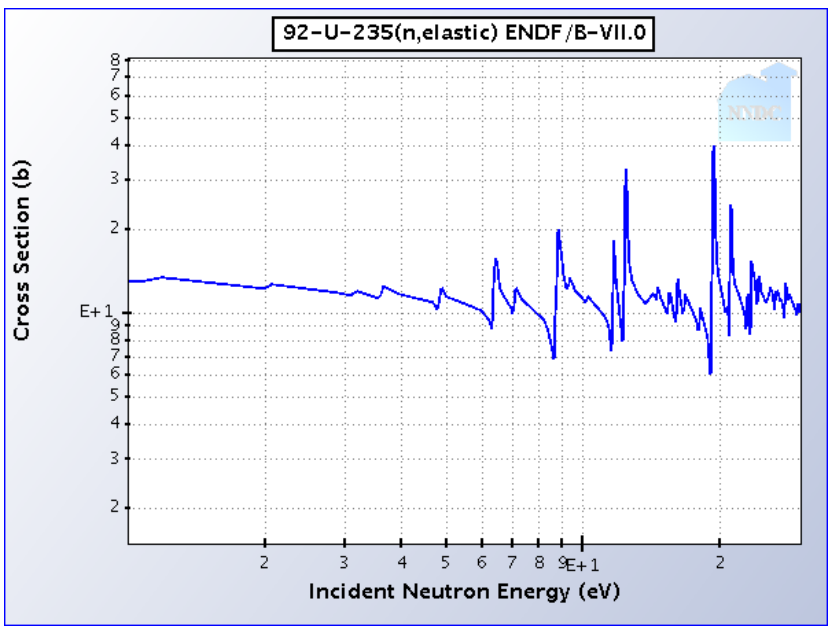

Figure 1.5: ^{238}U Elastic scattering cross section at 300 K [7]

The free gas scattering model can be modified to account for resonances in the cross section for heavy nuclides in the lower epithermal range as outlined in [10] and [11], but this method is based on an additional rejection test, which can be computationally inefficient. However, the impact of leaving the scattering cross section as a constant in the scattering model for heavy nuclides results in a significant bias in k_{eff}

for criticality calculations that involve Very High Temperature Reactors (VHTRs) and Light Water Reactors (LWRs) at hot full power conditions. Systems at higher temperatures are more affected by resonance scattering because the target nuclides gain speed as the temperature of the system increases. With this increase in target nuclide speed, the neutrons will experience a greater likelihood of gaining energy when they scatter off the target nuclide. In neutron scattering with heavy nuclides, there is a possibility that neutrons will gain enough energy to fall back into a resonance once they slow down past it. This is of concern in reactor analysis because neutrons have to reduce their speeds to less than 1 eV (thermal energy) in order to induce fission reactions in ^{235}U. If they are captured and lost from the system at energies above 1 eV, then there are fewer neutrons available to produce fission reactions at thermal energies. This additional absorption leads to a lower k_{eff} than what current Monte Carlo codes are predicting with the free gas scattering algorithm.

Therefore, it is important to account for the variation in the scattering cross section in the epithermal range, especially for ^{238}U, for reactor applications since it is considered to affect criticality calculations on the order of several hundred per cent mile (pcm) (1 pcm = 10^{-5}). Current methods that account for the resonances in the epithermal energy range involve an extra rejection test or modification to neutrons weights making the elastic scattering simulation less efficient in Monte Carlo codes. Chapters 2 and 3 will discuss these methods in greater detail.

1.4 Thesis goal

To develop an alternative method to account for scattering resonances in the epithermal range for heavy nuclides, which allows scattering parameters to be sampled directly in the laboratory frame.

1.5 Thesis outline

Chapter 2: Elastic scattering mechanics in the epithermal energy range will be discussed in great detail. Different types of resonances and nuclear reactions will be discussed and an in-depth review of the original free gas scattering algorithm will be presented. The effects of accounting for resonances in the scattering models will be analyzed by observing the changes in the differential scattering PDFs.

Chapter 3: Different methods developed by researchers to account for the varying scattering cross sections will be discussed. Detailed algorithms for scattering models used in Monte Carlo codes will be presented. The Doppler Broadened Rejection Correction Method (DBRC) [11] will be discussed along with the correction to the existing free gas scattering algorithm in Monte Carlo codes as a result of implementing DBRC. Finally, the independent implementation of this method in MCNP5 [6] and results will be presented in this chapter.

Chapter 4: A new method based on the Legendre moments of the differential scattering PDF will be discussed. This method is based on the equations derived by Blackshaw [12], which will be verified in this dissertation. Following the verification process, approximations made to the scattering cross sections that provide analytical solutions for the moments of the differential scattering PDF will be presented. Blackshaw's derivation for the P_1 moment had an error, and this correction is presented in Appendix D. This new equation was used to generate the analytical solution for the P_1 moment. Finally, comparisons of the P_0 and P_1 moments generated on-the-fly to those generated from a research Monte Carlo code with DBRC will be presented.

Chapter 5: Results from an alternative method to treat on-the-fly resonance scattering will be presented in this chapter. A brief algorithm will outline the generation of the moments on-the-fly. Criticality calculations to obtain k_{eff} were conducted for a standard LWR UO_2 pin cell from the Mosteller Benchmark problem set. Various scattering models were also used to run criticality calculations for a 17×17 Westinghouse fuel assembly using CASL benchmark specifications and the results are presented. Finally, a brief study on MOX fuel was conducted to analyze the importance of turning on a scattering model accounting for resonances in ^{239}Pu for the lower epithermal region.

Chapter 6: A summary of the lessons learned during work on this dissertation will be presented along with some recommendations for future work.

1.6 References

[1] J. J. Duderstadt and L. J. Hamilton, *Nuclear Reactor Analysis*, John Wiley & Sons, Inc. (1976).

[2] E. Larsen, NERS 543: Nuclear Reactor Theory II Class Notes, University of Michigan (2007).

[3] E. E. Lewis and W. F. Miller, Jr., *Computational Methods of Neutron Transport*, American Nuclear Society, Inc. (1993).

[4] M. H. Kalos and P. A. Whitlock, *Monte Carlo Methods*, John Wiley & Sons, Inc. (1986).

[5] R. R. Coveyou, R. R. Bate & R. K. Osborn, "Effect of Moderator Temperature Upon Flux In Infinite, Capturing Medium," *Journal of Nuclear Energy,* **2**, pp. 153-167 (1956).

[6] X-5 Monte Carlo Team, *MCNP – A General Monte Carlo N-Particle Transport Code, Version 5, Volume I: Overview and Theory*, LA-UR-03-1987, Los Alamos National Laboratory (2003).

[7] National Nuclear Data Center, *Evaluated Nuclear Data File (ENDF)*, Brookhaven National Laboratory <http://www.nndc.bnl.gov/sigma/index.jsp> (2012).

[8] E. Wolters, *Coordinate Transformation for Scattering Events*, Internal Report, University of Michigan, (2007).

[9] F. Brown, *Collision Physics*, Class Notes – Monte Carlo Techniques for Nuclear Systems, University of New Mexico (2011).

[10] B. Becker, *On the Influence of the Resonance Scattering Treatment in Monte Carlo Codes on High Temperature Reactor Characteristics,* Thesis, Institut fur Kernenergetik und Energiesysteme, Germany, (2010).

[11] B. Becker, R. Dagan and G. Lohnert, *Proof and implementation of the stochastic formula for ideal gas, energy dependent scattering kernel*, Annals of Nuclear Energy, **36**, pp. 470 – 474 (2009).

[12] G. L. Blackshaw, *Scattering of Low-Energy Neutrons In a Monatomic Gas Model Of A Multiplying System*, North Carolina State University, Raleigh, Ph.D. Thesis (1966).

CHAPTER 2

Nuclear Reactions And Scattering Mechanics

2.1 Introduction

In Chapter 1, the basics of Monte Carlo methods were introduced, omitting physical details regarding collision mechanics and nuclear reactions. In Chapter 2, the basic physical parameters attributed to the problems specified in this thesis will be discussed. We will examine different types of nuclear reactions, resonances, and elastic scattering collision mechanics in the neutron slowing down process.

A neutron in a nuclear reactor can undergo several reactions: nuclear fission (n, fission), radiative capture (n, γ), elastic scattering (n, n) and inelastic scattering (n, n'). After a neutron is born in a fission reaction, it has to slow down from fast neutron speeds to thermal speeds in order to trigger the next fission reaction. The fast energy range is generally considered to be above ~ 0.1 MeV and the thermal energy range is considered to be less than 1 eV. The epithermal energy range, 1 eV to 0.1 MeV, is also known as the slowing down range [1] and includes the resolved resonance range.

Different types of nuclear reactions in the neutron slowing down process are determined by using cross sections that are provided in the Evaluated Nuclear Data File (ENDF). ENDF-A contains complete and incomplete sets of data for each type of reaction in different nuclides [1]. ENDF-B contains complete nuclear data lists for all types of reactions in different isotopes from about 10^{-5} eV to 20 MeV. These files are available on the National Nuclear Data Center's (NNDC) website [2]. They can be processed using different codes like NJOY [3] or AMPX [4] to broaden the cross sections for various temperatures, which are then used in reactor analysis tools. Brookhaven National Laboratory in the United States maintains ENDF data sets. Different countries across the world produce their own sets of nuclear data: JENDL (Japan), JEFF (Europe),

ROSFOND (Russia) and CENDL (China). Figure 2.1 shows ^{238}U scattering cross sections for the three neutron energy ranges.

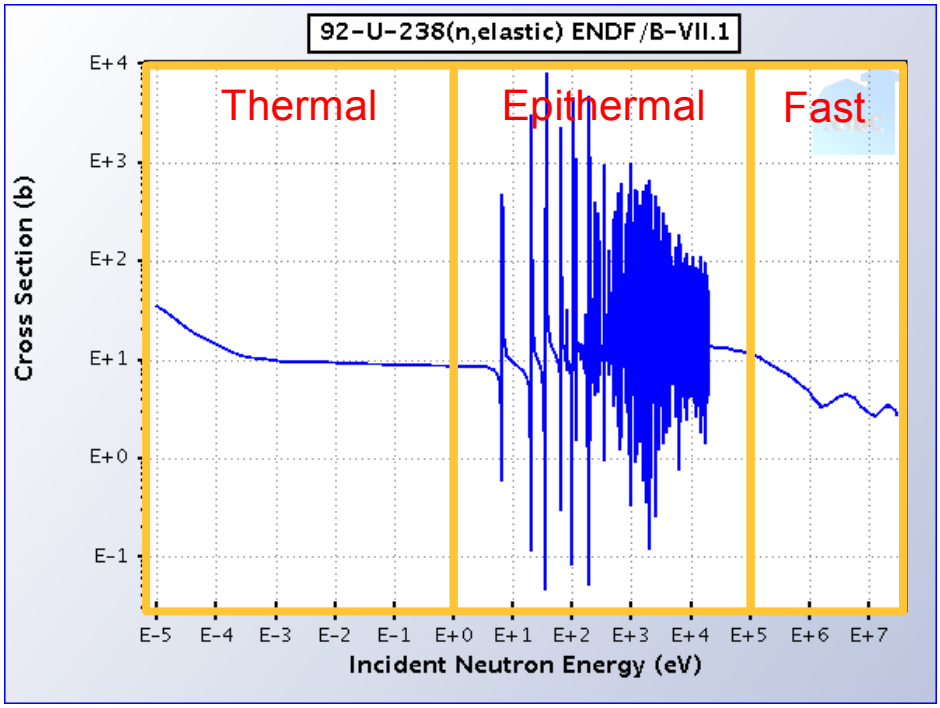

Figure 2.1: ^{238}U scattering cross section at 300 K [2]

The cross sections are almost constant for most of the thermal neutron energy range and adopt $1/v$ behavior for very small neutron energies [1]. There are well-defined and separated sharp peaks known as elastic scattering resonances in the epithermal neutron energy range. These resonances can be represented by the single-level Breit-Wigner formula or through other formulations like Adler-Adler or Reich-Moore equations.

There are many closely spaced resonances in the fast neutron energy range, which overlap, and resonances in this range are considered to be unresolved. Therefore, the cross section plot shows the average cross section value. There are several ways these cross sections are accounted for in the unresolved energy range. The average resonance spacing and partial widths are provided in the ENDF evaluations along with the probability distributions for the spacing and partial widths [5]. This information is used to generate self-shielded effective cross sections using codes like NJOY or they are used

to generate probability tables for the total cross section. These probability tables are then used in Monte Carlo codes to determine the type of nuclear reaction at high neutron energies [5].

When a neutron born after a fission reaction slows down from fast to thermal neutron energies, it has to avoid being lost through absorption, especially around resonances. More details regarding resonances will be provided in the following section.

2.2 Resonances

Resonances are sharply defined peaks in cross sections that form over very narrow energy ranges where there is a high likelihood of neutron interaction (scattering, fission, absorption, etc.) with the nucleus. These resonances occur when the center-of-mass energy plus the binding energy is close to an energy level of the compound nucleus resulting in the (temporary) absorption of a neutron by the target nucleus [1]. This compound nucleus is unstable and can decay through several reactions: elastic scattering, inelastic scattering, radiative capture or fission, all of which will be described in detail in this chapter.

$$ {}_{0}^{1}n + {}_{Z}^{A}X \rightarrow {}_{Z}^{A+1}X^{*} $$

$$ \text{neutron} + \text{target nucleus} \rightarrow \text{compound nucleus} $$

Z is the atomic number, A is the atomic mass number and X represents a general element. X^{*} denotes an element in an excited state.

An increase in the temperature of the system results in increased thermal motion of the target nucleus. As a result, the resonances in the nuclide experience Doppler broadening, where the resonance width widens while the magnitude of the peak decreases. The area under the peak remains relatively constant as the resonances broaden. Figure 2.2 illustrates the Doppler broadening phenomenon of the absorption cross section in ^{238}U from 300 K [2] to 1000 K [3].

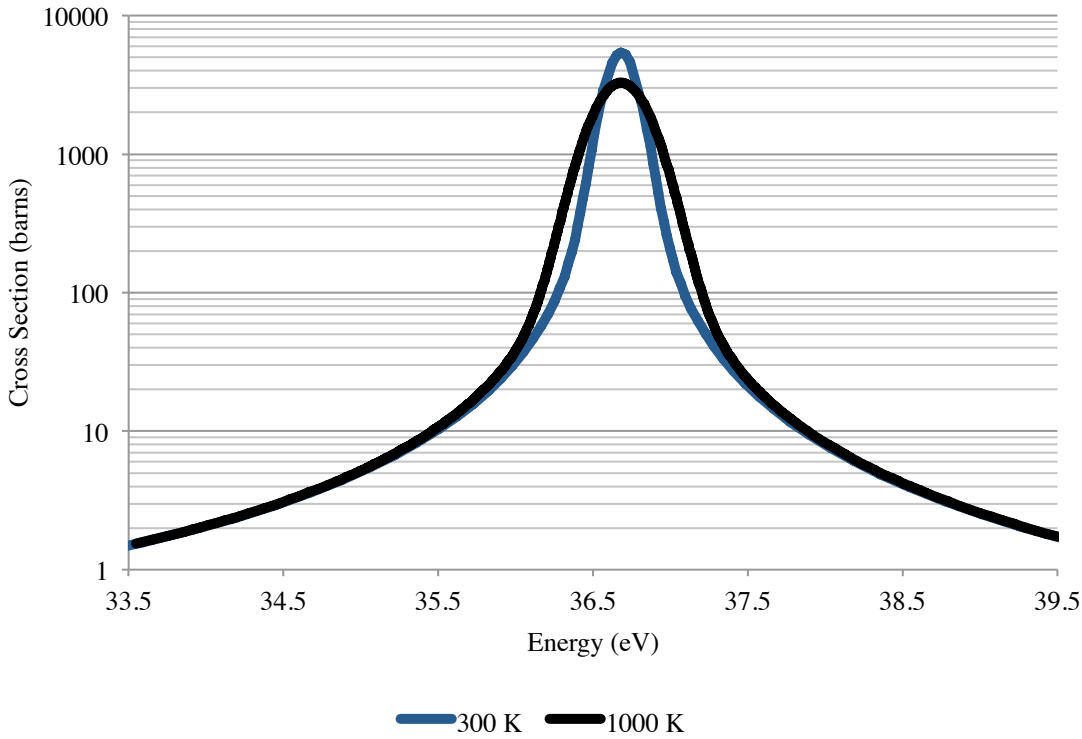

Figure 2.2: Doppler broadening of absorption cross sections in ^{238}U from 300 K to 1000 K

This behavior is important in reactor analysis as the temperature of the system increases because the probability of neutron absorption increases as it slows down from fast to thermal neutron energies due to broadening of the resonance widths. As a result, the neutron flux dips around these resonance regions. Consequently, the number of neutrons available to continue the fission chain reaction decreases with temperature, resulting in a reduction of k_{eff}.

2.3 Nuclear reactions

In this section, different types of nuclear reactions that neutrons undergo in a thermal fission reactor are discussed.

2.3.1 Fission

In nuclear fission, a neutron interacts with a fissile nucleus to form a compound nucleus, which spontaneously decays into two lighter nuclides and also expels some neutrons.

$$ {}_{0}^{1}n + {}_{Z_1}^{A_1}X \rightarrow {}_{Z_2}^{A_2}X + {}_{Z_3}^{A_3}X + neutrons + 200\,MeV $$

This is an exothermic reaction that releases approximately 200 MeV of energy [1]. The average number of neutrons released during a fission event is dependent on the nuclide with which the initial neutron interacts.

2.3.2 Radiative capture

In radiative capture, the excited compound nucleus reverts back to the target nucleus ground state with the release of a photon, also known as a gamma ray.

$$ {}_{0}^{1}n + {}_{Z}^{A}X \rightarrow {}_{Z}^{A+1}X^{*} \rightarrow {}_{Z}^{A+1}X + \gamma $$

Radiative capture is important to reactor analysis because a neutron is lost from the fission chain reaction during the slowing down process. The Breit-Wigner single-level resonance equation, Eq. (2.1), expresses the neutron energy dependence on the absorption cross section around a resonance [1] with the following equation:

$$ \sigma_{\gamma} = \frac{\sigma_o}{1+y^2}\frac{\Gamma_{\gamma}}{\Gamma}\sqrt{\frac{E_o}{E_c}}, \tag{2.1} $$

and,

$$ y = \frac{2}{\Gamma}\left(E_c - E_o\right). \tag{2.2} $$

E_c is the center of mass energy, E_o is the energy of the resonance, Γ is the total full width of half-maximum (FWHM) of the resonance, Γ_{γ} (radiative line width) is proportional to the probability that the compound nucleus will decay via gamma emission. The center-of-mass energy, E_c, is calculated from Eq. (2.3) [1],

$$E_c = \frac{M}{m+M} E, \tag{2.3}$$

where M is the mass of the target nucleus, m is the neutron mass and E is the incident neutron energy. σ_o is the total cross section at E_o shown in Eq. (2.4) [1],

$$\sigma_o = 4\pi \lambda\!\!\!^{-}_o{}^2 g \frac{\Gamma_n}{\Gamma}, \tag{2.4}$$

where $\lambda\!\!\!^{-}_o$ is the reduced neutron wavelength at E_o, Γ_n is the neutron line width which is proportional to the probability that the compound nucleus will decay with neutron emission and g represents the statistical spin factor. It is represented by the nuclear spin, I, and the total spin, J, [1]

$$g = \frac{2J+1}{2(2I+1)}. \tag{2.5}$$

The reduced neutron wavelength is calculated using $\lambda\!\!\!^{-} = \frac{\hbar}{\mu v}$ and μ, the reduced mass of the neutron-nucleus system, is found by $\mu = \frac{Am}{A+1}$, and v is the neutron speed at the resonance peak [6]. Using all these parameters, we are able to reconstruct single, separated resonances in nuclides.

2.3.3 Elastic scattering

Two forms of elastic scattering, potential and resonance elastic scattering, are described in detail in the following subsections.

2.3.3.1 Potential scattering

In potential scattering, a neutron scatters off a target nucleus due its nuclear potential, without the neutron penetrating the nuclear surface [1]. It is a billiard ball collision of a neutron with a nucleus, and there is no compound nucleus formation. The

potential scattering cross section is just the geometric cross section of the target nucleus represented by $\sigma_p = 4\pi R^2$, where R is the radius of the target nucleus [1].

2.3.3.2 Resonance elastic scattering

Elastic scattering resonances can occur in the low-lying epithermal region and this type of reaction is of particular interest to the work in this thesis. In elastic scattering around resonances, a neutron is absorbed by a nuclide and is then reemitted from the compound nucleus leaving the target nucleus in its ground state:

$$ {}_{0}^{1}n + {}_{Z}^{A}X \rightarrow {}_{Z}^{A+1}X^{*} \rightarrow {}_{0}^{1}n + {}_{Z}^{A}X $$

The neutron experiences a change in speed and direction after this interaction, but the energy and momentum is preserved before and after the interaction with the target nucleus. Elastic scattering occurs when the neutron energy is below the lowest excitation energy of the target nucleus [7].

Resonance elastic scattering cross sections are different from resonance capture cross sections. They have an interference region where the cross section dips before it rises to the peak, as shown in Figure 2.3. This region is caused by the quantum "interference" of possible elastic scattering states with potential scattering states.

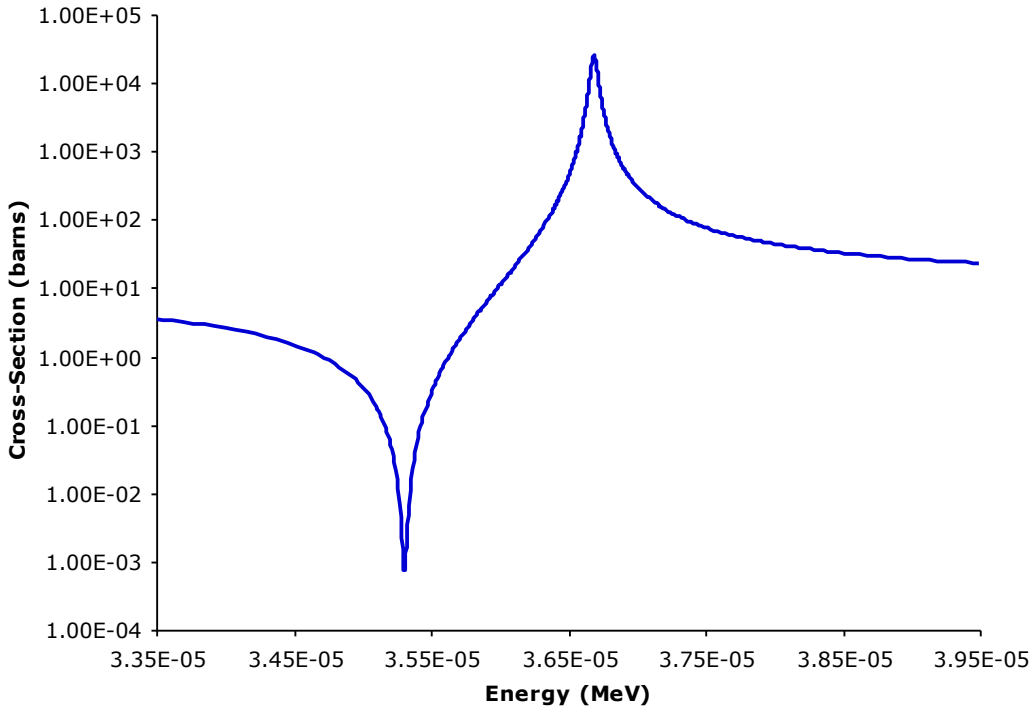

Figure 2.3: ^{238}U elastic resonance scattering cross section at 0 K

2.3.3.3 Scattering cross section

The scattering cross section can be represented by the single level Breit-Wigner formula [1]:

$$\sigma_s = \frac{\sigma_o}{1+y^2}\frac{\Gamma_n}{\Gamma}\sqrt{\frac{E_o}{E_c}} + \sigma_o \frac{2R}{\lambda\!\!\!^{-}_o}\frac{y}{1+y^2} + 4\pi R^2, \tag{2.6}$$

where σ_s = resonance scattering + interference scattering + potential scattering , and the other terms have been previously defined.

2.3.4 Inelastic scattering

A neutron interacting with a nucleus can experience inelastic scattering if the center-of-mass energy is higher than the lowest excitation level of the target nucleus. In this type of neutron interaction, kinetic energy is not conserved before and after the neutron collision with the nucleus. A neutron will transfer its energy to the target nucleus

so that the internal energy of the target nucleus changes and it becomes excited. The nucleus can then return to its ground state by emitting a gamma ray:

$$ {}_{0}^{1}n + {}_{Z}^{A}X \rightarrow {}_{0}^{1}n + {}_{Z}^{A}X^{*} \rightarrow {}_{0}^{1}n + {}_{Z}^{A}X + \gamma $$

Inelastic scattering generally occurs in the upper epithermal to fast neutron energy ranges.

2.4 Elastic scattering kinematics in free gas

As mentioned in the previous section, elastic scattering occurs when momentum and kinetic energy are conserved before and after a neutron interacts with a target nucleus. Elastic scattering occurs at all neutron energies, but we will consider the energy range from thermal to lower epithermal energies, where the neutron energy is small enough to be affected by the motion of the target nucleus.

In traditional Monte Carlo codes, elastic scattering collisions are treated in three different ways. In the thermal neutron energy range below ~ 1eV, chemical binding effects as well as the target motion is taken into account with the use of S(α,β) tables. For nuclides lacking S(α,β) tables, the free gas scattering treatment is used for all thermal energies where the target nuclides are assumed to be "free" and unbound. The free gas treatment is used in the lower epithermal energy range and thermal energy ranges for all nuclides. Above the threshold for free gas scattering, target-at-rest kinematics is used for fast neutron and higher epithermal neutron energies.

2.4.1 Collision mechanics in elastic scattering

To fully understand the relationship between the neutron velocity and target velocity, one must understand the collision mechanics in the laboratory frame and the center-of-mass frame. This is because collisions are analyzed in the center-of-mass frame and the exiting conditions of the neutrons are then converted back to the laboratory frame.

It is easier to execute collision mechanics in the center-of-mass frame because exiting neutron angles in this frame are assumed to be isotropic, and the target is at "rest".

After the collision is performed in the center-of-mass frame, the outgoing neutron energy is then computed in the laboratory frame [6].

Using conservation of momentum, the velocity of the center-of-mass, $\mathbf{v}_{\mathbf{CM}}$, in the laboratory frame is represented by,

$$\mathbf{v}_{\mathbf{CM}} = \frac{\mathbf{v} + A\mathbf{V}}{A+1}, \tag{2.7}$$

where **v** is the incident neutron velocity and **V** is the target velocity in the laboratory frame.

The neutron-nucleus interaction in the laboratory and CM frames are depicted below.

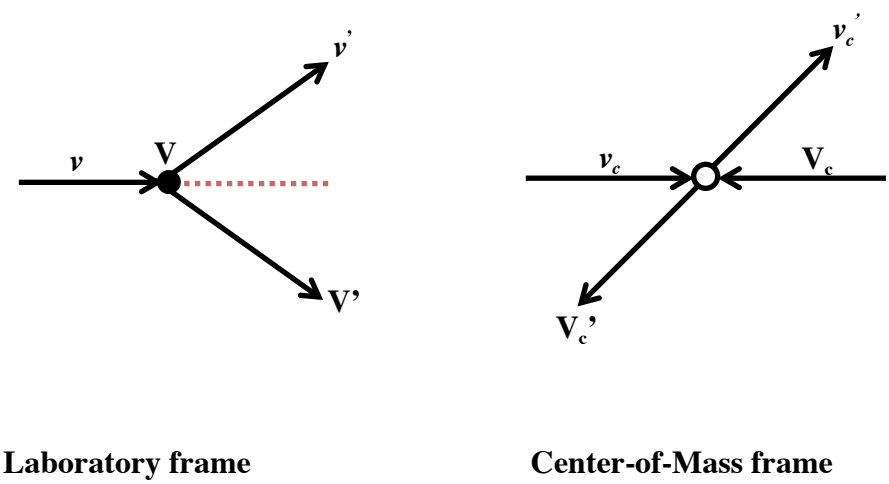

Figure 2.4: Velocity vectors in the laboratory and center-of-mass frames

Here $\boldsymbol{v}$ and $\boldsymbol{v'}$ are the incident and outgoing neutron velocities in the laboratory frame, and **V** and **V'** are the outgoing target nuclide velocity in the laboratory frame. The terms $\boldsymbol{v_c}$ and $\boldsymbol{v_c'}$ represent the incident and outgoing neutron velocities in the center-of-mass frame, and $\mathbf{V_c}$ and $\mathbf{V_c'}$ represent the incident and outgoing target nucleus velocities in the center-of-mass frame.

Since scattering is assumed to be isotropic in the center-of-mass frame, and neutron energy and momentum are conserved before and after the collision, the incident

neutron and final neutron speeds are equivalent in the center-of-mass system and can be represented by [6],

$$v_c = v_c' = \frac{A}{A+1} v_r, \tag{2.8}$$

where v_r is the relative speed of the neutron. If ϑ is the angle between the center-of-mass velocity and the outgoing neutron velocity in the center-of-mass frame, then the outgoing neutron speed, v', in the laboratory system is,

$$\left(\mathbf{v}_\mathbf{c}' + \mathbf{v}_\mathbf{CM}\right) \bullet \left(\mathbf{v}_\mathbf{c}' + \mathbf{v}_\mathbf{CM}\right) = v' = \sqrt{\left(\frac{A}{A+1} v_r\right)^2 + v_{CM}^2 + 2 v_{CM} \left(\frac{A}{A+1} v_r\right) \cos\vartheta}. \tag{2.9}$$

Therefore, the minimum exiting neutron speed, $v'_{\min}$, can be obtained if $\cos\vartheta$ = -1 and the maximum exiting neutron speed, $v'_{\max}$, is obtained when $\cos\vartheta$ = 1. They are shown below [6]:

$$\begin{aligned} v'_{\min} &= \left| v_{CM} - \frac{A}{A+1} v_r \right|, \\ v'_{\max} &= v_{CM} + \frac{A}{A+1} v_r. \end{aligned} \tag{2.10}$$

The final neutron speed in the laboratory system lies between $v'_{\min} \le v \le v'_{\max}$. Eq. (2.9) is used in current Monte Carlo codes to determine the exiting neutron speed in the laboratory frame.

2.5 Differential scattering probability distribution function

The scattering process in Monte Carlo codes, where the incident neutron experiences a change in angle and speed after the scattering process, is simulated by sampling for the target nuclide speed and the cosine of polar angle between the neutron and target. In the free gas model, the microscopic scattering cross section is assumed to be constant, hence it does not impact the probability of a change in the outgoing angle or speed of the neutron. Since this is clearly not the case for resonance scattering off heavy

nuclides, we need to consider the general case where the scattering cross section is not constant in energy. The change in neutron angle and speed due to a scattering collision is given by the double-differential scattering cross section, $\sigma_s\left(E \rightarrow E', \mathbf{\Omega} \rightarrow \mathbf{\Omega}'\right)$, which is proportional to the probability that a neutron with an incident speed and angle will scatter out with a specific energy and angle [1]. Integrating $\sigma_s\left(E \rightarrow E', \mathbf{\Omega} \rightarrow \mathbf{\Omega}'\right)$ over all polar and azimuthal angles gives the energy-dependent differential scattering cross section probability as a function of incident energy and independent of the angle, as shown in Eq. (2.11),

$$\sigma_s\left(E \rightarrow E'\right) = \int_{4\pi} \sigma_s\left(E \rightarrow E', \mathbf{\Omega} \rightarrow \mathbf{\Omega}'\right) d\mathbf{\Omega}'. \tag{2.11}$$

The differential scattering cross section can then be expressed in terms of the total scattering cross section,

$$\sigma_s\left(E \rightarrow E'\right) = \sigma_s\left(E\right) P\left(E \rightarrow E'\right),$$

where $P\left(E \rightarrow E'\right) dE'$ is the probability that a neutron scattering with an incident neutron energy, E, will scatter out of the collision with energy, E', in the interval E' and $E' + dE'$. $P\left(E \rightarrow E'\right)$ is referred to as the differential scattering PDF.

2.5.1 Effect of cross sections on the differential scattering PDF

Details and assumptions associated with the free gas scattering model, implemented in current Monte Carlo codes, were presented in Section 1.3. In the following subsections, the differential scattering PDF generated by the free gas scattering model will be compared to two other scattering models: asymptotic and modified free gas scattering.

2.5.1.1 Asymptotic scattering

Deterministic codes also assume constant scattering cross sections in the low-lying epithermal neutron energy range, but additionally assume that the target nucleus is at rest. This means that the final neutron energy lies between $\alpha E_{initial} \leq E_{final} \leq E_{initial}$,

where $\alpha = \left(\frac{A-1}{A+1}\right)^2$. The target is assumed to be at rest because the incident neutron energy is thought to be far greater than the target nucleus energy. As a result, the target nucleus speed is considered to be zero relative to the neutron speed in the epithermal region. This is not a valid assumption to make for all scenarios because at high temperatures, the target nucleus motion increases and can contribute to neutron energy gain even if the neutron is colliding with a heavy nucleus at epithermal energies. Therefore, deterministic codes do not predict any upscattering effects in the epithermal range with the asymptotic or target-at-rest scattering model.

2.5.1.2 Modified free gas scattering

It is important to account for scattering resonances in heavy nuclides in the lower epithermal region because the effects they have on neutron moderation and absorption are not negligible. The varying resonances are important in reactor calculations because they contribute to the additional probability of neutrons scattering past an absorption resonance, gaining energy and falling back into the absorption resonance.

The Doppler Broadened Rejection Correction (DBRC) method was developed by Becker *et. al.* [9] where the resonances in the scattering cross sections for heavy nuclides are taken into account in the free gas model. The modified scattering model uses the scattering cross section dependent on the relative speed of the neutron, $\sigma_s\left(|\mathbf{v}-\mathbf{V}|\right)$. The modified bivariate scattering PDF can then be shown to be,

$$P(V,\mu\,|\,v)\,dV\,d\mu = \frac{\left(\frac{\alpha}{\pi}\right)^{3/2}\sigma_s\left(|\mathbf{v}-\mathbf{V}|\right)|\mathbf{v}-\mathbf{V}|\,V^2 e^{-\alpha V^2}\,2\pi\,dV\,d\mu}{\sigma_{eff,s}\left(v\right)}.$$

This method and the detailed algorithm for Monte Carlo codes will be discussed in detail in Chapter 3.

Figures 2.5(a) and 2.5(b) illustrate two resonances in ^{238}U, peaked at 36.67 eV and 6.67 eV.

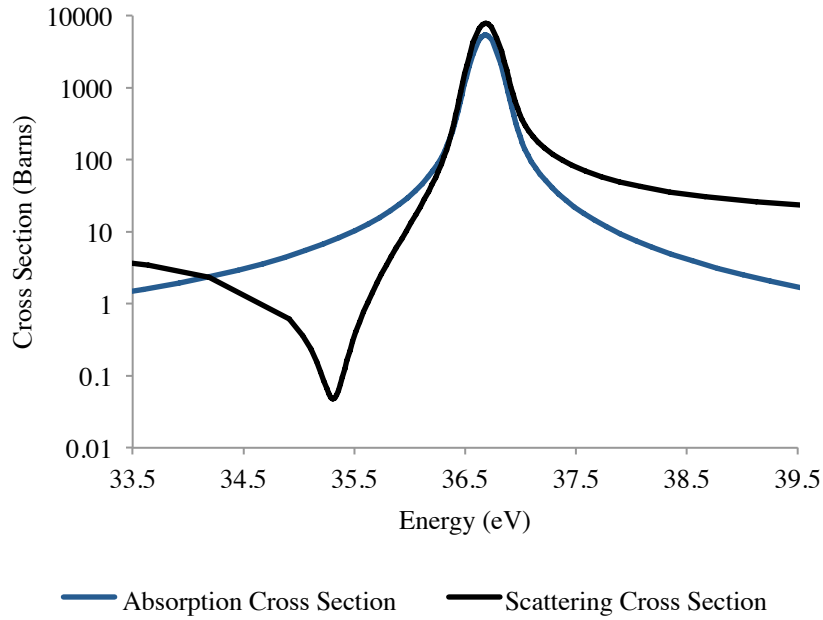

(a)

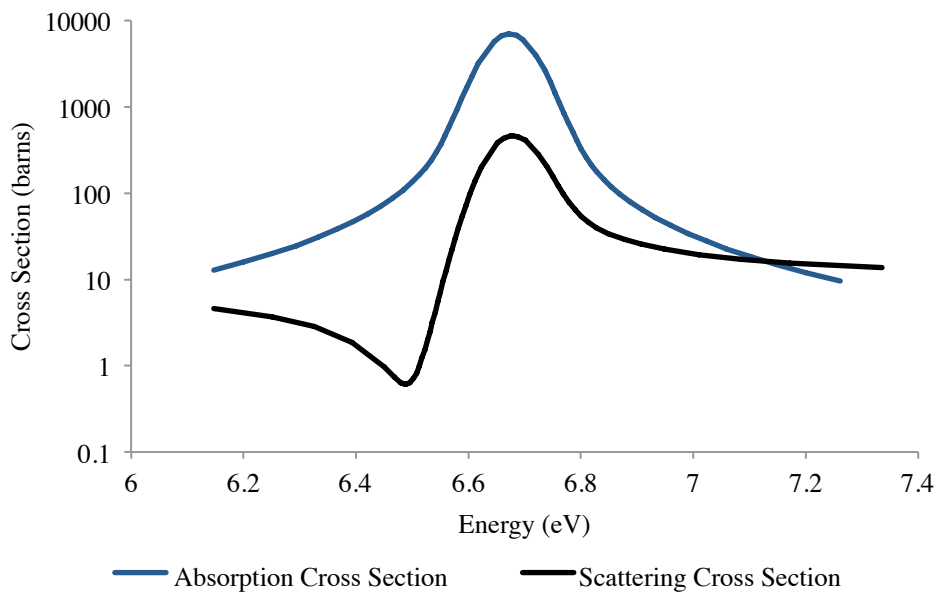

(b)

Figures 2.5: (a) Scattering and (b) absorption cross sections for ^{238}U around 36.67 eV and 6.67 eV resonances at 300 K [2]

Figure 2.5 (a) shows the 36.67 eV resonance in ^{238}U, which has a large scattering to absorption cross section ratio. In this case, a neutron that has slowed down past a

resonance can scatter back into the resonance with greater likelihood than a neutron around the resonance depicted in Figure 2.5 (b). Figure 2.5 (b) shows the 6.67 eV resonance in ^{238}U, which has a lower scattering to absorption ratio. The probability of neutrons with energies around the vicinity of the resonance is low due to the large absorption cross section. Therefore, the probability of a scattering reaction is reduced. As a result, the effects of taking into account the resonances with low scattering to absorption ratios become less important.

2.5.1.3 Comparison of differential scattering PDFs from different scattering models

Figure 2.6 shows the difference in the differential scattering PDF from various scattering models that have been discussed: asymptotic scattering (target-at-rest kinematics), free gas (FG) scattering, and modified free gas scattering, also known as DBRC, which essentially gives the exact energy dependence. In this figure, the probability that a neutron with an incident neutron energy, *E*, will scatter into outgoing energies, *E'*, after one collision is shown. For this case, neutrons have an incident energy of 6.52 eV, and they scatter in a purely homogenous medium of ^{238}U at 1000 K.

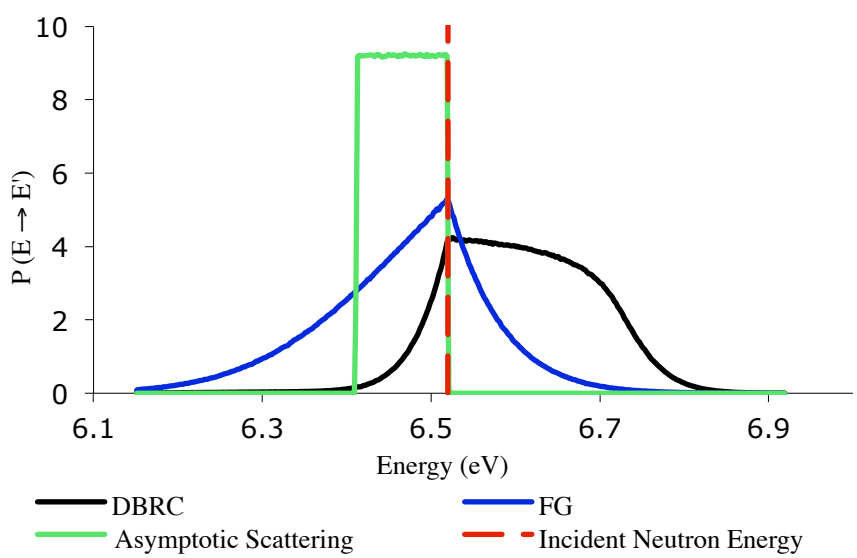

Figure 2.6: Comparison of different scattering models for ^{238}U at 1000 K and for incident neutron energy of 6.52 eV

In Figure 2.6, the red line indicates the incident neutron energy at 6.52 eV. All data points to the right of the red line indicates neutron upscatter (energy gain) and all data points to the left represent downscatter. The green line represents the energy transfer obtained from the asymptotic scattering model. The plot shows that there is no upscatter with asymptotic scattering, consistent with the assumption that the target is at rest. The blue line illustrates the results from the free gas scattering model. This model does indicate some neutron upscattering because it accounts for thermal motion of the target nuclides. But, the cross sections are held constant, and consequently, the scattering model is not accurate. Finally, the black line indicates the results provided by DBRC (modified free gas scattering model), which shows that there is significant upscattering when the thermal motion of the target nuclides and the resonance cross sections are taken into account.

As shown in Figure 2.5(b), the peak of the absorption resonance occurs at around 6.67 eV. In Figure 2.6, neutrons with 6.52 eV incident energy are more likely to gain energy around the resonance peak and experience higher absorption. The figure clearly shows the importance of taking into account target nucleus motion and the resonances due to the significant gain in energy of the neutron that our current scattering models are neglecting.

2.6 Summary

The results from the three scattering models demonstrate the importance of accounting for resonances and target motion in the epithermal region when predicting the correct behavior of neutrons slowing down through the resonance range. Criticality calculations have shown that k_{eff} can be off by several hundred pcm for LWR and VHTR calculations. Algorithms to simulate the conventional free gas scattering model and DBRC will be presented in detail in the next chapter.

2.7 References

[1] J. J. Duderstadt and L. J. Hamilton, *Nuclear Reactor Analysis*, John Wiley & Sons, Inc. (1976).

[2] National Nuclear Data Center, *Evaluated Nuclear Data File (ENDF)*, Brookhaven National Laboratory <http://www.nndc.bnl.gov/exfor/endf00.jsp> (2012).

[3] R. E. MacFarlane and D. W. Muir, *The NJOY Nuclear Data Process System Version 91*, LA-12740-M, Los Alamos National Laboratory (1994).

[4] N. M. Greene, W. E. Ford III, L. M. Petrie and J. W. Arwood, *AMPX-77 A Modular Code System for Generating Coupled Multigroup Neutron Gamma Cross Section Libraries from ENDF/B-IV and/or ENDF/B-V*, ORNL/CSD/TM-283, Oak Ridge National Laboratory (1992).

[5] T-2 Nuclear Information Service, *Unresolved Resonances,* Los Alamos National Laboratory <http://t2.lanl.gov/endf/intro16.html> (1998).

[6] G. I. Bell and S. Glasstone, *Nuclear Reactor Theory,* Van Nostrand Reinhold Company (1970).

[7] S. A. Dupree and S. K. Fraley, *A Monte Carlo Primer: A Practical Approach to Radiation Transport,* Kluwer Academic/Plenum Publishers, New York (2002).

[8] B. Becker, R. Dagan and G. Lohnert, *Proof and implementation of the stochastic formula for ideal gas, energy dependent scattering kernel*, Annals of Nuclear Energy, **36**, pp. 470 – 474 (2009).

[9] T. Högberg, *Monte Carlo Calculations of Neutron Thermalization In a Heterogeneous System,* Journal of Nuclear Energy, Part A: Reactor Science, **12**, pp. 145-150 (1960).

[10] G. L. Blackshaw, *Scattering of Low-Energy Neutrons In a Monatomic Gas Model of a Multiplying System,* Ph.D. Dissertation in Nuclear Engineering, North Carolina State University (1966).

[11] E. Larsen, NERS 543: Nuclear Reactor Theory II Class Notes, University of Michigan (2007).

[12] E. E. Lewis and W. F. Miller, Jr., *Computational Methods of Neutron Transport*, American Nuclear Society, Inc. (1993).

[13] R. R. Coveyou, R. R. Bate and R. K. Osborn, *Effect of Moderator Temperature Upon Flux In Infinite, Capturing Medium*, Journal of Nuclear Energy, **2**, pp. 153-167 (1956).

[14] X-5 Monte Carlo Team, *MCNP – A General Monte Carlo N-Particle Transport Code, Version 5, Volume I: Overview and Theory*, LA-UR-03-1987, Los Alamos National Laboratory (2003).

CHAPTER 3

Analysis Of Existing Scattering Models

3.1 Introduction

Chapters 1 and 2 discussed stochastic simulation of neutrons in Monte Carlo codes and the physics behind the important nuclear reactions for reactor analysis. In Chapter 2, we discussed conventional scattering models used in reactor analysis methods today and their drawbacks. In this chapter, we will examine the existing scattering models in more detail and the algorithms used to implement these models in Monte Carlo codes.

In Chapter 1, Eq. (1.20), it was shown that it is possible to analytically integrate the double-integral equation for the effective scattering cross section if one assumes constant scattering cross section and a Maxwell-Boltzmann energy distribution for target nuclide motion. Assuming constant scattering cross sections was reasonable for most cases because light nuclides have nearly constant cross sections in the epithermal energy range. Moreover, moderation due to scattering off heavy nuclides was often negligible, thus justifying the use of constant scattering cross sections even for heavy nuclides in conventional scattering models. Thus the bivariate PDF for scattering was based on constant scattering cross sections, as discussed in Chapters 1 and 2.

Based on these simplifying assumptions, it is still not possible to analytically sample target nucleus speed and approaching polar angle from the bivariate PDF without using a rejection technique or constructing the cumulative distribution function (CDF) for all incident neutron energies from a discretized PDF to sample for the scattering parameters. The latter method was computationally expensive and was not feasible to implement until recently with the huge gains in computing performance. A Monte Carlo scheme that involved a rejection technique proposed by H. Kahn [1] was implemented as the free gas scattering kernel in the Monte Carlo N-Particle (MCNP) [2] transport code to

sample the target nucleus speed and cosine of polar angle between the neutron and target. The free gas scattering kernel can be activated in MCNP when target nuclides have a temperature of less than $400kT$ (~10 eV) where k is the Boltzmann constant and T is the temperature of the target.

The original free gas scattering kernel does not provide the correct differential scattering kernel for neutron scatter, especially off heavy nuclides as demonstrated in the previous chapter. Recent studies by M. Ouisloumen *et. al.* [3], W. Rothenstein *et. al.* [4], B. Becker *et. al.* [5] and D. Lee *et. al.* [6] showed that when cross section dependence on relative neutron speed was taken into account, resonance scattering off heavy nuclides caused the neutron to gain speed with greater likelihood than previously considered. This work performed on resonance scattering raised an issue about scattering models that need to be implemented in the epithermal energy range for reactor calculations. The use of HPCs facilitate faster and more accurate Monte Carlo calculations with large numbers of particles and cycles, and the effects of the assumptions in the current free gas scattering kernel are now evident and no longer in the noise range. Very High Temperature Reactor (VHTR) calculations seem to be most affected by resonance scattering, but it can also be significant in LWRs at hot full power conditions [6].

In this chapter, the Doppler Broadened Rejection Correction (DBRC) method developed by B. Becker *et. al.* [5] will be discussed. An overview of its independent implementation in MCNP5 to study the differences in benchmark problems with conventional free gas scattering model and DBRC will be presented. DBRC was selected over other methods to account for resonance scattering because it is based on the free gas scattering kernel on which MCNP5 currently operates. It was also important to independently implement DBRC in MCNP5 in order to have a reliable code to benchmark alternative resonance scattering models developed in this thesis.

3.2 Literature survey on scattering methods development

Several methods account for neutrons slowing down in an absorbing/scattering media where the target nuclides are in thermal motion. These methods, however, focus on changing the integral equations to differential equations and using numerical methods to solve the differential equations. One of the main assumptions used in all these models is that the scattering cross sections remain constant, thereby simplifying the calculations.

Coveyou *et. al.* [1] presented a Monte Carlo method proposed by H. Kahn [1] to sample for target nuclide speed and cosine of polar angle to form the well known free gas scattering kernel, which is implemented in MCNP5.

Marchuk *et. al.* [7], and Blackshaw *et. al.* [8] focused on approximating the differential scattering probability for cross sections that are not constant using Legendre expansions to calculate the moments. M. Ouisloumen *et. al.* [3] also used Legendre expansions to calculate the differential scattering probability using the P_0 moment for cross sections that are a function of relative speed of the neutron. Their studies showed that resonance upscattering was important. B. Becker *et. al.* [5] modified the free gas scattering kernel proposed by H. Kahn to account for resonance scattering effects.

D. Lee *et. al.* [6] discretized the bivariate scattering PDF and constructed a discrete CDF that could then be used to sample for the target nuclide speed and the cosine of polar angle. However, they found this approach was computationally expensive. Later, they implemented an accelerated scheme where the neutron was assigned a weight as shown,

$$w_{i+1} = w_i \frac{\sigma_t\left(v_r\right)\frac{v_r}{v'} + \sigma_b}{\sigma_t^{eff}\left(v'\right)\frac{v_r}{v'} + \sigma_b}, \tag{3.1}$$

where σ_t is the total cross section, σ_t^{eff} is the effective total cross section, σ_b is the background cross section, v_r is the relative neutron speed and v' is the incident neutron speed. D. Lee *et. al.* [6] obtained results comparable to B. Becker *et. al.* [5] and M. Ouisloumen *et. al.* [3].

T. Mori *et. al.* [9] also developed a similar method and applied a correction factor for the neutron weight as shown,

$$f = \frac{\sigma_s\left(v_r\right)}{\sigma_s^{eff}\left(v'\right)}, \tag{3.2}$$

where σ_s is the scattering cross section and σ_s^{eff} is the effective scattering cross section. Their results were also comparable to results published by D. Lee *et. al.* [6]. More recently, G. Arnabas *et. al.* [10] presented a paper on the use of Blatt-Beidenharn coefficients to generate moments of the differential scattering kernel.

All this recent work on resonance scattering showed the importance of accounting for resonance scattering in reactor calculations and illustrated the need to account for resonance scattering in MCNP.

3.3 Free gas scattering

3.3.1 Original free gas scattering model and algorithm

In this section, we present the details for the free gas scattering algorithm that was developed in the 1950s for continuous energy Monte Carlo codes. It is based on three main assumptions:

- Target nuclides are unbound,
- Unbound nuclei are in a Maxwell-Boltzmann distribution in energy,
- The microscopic scattering cross section is constant.

Using these assumptions, the bivariate scattering PDF is sampled for the target nuclide speed and cosine of polar angle. We can rewrite Eq. (1.20) as,

$$P(V,\mu \mid v)\,dV\,d\mu = C\cdot\left[P_1\cdot f_1(V)dV \;+\; P_2\cdot f_2(V)dV\right]\cdot\frac{d\mu}{2}\cdot\frac{|\mathbf{v}-\mathbf{V}|}{v+V}\;, \tag{3.3}$$

where $P_1 = \dfrac{v}{v+2/\sqrt{\pi\alpha}}$, $\qquad P_2 = 1-P_1$,

$f_1(V) = 4\sqrt{\frac{\alpha^3}{\pi}}V^2 e^{-\alpha V^2}$, $\qquad f_2(V) = 2\alpha^2 V^3 e^{-\alpha V^2}$,

$C = \sigma_s / \sigma_{eff,s}(v)$.

Here $f_1(V)$ *and* $f_2(V)$ are two different forms of the Maxwell-Boltzmann distribution in energy for the target nuclides. P_1 and P_2 are probabilities, which are used to decide the target speed. The algorithm can be implemented in the following manner:

Step 1: We start off with the terms within the square bracket. Choose a random number, ξ_1, and test P_1 against ξ_1.

a. *If* $\xi < P_1$ then choose the target speed from $f_1(V)$ where $V \in [0,\infty]$, and

$$V = \sqrt{-\frac{1}{\alpha}\left(\ln \xi_a + \ln \xi_b \cos^2\left(\frac{\pi}{2}\xi_c\right)\right)}.$$

b. Else, choose the target speed from $f_2(V)$ where $V \in [0,\infty]$, and

$$V = \sqrt{-\frac{1}{\alpha}\ln\left(\xi_a \xi_b\right)}.$$

Step 2: Choose the cosine of polar angle, μ, between the incident neutron and the target nuclide in the center-of-mass frame from an isotropic distribution, $\frac{d\mu}{2}$, where $\mu \in [-1,1]$ and $\mu = 2\xi - 1$.

Step 3: Choose a random number, ξ_2, and test $\frac{|\mathbf{v}-\mathbf{V}|}{v+V}$ against ξ_2.

a. If $\xi_2 > \frac{|\mathbf{v}-\mathbf{V}|}{v+V}$, reject all scattering parameters and restart from Step 1 until Step 3b. is achieved.

b. Else, accept the scattering parameters, target speed, V, and cosine of polar angle, μ.

i. Determine cosine of polar angle and azimuthal angle for the exiting neutron in the laboratory frame.

ii. Calculate the final exiting neutron speed in the laboratory frame.

This algorithm is implemented in many Monte Carlo codes, i.e. MCNP, to treat elastic scattering. Assuming a constant scattering cross section in the vicinity of resonances in heavy nuclides will result in incorrect differential scattering PDFs. This effect leads to about 200 pcm differences in Hot Full Power criticality calculations in LWRs and about 400 pcm differences in VHTRs [6]. Therefore, it is important to take into account resonance scattering cross sections in heavy nuclides when sampling for the target speed and cosine of polar angle between the target and neutron.

3.3.2 Constructing the discretized bivariate PDF

Before presenting the algorithm for the DBRC method, it was important to develop an intuitive sense for the accuracy and efficiency of this method in Monte Carlo codes. To do this, the bivariate PDF in Eq. (3.3) was studied by discretizing it in the following manner:

$$P_{ij} = \frac{v_{ij}\sigma_s(v_{ij})M_j}{\sum_{i=1}^{N_i}\sum_{j=1}^{N_j} v_{ij}\sigma_s(v_{ij})M_j}, \tag{3.4}$$

where grid i represents cosine angles between -1.0 and +1.0 and $\Delta\mu_i$ was set to 0.02. Grid j represents the target speed, V, from 0 to 990 m/s with ΔV_j set to 10 m/s. The term M_j represents the Maxwell-Boltzmann distribution in energy of the target nuclides, v_{ij} represents the relative neutron speeds for varying target nuclide speeds and cosine angles on the grid, and $\sigma_s(v_{ij})$ represents the zero Kelvin scattering cross section as a function of the relative speed of the neutron.

The discretized bivariate PDF in Eq. (3.4) was used to study the effect of scattering resonances in heavy nuclides. For this study, the scattering medium was ^{238}U and the 36.67 eV resonance was chosen since this is a scattering resonance that is known to be particularly important for the resonance upscattering effect [9], [10]. First, the bivariate PDF was constructed for 36.0 eV incident neutron energy scattering in ^{238}U at 1000 K. The step-by-step change in each of the parameters (v_{ij}, $\sigma_s(v_{ij})$, M_j) over the range of i and j was studied.

Figure 3.1 illustrates the Maxwell-Boltzmann distribution, M_j, of the target nuclei. The figure shows that the Maxwell-Boltzmann distribution is independent of the cosine of polar angle, as expected, but is a function of the nuclei speeds. Figure 3.2 shows the scattering cross section as a function of the relative speed of the neutron, $\sigma_s(v_{ij})$, which does depend on the target speed and polar angle of approach. The plot shows that this variation in cross section peaks over a very narrow range of target speeds and polar angle, a consequence of the strongly varying cross section in the vicinity of the resonance. Figure 3.3 shows the relative neutron energy variation over angle and target speeds, v_{ij}. After combining these parameters and normalizing them, we obtain Figure 3.4, which shows the discretized bivariate scattering PDF, P_{ij}. Figure 3.4 shows that the scattering probability is close to zero for a wide range of angle and target speeds, peaking for a narrow region of angle and target speeds.

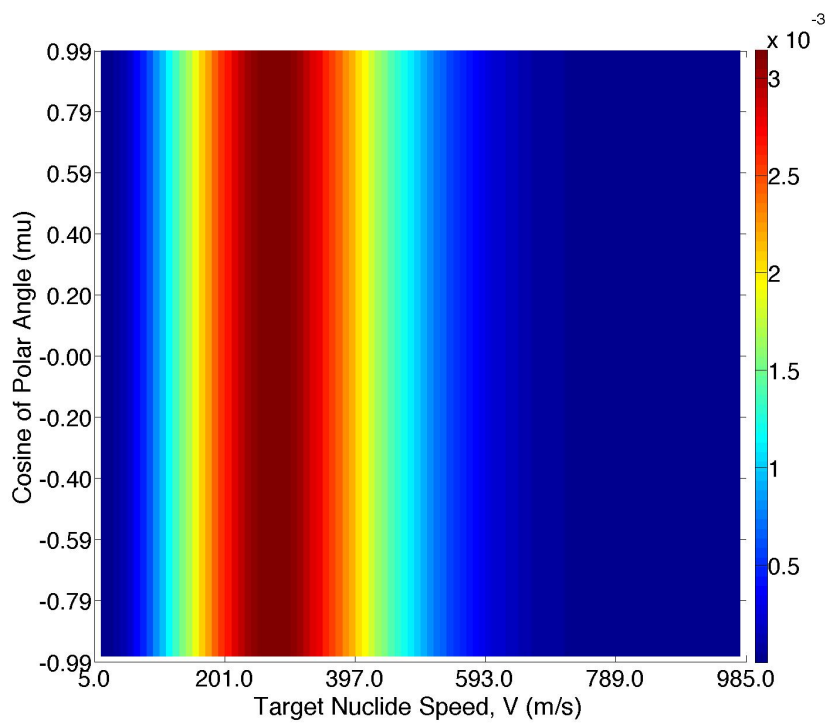

Figure 3.1: Maxwell-Boltzmann distribution (M_j) ^{238}U nuclei at 1000 K

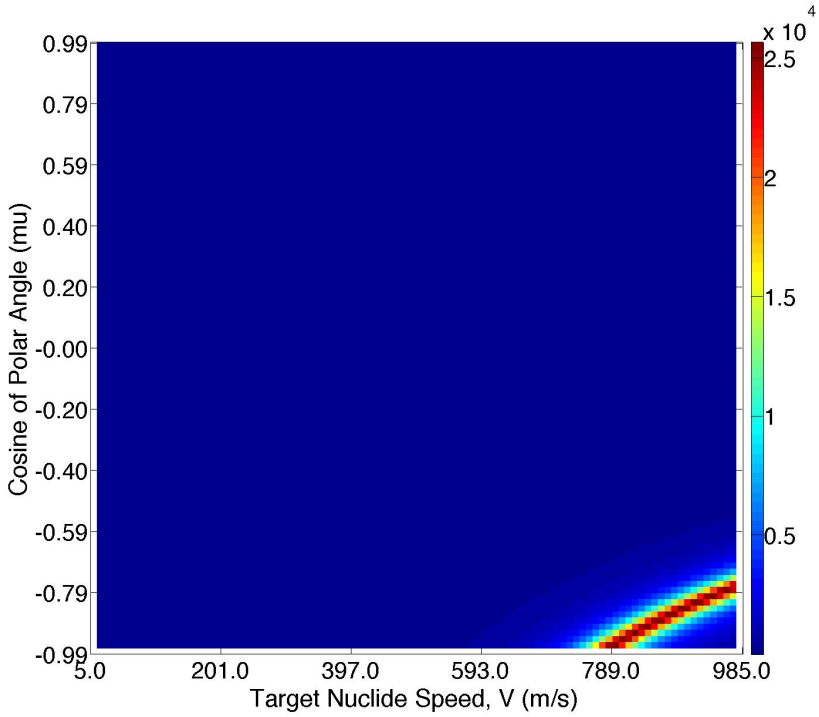

Figure 3.2: Zero Kelvin ^{238}U scattering cross sections as a function of the relative speed of the neutron ($\sigma_s(v_{ij})$) for 36.0 eV incident neutron energy

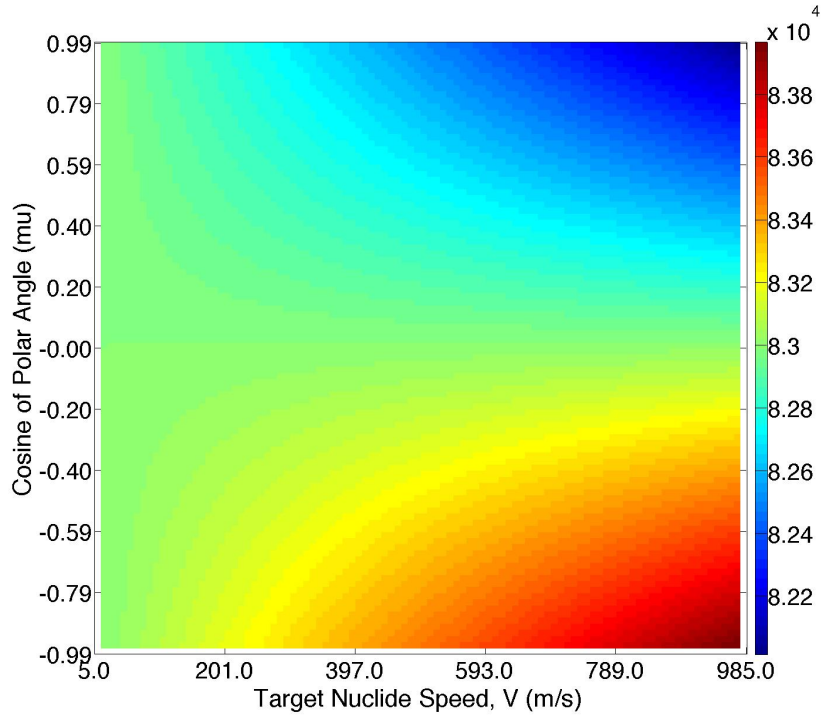

Figure 3.3: Relative speed of the neutron (v_{ij}) for 36.0 eV incident neutron energy

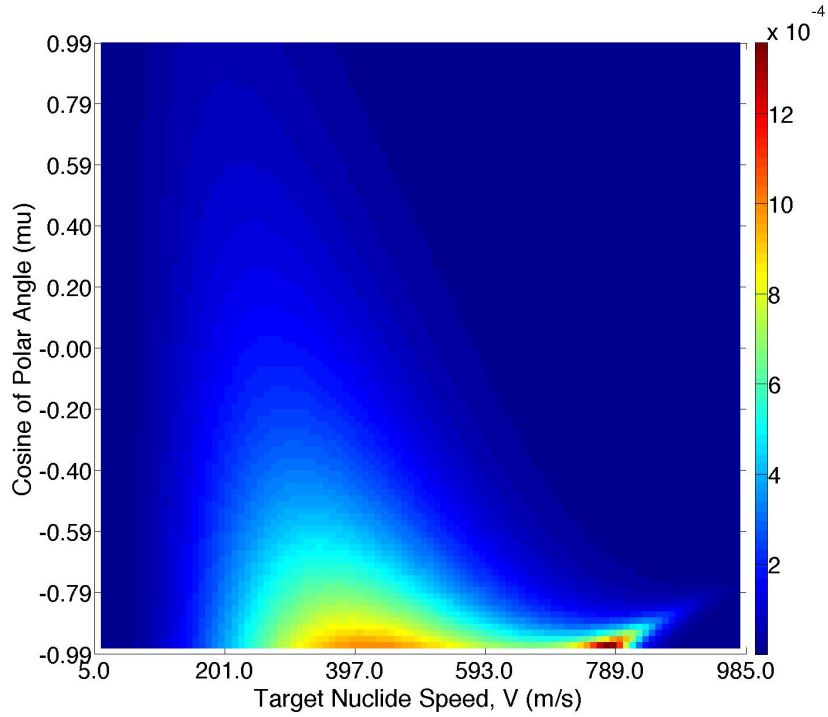

Figure 3.4: Bivariate scattering PDF (P_{ij}) for incident neutron energy of 36.0 eV and ^{238}U at 1000 K

When implementing an extra rejection technique to select the target speed and angle in the DBRC method, one can now understand why it would be extremely inefficient. That is, by choosing the target speed from all ranges, $V \in [0,\infty]$, and angle from $\mu \in [-1,1]$, these selected values have to pass the rejection tests. If the probability of scatter is going to be close to zero for most of the range of cosine of polar angles and target nuclide speeds, then the rejection becomes very inefficient. This is the reason why there are many rejections near the resonance and the DBRC method will be slow.

A sensitivity study was performed by varying the incident neutron energy while holding the temperature of ^{238}U at 1000 K. The incident neutron energy was varied from 36.0 eV to 36.25 eV to 36.50 eV. Figures 3.5 (a), (b) and (c) show that the peaked behavior is consistent, and that it does not change even when the incident neutron energies vary near the resonance. Next, the incident neutron energy was held at 36.25 eV and the temperature was varied. Figures 3.6 (a), (b), (c), (d) and (e) show that this peaked behavior does not change even when the temperature of the system was varied.

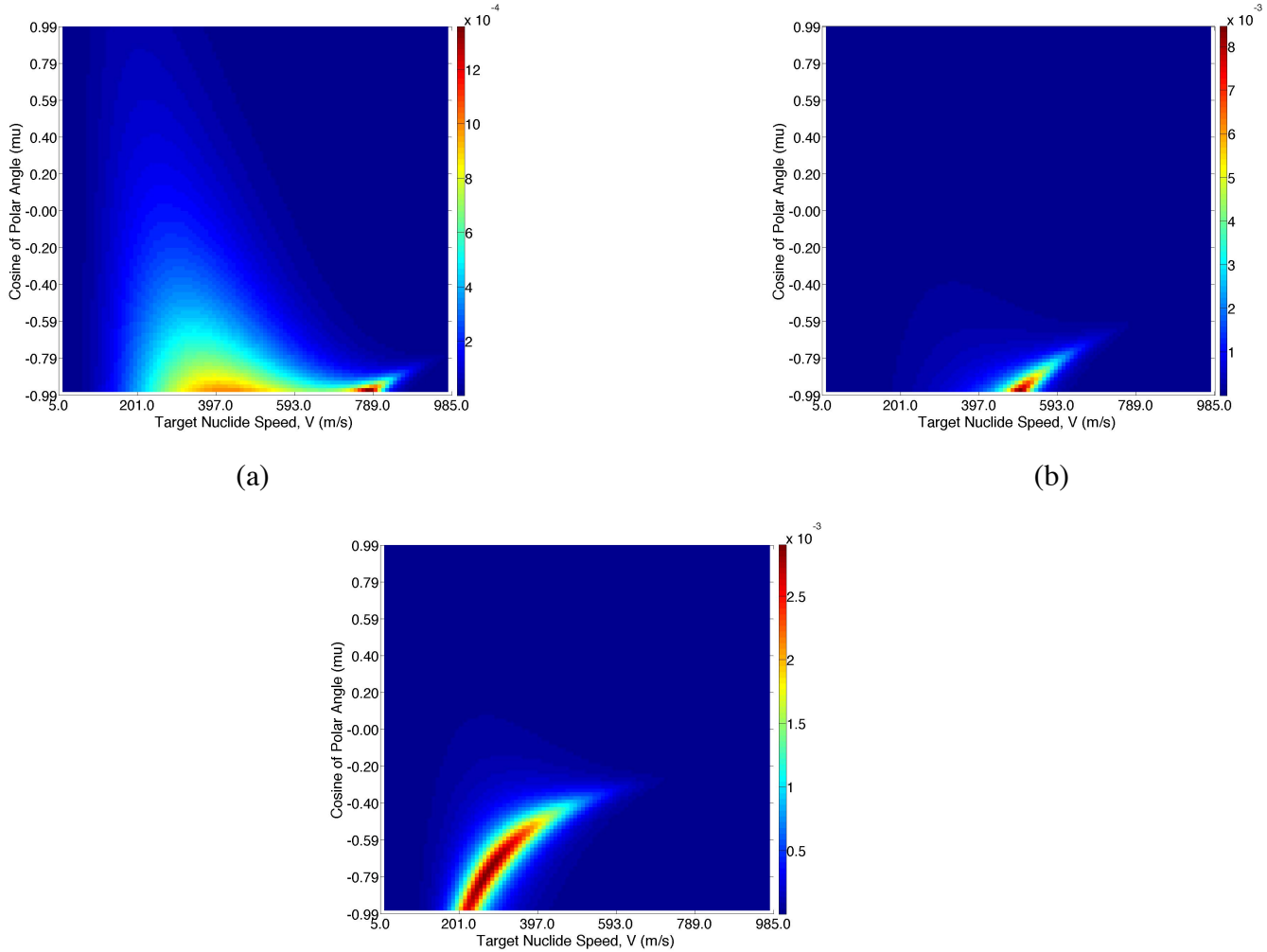

Figure 3.5: Bivariate scattering PDFs for incident neutron energies of (a) 36.0 eV, (b) 36.25 eV and (c) 36.50 eV for ^{238}U at 1000 K

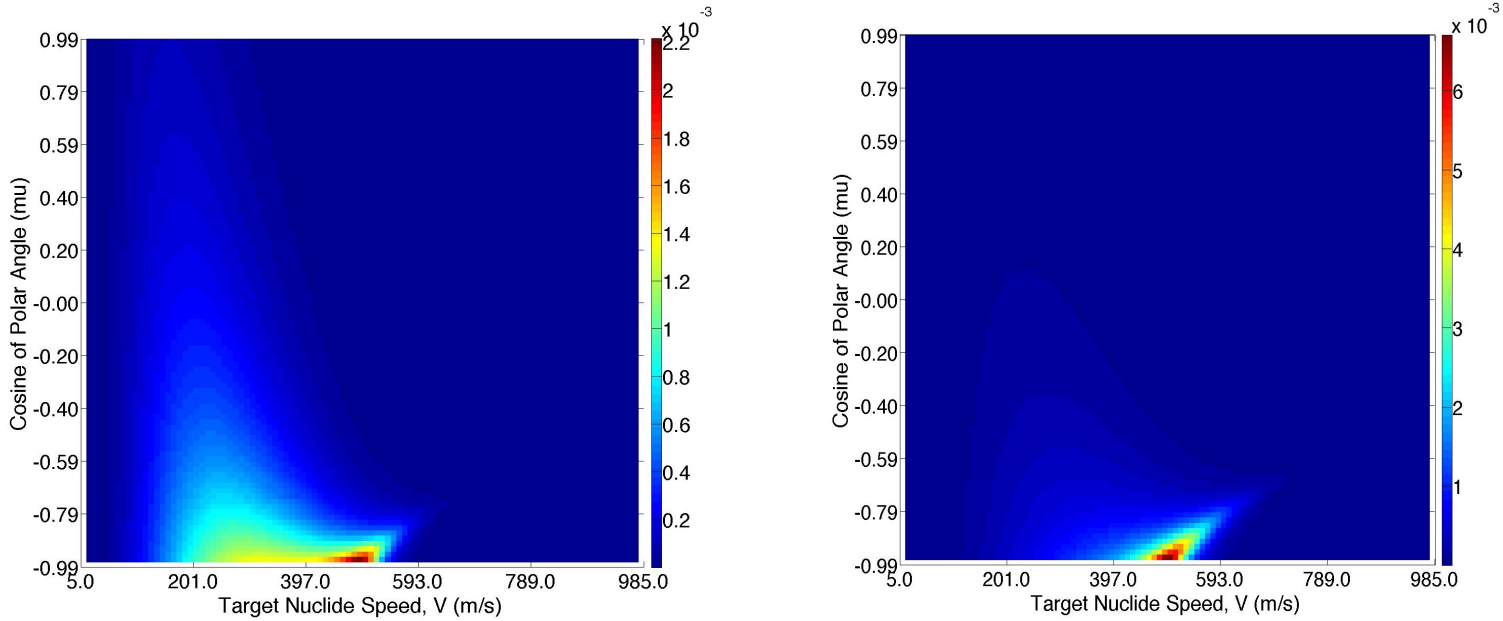

(a) (b)

Figure 3.6: Bivariate scattering PDFs at (a) 500 K, (b) 750 K (36.25 eV incident neutron energy and ^{238}U at 1000 K)

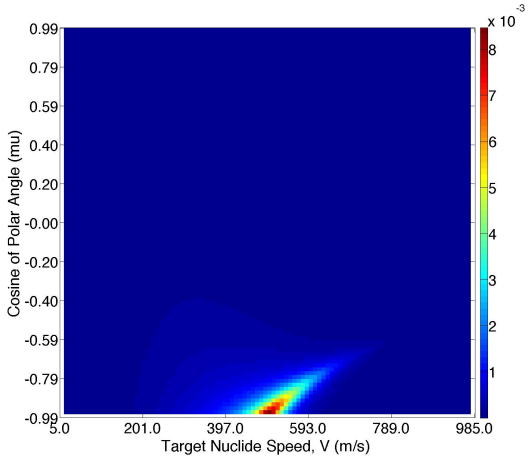

(c)

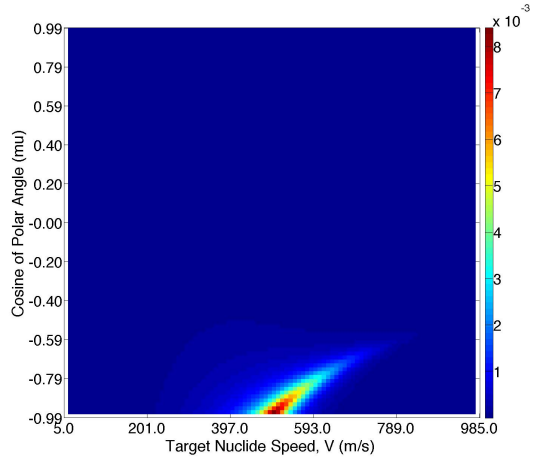

(d)

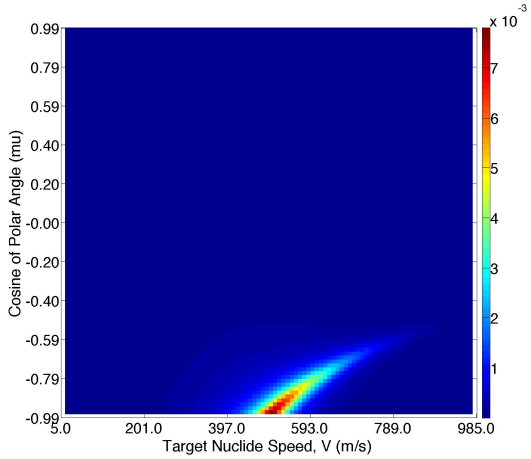

(e)

Figure 3.6: Bivariate scattering PDFs at (c) 1000 K, (d) 1250 K and (e) 1500 K (36.25 eV incident neutron energy and ^{238}U at 1000 K)

3.3.3 Modified free gas scattering algorithm

In the DBRC method, the original free gas algorithm remained intact except for an additional constraint based on scattering cross sections, which are not assumed to be constant. This additional constraint is shown in Eq. (3.5). It is the ratio of the zero Kelvin scattering cross section for the relative neutron speed and the maximum zero Kelvin scattering cross section in a specific energy range, E_ε ,

$$P(V,\mu \mid v)\,dV\,d\mu = \frac{1}{\sigma_{eff,s}(v)}\begin{bmatrix} 4\pi\left(\frac{\alpha}{\pi}\right)^{3/2} vV^2 e^{-\alpha V^2}\,dV\,\frac{d\mu}{2} + \ldots \\ \\ \ldots 4\pi\left(\frac{\alpha}{\pi}\right)^{3/2} V^3 e^{-\alpha V^2}\,dV\,\frac{d\mu}{2} \end{bmatrix}\left(\frac{|\mathbf{v}-\mathbf{V}|}{v+V}\right)\left(\frac{\sigma(E_r,0)}{\sigma_{\max}(E_{\Delta E},0)}\right). \tag{3.5}$$

E_r is the relative neutron energy and $E_{\Delta E}$ is the energy range in which the maximum scattering cross section is determined. ΔE is a dimensionless quantity that equates to $\sqrt{AE/kT}$, and ranges from ± 4.0 , where E is the incident neutron energy. This energy range was chosen to perform the rejection test because the tails of the scattering distribution are expected to become very small, and approach zero.

The following steps establish the energy interval, $E_{\Delta E}$:

$$\sqrt{\frac{AE}{kT}} + 4 = \sqrt{\frac{AE_{\max}}{kT}},$$

$$E_{\max} = \frac{kT}{A}\left(\sqrt{\frac{AE}{kT}} + 4\right)^2. \tag{3.6}$$

And,

$$\sqrt{\frac{AE}{kT}} - 4 = \sqrt{\frac{AE_{\min}}{kT}},$$

$$E_{\min} = \frac{kT}{A}\left(\sqrt{\frac{AE}{kT}} - 4\right)^2. \tag{3.7}$$

Here,

$$E_{\Delta E} = E_{\max} - E_{\min} \,. \tag{3.8}$$

After converting Eqs. (3.6) and (3.7) into units of neutron speed (m/s), the rejection bounds are,

$$v_{\max} = v + 4\sqrt{\frac{2kT}{Am}}, \tag{3.9}$$

and,

$$v_{\min} = v - 4\sqrt{\frac{2kT}{Am}}. \tag{3.10}$$

Here, v is the incident neutron speed, k is the Boltzmann constant, T is the temperature of the target nuclide, A is the atomic mass number for the target nucleus and m is the neutron mass.

Eq. (3.5) can be rewritten in the following form:

$$P\left(V,\mu \mid v\right) dV\, d\mu = C \cdot \left[P_1 \cdot f_1(V) dV \;\; + \;\; P_2 \cdot f_2(V) dV\right] \cdot \frac{d\mu}{2} \cdot \frac{|\mathbf{v} - \mathbf{V}|}{v + V} \frac{\sigma_s\left(v_r\right)}{\sigma_{s,\max}\left(v_{\Delta v}\right)}, \tag{3.11}$$

where $P_1 = \dfrac{v}{v + 2/\sqrt{\pi\alpha}}$, $\qquad P_2 = 1 - P_1$,

$f_1(V) = 4\sqrt{\frac{\alpha^3}{\pi}} V^2 e^{-\alpha V^2}$, $\qquad f_2(V) = 2\alpha^2 V^3 e^{-\alpha V^2}$,

$C = \sigma_s / \sigma_{eff,s}(v)$.

The modified algorithm consists of adding an additional rejection in the original Step 3 in Section 3.3.1.

Step 1: Choose a random number, ξ_1, and test P_1 against ξ_1.

a. If $\xi_1 < P_1$, choose target speed from $4\left(\frac{\alpha}{\pi}\right)^{3/2} V^2 e^{-\alpha V^2}$ where $V \in [0,\infty]$, and

$$V = \sqrt{-\frac{1}{\alpha}\left(\ln \xi_a + \ln \xi_b \cos^2\left(\frac{\pi}{2}\xi_c\right)\right)}.$$

b. Else, choose target speed from $2\alpha^2 V^3 e^{-\alpha V^2}$ where $V \in [0,\infty]$, and

$$V = \sqrt{-\frac{1}{\alpha}\ln\left(\xi_a \xi_b\right)}.$$

Step 2: Once the target speed has been selected, choose the cosine of polar angle, μ, of approach between the neutron and the target in the center of mass frame from an isotropic distribution, $\frac{d\mu}{2}$ where $\mu \in [-1,1]$ and $\mu = 2\xi - 1$.

Step 3: Choose a random number, ξ_2, and test $\frac{|\mathbf{v}-\mathbf{V}|}{v+V}$ against ξ_2.

a. If $\xi_2 > \frac{|\mathbf{v}-\mathbf{V}|}{v+V}$, reject all scattering parameters and restart from Step 1.

b. Else, choose a random number, ξ_3, and test $\frac{\sigma_s(v_r)}{\sigma_{s,\max}(v_\varepsilon)}$ against ξ_3.

c. If $\xi_3 < \frac{\sigma_s(v_r)}{\sigma_{s,\max}(v_\varepsilon)}$ accept the scattering parameters: target speed, V, and cosine of polar angle of incidence, μ, of the neutron in the COM frame.

i. Determine the cosine of polar angle, and the azimuthal angle for the exiting neutron in the laboratory frame.

ii. Calculate the final exiting neutron speed in the laboratory frame.

d. Else, reject the scattering parameters and repeat from Step 1 until Step 3c is been achieved.

After the target nuclide speed and cosine of polar angle are selected and the two variables have passed the first rejection test, the samples are not yet accepted, as they

would be in the original free gas scattering algorithm. Instead, the sampled scattering parameters have to pass the second rejection test in order to be accepted.

3.3.4 Comparison of scattering models

A research Monte Carlo code with different scattering models was set up to compare the differences in the differential scattering kernel. In Chapter 2, the results from the original free gas model have already been compared to DBRC and the asymptotic scattering model for 6.52 incident neutron energy just below the 6.67 eV resonance. In this section, the differences in the scattering models at neutron energies above and below the 6.67 eV resonance will be analyzed at 300 K and 1000 K. The reference case is DBRC, which is considered to give us the true differential scattering PDF.

In Figures 3.7 – 3.10, the blue line represents the original free gas scattering model, the black line represents DBRC, which accounts for resonance scattering effects, and the green line represents the asymptotic scattering model where the target is assumed to be at rest. The red line indicates the incident neutron energy. Data points to the left of the red line indicates downscatter after one collision and all data points to the right show upscatter after one collision with the target nuclide.

Figures 3.7 and 3.8 show the differences in differential scattering PDF between the scattering models for 6.52 eV incident neutron energy slightly below the resonance peak energy. They illustrate the significantly higher neutron upscattering at 300 K and 1000 K with DBRC. The asymptotic scattering model does not show any neutron upscatter because target-at-rest kinematics was used. These figures indicate that for neutron energies slightly below the resonance, it is important to account for the resonance in the scattering model.

The next step was to evaluate the differences in the scattering models for 7.2 eV incident neutron energy, slightly above the resonance. The results for this case are shown in Figures 3.9 and 3.10.

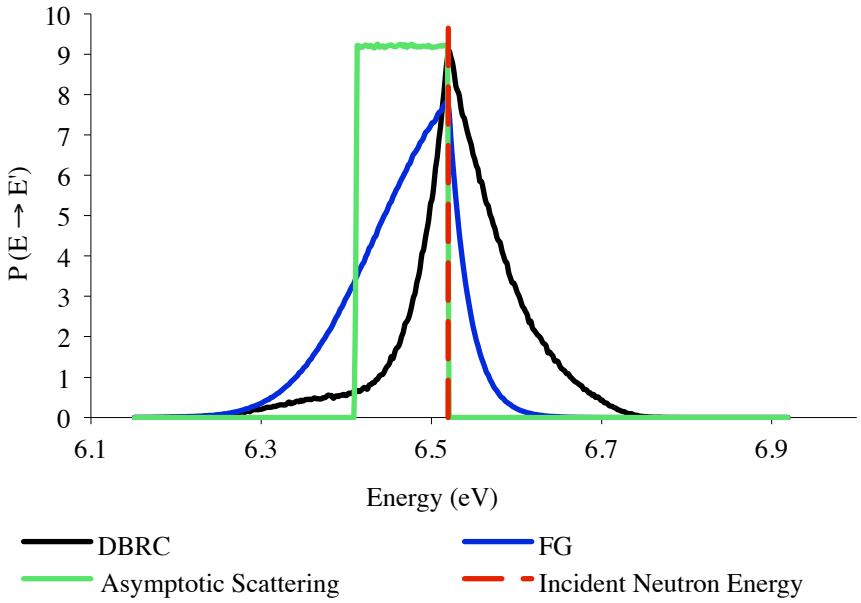

Figure 3.7: Incident neutron energy of 6.52 eV and ^{238}U at 300 K

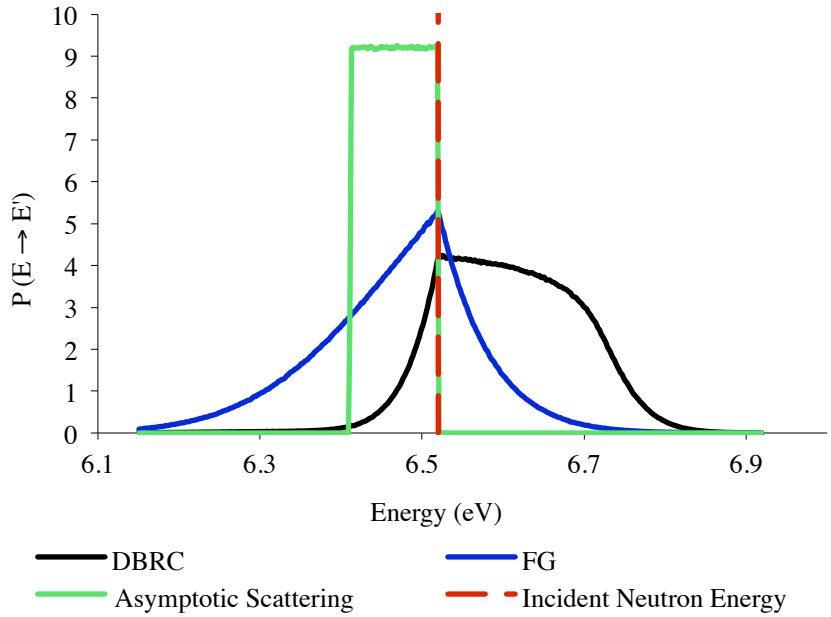

Figure 3.8: Incident neutron energy of 6.52 eV and ^{238}U at 1000 K

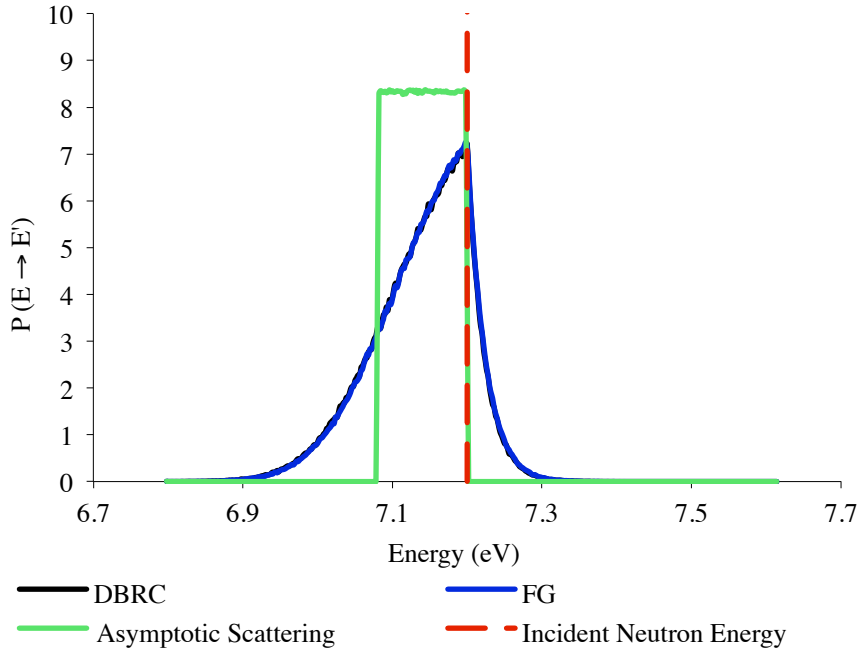

Figure 3.9: Incident neutron energy of 7.2 eV and ^{238}U at 300 K

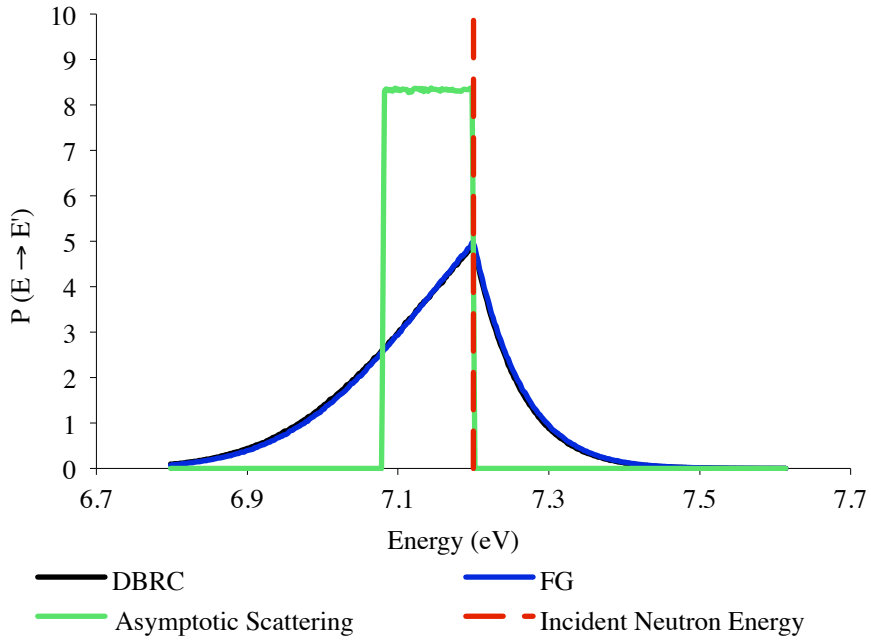

Figure 3.10: Incident neutron energy of 7.2 eV and ^{238}U at 1000 K

The asymptotic scattering model once again does not show any neutron upscattering. However, the free gas scattering model and DBRC provide similar results,

which shows that it is not important to implement an expensive method that accounts for resonance scattering for the entire epithermal range. It is important, however, to identify the energy ranges relevant to resonance elastic scattering.

The next step was to implement DBRC into MCNP5 so that it provided a reliable benchmark for an alternative on-the-fly resonance scattering method developed for this thesis work.

3.4 MCNP5 with DBRC

A separate module was created to contain all the calculations required to make the scattering decision regarding the target nuclide speed and the cosine of the polar angle between the neutron and target. This module contains a function that determines the decision of the second rejection test using a subroutine that reads in all the 0 K scattering cross section values for ^{238}U. It also contains subroutines that use the target speed and cosine of polar angle selected in tgtvel.F90 to determine the incident neutron energy range, $E_{\Delta E}$, that needs to be considered. Next, the corresponding maximum cross section value within this energy range, and the scattering cross section for the relative neutron speed are determined and then used to decide the second rejection test. The upper energy limit that activates the use of free gas scattering kernel was set in colidn.F90 at 210 eV as recommended by B. Becker in his thesis [11].

3.4.1 Temperature effects on differential scattering kernel

The scattering kernel is a function of temperature and upscattering percentages increase as the temperature of the target material increases. Figure 3.11 shows how the differential scattering kernel changes with temperature.

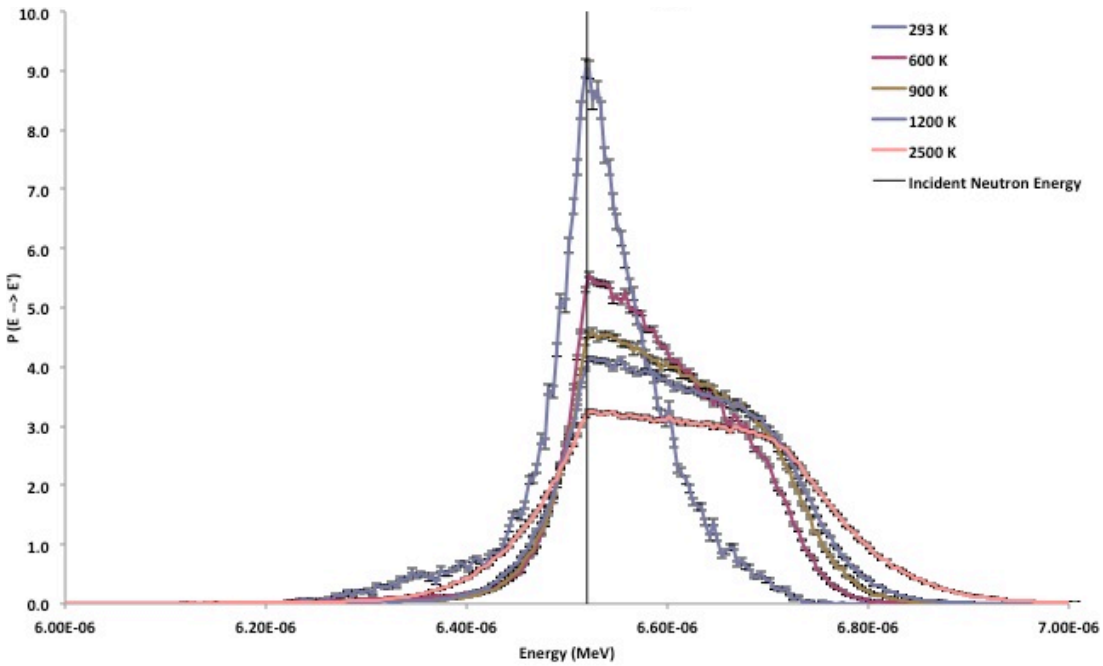

Figure 3.11: Scattering kernel for ^{238}U at varying temperatures for incident neutron energy of 6.52 eV

For benchmarking, the upscattering percentages were calculated for specific incident neutron energies around low-lying resonances in ^{238}U and these values were compared to values obtained by Ouisloumen *et. al.* [3] and D. Lee *et. al.* [6]. Table 3-1 shows the comparison between upscatter percentages from the different resonance scattering treatments.

Table 3-1: Upscatter percentages for varying incident neutron energies for ^{238}U at 1000 K

Resonance (eV)	**Neutron Energy (eV)**	**Ouisloumen *et. al.* Results [3]**	**D. Lee *et. al.* Results [6] (1 σ std. dev)**	**Modified MCNP5 Results (1 σ std. dev)**
6.67	6.52	82.03	83.40 (0.04)	83.64 (0.19)
	7.20	28.12	28.20 (0.01)	28.03 (0.05)
36.67	36.25	54.23	55.28 (0.06)	53.69 (0.01)
	37.20	7.95	7.26 (0.01)	7.72 (0.02)

The results showed that the upscattering percentages from modified MCNP5 compared very well with results obtained through different methods developed by Ouisloumen *et. al.* [3] and D. Lee *et. al* [6]. The broadening of these scattering PDFs as a function of

temperatures also showed why resonances in the epithermal region have more of an effect on High Temperatures Reactors (HTRs).

3.4.2 Mosteller benchmark problem

The Mosteller benchmark problem [12], [13] for an LWR pin cell with UO_2 fuel was chosen to benchmark MCNP5 results with resonance scattering to the results published in [6] and [9]. ENDF/B-VII.0 cross sections were used for this calculation, and zirconium isotope abundances for natural zirconium were obtained from NIST [14] and used as weight fractions for pure zirconium in the benchmark problem. The values obtained from NIST are presented in Table 3-2.

Table 3-2: Natural Zirconium isotope abundances [14]

	Abundance (%)
Zr-90	51.45
Zr-91	11.22
Zr-92	17.15
Zr-94	17.38
Zr-96	2.8

The MCNP5 setup in Figure 3.12 shows the LWR pin cell that was modeled in Mosteller benchmark problems.

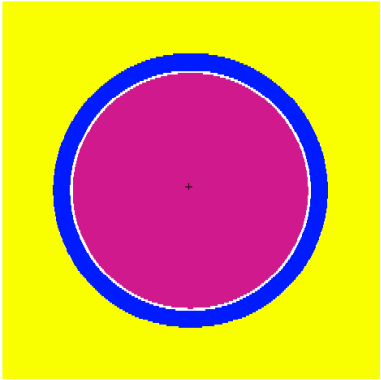

Figure 3.12: LWR pin cell in Mosteller benchmark [12]

In order to calculate the Fuel Temperature Coefficient (FTC), two sets of calculations were performed in MCNP5. The first was at Hot Zero Power (HZP) conditions where the fuel, cladding and moderator were set to a temperature of 600 K.

The second set of calculations were done under Hot Full Power (HFP) conditions where the fuel temperature was set at 900 K and the cladding and moderator temperatures were set to 600 K.

FTC was calculated using Eq (3.12),

$$FTC = \left(\frac{1}{k_{HZP}} - \frac{1}{k_{HFP}} \right) \times \frac{10^5}{\Delta T}, \tag{3.12}$$

where ΔT is 300K.

MCNP5 results with free gas scattering are presented in Table 3-3. The results obtained from this benchmark exercise for 0.711 wt%, 1.6 wt% and 5.0 wt% cases were within one standard deviation of the corresponding results presented in [9] except for the 3.1 wt% case. For this case, the result was just slightly higher than two standard deviations.

Table 3-3: MCNP5 k_{eff} results with constant free gas scattering

wt%	k_{eff} at HZP			k_{eff} at HFP			FTC (pcm/K)		
0.711	0.66569	±	0.00019	0.65987	±	0.00020	-4.42	±	0.21
1.6	0.96124	±	0.00026	0.95295	±	0.00025	-3.02	±	0.13
2.4	1.09913	±	0.00026	1.08986	±	0.00029	-2.58	±	0.11
3.1	1.17657	±	0.00030	1.16777	±	0.00027	-2.13	±	0.10
3.9	1.23944	±	0.00028	1.23009	±	0.00027	-2.04	±	0.09
4.5	1.27495	±	0.00032	1.26542	±	0.00027	-1.97	±	0.09
5.0	1.29920	±	0.00034	1.28911	±	0.00029	-2.01	±	0.09

Table 3-4 shows results obtained when resonance free gas scattering was taken into account. The FTC decreased after resonance scattering was taken into account. FTC for 4.5 wt% ^{235}U looks slightly higher than those at 3.9 wt% and 5.0 wt% due to statistical fluctuations. An independent check on the FTC was conducted using the same code and the values for FTCs were comparable to results presented in [9] and [10]. This led to the conclusion that the FTCs oscillate due to statistical fluctuations unavoidable in Monte Carlo methods and as the number of particles and cycles were increased, the FTCs became more stable.

The results for 0.711 wt%, 1.6 wt%, 3.1 wt% and 5.0 wt% cases in Table 3-3 were within one standard deviation of the results presented in [9]. For all the cases

presented in Table 3-3, most of them were within two standard deviations of the results presented in [10], except for three cases, 3.1 wt%, 3.9 wt%, and 5.0 wt%, which were slightly above two standard deviations. The results presented in [9] and [10] were obtained using different Monte Carlo techniques than those used to generate the results in Tables 3-3 and 3-4. Therefore, the results from MCNP5 with DBRC compared very well other resonance scattering treatments presented in [9] and [10].

Table 3-4: MCNP5 k_{eff} results with resonance free gas scattering

wt%	k_{eff} at HZP			k_{eff} at HFP			FTC (pcm/K)		
0.711	0.66541	±	0.00022	0.65909	±	0.00020	-4.80	±	0.23
1.6	0.96044	±	0.00026	0.95142	±	0.00022	-3.29	±	0.12
2.4	1.09889	±	0.00027	1.08877	±	0.00029	-2.82	±	0.11
3.1	1.17613	±	0.00026	1.16563	±	0.00028	-2.55	±	0.09
3.9	1.23924	±	0.00029	1.22866	±	0.00030	-2.32	±	0.09
4.5	1.27460	±	0.00025	1.26271	±	0.00031	-2.46	±	0.08
5.0	1.29860	±	0.00029	1.28748	±	0.00030	-2.22	±	0.08

The results show that FTCs decreased as expected when resonance free gas scattering was taken into account. Figure 3.13 illustrates the difference in FTCs computed in MCNP5 with constant and resonance free gas scattering models. The figure depicts the negative shift in FTC because of resonance scattering.

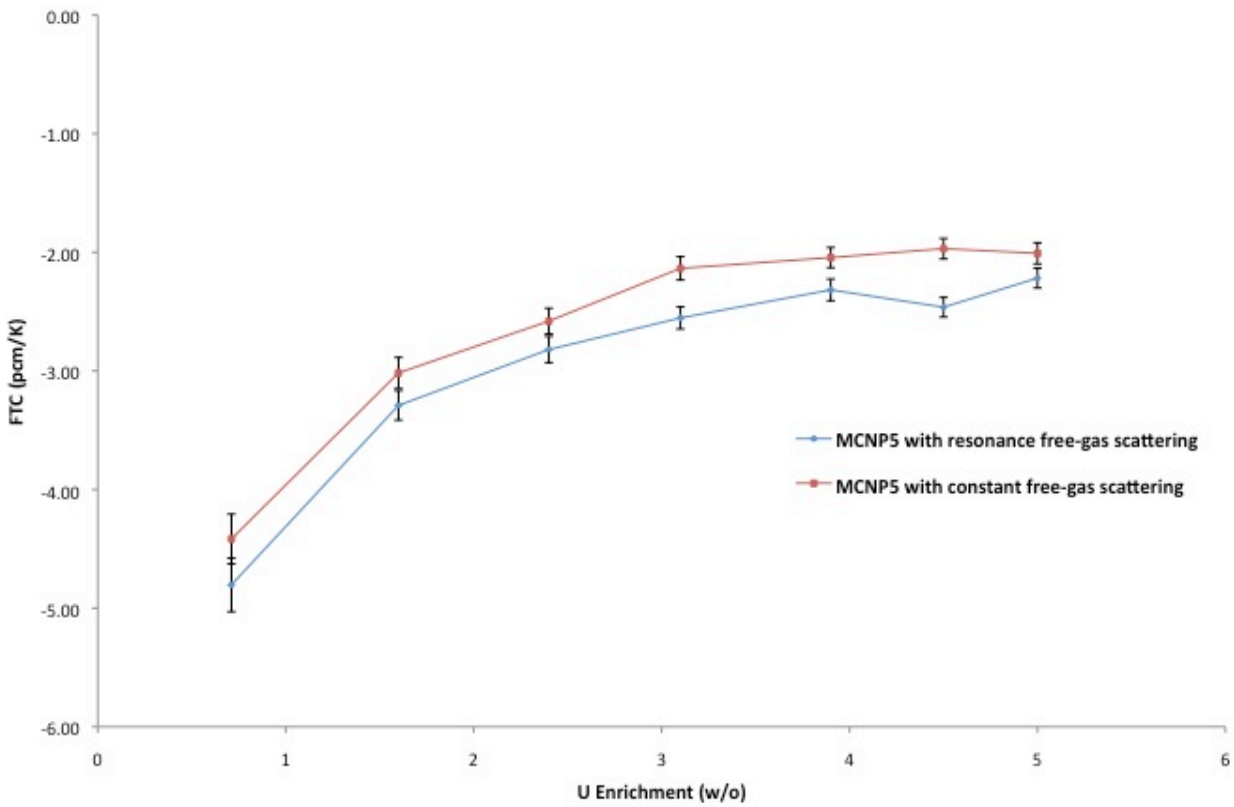

Figure 3.13: FTCs for UO_2 pin cell

Table 3-5 shows that the difference in k_{eff} increases with fuel temperature due to resonance scattering. The difference is on the order of several hundred pcm for LWR pin cell calculations at full power. This clearly shows that resonance scattering cannot be ignored in full power reactor calculations for LWRs and VHTRs.

Table 3-5: Difference in k_{eff} due to resonance free gas scattering

wt%	HZP (pcm)			HFP (pcm)		
0.711	-28	±	29	-78	±	28
1.6	-80	±	37	-153	±	33
2.4	-24	±	37	-109	±	41
3.1	-44	±	40	-214	±	39
3.9	-20	±	40	-143	±	40
4.5	-35	±	41	-271	±	41
5.0	-60	±	45	-163	±	42

3.4.2.1 Computational time study

A study on computational time was conducted for criticality calculations with resonance scattering in free gas for energies below 210 eV. The time it takes to run these criticality problems increased with the temperature of the fuel. Table 3-6 indicates a greater than 10% increase in computational time for HFP cases and about 6 – 9 % increase in computational time for HZP cases.

Table 3-6: Time difference (%) between standard and modified MCNP5

	TIME DIFFERENCE (%)	
wt%	**HZP**	**HFP**
0.711	7	11
3.1	9	13
5.0	6	12

3.4.3 Energy limits for resonance free gas scattering

A study was conducted on FTC behavior when changing the upper energy limit at which resonance free gas scattering is invoked. The results from this parametric study on varying energy limits for free gas scattering are presented in Table 3-7.

Table 3-7: FTCs due to varying energy limits for resonance free gas scattering

Energy Limit	**0.711 wt% FTC (pcm/K)**	**3.1 wt% FTC (pcm/K)**	**5.0 wt% FTC (pcm/K)**
50	-5.11 ± 0.22	-2.60 ± 0.10	-2.20 ± 0.08
90	-4.88 ± 0.20	-2.60 ± 0.09	-2.34 ± 0.08
150	-4.90 ± 0.20	-2.72 ± 0.09	-2.28 ± 0.08
210	-4.80 ± 0.23	-2.55 ± 0.09	-2.22 ± 0.08
250	-4.91 ± 0.21	-2.67 ± 0.10	-2.26 ± 0.09
500	-4.66 ± 0.21	-2.62 ± 0.11	-2.23 ± 0.08
1000	-4.90 ± 0.20	-2.57 ± 0.10	-2.29 ± 0.08

The results show that FTCs oscillate around similar values after the upper energy limit was set above 50 eV. However, for 500 eV, FTC for 0.711 wt% U was slightly lower than other cases. This value is reasonable because it is within two standard deviations of the corresponding results above the 50 eV upper limit. The results suggest that there is no need to invoke the modified free gas scattering kernel above 90 eV for ^{238}U when analyzing FTCs. These upper limits will be different for other nuclides since the number

of resonances and peak energies of resonances will be different in the low-lying epithermal range. As a result, neutron upscattering percentages will vary accordingly.

3.5 Conclusion

The DBRC method developed by Becker *et. al.* [5] was correctly implemented in MCNP5-1.60. Criticality calculations using the modified resonance free gas scattering model at room temperature does not indicate significant upscattering effects. Criticality studies on LWR pin cells using the modified resonance free gas scattering model showed that k_{eff} does not change considerably in LWRs unless full power criticality studies are being performed. Resonance scattering is expected to affect criticality and safety studies for only very specific problems, namely those that involve high-temperature calculations. HFP and HZP temperature conditions in a VHTR are much higher than those for LWRs, and as a result, criticality and safety studies using elastic scattering resonances in the free gas scattering kernel are expected to affect VHTR criticality analysis more so than LWR criticality and safety studies. Studies by D. Lee *et. al.* [6] showed k_{eff} reduction on the order of 400 pcm in VHTRs when accounting for resonance scattering effects. Parameter studies in this chapter showed that there is no need to invoke the modified free gas scattering kernel above 90 eV neutron energies in ^{238}U when analyzing FTCs, and this limit can vary depending on the target nuclide. In the next chapter, we will focus on an alternative scattering model to account for resonance scattering in an efficient and accurate way during the random walk of the neutrons, effectively yielding an "on-the-fly" generation of the Doppler-broadened differential scattering cross section.

3.6 References

[1] R. R. Coveyou, R. R. Bate and R. K. Osborn, *Effect of Moderator Temperature Upon Neutron Flux In Infinite, Capturing Medium*, Journal of Nuclear Energy, **2**, pp. 153-167 (1956).

[2] X-5 Monte Carlo Team, *MCNP – A General Monte Carlo N-Particle Transport Code, Version 5, Volume I: Overview and Theory*, LA-UR-03-1987, Los Alamos National Laboratory (2003).

[3] M. Ouisloumen and R. Sanchez, *A Model for Neutron Scattering Off Heavy Isotopes That Accounts for Thermal Agitation Effects*, Nuclear Science and Engineering, **107**, pp. 189-200 (1991).

[4] W. Rothenstein and R. Dagan, *Ideal gas scattering kernel for energy dependent cross section*, Annals of Nuclear Energy, **25**, pp. 209 – 222 (1998).

[5] B. Becker, R. Dagan and G. Lohnert, *Proof and implementation of the stochastic formula for ideal gas, energy dependent scattering kernel*, Annals of Nuclear Energy, **36**, pp. 470 – 474 (2009).

[6] D. Lee, K. Smith and J. Rhodes, *The impact of ^{238}U resonance elastic scattering approximations on thermal reactor Doppler reactivity*, Annals of Nuclear Energy, **36**, pp. 274-280 (2009).

[7] G. J. Marchuk, V. G. Turchin, V. N. Smelov and G. A. Il'yasova, *Proceedings from Brookhaven Conference on Neutron Thermalization*, II, pp. 706 (1962).

[8] G. L. Blackshaw and R. L. Murray, *Scattering Functions for Low-Energy Neutron Collisions in a Maxwellian Monatomic Gas*, Nuclear Science and Engineering, **27**, pp. 520-532 (1967).

[9] T. Mori and Y. Nagaya, *Comparison of Resonance Elastic Scattering Models Newly Implemented in MVP Continuous-Energy Monte Carlo Code*, Journal of Nuclear Science and Technology, Vol 46, No. 8, pp. 793-798 (2009).

[10] D. Lee, K. Smith and J. Rhodes, *The impact of ^{238}U resonance elastic scattering approximations on LWR Doppler reactivity*, International Conference on Reactor Physics, Interlaken, Switzerland (2008).

[11] B. Becker, *On the Influence of the Resonance Scattering Treatment in Monte Carlo Codes on High Temperature Reactor Characteristics*, Thesis, Institut fur Kernenergetik und Energiesysteme, Germany (2010).

[12] R. D. Mosteller, *Computational Benchmarks for the Doppler Reactivity Defect*, LA-UR-06-2968, Los Alamos National Laboratory.

[13] R. D. Mosteller, *ENDF/B-V, ENDF/B-VI, and ENDF/B-VII.0 Results for the Doppler-defect Benchmark*, Proceedings from M&C+SNA, Monterey, CA (2007).

[14] National Institute of Standards and Technology, *Atomic Data for Zirconium (Zr)*, Handbook of Basic Atomic Spectroscopic Data – online version (2011).

CHAPTER 4

Legendre Moments Of The Differential Scattering Probability Distribution Function

4.1 Introduction

In Chapter 3, the discretized bivariate probability distribution functions (PDFs) showed that the scattering probability is very close to zero for most of the target speeds and polar angle cosines. A rejection method would be slow, since choosing target speed and a polar angle cosine from all ranges that passed the rejection test was cumbersome. For the purpose of this dissertation, we decided to focus on a method that would enable us to go directly from incident neutron energy in the laboratory frame to calculating the outgoing neutron energy in the laboratory frame. For this reason, we looked at the moments of the differential scattering PDF that would allow us to predict the exiting conditions of the neutron in the laboratory frame. There are several methods that focus on the moments of the differential scattering PDF, but they all use the exact scattering cross sections. We focused our efforts on the development of a method that would allow us to store coefficients or shape functions, which we can use to generate the moments on-the-fly for use in Monte Carlo codes. The true moments were generated using Doppler Broadened Rejection Correction (DBRC) method from a research Monte Carlo code that can be compared with the numerical results of the moments that are generated on-the-fly. The process behind the generation of these moments with DBRC as well as the equations and processes behind the new method to generate these moments, will be explained in this chapter.

4.2 Generating moments using DBRC

Legendre moments of the differential scattering PDF had to be extracted from the modified free gas scattering model with DBRC in order to check the accuracy of the

method that was developed for this dissertation. The moments of the differential scattering PDF were found using the following relation:

$$P_n\left(v \to v'\right) = \sum_{j>0} P\left(v \to v', \mu_{lab,j}\right) P_n\left(\mu_{lab,j}\right) \tag{4.1}$$

where, j represents the discretized bins for the cosine of polar angle between the incoming and outgoing neutron velocities in the laboratory frame and $P_n\left(\mu_{lab,j}\right)$ is the nth Legendre polynomial. The first six Legendre polynomials are shown below:

$$P_0\left(\mu_{lab,j}\right) = 1,$$

$$P_1\left(\mu_{lab,j}\right) = \mu_{lab,j},$$

$$P_2\left(\mu_{lab,j}\right) = \frac{3\mu_{lab,j}^2 - 1}{2},$$

$$P_3\left(\mu_{lab,j}\right) = \frac{5\mu_{lab,j}^3 - 3\mu_{lab,j}}{2},$$

$$P_4\left(\mu_{lab,j}\right) = \frac{35\mu_{lab,j}^4 - 30\mu_{lab,j}^2 + 3}{8},$$

$$P_5\left(\mu_{lab,j}\right) = \frac{63\mu_{lab,j}^5 - 70\mu_{lab,j}^3 + 15\mu_{lab,j}}{8}.$$

The cosine of polar angle in laboratory frame, μ_{lab}, can be determined by using the following equation, derived in Appendix A [1]:

$$\mu_{lab} = \cos\theta = \cos\alpha\cos\beta + \sin\alpha\sin\beta\cos\varphi.$$

where θ is the angle between the incoming and outgoing neutron velocities in the laboratory frame, β is the angle between the center-of-mass velocity and the incident neutron velocity in laboratory frame, α is the angle between the center-of-mass velocity

and the outgoing neutron velocity in the laboratory frame, and φ is the azimuthal angle in the laboratory frame.

With this information, the true differential scattering PDF, $P\left(v \rightarrow v', \mu_{lab,j}\right)$, was constructed using DBRC in Monte Carlo. The Legendre expansions were applied for the moments of interest to solve for $P\left(v \rightarrow v'\right)$. The six Legendre moments of the differential scattering PDF obtained from the research Monte Carlo code are presented in Figure 4.1. They compared very well to the Legendre moments of the PDF presented in [2] and provided confidence that the moments generated by the research code was correct. These moments were then used for comparison to the moments generated from the alternative on-the-fly scheme developed for this dissertation. It is possible to obtain negative probabilities in PDFs formed from truncated Legendre expansions. Treating this unphysical behavior in Monte Carlo sampling will be discussed at the end of this chapter.

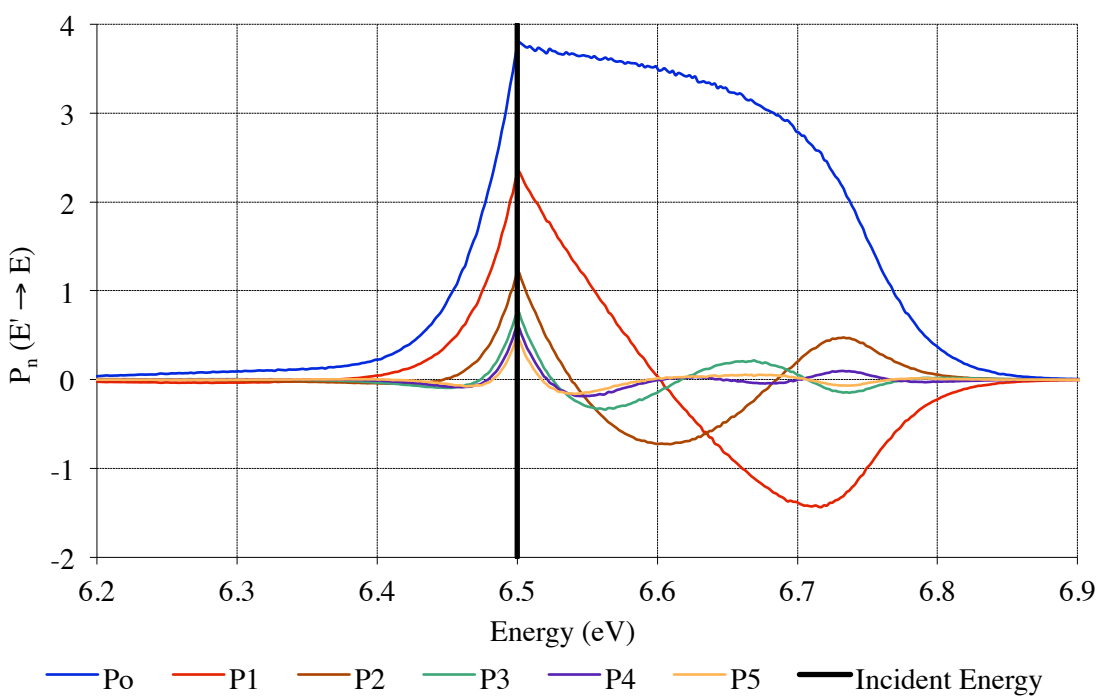

Figure 4.1: Legendre moments of differential scattering PDFs generated with DBRC for incident neutron energy of 6.5 eV scattering in ^{238}U at 1000 K

4.3 Developing an alternative on-the-fly resonance scattering method

There were many researchers who developed equations that calculated moments of the differential scattering PDFs, as discussed in Chapter 3. M. Ouisloumen *et. al.* [3] developed a set of equations that use the exact, tabulated scattering cross sections to generate the moments, and showed numerical results for the P_0 moments of the differential scattering PDFs. Generating these moments on-the-fly during a Monte Carlo simulation can be slow and requires the storage of 0 K cross sections for isotopes of interest. Blackshaw *et. al.* [4] developed a set of equations in the 1960s for the zeroth and first moments of the differential scattering PDF. However, their work has not been implemented anywhere, and numerical results for the equations were not shown for exact cross sections in Blackshaw's dissertation [5]. The equations presented in his dissertation were the starting point for the work described in this section.

In this section, Blackshaw's equations will be reviewed, and these equations for the moments of the differential scattering PDFs were validated for accuracy since numerical results have not been reported. Finally, an approximation to the cross section that will allow us to generate these moments on-the-fly will be presented as well.

4.3.1 P_0 Moment of the differential scattering kernel

Blackshaw's equations are of interest to work in this dissertation because we are forming an approximation for the neutron speed-dependent scattering cross section, which can be used to generate the moments of differential scattering PDF, $P_n\left(v \rightarrow v'\right)$, on-the-fly. These moments can be used to sample the exiting neutron speed and angle without having to go through the cumbersome collision mechanics in the center-of-mass frame and subsequent conversion of scattering parameters from center-of-mass to laboratory frame. Of course, truncated Legendre expansions for the differential scattering cross section will introduce some error in the resultant exiting speed and angles, and this will be assessed later.

Blackshaw [5] derived equations for the moments of the differential scattering distribution for both the downscatter and upscatter of neutrons. It must be noted these distributions are not normalized, hence are not moments of the true PDF. They must be normalized so that the moments of the PDF can be obtained, but this will be discussed in

greater detail later. In [5], Blackshaw presented equations to produce the differential neutron scatter with initial speed, v, into final speed, v', within the laboratory frame. A more in-depth review of the derivation is presented in his dissertation [5].

The moments of the differential scattering distribution can be obtained from the exact differential scattering distribution:

$$K(v,v') = \iiint_{\phi\mu V} v_r \sigma_s(v_r) M(V) P(v,v') dV\, d\mu\, d\phi. \tag{4.2}$$

Here, v_r is the relative speed of the neutron, $\sigma_s(v_r)$ is the zero Kelvin scattering cross section dependent on the relative speed of the neutron, $M(V)$ is the Maxwell-Boltzmann distribution of the target nuclides, and $P(v,v')$ is the probability that a neutron of incident neutron speed, v, will scatter into outgoing speed, v'. The exact differential scattering distribution is obtained after integration over all range of target speeds, the cosine of polar angle between initial neutron velocity and target velocity in the laboratory frame, μ, and azimuthal angle, ϕ.

Eq. 4.2 can be used to represent the moments:

$$K_n(v,v') = \iint_{\phi\mu} P_n(\mu_o) K(v,v') d\mu_o\, d\phi_o, \tag{4.3}$$

where μ_o represents the cosine of polar angle between the initial and final neutron velocities in the laboratory frame, $K_n(v,v')$ is the moment of the exact differential scattering distribution and $P_n(\mu_o)$ is the nth Legendre polynomial.

In [5], Blackshaw manipulates Eqs. (4.2) and (4.3) to derive Eq. (4.4),

$$\begin{aligned} K_0(v,v') = {} & \frac{B^3}{\sqrt{\pi}} \left(\frac{A+1}{A}\right)^2 \frac{v'}{v} \exp\left(\frac{B^2 v^2}{A}\right) \times \ldots \\ & \int_{v_r} v_r \sigma_s(v_r) \exp\left(-\frac{B^2 v_r^2}{A+1}\right) dv_r \int_{v_c} \exp\left(-B^2 \left(\frac{A+1}{A}\right) v_c^2\right) dv_c, \end{aligned} \tag{4.4}$$

where A represents the atomic mass, v_c represents the speed of the center-of-mass in the laboratory frame, v_r is the relative speed of the neutron, B is a constant, M is the target nuclide mass, k is the Boltzmann constant and T is the temperature of the nuclide. Here, $v_c^2 = \frac{v^2 + (AV)^2 + 2AvV\mu}{(A+1)^2}$, $v_r^2 = v^2 + V^2 - 2vV\mu$, and $B^2 = \frac{M}{2kT}$.

After further algebraic manipulations, the P_0 moment of the differential scattering distribution, $K_0(v,v')$, for both, downscattering and upscattering, cases are discussed in the following sections.

4.3.1.1 Downscatter case

The zeroth moment of the differential scattering kernel for downscattering is:

$$K_{0,down}(v,v') = \frac{h^3}{2B}\frac{v'}{v}\exp\left[\frac{B^2v^2}{A}\right]\times\ldots$$

$$\left\{\begin{array}{l} \displaystyle\int_{\frac{h^2(v-v')}{2B^2}}^{\frac{h^2(v+v')}{2B^2}} v_r\sigma_s(v_r)\exp\left(-\frac{B^4v_r^2}{Ah^2}\right)\left[erf\left(hv'+\frac{B^2v_r}{h}\right)-erf\left(hv-\frac{B^2v_r}{h}\right)\right]dv_r + \\ \displaystyle\int_{\frac{h^2(v+v')}{2B^2}}^{\infty} v_r\sigma_s(v_r)\exp\left(-\frac{B^4v_r^2}{Ah^2}\right)\left[erf\left(hv'+\frac{B^2v_r}{h}\right)-erf\left(\frac{B^2v_r}{h}-hv'\right)\right]dv_r \end{array}\right\}, \quad (4.5)$$

where h is a constant, $h^2 = \left(\frac{A+1}{A}\right)B^2$.

4.3.1.2 Upscatter case

A similar equation was found for the upscattering case, when v and v' in the integrand and limits of the integral are interchanged in Eq. (4.5),

$$K_{0,up}\left(v,v'\right)=\frac{h^3}{2B}\frac{v'}{v}\exp\left[\frac{B^2v^2}{A}\right]\times\ldots$$

$$\left\{\begin{array}{l}\displaystyle\int_{\frac{h^2(v'-v)}{2B^2}}^{\frac{h^2(v+v')}{2B^2}} v_r\sigma_s\left(v_r\right)\exp\left(-\frac{B^4v_r^2}{Ah^2}\right)\left[erf\left(hv+\frac{B^2v_r}{h}\right)-erf\left(hv'-\frac{B^2v_r}{h}\right)\right]dv_r+\\ \displaystyle\int_{\frac{h^2(v+v')}{2B^2}}^{\infty} v_r\sigma_s\left(v_r\right)\exp\left(-\frac{B^4v_r^2}{Ah^2}\right)\left[erf\left(hv+\frac{B^2v_r}{h}\right)-erf\left(\frac{B^2v_r}{h}-hv\right)\right]dv_r\end{array}\right\}. \tag{4.6}$$

As discussed earlier, the equations derived by Blackshaw are not moments of the differential scattering PDF since the downscatter and upscatter distributions were not normalized.

4.3.1.3 Normalized general expressions for moments of differential scattering PDFs

General expressions for the normalized distribution for the moments of the differential scattering PDF for both downscattering and upscattering cases are given by,

$$P_{n,\,down}\left(v,v'\right)=\frac{K_{n,\,down}\left(v,v'\right)}{\int_{v'}K_{n,\,down}\left(v,v'\right)dv'+\int_{v'}K_{n,\,up}\left(v,v'\right)dv'},\qquad (v'<v)$$

$$P_{n,\,up}\left(v,v'\right)=\frac{K_{n,\,up}\left(v,v'\right)}{\int_{v'}K_{n,\,down}\left(v,v'\right)dv'+\int_{v'}K_{n,\,up}\left(v,v'\right)dv'},\qquad (v'>v)$$

where n represents the order of the Legendre moments.

4.3.2 Testing Blackshaw's equation

As mentioned earlier, Blackshaw did not provide any numerical results for his equations using actual scattering cross sections. It was important to check if the equations were derived correctly, so that any approximations made to them would also provide the correct solution. It must be noted that the relative neutron speed-dependent cross sections used in the equations are for the 0 K scattering cross sections. We compared the P_0 moment of the differential scattering PDF obtained from Monte Carlo with DBRC to the solution from Blackshaw's equation [5]. To do this comparison, Eqs. (4.5) and (4.6) were integrated numerically and normalized. If the equations are not normalized, then Blackshaw's equations represent just the Legendre moments of a differential scattering distribution and not the differential scattering PDF. The zeroth moment of the differential scattering PDF was generated for the 6.5 eV incident neutron energy, which is slightly lower than the 6.67 eV peak energy of the resonance in ^{238}U. The temperature of ^{238}U was at 1000 K. The results are presented in Figure 4.2. The red line represents the numerically integrated solution of Blackshaw's equations and the dotted black line represents the solution obtained from the research Monte Carlo code with DBRC. The resulting normalized distribution compared very well to the Monte Carlo result giving confidence in Blackshaw's equations and its potential application in Monte Carlo codes.

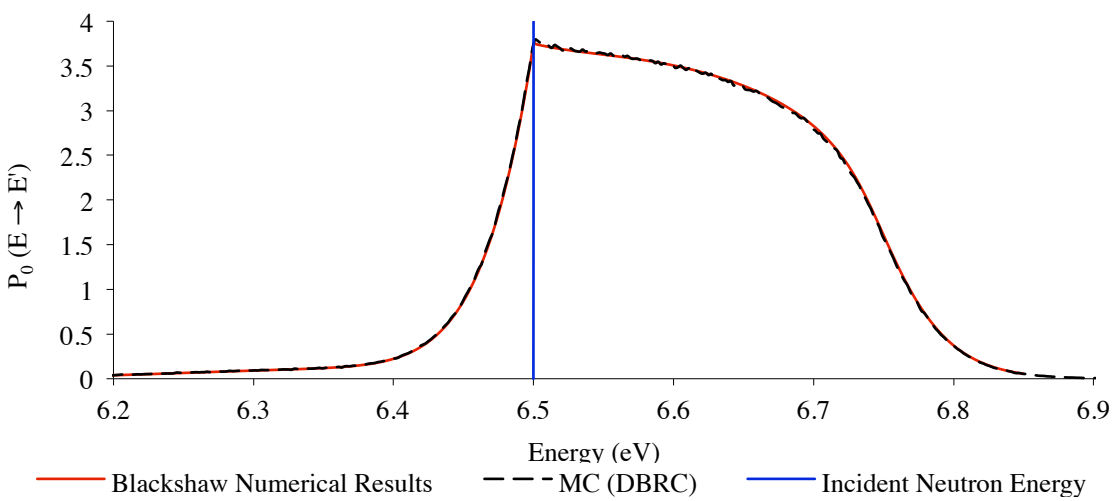

Figure 4.2: Comparison of P_0 moment of differential scattering PDFs from DBRC and Eqs. (4.6) and (4.7) for incident neutron energy of 6.5 eV scattering in ^{238}U at 1000 K

4.3.2.1 Sensitivity study on the integration limits for the moments of the differential scattering kernel

During the numerical integration process, it was noted that the integration steps for the relative speed of the neutron had to be kept very small. Keeping the integration steps really large led to oscillations in the numerical results. Figure 4.3 shows the numerical results for various integration steps of 10, 50, 100 and 200 m/s and these results are compared to P_0 moment obtained from Monte Carlo.

It should also be noted that the original integration limits in Eqs. (4.5) and (4.6) slowed down the numerical integration exceedingly when the steps were only 10 m/s, which consequently led to the adjustment of the integral limit. At first, the lower limit of the first integral term in Eqs. (4.5) and (4.6) was modified to represent the outgoing neutron speed subtracted from the incident neutron speed, $v - v'$, for the downscattering case and vice versa for the upscattering case. The upper limit of the second integral term was modified to represent the sum of the incident neutron speed and the outgoing neutron speed, $v + v'$.

This alteration to the integral limits allowed the numerical integration to be significantly faster. The probability of outgoing neutron energy higher and lower than the modified bounds is significantly smaller for 6.5 eV incident neutron energy, and their contribution to the integral is negligible.

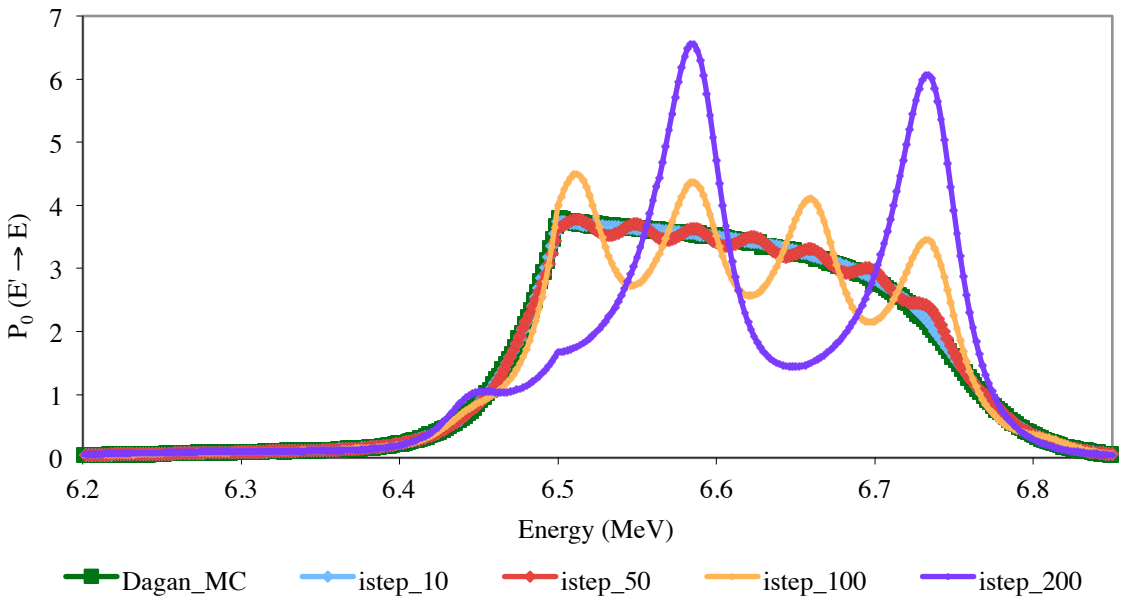

Figure 4.3: Sensitivity study on integration steps for P_0 moment using Eqs. (4.6) and (4.7) in ^{238}U at 1000 K for incident neutron energy of 6.5 eV [Modified limits used]

The green line represents the Monte Carlo results obtained using the DBRC method. The blue line represents the numerical integration results of Eqs. (4.5) and (4.6) which were then normalized for integration steps of 10 m/s. The red line represents the results with steps of 50 m/s, the orange line represents steps of 100 m/s and finally, the purple line represents steps of 200 m/s.

While generating the differential scattering PDFs, the tails of the PDFs were also found to be very close to zero outside the ranges of the limits used to find the maximum scattering cross section in DBRC. These limits were used in DBRC to perform the second rejection test as discussed in Chapter 3, Eqs. (3.9) and (3.10). The lower limit of the first integral in Eqs. (4.5) and (4.6), $\frac{h^2(v-v')}{2B^2}$ and $\frac{h^2(v'-v)}{2B^2}$, were modified to Eq. (3.10) and the upper limit of the second integral, ∞, were modified to Eq. (3.9).

These modified bounds were tested and Figure 4.4 shows the comparison between the results with the original bounds, modified bounds and the Monte Carlo result. The blue line shows results from the normalized numerically integrated Eqs. (4.5) and (4.6) with the original bounds. The red line represents results with modified bounds for the integrals and the green line represents the Monte Carlo results obtained from DBRC.

Both these lines overlap and their results match very closely. This sensitivity study showed that the moments of the differential scattering PDFs could be generated relatively quickly and accurately with the modified bounds used to perform the second rejection test in DBRC.

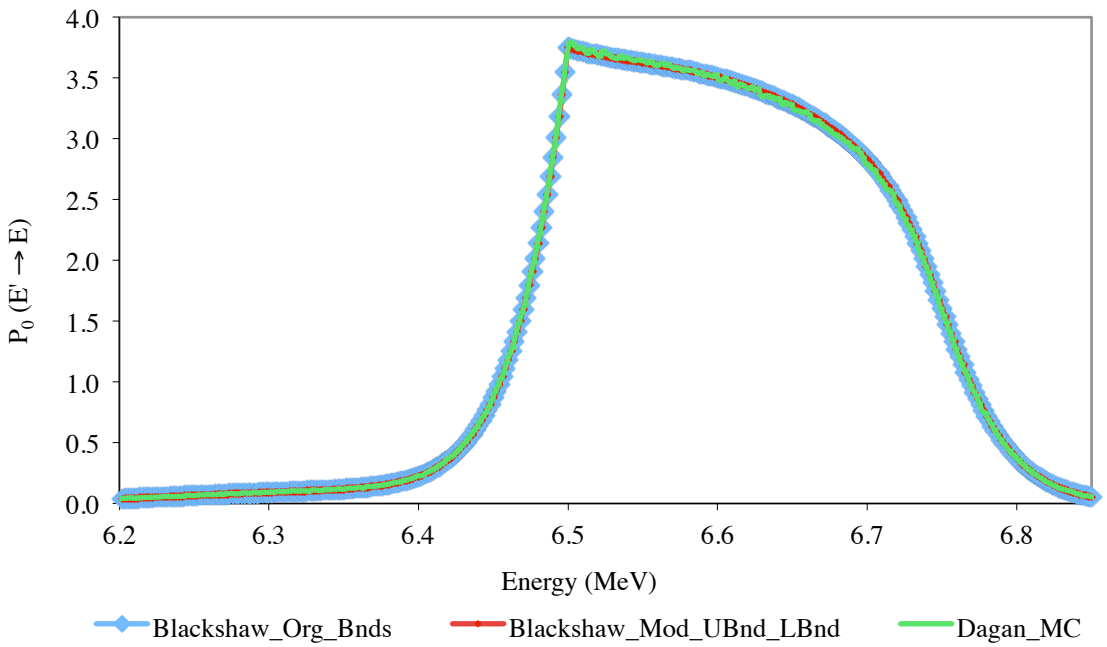

Figure 4.4: Sensitivity study on upper and lower bounds of the integrals for P_0 Moment for ^{238}U at 1000 K and incident neutron energy of 6.5 eV
[Integration steps of 10 m/s]

4.3.2.2 Sensitivity study on P_0 moment for varying incident neutron energies around a resonance

A study was conducted on differences in the differential scattering PDF for varying incident neutron energies around 6.67 eV resonance. These differences were noted between the original free gas scattering kernel in Monte Carlo and the normalized numerically integrated results for P_0 moments of the differential scattering PDFs derived by Blackshaw. In Figures 4.5 and 4.6, the grey line in the background represents the scattering cross section. Figure 4.5 illustrates the differential scattering PDF produced by the original free gas scattering kernel. The figure shows that for neutron energies just below the peak resonance energy, the free gas scattering model does not provide any increase in neutron upscattering.

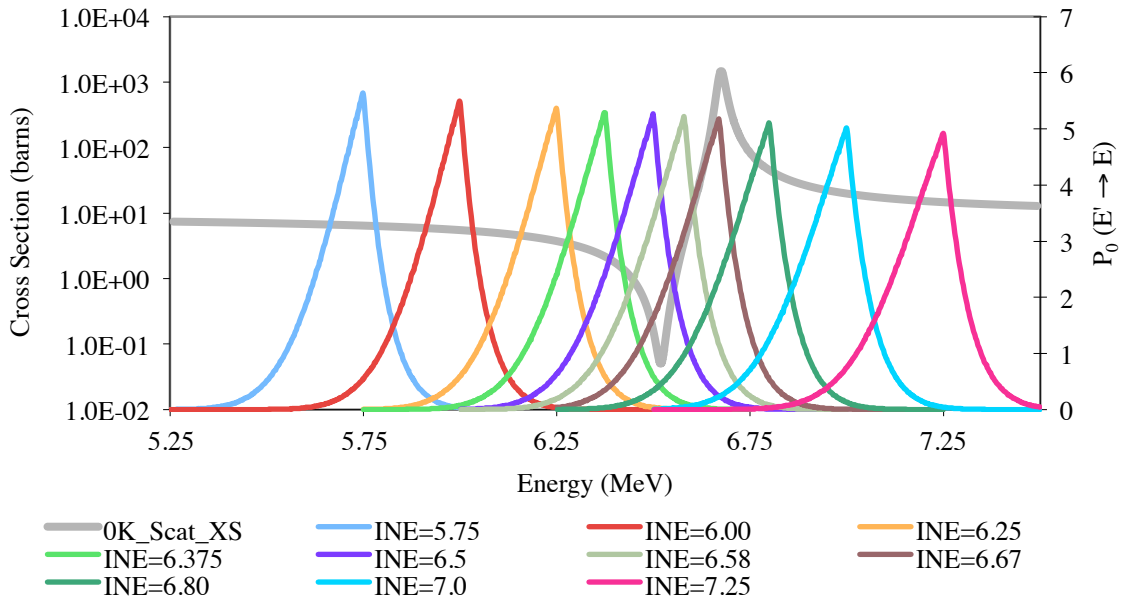

Figure 4.5: Sensitivity study of differential scattering PDF using free gas for varying incident neutron energies in ^{238}U at 1000 K
(INE – Incident Neutron Energy in eV)

Figure 4.6 shows the normalized numerically integrated results from Eqs. (4.5) and (4.6) for the P_0 moment of the differential scattering PDF using the exact scattering cross sections around the resonance. The results, which are synonymous to DBRC results, show increased upscattering for neutron energies slightly below the peak resonance energy. As neutron energies move further away from the resonance peak, the original free gas scattering model is in agreement with the P_0 moment of the differential scattering PDF, which accounts for the resonance.

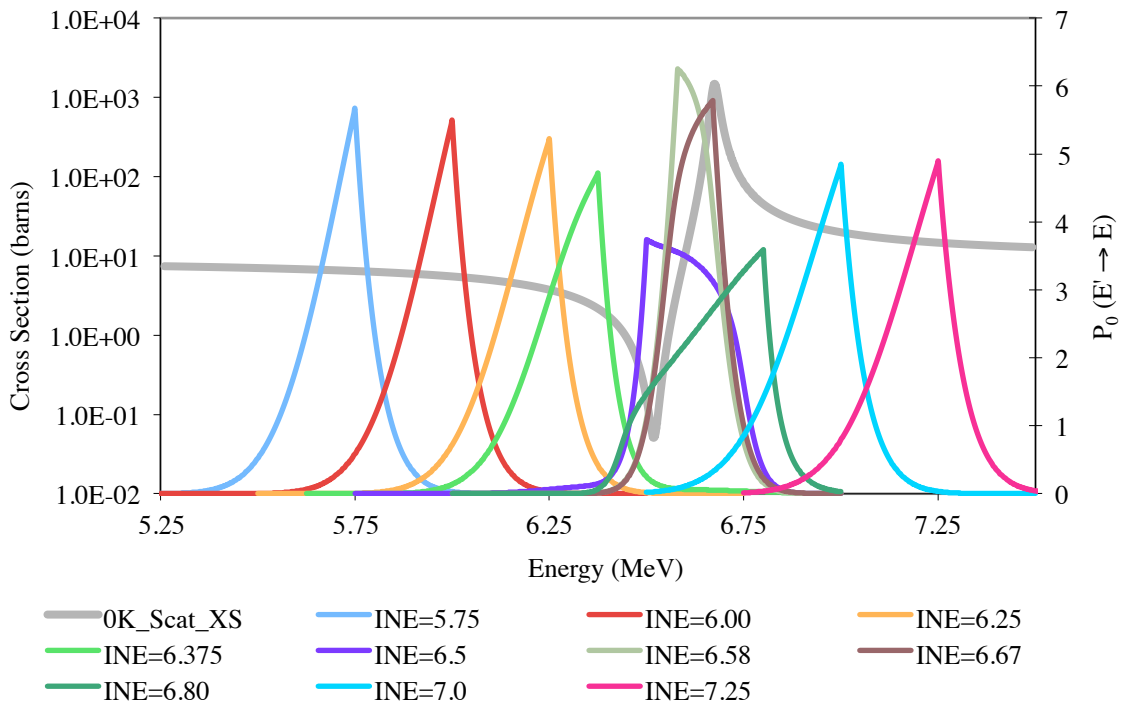

Figure 4.6: Sensitivity study of differential resonance scattering PDF for varying incident neutron energies in ^{238}U at 1000 K
(INE – Incident Neutron Energy in eV)

Figure 4.7 shows the superimposed results from the differential scattering PDFs obtained using the original free gas scattering model and the P_0 moment from Eqs. (4.5) and (4.6). As noted earlier, the plot shows that the differential scattering PDFs obtained from free gas and Eqs. (4.5) and (4.6) which account for the resonance, do not differ significantly from each other until the incident neutron energies are closer to the resonance peak. This suggests that any scattering model that utilizes resonance elastic scattering cross sections does not need to be turned on for the entire epithermal region, but can be set by the user around specific resonances of interest for their relevant applications.

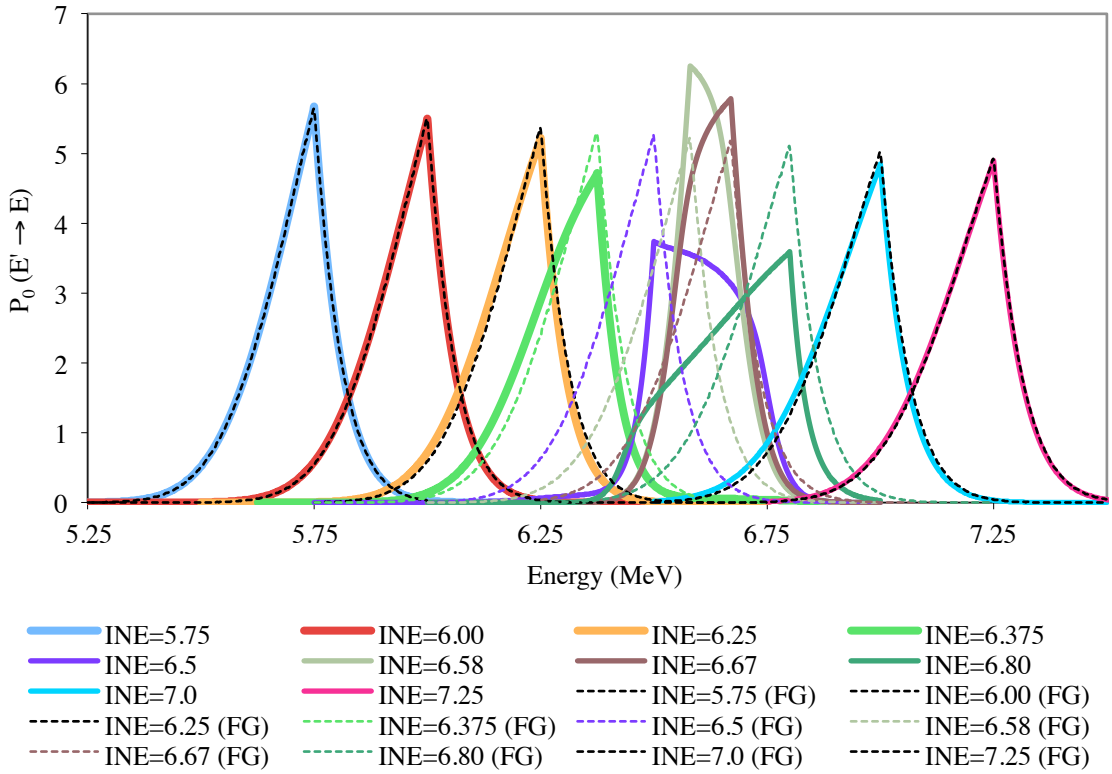

Figure 4.7: Comparison of results of P_0 moment of differential scattering PDFs using free gas scattering and Eqs (4.5) and (4.6)

4.4 Approximating Blackshaw's equation

The next step was to use Eqs. (4.5) and (4.6) to find an analytical solution to the integral by approximating the relative neutron speed-dependent cross section function. To begin the study for an approximation of the scattering cross section, the 36.67 eV resonance in ^{238}U was chosen. This resonance contributed to a significant bias in reactor analysis calculations caused by the large scattering to absorption ratio as explained in Chapter 2. Therefore, initial benchmarking was done for incident neutron energies around this important resonance for reactor analysis.

We first looked at assuming a Single-Level Breit Wigner model for the scattering cross section, using Taylor series expansions to linearize the exponential and error functions. This proved to be an inefficient method. It required high order functions for an accurate approximation and the resulting analytical integral was messy causing precision issues. These issues arose because very large numbers were multiplied by very small numbers. The specific function that contributed to the precision issue was the

exponential function within the integral, $\exp\left(-cv_r^2\right)$. It is a function of relative speed squared, which in the case for neutron speeds around the 36.67 eV resonance can be on the order of 80,000 m/s squared.

The study gave insight into the type of functions that can be used to represent the speed-dependent scattering cross sections that will result in analytical solutions for Eqs. (4.5) and (4.6). Using a constant scattering cross section will result in an integral that can be analytically integrated as Blackshaw showed in his thesis [5]. Also, assuming the cross section to take on the form of an exponential function, $\exp\left(-cv_r^2\right)$, will lead to an analytical solution. In our study of the integral, we found that even-ordered functions that approximate the neutron speed-dependent cross section would also lead to an analytical solution of Blackshaw's equation. Blackshaw did not mention this approximation in his journal paper [4], but he mentioned this approximation in his dissertation [5]. He applied it to the exact scattering distribution, but not to the moments. Therefore, all work done with the approximations on the moments is new. The next step was to determine if such an approximation to the cross section was sufficient to predict the P_0 moment of the differential scattering PDF accurately.

4.4.1 Second order fit for cross section

For simplicity, the cross section term is taken to be of the form:

$$\sigma_s\left(v_r\right) = a_0 + a_1 v_r^2. \tag{4.7}$$

The coefficients, a_o and a_1, were found by interpolating between two points. Since we know two sets of data points, $\{v_{r1}, \sigma_{s1}(v_{r1})\}$ and $\{v_{r2}, \sigma_{s2}(v_{r2})\}$, we can solve for a_o and a_1, using the linear system of equations:

$$\sigma_s\left(v_r\right) = a_0 + a_1 v_{r1}^2,$$
$$\sigma_s\left(v_r\right) = a_0 + a_1 v_{r2}^2.$$

Since this is not a high-order fit, the energy range for the cross section has to be split into 24 different regions to replicate the zero Kelvin scattering cross section relatively accurately for the 36.67 eV resonance. Figure 4.8 shows the fits superimposed onto the exact, zero Kelvin scattering cross section data for ^{238}U around the 36.67 eV resonance.

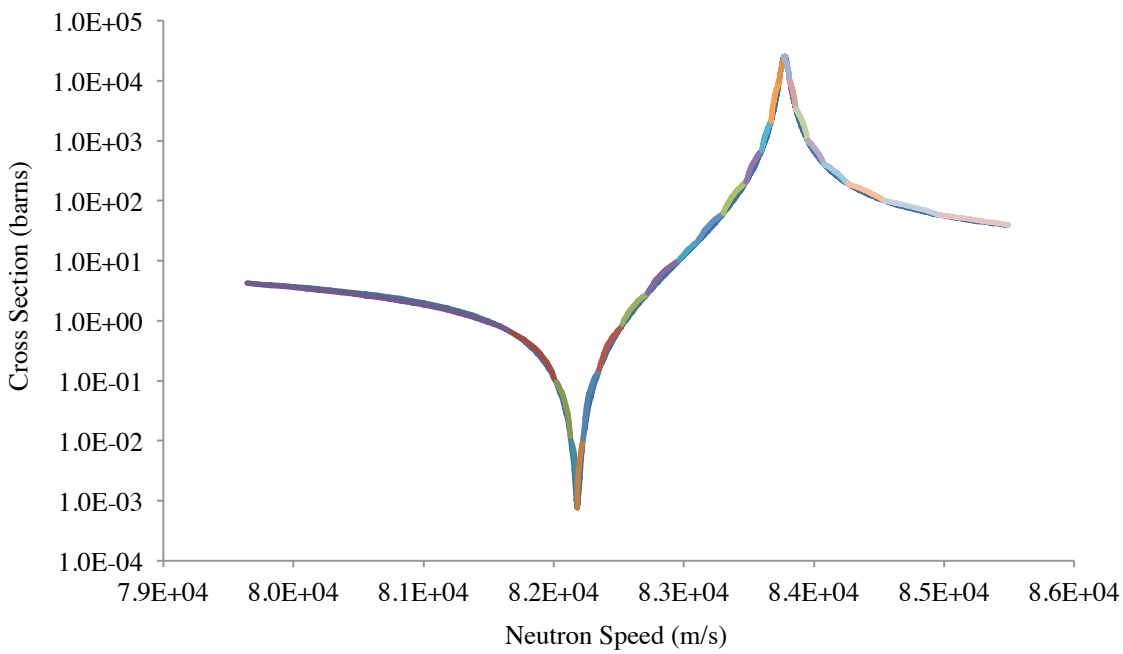

Figure 4.8: Piecewise interpolation using the form $\sigma_s(v_r) = a_0 + a_1 v_r^2$ around 36.67 eV resonance in ^{238}U

In Figure 4.8, the different colors represent the cross sections in their corresponding piecewise region. The coefficients for each of the regions starting from the lowest neutron speeds are indicated in Appendix B, Section B.1.

The equations after making the substitution for the cross sections are presented in the case of neutron downscattering:

$$K_{0,down}\left(v,v'\right)=\frac{h^3}{2B}\frac{v'}{v}\exp\left[\frac{B^2v^2}{A}\right]\times\ldots$$

$$\left\{\begin{array}{l}\displaystyle\int_{v_{\min}=v-4\sqrt{\frac{2kT}{Am}}}^{\frac{h^2(v+v')}{2B^2}} v_r\left(a_0+a_1v_r^2\right)\exp\left(-\frac{B^4v_r^2}{Ah^2}\right)\left[erf\left(hv'+\frac{B^2v_r}{h}\right)-erf\left(hv-\frac{B^2v_r}{h}\right)\right]dv_r+\\ \displaystyle\int_{\frac{h^2(v+v')}{2B^2}}^{v_{\max}=v+4\sqrt{\frac{2kT}{Am}}} v_r\left(a_0+a_1v_r^2\right)\exp\left(-\frac{B^4v_r^2}{Ah^2}\right)\left[erf\left(hv'+\frac{B^2v_r}{h}\right)-erf\left(\frac{B^2v_r}{h}-hv'\right)\right]dv_r\end{array}\right\}. \tag{4.8}$$

The upscatter case can be expressed as,

$$K_{0,up}\left(v,v'\right)=\frac{h^3}{2B}\frac{v'}{v}\exp\left[\frac{B^2v^2}{A}\right]\times\ldots$$

$$\left\{\begin{array}{l}\displaystyle\int_{v_{\min}=v-4\sqrt{\frac{2kT}{Am}}}^{\frac{h^2(v+v')}{2B^2}} v_r\left(a_0+a_1v_r^2\right)\exp\left(-\frac{B^4v_r^2}{Ah^2}\right)\left[erf\left(hv+\frac{B^2v_r}{h}\right)-erf\left(hv'-\frac{B^2v_r}{h}\right)\right]dv_r+\\ \displaystyle\int_{\frac{h^2(v+v')}{2B^2}}^{v_{\max}=v+4\sqrt{\frac{2kT}{Am}}} v_r\left(a_0+a_1v_r^2\right)\exp\left(-\frac{B^4v_r^2}{Ah^2}\right)\left[erf\left(hv+\frac{B^2v_r}{h}\right)-erf\left(\frac{B^2v_r}{h}-hv\right)\right]dv_r\end{array}\right\}. \tag{4.9}$$

The solutions for Eqs. (4.8) and (4.9) will be presented in the next few sections. These solutions can be simplified further, and this simplification process will also be presented. In all the equations, *ubnd* represents the upper bound of the integral, and *lbnd* represents the lower bound of the integral. All the solutions presented in this dissertation are the solutions for the indefinite integrals presented in Eqs. (4.8) and (4.9). The integral bounds must be substituted into these solutions in order to obtain the final answer.

4.4.1.1 Solution for the first integral in the downscattering case

The solution for the first integral in the downscattering case in Eq. (4.8) is given below:

$$C\int v_r\left(a_0+a_1v_r^2\right)\exp\left(-\frac{B^4v_r^2}{Ah^2}\right)\left[erf\left(hv'+\frac{B^2v_r}{h}\right)-erf\left(hv-\frac{B^2v_r}{h}\right)\right]dv_r$$

$$=\left.\left\{\begin{array}{l}\frac{(A+1)^2}{4AM}\frac{v'}{v}\left(a_0M+(3+2A)a_1kT+a_1Mv^2\right)erf\left[\sqrt{\frac{M}{2kT}}(v_r-v)\right]+\\ \boxed{\frac{(A+1)^2}{4A}a_1\sqrt{\frac{2kT}{\pi M}}\frac{v'}{v}(v'-v_r)\exp\left[\frac{M}{2AkT}\left(v^2-(A+1)v'^2-2Av'v_r-Av_r^2\right)\right]}-\\ \frac{(A+1)^2}{4A}a_1\sqrt{\frac{2kT}{\pi M}}\frac{v'}{v}(v+v_r)\exp\left[-\frac{M}{2kT}(v-v_r)^2\right]+\\ \boxed{\frac{(A+1)^2}{4AM}\frac{v'}{v}\left((3+2A)a_1kT+M\left(a_0+a_1v'^2\right)\right)\exp\left[\frac{M}{2AkT}\left(v^2-v'^2\right)\right]erf\left[\sqrt{\frac{M}{2kT}}(v'+v_r)\right]}+\\ \frac{(A+1)^{5/2}}{4A^{3/2}M}\frac{v'}{v}\left(2(A+1)a_1kT+M\left(a_0+a_1v_r^2\right)\right)\exp\left[\frac{M}{2A(A+1)kT}\left((A+1)v^2-Av_r^2\right)\right]\times\\ \left[erf\left[\sqrt{\frac{M}{2A(A+1)kT}}\left((A+1)v-Av_r\right)\right]-\boxed{erf\left[\sqrt{\frac{M}{2A(A+1)kT}}\left((A+1)v'+Av_r\right)\right]}\right]\end{array}\right\}\right|_{lbnd}^{ubnd}$$

where, $C=\frac{h^3}{2B}\frac{v'}{v}\exp\left[\frac{B^2v^2}{A}\right]$.

A closer look at the term in the red box shows that the term with the exponential function is a very large negative number. This large negative number arises from neutron speed, which is on the order of 10^4 m/s. This means that the exponential term is a very small number and the contribution from this term is negligible or zero.

$$\frac{(A+1)^2}{4A} a_1 \sqrt{\frac{2kT}{\pi M}} \frac{v'}{v} (v' - v_r) \exp\left[\frac{M}{2AkT}\left(v^2 - (A+1)v'^2 - 2Av'v_r - Av_r^2\right)\right]$$

$$\approx \frac{(A+1)^2}{4A} a_1 \sqrt{\frac{2kT}{\pi M}} \frac{v'}{v} (v' - v_r) \exp[-\infty]$$

$$= 0$$

A close look at the term in the blue box shows that only the error function is dependent on the relative speed and the rest of the terms are known constants. The term within the error function is so large that the error function will be almost one. This means that we are left with only the constants, which will cancel out during the integration and this term can be neglected.

$$\frac{(A+1)^2}{4AM} \frac{v'}{v} \left((3+2A)a_1 kT + M\left(a_0 + a_1 v'^2\right)\right) \exp\left[\frac{M}{2AkT}\left(v^2 - v'^2\right)\right] \times \ldots$$
$$\left\{ erf\left[\sqrt{\frac{M}{2kT}}\left(v' + ubnd\right)\right] - erf\left[\sqrt{\frac{M}{2kT}}\left(v' + lbnd\right)\right]\right\}$$

$$\approx \frac{(A+1)^2}{4AM} \frac{v'}{v} \left((3+2A)a_1 kT + M\left(a_0 + a_1 v'^2\right)\right) \exp\left[\frac{M}{2AkT}\left(v^2 - v'^2\right)\right] \left\{ erf[\infty] - erf[\infty]\right\}$$

$$= \frac{(A+1)^2}{4AM} \frac{v'}{v} \left((3+2A)a_1 kT + M\left(a_0 + a_1 v'^2\right)\right) \exp\left[\frac{M}{2AkT}\left(v^2 - v'^2\right)\right] \{1 - 1\}$$

$$= 0$$

The term in the green box becomes one since the error function of a large number is approximately equal to one.

$$erf\left[\sqrt{\frac{M}{2A(A+1)kT}}\left((A+1)v' + Av_r\right)\right] \approx erf[\infty] = 1$$

After considering all the simplifications, the solution of the first indefinite integral for the downscattering case leads to the following form:

$$\left\{\begin{array}{l}\frac{(A+1)^2}{4AM}\frac{v'}{v}\left(a_0M+(3+2A)a_1kT+a_1Mv^2\right)erf\left[\sqrt{\frac{M}{2kT}}(v_r-v)\right]- \\ \frac{(A+1)^2}{4A}a_1\sqrt{\frac{2kT}{\pi M}}\frac{v'}{v}(v+v_r)\exp\left[-\frac{M}{2kT}(v-v_r)^2\right]+ \\ \frac{(A+1)^{5/2}}{4A^{3/2}M}\frac{v'}{v}\left(2(A+1)a_1kT+M\left(a_0+a_1v_r^2\right)\right)\times\ldots \\ \quad\exp\left[\frac{M}{2A(A+1)kT}\left((A+1)v^2-Av_r^2\right)\right]\times\ldots \\ \quad\left[erf\left[\sqrt{\frac{M}{2A(A+1)kT}}\left((A+1)v-Av_r\right)\right]-1\right]\end{array}\right\}\Bigg|_{v_{\min}=v-4\sqrt{\frac{2kT}{Am}}}^{\frac{h^2(v+v')}{2B^2}} \tag{4.10}$$

4.4.1.2 Solution for the second integral in the downscattering case

The solution for the second indefinite integral in the downscattering case in Eq. (4.8) is given below:

$$C\int v_r\left(a_0+a_1v_r^2\right)\exp\left(-\frac{B^4v_r^2}{Ah^2}\right)\left[erf\left(hv'+\frac{B^2v_r}{h}\right)-erf\left(\frac{B^2v_r}{h}-hv'\right)\right]dv_r$$

$$=\left|\begin{array}{l}\left\{\begin{array}{l}-\frac{(A+1)^2}{4AM}\frac{v'}{v}\left(a_0M+(3+2A)a_1kT+a_1Mv'^2\right)\exp\left[\frac{M}{2AkT}\left(v^2-v'^2\right)\right]\times\ldots \\ \qquad erf\left[\sqrt{\frac{M}{2kT}}\left(v_r-v'\right)\right]+ \\ \boxed{\frac{(A+1)^2}{4A}a_1\sqrt{\frac{2kT}{\pi M}}\frac{v'}{v}\left(v'-v_r\right)\exp\left[\frac{M}{2AkT}\left(v^2-(A+1)v'^2-2Av'v_r-Av_r^2\right)\right]}+ \\ \frac{(A+1)^2}{4A}a_1\sqrt{\frac{2kT}{\pi M}}\frac{v'}{v}\left(v'+v_r\right)\exp\left[\frac{M}{2AkT}\left(v^2-(A+1)v'^2+2Av'v_r-Av_r^2\right)\right]+ \\ \boxed{\begin{array}{l}\frac{(A+1)^2}{4AM}\frac{v'}{v}\left((3+2A)a_1kT+M\left(a_0+a_1v'^2\right)\right)\exp\left[\frac{M}{2AkT}\left(v^2-v'^2\right)\right]\times\ldots \\ \qquad erf\left[\sqrt{\frac{M}{2kT}}\left(v'+v_r\right)\right]-\end{array}} \\ \frac{(A+1)^{5/2}}{4A^{3/2}M}\frac{v'}{v}\left(2(A+1)a_1kT+M\left(a_0+a_1v_r^2\right)\right)\exp\left[\frac{M}{2A(A+1)kT}\left((A+1)v^2-Av_r^2\right)\right]\times\ldots \\ \qquad \left[erf\left[\sqrt{\frac{M}{2A(A+1)kT}}\left((A+1)v'-Av_r\right)\right]+\boxed{erf\left[\sqrt{\frac{M}{2A(A+1)kT}}\left((A+1)v'+Av_r\right)\right]}\right]\end{array}\right\}\end{array}\right|_{lbnd}^{ubnd}$$

where, $C=\frac{h^3}{2B}\frac{v'}{v}\exp\left[\frac{B^2v^2}{A}\right]$.

Once again, the color-coded boxes highlight the terms eliminated from the solution for the indefinite integral due to the nature of the numbers that are substituted into them. The term in the red box shows that the term within the exponential function is a very large negative number, meaning the exponential function becomes a very small number and the contribution from this term is negligible.

$$\frac{(A+1)^2}{4A} a_1 \sqrt{\frac{2kT}{\pi M}} \frac{v'}{v} (v' - v_r) \exp\left[\frac{M}{2AkT}\left(v^2 - (A+1)v'^2 - 2Av'v_r - Av_r^2\right)\right]$$

$$\approx \frac{(A+1)^2}{4A} a_1 \sqrt{\frac{2kT}{\pi M}} \frac{v'}{v} (v' - v_r) \exp[-\infty]$$

$$= 0$$

Again, the term in the blue box shows that only the error function is dependent on the relative speed and the rest of the terms are known constants. The term within the error function is so large that the error function will be almost one. This means that the constants will cancel out during integration and this term can be neglected.

$$\frac{(A+1)^2}{4AM} \frac{v'}{v} \left((3+2A)a_1 kT + M\left(a_0 + a_1 v'^2\right)\right) \exp\left[\frac{M}{2AkT}\left(v^2 - v'^2\right)\right] \times \ldots$$
$$\left\{ erf\left[\sqrt{\frac{M}{2kT}}\left(v' + ubnd\right)\right] - erf\left[\sqrt{\frac{M}{2kT}}\left(v' + lbnd\right)\right]\right\}$$

$$\approx \frac{(A+1)^2}{4AM} \frac{v'}{v} \left((3+2A)a_1 kT + M\left(a_0 + a_1 v'^2\right)\right) \exp\left[\frac{M}{2AkT}\left(v^2 - v'^2\right)\right] \left\{ erf[\infty] - erf[\infty]\right\}$$

$$= \frac{(A+1)^2}{4AM} \frac{v'}{v} \left((3+2A)a_1 kT + M\left(a_0 + a_1 v'^2\right)\right) \exp\left[\frac{M}{2AkT}\left(v^2 - v'^2\right)\right] \{1 - 1\}$$

$$= 0$$

Again, the term in the green box contains an error function of a large number, which is approximately equal to one.

$$erf\left[\sqrt{\frac{M}{2A(A+1)kT}}\left((A+1)v'+Av_r\right)\right]\approx erf\left[\infty\right]=1$$

After simplification, the second integral for the downscattering case takes on the following form:

$$\left|\left\{\begin{array}{l}
-\frac{(A+1)^2}{4AM}\frac{v'}{v}\left(a_0M+(3+2A)a_1kT+a_1Mv'^2\right)\times\ldots \\
\qquad\exp\left[\frac{M}{2AkT}\left(v^2-v'^2\right)\right]erf\left[\sqrt{\frac{M}{2kT}}\left(v_r-v'\right)\right]+ \\
\\
\frac{(A+1)^2}{4A}a_1\sqrt{\frac{2kT}{\pi M}}\frac{v'}{v}\left(v'+v_r\right)\times\ldots \\
\qquad\exp\left[\frac{M}{2AkT}\left(v^2-(A+1)v'^2+2Av'v_r-Av_r^2\right)\right]- \\
\\
\frac{(A+1)^{5/2}}{4A^{3/2}M}\frac{v'}{v}\left(2(A+1)a_1kT+M\left(a_0+a_1v_r^2\right)\right)\times\ldots \\
\qquad\exp\left[\frac{M}{2A(A+1)kT}\left((A+1)v^2-Av_r^2\right)\right]\times\ldots \\
\qquad\left[erf\left[\sqrt{\frac{M}{2A(A+1)kT}}\left((A+1)v'-Av_r\right)\right]+1\right]
\end{array}\right\}\right|_{\frac{h^2(v+v')}{2B^2}}^{v_{\max}=v+4\sqrt{\frac{2kT}{Am}}} \tag{4.11}$$

4.4.1.3 Solution for the first integral in the upscattering case

The solution for the first indefinite integral in the upscattering case in Eq. (4.9) is given below:

$$C\int v_r\left(a_0+a_1v_r^2\right)\exp\left(-\frac{B^4v_r^2}{Ah^2}\right)\left[erf\left(hv+\frac{B^2v_r}{h}\right)-erf\left(hv'-\frac{B^2v_r}{h}\right)\right]dv_r$$

$$=\left\{\begin{array}{l}
\boxed{\frac{(A+1)^2}{4AM}\frac{v'}{v}\left(a_0M+(3+2A)a_1kT+a_1Mv^2\right)erf\left[\sqrt{\frac{M}{2kT}}(v+v_r)\right]+} \\
\boxed{\frac{(A+1)^2}{4A}a_1\sqrt{\frac{2kT}{\pi M}}\frac{v'}{v}(v-v_r)\exp\left[-\frac{M}{2kT}(v+v_r)^2\right]}- \\
\frac{(A+1)^2}{4A}a_1\sqrt{\frac{2kT}{\pi M}}\frac{v'}{v}(v'+v_r)\exp\left[\frac{M}{2AkT}\left(v^2-(A+1)v'^2+2Av'v_r-Av_r^2\right)\right]+ \\
\frac{(A+1)^2}{4AM}\frac{v'}{v}\left((3+2A)a_1kT+M\left(a_0+a_1v'^2\right)\right)\exp\left[\frac{M}{2AkT}\left(v^2-v'^2\right)\right]\times\ldots \\
\qquad erf\left[\sqrt{\frac{M}{2kT}}(v_r-v')\right]+ \\
\frac{(A+1)^{5/2}}{4A^{3/2}M}\frac{v'}{v}\left(2(A+1)a_1kT+M\left(a_0+a_1v_r^2\right)\right)\times\ldots \\
\qquad \exp\left[\frac{M}{2A(A+1)kT}\left((A+1)v^2-Av_r^2\right)\right]\times\ldots \\
\qquad \left[erf\left[\sqrt{\frac{M}{2A(A+1)kT}}\left((A+1)v'-Av_r\right)\right]-\boxed{erf\left[\sqrt{\frac{M}{2A(A+1)kT}}\left((A+1)v+Av_r\right)\right]}\right]
\end{array}\right\}\Bigg|_{lbnd}^{ubnd}$$

where, $C=\frac{h^3}{2B}\frac{v'}{v}\exp\left[\frac{B^2v^2}{A}\right]$.

The color-coded boxes represent the terms that can be eliminated due to terms canceling out or numbers becoming zero. From now on, details regarding the simplifications made to the terms in the boxes will not be presented in great detail as it was in the previous two sections for the downscattering case. The term in the blue box contains an error function in which the term is a large number. The resulting error function will be equivalent to one and the constants will cancel out. The terms within the exponential function in the red box contains a very large negative term and so the exponential function will be a very small number, close to zero, and can be neglected. In the green box, the term within the error function is a very large number and the error function becomes equivalent to one. After the simplifications, the solution for the first integral for the upscattering case takes on the following form:

$$\left\{\begin{array}{l} -\dfrac{(A+1)^2}{4A} a_1 \sqrt{\dfrac{2kT}{\pi M}} \dfrac{v'}{v}\left(v'+v_r\right)\times\ldots \\ \quad \exp\left[\dfrac{M}{2AkT}\left(v^2-(A+1)v'^2+2Av'v_r-Av_r^2\right)\right]+ \\ \\ \dfrac{(A+1)^2}{4AM}\dfrac{v'}{v}\left((3+2A)a_1kT+M\left(a_0+a_1v'^2\right)\right)\exp\left[\dfrac{M}{2AkT}\left(v^2-v'^2\right)\right]\times\ldots \\ \quad erf\left[\sqrt{\dfrac{M}{2kT}}\left(v_r-v'\right)\right]+ \\ \\ \dfrac{(A+1)^{5/2}}{4A^{3/2}M}\dfrac{v'}{v}\left(2(A+1)a_1kT+M\left(a_0+a_1v_r^2\right)\right)\times\ldots \\ \quad \exp\left[\dfrac{M}{2A(A+1)kT}\left((A+1)v^2-Av_r^2\right)\right]\times\ldots \\ \quad \left[erf\left[\sqrt{\dfrac{M}{2A(A+1)kT}}\left((A+1)v'-Av_r\right)\right]-1\right] \end{array}\right\}\Bigg|_{v_{\min}=v-4\sqrt{\frac{2kT}{Am}}}^{\frac{h^2(v+v')}{2B^2}} \tag{4.12}$$

4.4.1.4 Solution for the second integral in the upscattering case

The solution for the second indefinite integral for the upscattering in Eq. (4.9) is presented below.

$$
C\int_{lbnd}^{ubnd} v_r\left(a_0+a_1v_r^2\right)\exp\left(-\frac{B^4v_r^2}{Ah^2}\right)\left[erf\left(hv+\frac{B^2v_r}{h}\right)-erf\left(\frac{B^2v_r}{h}-hv\right)\right]dv_r
$$

$$
=\left\{\begin{array}{l}
-\frac{(A+1)^2}{4AM}\frac{v'}{v}\left(a_0M+(3+2A)a_1kT+a_1Mv^2\right)erf\left[\sqrt{\frac{M}{2kT}}(v_r-v)\right]+ \\
\boxed{\frac{(A+1)^2}{4A}a_1\sqrt{\frac{2kT}{\pi M}}\frac{v'}{v}(v-v_r)\exp\left[-\frac{M}{2kT}(v+v_r)^2\right]}+ \\
\frac{(A+1)^2}{4A}a_1\sqrt{\frac{2kT}{\pi M}}\frac{v'}{v}(v+v_r)\exp\left[-\frac{M}{2kT}(v-v_r)^2\right]+ \\
\boxed{\frac{(A+1)^2}{4AM}\frac{v'}{v}\left((3+2A)a_1kT+M\left(a_0+a_1v^2\right)\right)erf\left[\sqrt{\frac{M}{2kT}}(v+v_r)\right]}- \\
\frac{(A+1)^{5/2}}{4A^{3/2}M}\frac{v'}{v}\left(2(A+1)a_1kT+M\left(a_0+a_1v_r^2\right)\right)\exp\left[\frac{M}{2A(A+1)kT}\left((A+1)v^2-Av_r^2\right)\right]\times \\
\quad\left[erf\left[\sqrt{\frac{M}{2A(A+1)kT}}\left((A+1)v-Av_r\right)\right]+\boxed{erf\left[\sqrt{\frac{M}{2A(A+1)kT}}\left((A+1)v+Av_r\right)\right]}\right]
\end{array}\right\}\Bigg|_{lbnd}^{ubnd}
$$

where, $C=\frac{h^3}{2B}\frac{v'}{v}\exp\left[\frac{B^2v^2}{A}\right]$.

The term in the red box contains a very large negative term in the exponential function, and the terms within the red box can be neglected since the exponential function becomes zero. In the blue box, the term within the error function is very large, and the function becomes one. The terms left are all constants, which cancel out after the integration. Again, the error function within the green box contains a very large term

which results in the error function becoming one. After the simplifications, the resulting solution to the second integral for the upscattering case becomes,

$$\left\{\begin{array}{l} -\frac{(A+1)^2}{4AM}\frac{v'}{v}\left(a_0M+(3+2A)a_1kT+a_1Mv^2\right)erf\left[\sqrt{\frac{M}{2kT}}(v_r-v)\right]+ \\ \frac{(A+1)^2}{4A}a_1\sqrt{\frac{2kT}{\pi M}}\frac{v'}{v}(v+v_r)\exp\left[-\frac{M}{2kT}(v-v_r)^2\right]- \\ \frac{(A+1)^{5/2}}{4A^{3/2}M}\frac{v'}{v}\left(2(A+1)a_1kT+M\left(a_0+a_1v_r^2\right)\right)\times\ldots \\ \qquad \exp\left[\frac{M}{2A(A+1)kT}\left((A+1)v^2-Av_r^2\right)\right]\times\ldots \\ \qquad \left[erf\left[\sqrt{\frac{M}{2A(A+1)kT}}\left((A+1)v-Av_r\right)\right]+1\right] \end{array}\right\}\Bigg|_{\frac{h^2(v+v')}{2B^2}}^{v_{\max}=v+4\sqrt{\frac{2kT}{Am}}} \tag{4.13}$$

4.4.2 Fourth order fit for cross section

In the previous section, we looked at the solutions for Eqs. (4.8) and (4.9) using the second order approximation for the scattering cross section. In this section, we will look at the solutions using the fourth order approximation. Instead of interpolating between points to generate the coefficients as in the second order case, the coefficients for the fourth order case were generated using least squares fitting using Mathematica [8]. Fewer piecewise regions are required to generate the moments when going up higher orders. The coefficients and their speed ranges are provided in Appendix B, Section B.2. The cross section fits are shown in Figure 4.9. Each colored line in Figure 4.9 represents a piecewise region.

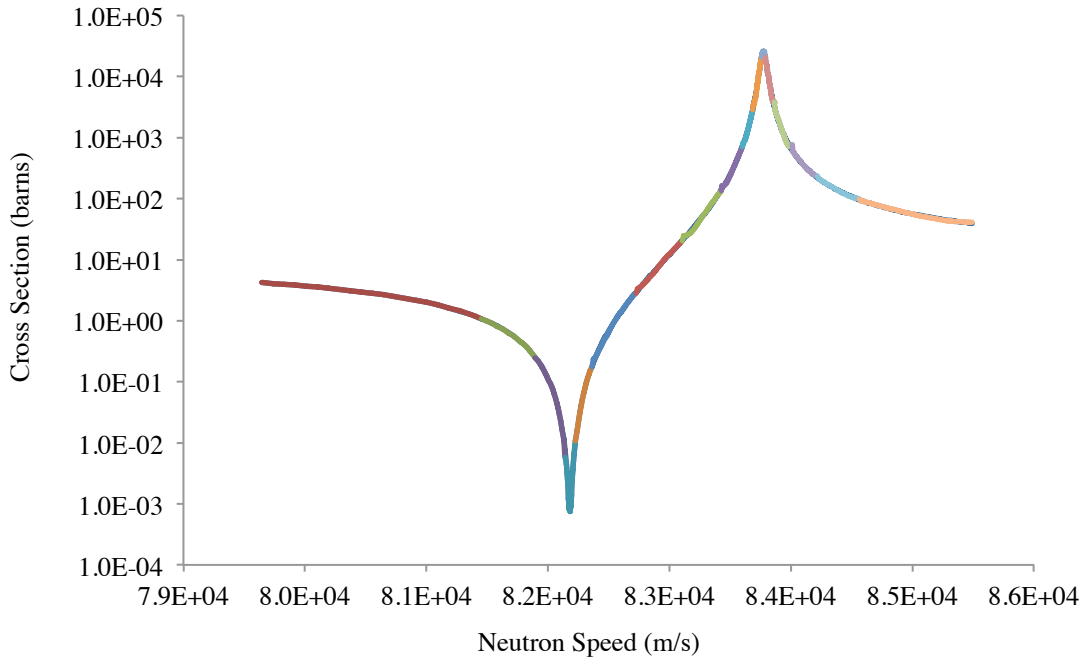

Figure 4.9: Piecewise least squares fitting using the form $\sigma_s(v_r) = a_0 + a_1 v_r^2 + a_2 v_r^4$ around 36.67 eV resonance in ^{238}U.

The equations after making the fourth order approximation for the cross section are presented below for both cases, neutron downscattering and upscattering:

$$K_{0,down}(v,v') = \frac{h^3}{2B}\frac{v'}{v}\exp\left[\frac{B^2v^2}{A}\right]\times\ldots$$

$$\left\{\begin{array}{l} \displaystyle\int_{\frac{h^2(v-v')}{2B^2}}^{\frac{h^2(v+v')}{2B^2}} v_r\left(a_0 + a_1 v_r^2 + a_2 v_r^4\right)\exp\left(-\frac{B^4 v_r^2}{Ah^2}\right)\left[erf\left(hv' + \frac{B^2 v_r}{h}\right) - erf\left(hv - \frac{B^2 v_r}{h}\right)\right]dv_r + \\ \displaystyle\int_{\frac{h^2(v+v')}{2B^2}}^{\infty} v_r\left(a_0 + a_1 v_r^2 + a_2 v_r^4\right)\exp\left(-\frac{B^4 v_r^2}{Ah^2}\right)\left[erf\left(hv' + \frac{B^2 v_r}{h}\right) - erf\left(\frac{B^2 v_r}{h} - hv'\right)\right]dv_r \end{array}\right\} \quad (4.14)$$

$$K_{0,up}\left(v,v'\right)=\frac{h^3}{2B}\frac{v'}{v}\exp\left[\frac{B^2v^2}{A}\right]\times\ldots$$

$$\left\{\begin{array}{l}\displaystyle\int_{\frac{h^2(v'-v)}{2B^2}}^{\frac{h^2(v+v')}{2B^2}} v_r\left(a_0+a_1v_r^2+a_2v_r^4\right)\exp\left(-\frac{B^4v_r^2}{Ah^2}\right)\left[erf\left(hv+\frac{B^2v_r}{h}\right)-erf\left(hv'-\frac{B^2v_r}{h}\right)\right]dv_r+\\ \displaystyle\int_{\frac{h^2(v+v')}{2B^2}}^{\infty} v_r\left(a_0+a_1v_r^2+a_2v_r^4\right)\exp\left(-\frac{B^4v_r^2}{Ah^2}\right)\left[erf\left(hv+\frac{B^2v_r}{h}\right)-erf\left(\frac{B^2v_r}{h}-hv\right)\right]dv_r\end{array}\right\} \tag{4.15}$$

Once again note that this is a distribution and not the P_0 moment of the differential scattering PDF, so it must be normalized. The solutions for the indefinite integrals in Eqs. (4.14) and (4.15) will be presented in the next few sections. The upper bound of the second integral and lower bound of the first integral should be modified to Eqs. (3.9) and (3.10) for faster calculations. These solutions were further simplified due to the nature of the values used in these equations. Once again, in all the equations presented in the next few sections, *ubnd* represents the upper bound of the integral and *lbnd* represents the lower bound of the integral. Details from the simplification process will be neglected and final forms of the equations are presented in the next sections. Again, the exponential function within the red box becomes zero due to the very large negative number present in the function. The terms within the blue box become a constant, which will cancel out when the bounds of the integrals are substituted. This is because the error function will become one, and the rest of the terms are constants, which eventually cancel out. This term can be ignored in the final solution. Finally, the terms within the green box become unity because the error function contains a large value.

4.4.2.1 Solution for the first integral in the downscattering case

$$
\left.\begin{aligned}
&\frac{(A+1)^2}{4AM^2}\frac{v'}{v}erf\left[\sqrt{\frac{M}{2kT}}\left(v_r-v\right)\right]\times\ldots\\
&\qquad\begin{pmatrix}a_0M^2+kT\left(\left(3+2A\right)a_1M+\left(15+4A\left(5+2A\right)\right)a_2kT\right)+\\ M\left(a_1M+2\left(5+2A\right)a_2kT\right)v^2+a_2M^2v^4\end{pmatrix}-\\
&\frac{(A+1)^2}{4AM^{3/2}}\frac{v'}{v}\sqrt{\frac{2kT}{\pi}}\exp\left[-\frac{M}{2kT}\left(v-v_r\right)^2\right]\times\ldots\\
&\qquad\left(a_1M\left(v+v_r\right)+a_2\begin{pmatrix}kT\left(9v+4Av+7v_r+4Av_r\right)+\\ M\left(v+v_r\right)\left(v^2+v_r^2\right)\end{pmatrix}\right)-\\
&\boxed{\begin{aligned}&\frac{(A+1)^2}{4AM^{3/2}}\frac{v'}{v}\sqrt{\frac{2kT}{\pi}}\exp\left[\frac{M}{2AkT}\left(v^2-\left(A+1\right)v'^2-2Av'v_r-Av_r^2\right)\right]\times\ldots\\ &\qquad\begin{pmatrix}a_1M\left(v_r-v'\right)+\\ a_2\begin{pmatrix}kT\left(-9v'-4Av'+7v_r+4Av_r\right)-\\ M\left(v'-v_r\right)\left(v'^2+v_r^2\right)\end{pmatrix}\end{pmatrix}+\end{aligned}}\\
&\boxed{\begin{aligned}&\frac{(A+1)^2}{4AM^2}\frac{v'}{v}\exp\left[\frac{M}{2AkT}\left(v^2-v'^2\right)\right]erf\left[\sqrt{\frac{M}{2kT}}\left(v'+v_r\right)\right]\times\ldots\\ &\qquad\begin{pmatrix}a_0M^2+kT\left(\left(3+2A\right)a_1M+\left(15+4A\left(5+2A\right)\right)a_2kT\right)+\\ M\left(a_1M+2\left(5+2A\right)a_2kT\right)v'^2+a_2M^2v'^4\end{pmatrix}+\end{aligned}}\\
&\frac{(A+1)^{5/2}}{4A^{3/2}M^2}\frac{v'}{v}\exp\left[\frac{M}{2A\left(A+1\right)kT}\left(\left(A+1\right)v^2-Av_r^2\right)\right]\\
&\qquad\begin{pmatrix}a_0M^2+2\left(A+1\right)kT\left(a_1M+4\left(A+1\right)a_2kT\right)+\\ M\left(a_1M+4\left(A+1\right)a_2kT\right)v_r^2+a_2M^2v_r^4\end{pmatrix}\times\ldots\\
&\qquad\left[erf\left[\sqrt{\frac{M}{2A\left(A+1\right)kT}}\left(\left(A+1\right)v-Av_r\right)\right]-\boxed{erf\left[\sqrt{\frac{M}{2A\left(A+1\right)kT}}\left(\left(A+1\right)v'+Av_r\right)\right]}\right]
\end{aligned}\right\}\Bigg|_{lbnd}^{ubnd}
$$

After further simplification, the solution for the first indefinite integral for downscatter in Eq. (4.14) is:

$$\left\{\begin{array}{l}
\frac{(A+1)^2}{4AM^2}\frac{v'}{v}erf\left[\sqrt{\frac{M}{2kT}}(v_r-v)\right]\times\ldots \\
\qquad\left(\begin{array}{l}a_0M^2+kT\left((3+2A)a_1M+(15+4A(5+2A))a_2kT\right)+\\ M\left(a_1M+2(5+2A)a_2kT\right)v^2+a_2M^2v^4\end{array}\right)- \\
\\
\frac{(A+1)^2}{4AM^{3/2}}\frac{v'}{v}\sqrt{\frac{2kT}{\pi}}\exp\left[-\frac{M}{2kT}(v-v_r)^2\right]\times\ldots \\
\qquad\left(a_1M(v+v_r)+a_2\left(\begin{array}{l}kT(9v+4Av+7v_r+4Av_r)+\\ M(v+v_r)(v^2+v_r^2)\end{array}\right)\right)+ \\
\\
\frac{(A+1)^{5/2}}{4A^{3/2}M^2}\frac{v'}{v}\exp\left[\frac{M}{2A(A+1)kT}\left((A+1)v^2-Av_r^2\right)\right] \\
\qquad\left(\begin{array}{l}a_0M^2+2(A+1)kT\left(a_1M+4(A+1)a_2kT\right)+\\ M\left(a_1M+4(A+1)a_2kT\right)v_r^2+a_2M^2v_r^4\end{array}\right)\times\ldots \\
\qquad\left[erf\left[\sqrt{\frac{M}{2A(A+1)kT}}\left((A+1)v-Av_r\right)\right]-1\right]
\end{array}\right\}\Bigg|_{v_{\min}=v-4\sqrt{\frac{2kT}{Am}}}^{\frac{h^2(v+v')}{2B^2}} \tag{4.16}$$

4.4.2.2 Solution for second integral for downscattering case

$$
\left.\begin{aligned}
&-\frac{(A+1)^2}{4AM^2}\frac{v'}{v}\exp\left[\frac{M}{2AkT}\left(v^2-v'^2\right)\right]erf\left[\sqrt{\frac{M}{2kT}}\left(v_r-v'\right)\right]\times\ldots\\
&\qquad\begin{pmatrix}a_0M^2+kT\left((3+2A)a_1M+\left(15+4A(5+2A)\right)a_2kT\right)+\\ M\left(a_1M+2(5+2A)a_2kT\right)v'^2+a_2M^2v'^4\end{pmatrix}+\\
&\boxed{\begin{aligned}&\frac{(A+1)^2}{4AM^2}\frac{v'}{v}\exp\left[\frac{M}{2AkT}\left(v^2-v'^2\right)\right]erf\left[\sqrt{\frac{M}{2kT}}\left(v'+v_r\right)\right]\times\ldots\\ &\qquad\begin{pmatrix}a_0M^2+kT\left((3+2A)a_1M+\left(15+4A(5+2A)\right)a_2kT\right)+\\ M\left(a_1M+2(5+2A)a_2kT\right)v'^2+a_2M^2v'^4\end{pmatrix}-\end{aligned}}\\
&\frac{(A+1)^{5/2}}{4A^{3/2}M^2}\frac{v'}{v}\exp\left[\frac{M}{2A(A+1)kT}\left((A+1)v^2-Av_r^2\right)\right]\times\ldots\\
&\qquad\begin{pmatrix}a_0M^2+2(A+1)kT\left(a_1M+4(A+1)a_2kT\right)+\\ M\left(a_1M+4(A+1)a_2kT\right)v_r^2+a_2M^2v_r^4\end{pmatrix}\times\ldots\\
&\qquad\left[erf\left[\sqrt{\frac{M}{2A(A+1)kT}}\left((A+1)v'-Av_r\right)\right]+\boxed{erf\left[\sqrt{\frac{M}{2A(A+1)kT}}\left((A+1)v'+Av_r\right)\right]}\right]+\\
&\frac{(A+1)^2}{4AM^{3/2}}\frac{v'}{v}\sqrt{\frac{2kT}{\pi}}\exp\left[\frac{M}{2AkT}\left(v^2-(A+1)v'^2+2Av'v_r-Av_r^2\right)\right]\times\ldots\\
&\qquad\begin{pmatrix}v'\left((9+4A)a_2kT+M\left(a_1+a_2\left(v'^2+v_r^2\right)\right)\right)+\\ v_r\left((7+4A)a_2kT+M\left(a_1+a_2\left(v'^2+v_r^2\right)\right)\right)\end{pmatrix}+\\
&\boxed{\begin{aligned}&\frac{(A+1)^2}{4AM^{3/2}}\frac{v'}{v}\sqrt{\frac{2kT}{\pi}}\exp\left[\frac{M}{2AkT}\left(v^2-(A+1)v'^2-2Av'v_r-Av_r^2\right)\right]\times\ldots\\ &\qquad\begin{pmatrix}v'\left((9+4A)a_2kT+M\left(a_1+a_2\left(v'^2+v_r^2\right)\right)\right)-\\ v_r\left((7+4A)a_2kT+M\left(a_1+a_2\left(v'^2+v_r^2\right)\right)\right)\end{pmatrix}\end{aligned}}
\end{aligned}\right\}\Bigg|_{lbnd}^{ubnd}
$$

After further simplification, the solution for the second indefinite integral for downscatter in Eq. (4.14) is:

$$\left.\begin{cases} -\dfrac{(A+1)^2}{4AM^2}\dfrac{v'}{v}\exp\left[\dfrac{M}{2AkT}\left(v^2-v'^2\right)\right]erf\left[\sqrt{\dfrac{M}{2kT}}\left(v_r-v'\right)\right]\times\ldots \\ \qquad \begin{pmatrix} a_0M^2+kT\left((3+2A)a_1M+\left(15+4A(5+2A)\right)a_2kT\right)+ \\ M\left(a_1M+2(5+2A)a_2kT\right)v'^2+a_2M^2v'^4 \end{pmatrix}- \\ \\ \dfrac{(A+1)^{5/2}}{4A^{3/2}M^2}\dfrac{v'}{v}\exp\left[\dfrac{M}{2A(A+1)kT}\left((A+1)v^2-Av_r^2\right)\right]\times\ldots \\ \qquad \begin{pmatrix} a_0M^2+2(A+1)kT\left(a_1M+4(A+1)a_2kT\right)+ \\ M\left(a_1M+4(A+1)a_2kT\right)v_r^2+a_2M^2v_r^4 \end{pmatrix}\times\ldots \\ \qquad \left[erf\left[\sqrt{\dfrac{M}{2A(A+1)kT}}\left((A+1)v'-Av_r\right)\right]+1\right]+ \\ \\ \dfrac{(A+1)^2}{4AM^{3/2}}\dfrac{v'}{v}\sqrt{\dfrac{2kT}{\pi}}\exp\left[\dfrac{M}{2AkT}\left(v^2-(A+1)v'^2+2Av'v_r-Av_r^2\right)\right]\times\ldots \\ \qquad \begin{pmatrix} v'\left((9+4A)a_2kT+M\left(a_1+a_2\left(v'^2+v_r^2\right)\right)\right)+ \\ v_r\left((7+4A)a_2kT+M\left(a_1+a_2\left(v'^2+v_r^2\right)\right)\right) \end{pmatrix} \end{cases}\right|_{\frac{h^2(v+v')}{2B^2}}^{v_{\max}=v+4\sqrt{\frac{2kT}{Am}}} \tag{4.17}$$

4.4.2.3 Solution for first integral for upscattering case

$$
\left\{
\begin{aligned}
&\boxed{\begin{aligned}
&\frac{(A+1)^2}{4AM^2}\frac{v'}{v}erf\left[\sqrt{\frac{M}{2kT}}\left(v_r+v\right)\right]\times\ldots\\
&\quad\begin{pmatrix} a_0M^2+kT\left(\left(3+2A\right)a_1M+\left(15+4A\left(5+2A\right)\right)a_2kT\right)+\\ M\left(a_1M+2\left(5+2A\right)a_2kT\right)v^2+a_2M^2v^4\end{pmatrix}+
\end{aligned}}\\
&\boxed{\begin{aligned}
&\frac{(A+1)^2}{4AM^{3/2}}\frac{v'}{v}\sqrt{\frac{2kT}{\pi}}\exp\left[-\frac{M}{2kT}\left(v+v_r\right)^2\right]\times\ldots\\
&\quad\left(a_1M\left(v-v_r\right)+a_2\begin{pmatrix} kT\left(9v+4Av-7v_r-4Av_r\right)+\\ M\left(v-v_r\right)\left(v^2+v_r^2\right)\end{pmatrix}\right)-
\end{aligned}}\\
&\frac{(A+1)^2}{4AM^{3/2}}\frac{v'}{v}\sqrt{\frac{2kT}{\pi}}\exp\left[\frac{M}{2AkT}\left(v^2-\left(A+1\right)v'^2+2Av'v_r-Av_r^2\right)\right]\times\ldots\\
&\quad\left(a_1M\left(v_r+v'\right)+a_2\begin{pmatrix} kT\left(9v'+4Av'+7v_r+4Av_r\right)+\\ M\left(v'+v_r\right)\left(v'^2+v_r^2\right)\end{pmatrix}\right)+\\
&\frac{(A+1)^2}{4AM^2}\frac{v'}{v}\exp\left[\frac{M}{2AkT}\left(v^2-v'^2\right)\right]erf\left[\sqrt{\frac{M}{2kT}}\left(v_r-v'\right)\right]\times\ldots\\
&\quad\begin{pmatrix} a_0M^2+kT\left(\left(3+2A\right)a_1M+\left(15+4A\left(5+2A\right)\right)a_2kT\right)+\\ M\left(a_1M+2\left(5+2A\right)a_2kT\right)v'^2+a_2M^2v'^4\end{pmatrix}+\\
&\frac{(A+1)^{5/2}}{4A^{3/2}M^2}\frac{v'}{v}\exp\left[\frac{M}{2A\left(A+1\right)kT}\left(\left(A+1\right)v^2-Av_r^2\right)\right]\times\ldots\\
&\quad\begin{pmatrix} a_0M^2+2\left(A+1\right)kT\left(a_1M+4\left(A+1\right)a_2kT\right)+\\ M\left(a_1M+4\left(A+1\right)a_2kT\right)v_r^2+a_2M^2v_r^4\end{pmatrix}\times\\
&\quad\left[erf\left[\sqrt{\frac{M}{2A\left(A+1\right)kT}}\left(\left(A+1\right)v'-Av_r\right)\right]-\boxed{erf\left[\sqrt{\frac{M}{2A\left(A+1\right)kT}}\left(\left(A+1\right)v+Av_r\right)\right]}\right]
\end{aligned}
\right\}\Bigg|_{lbnd}^{ubnd}
$$

After further simplification, the solution for the first indefinite integral for upscatter in Eq. (4.15) is:

$$\left.\begin{cases} -\dfrac{(A+1)^2}{4AM^{3/2}}\dfrac{v'}{v}\sqrt{\dfrac{2kT}{\pi}}\exp\left[\dfrac{M}{2AkT}\left(v^2-(A+1)v'^2+2Av'v_r-Av_r^2\right)\right]\times\ldots \\ \qquad\left(a_1M(v_r+v')+a_2\begin{pmatrix} kT(9v'+4Av'+7v_r+4Av_r)+ \\ M(v'+v_r)(v'^2+v_r^2)\end{pmatrix}\right)+ \\ \\ \dfrac{(A+1)^2}{4AM^2}\dfrac{v'}{v}\exp\left[\dfrac{M}{2AkT}\left(v^2-v'^2\right)\right]erf\left[\sqrt{\dfrac{M}{2kT}}(v_r-v')\right]\times\ldots \\ \qquad\begin{pmatrix} a_0M^2+kT\left((3+2A)a_1M+(15+4A(5+2A))a_2kT\right)+ \\ M\left(a_1M+2(5+2A)a_2kT\right)v'^2+a_2M^2v'^4\end{pmatrix}+ \\ \\ \dfrac{(A+1)^{5/2}}{4A^{3/2}M^2}\dfrac{v'}{v}\exp\left[\dfrac{M}{2A(A+1)kT}\left((A+1)v^2-Av_r^2\right)\right]\times\ldots \\ \qquad\begin{pmatrix} a_0M^2+2(A+1)kT\left(a_1M+4(A+1)a_2kT\right)+ \\ M\left(a_1M+4(A+1)a_2kT\right)v_r^2+a_2M^2v_r^4\end{pmatrix}\times \\ \qquad\left[erf\left[\sqrt{\dfrac{M}{2A(A+1)kT}}\left((A+1)v'-Av_r\right)\right]-1\right] \end{cases}\right|_{v_{\min}=v-4\sqrt{\frac{2kT}{Am}}}^{\frac{h^2(v+v')}{2B^2}} \tag{4.18}$$

4.4.2.4 Solution for second integral for upscattering case

$$
\left\{
\begin{aligned}
&-\frac{(A+1)^2}{4AM^2}\frac{v'}{v}erf\left[\sqrt{\frac{M}{2kT}}(v_r-v)\right]\times\ldots \\
&\qquad\begin{pmatrix} a_0M^2+kT\left((3+2A)a_1M+(15+4A(5+2A))a_2kT\right)+ \\ M\left(a_1M+2(5+2A)a_2kT\right)v^2+a_2M^2v^4 \end{pmatrix}+ \\
&\boxed{\begin{aligned}&\frac{(A+1)^2}{4AM^2}\frac{v'}{v}erf\left[\sqrt{\frac{M}{2kT}}(v+v_r)\right]\times\ldots \\ &\qquad\begin{pmatrix} a_0M^2+kT\left((3+2A)a_1M+(15+4A(5+2A))a_2kT\right)+ \\ M\left(a_1M+2(5+2A)a_2kT\right)v^2+a_2M^2v^4 \end{pmatrix}-\end{aligned}} \\
&\frac{(A+1)^{5/2}}{4A^{3/2}M^2}\frac{v'}{v}\exp\left[\frac{M}{2A(A+1)kT}\left((A+1)v^2-Av_r^2\right)\right]\times\ldots \\
&\qquad\begin{pmatrix} a_0M^2+2(A+1)kT\left(a_1M+4(A+1)a_2kT\right)+ \\ M\left(a_1M+4(A+1)a_2kT\right)v_r^2+a_2M^2v_r^4 \end{pmatrix}\times\ldots \\
&\qquad\left[erf\left[\sqrt{\frac{M}{2A(A+1)kT}}\left((A+1)v-Av_r\right)\right]+\boxed{erf\left[\sqrt{\frac{M}{2A(A+1)kT}}\left((A+1)v+Av_r\right)\right]}\right]+ \\
&\frac{(A+1)^2}{4AM^{3/2}}\frac{v'}{v}\sqrt{\frac{2kT}{\pi}}\exp\left[-\frac{M}{2kT}(v-v_r)^2\right]\times\ldots \\
&\qquad\begin{pmatrix} v\left((9+4A)a_2kT+M\left(a_1+a_2\left(v^2+v_r^2\right)\right)\right)+ \\ v_r\left((7+4A)a_2kT+M\left(a_1+a_2\left(v^2+v_r^2\right)\right)\right) \end{pmatrix}+ \\
&\boxed{\begin{aligned}&\frac{(A+1)^2}{4AM^{3/2}}\frac{v'}{v}\sqrt{\frac{2kT}{\pi}}\exp\left[-\frac{M}{2kT}(v+v_r)^2\right]\times\ldots \\ &\qquad\begin{pmatrix} v\left((9+4A)a_2kT+M\left(a_1+a_2\left(v^2+v_r^2\right)\right)\right)- \\ v_r\left((7+4A)a_2kT+M\left(a_1+a_2\left(v^2+v_r^2\right)\right)\right) \end{pmatrix}\end{aligned}}
\end{aligned}
\right\}\Bigg|_{lbnd}^{ubnd}
$$

After further simplification, the solution for the second indefinite integral for upscatter in Eq. (4.15) is:

$$\left\{\begin{array}{l}
-\dfrac{(A+1)^2}{4AM^2}\dfrac{v'}{v}erf\left[\sqrt{\dfrac{M}{2kT}}\left(v_r-v\right)\right]\times\ldots \\
\qquad\left(\begin{array}{l} a_0M^2+kT\left(\left(3+2A\right)a_1M+\left(15+4A\left(5+2A\right)\right)a_2kT\right)+ \\ M\left(a_1M+2\left(5+2A\right)a_2kT\right)v^2+a_2M^2v^4 \end{array}\right)- \\
\\
\dfrac{(A+1)^{5/2}}{4A^{3/2}M^2}\dfrac{v'}{v}\exp\left[\dfrac{M}{2A(A+1)kT}\left((A+1)v^2-Av_r^2\right)\right]\times\ldots \\
\qquad\left(\begin{array}{l} a_0M^2+2(A+1)kT\left(a_1M+4(A+1)a_2kT\right)+ \\ M\left(a_1M+4(A+1)a_2kT\right)v_r^2+a_2M^2v_r^4 \end{array}\right)\times\ldots \\
\qquad\left[erf\left[\sqrt{\dfrac{M}{2A(A+1)kT}}\left((A+1)v-Av_r\right)\right]+1\right]+ \\
\\
\dfrac{(A+1)^2}{4AM^{3/2}}\dfrac{v'}{v}\sqrt{\dfrac{2kT}{\pi}}\exp\left[-\dfrac{M}{2kT}\left(v-v_r\right)^2\right]\times\ldots \\
\qquad\left(\begin{array}{l} v\left(\left(9+4A\right)a_2kT+M\left(a_1+a_2\left(v^2+v_r^2\right)\right)\right)+ \\ v_r\left(\left(7+4A\right)a_2kT+M\left(a_1+a_2\left(v^2+v_r^2\right)\right)\right) \end{array}\right)
\end{array}\right\}\Bigg|_{\frac{h^2(v+v')}{2B^2}}^{v_{\max}=v+4\sqrt{\frac{2kT}{Am}}} \tag{4.19}$$

4.4.3 Results

Eqs. (4.10) – (4.13), presented for the second order fit, were used to generate the scattering distribution and then were normalized to generate the P_0 moment of the scattering kernel. This was compared to the results obtained from Eqs. (4.16) – (4.19) for the fourth order fit and normalized once again to generate the P_0 moment. The results were also compared against the P_0 moment obtained from the research Monte Carlo code with DBRC.

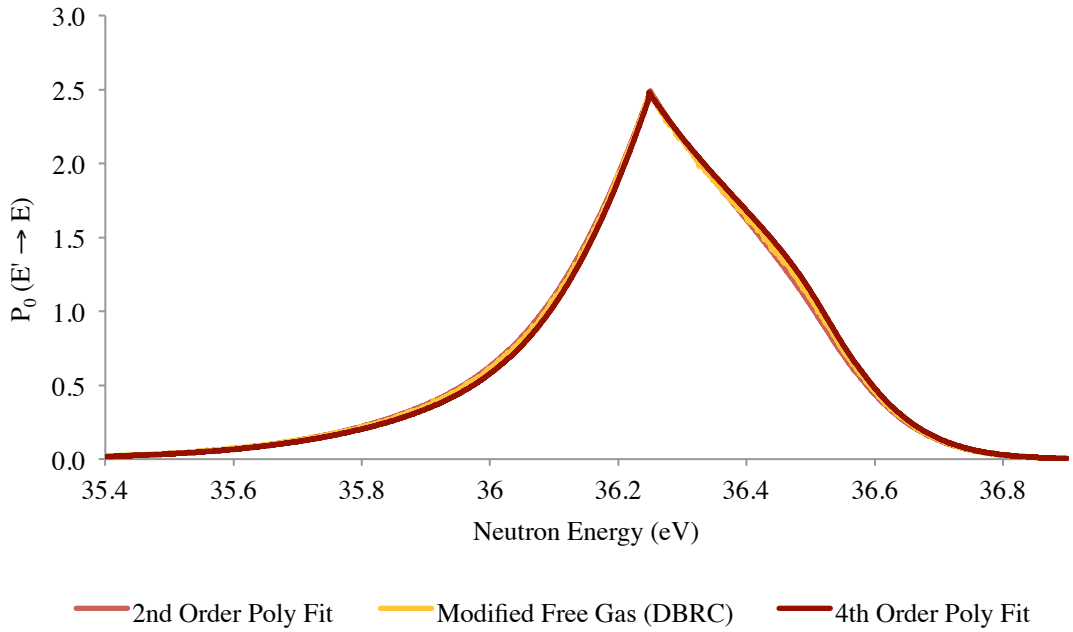

Figure 4.10: Comparison of P_0 moment of differential scattering PDF for ^{238}U at 1000 K and incident neutron speed of 36.25 eV

Figure 4.10 shows that the P_0 moment of the scattering kernel obtained with a simple approximation to the cross section provides very good results in comparison to the true P_0 moment obtained from Monte Carlo. Consequently, the P_0 moment can be used in a Monte Carlo code to predict the outgoing speed of a neutron with acceptable accuracy. Specifically, given an incident neutron energy in the laboratory frame, the outgoing energy can be sampled from the P_0 moment of the differential scattering PDF. The outgoing angle in the laboratory frame after the collision can be sampled from an isotropic distribution, where the cosine of polar angle is sampled uniformly from -1 to 1.

In order to sample the angle from a PDF other than an isotropic distribution, we have to generate higher moments. In the next section, the P_1 moment of the differential scattering PDF will be discussed. Then, using the P_0 and P_1 moments, we can form a PDF to sample for the outgoing angle of the neutron after the collision.

4.4.4 P_1 moment of differential scattering kernel

Blackshaw derived equations for the P_1 moment of the differential scattering kernel for both downscattering and upscattering cases in his dissertation [5]. However, after applying the second order approximation to the cross section and integrating the

equations, the correct first moment could not be obtained. This led to a detailed review of his derivation in [5] and a mistake was found. The mistake was corrected and the detailed derivation of the corrected P_1 moment is presented in Appendix D. The final set of equations obtained for both cases are presented below.

Downscatter ($v' < v$):

$$
\begin{aligned}
K_{1,down}(v,v') = {} & \frac{h^4}{4\sqrt{\pi}Bv^2} Exp\left[\frac{B^2v^2}{A}\right]\times\ldots \\
& \left[\int_{\frac{h^2(v-v')}{2B^2}}^{\frac{h^2(v+v')}{2B^2}} v_r\sigma(v_r)Exp\left[-\frac{B^4v_r^2}{Ah^2}\right]\times\ldots \right. \\
& \left\{\begin{array}{l}
\left[v\left(v'^2+\frac{1}{2h^2}\right)+\frac{B^2}{h^2}v_r\left(v'^2-\frac{1}{2h^2}\right)-\frac{B^4}{h^4}vv_r^2-\frac{B^6}{h^6}v_r^3\right]Exp\left[-\left(hv-\frac{B^2}{h}v_r\right)^2\right]- \\
\left[v'\left(v^2+\frac{1}{2h^2}\right)+\frac{B^2}{h^2}v_r\left(\frac{1}{2h^2}-v^2\right)-\frac{B^4}{h^4}v'v_r^2+\frac{B^6}{h^6}v_r^3\right]Exp\left[-\left(hv'+\frac{B^2}{h}v_r\right)^2\right]+ \\
\sqrt{\pi}h\left[-v'^2\left(v^2-\frac{1}{2h^2}\right)+\frac{1}{2h^2}\left(v^2+\frac{1}{2h^2}\right)+\frac{B^4}{h^4}v_r^2\left(v'^2+v^2-\frac{1}{h^2}\right)-\frac{B^8}{h^8}v_r^4\right]\times\ldots \\
\quad\left[Erf\left(hv'+\frac{B^2}{h}v_r\right)-Erf\left(hv-\frac{B^2}{h}v_r\right)\right]
\end{array}\right\}dv_r \; + \\
& \int_{\frac{h^2(v+v')}{2B^2}}^{\infty} v_r\sigma(v_r)Exp\left[-\frac{B^4v_r^2}{Ah^2}\right]\times\ldots \\
& \left\{\begin{array}{l}
\left[-v'\left(v^2+\frac{1}{2h^2}\right)+\frac{B^2}{h^2}v_r\left(\frac{1}{2h^2}-v^2\right)+\frac{B^4}{h^4}v'v_r^2+\frac{B^6}{h^6}v_r^3\right]Exp\left[-\left(\frac{B^2}{h}v_r-hv'\right)^2\right]- \\
\left[v'\left(v^2+\frac{1}{2h^2}\right)+\frac{B^2}{h^2}v_r\left(\frac{1}{2h^2}-v^2\right)-\frac{B^4}{h^4}v'v_r^2+\frac{B^6}{h^6}v_r^3\right]Exp\left[-\left(hv'+\frac{B^2}{h}v_r\right)^2\right]+ \\
\sqrt{\pi}h\left[-v'^2\left(v^2-\frac{1}{2h^2}\right)+\frac{1}{2h^2}\left(v^2+\frac{1}{2h^2}\right)+\frac{B^4}{h^4}v_r^2\left(v'^2+v^2-\frac{1}{h^2}\right)-\frac{B^8}{h^8}v_r^4\right]\times\ldots \\
\quad\left[Erf\left(hv'+\frac{B^2}{h}v_r\right)-Erf\left(\frac{B^2}{h}v_r-hv'\right)\right]
\end{array}\right\}dv_r \left.\right]
\end{aligned}
\tag{4.20}
$$

Upscatter ($v' > v$):

$$K_{1,up}\left(v,v'\right)=\frac{h^4}{4\sqrt{\pi}Bv^2}Exp\left[\frac{B^2v^2}{A}\right]\times\ldots$$

$$\left[\begin{array}{l}
\displaystyle\int_{\frac{h^2(v'-v)}{2B^2}}^{\frac{h^2(v+v')}{2B^2}} v_r\sigma\left(v_r\right)Exp\left[-\frac{B^4v_r^2}{Ah^2}\right]\times\ldots \\
\left\{\begin{array}{l}
\left[v'\left(v^2+\frac{1}{2h^2}\right)+\frac{B^2}{h^2}v_r\left(v^2-\frac{1}{2h^2}\right)-\frac{B^4}{h^4}v'v_r^2-\frac{B^6}{h^6}v_r^3\right]Exp\left[-\left(hv'-\frac{B^2}{h}v_r\right)^2\right]- \\
\left[v\left(v'^2+\frac{1}{2h^2}\right)+\frac{B^2}{h^2}v_r\left(\frac{1}{2h^2}-v'^2\right)-\frac{B^4}{h^4}vv_r^2+\frac{B^6}{h^6}v_r^3\right]Exp\left[-\left(hv+\frac{B^2}{h}v_r\right)^2\right]+ \\
\sqrt{\pi}h\left[-v^2\left(v'^2-\frac{1}{2h^2}\right)+\frac{1}{2h^2}\left(v'^2+\frac{1}{2h^2}\right)+\frac{B^4}{h^4}v_r^2\left(v'^2+v^2-\frac{1}{h^2}\right)-\frac{B^8}{h^8}v_r^4\right]\times\ldots \\
\quad\left[Erf\left(hv+\frac{B^2}{h}v_r\right)-Erf\left(hv'-\frac{B^2}{h}v_r\right)\right]
\end{array}\right\}dv_r \\
+ \\
\displaystyle\int_{\frac{h^2(v+v')}{2B^2}}^{\infty} v_r\sigma\left(v_r\right)Exp\left[-\frac{B^4v_r^2}{Ah^2}\right]\times\ldots \\
\left\{\begin{array}{l}
\left[-v\left(v'^2+\frac{1}{2h^2}\right)+\frac{B^2}{h^2}v_r\left(\frac{1}{2h^2}-v'^2\right)+\frac{B^4}{h^4}vv_r^2+\frac{B^6}{h^6}v_r^3\right]Exp\left[-\left(\frac{B^2}{h}v_r-hv\right)^2\right]- \\
\left[v\left(v'^2+\frac{1}{2h^2}\right)+\frac{B^2}{h^2}v_r\left(\frac{1}{2h^2}-v'^2\right)-\frac{B^4}{h^4}vv_r^2+\frac{B^6}{h^6}v_r^3\right]Exp\left[-\left(hv+\frac{B^2}{h}v_r\right)^2\right]+ \\
\sqrt{\pi}h\left[-v^2\left(v'^2-\frac{1}{2h^2}\right)+\frac{1}{2h^2}\left(v'^2+\frac{1}{2h^2}\right)+\frac{B^4}{h^4}v_r^2\left(v'^2+v^2-\frac{1}{h^2}\right)-\frac{B^8}{h^8}v_r^4\right]\times\ldots \\
\quad\left[Erf\left(hv+\frac{B^2}{h}v_r\right)-Erf\left(\frac{B^2}{h}v_r-hv\right)\right]
\end{array}\right\}dv_r
\end{array}\right] \tag{4.21}$$

The second order approximation to the cross section was applied, $\sigma_s\left(v_r\right)=a_0+a_1v_r^2$, and the solutions are presented in the next few subsections. The solutions for the P_1 moment presented in this chapter have already been simplified and

this simplification process has not been shown. Only the final equations are presented in the following subsections.

4.4.4.1 Solution for first integral for downscattering case

The solution for the first indefinite integral for downscattering in Eq. (4.209) consists of four parts, which are shown in this section,

$$Integral\_1\_down = \left[Int1pt1 + Int1pt2 + Int1pt3 + Int1pt4 \right]_{v_{\min}=v-4\sqrt{\frac{2kT}{Am}}}^{\frac{h^2(v+v')}{2B^2}} \tag{4.22}$$

The four terms are:

$$Int1pt1 = \frac{1}{8A^2M^{3/2}v^2\sqrt{2\pi kT}}\exp\left[-\frac{M}{2kT}\left(v-v_r\right)^2\right]\times$$

$$\left[\begin{array}{l}
24A^5a_1k^2T^2\left(v+v_r\right)-Mvv'^2\left(a_0M+2a_1kT+a_1Mv_r^2\right)+ \\
2A^4kT\left(2a_0M\left(v+v_r\right)+a_1\left(kT\left(31v+25v_r\right)+M\left(v+v_r\right)\left(v^2-2v'^2+3v_r^2\right)\right)\right)- \\
A\left(\begin{array}{l} a_0M\left(kTv+Mv'^2\left(3v+v_r\right)\right)+ \\ a_1\left(\begin{array}{l} 2k^2T^2v+M^2v'^2v_r^2\left(3v+v_r\right)+ \\ kTM\left(2v^3+10vv'^2+2v^2v_r+4v'^2v_r+vv_r^2\right)\end{array}\right)\end{array}\right)+ \\
A^2\left(\begin{array}{l} a_0M\left(kT\left(2v+v_r\right)+M\left(-3vv'^2-2v'^2v_r+vv_r^2\right)\right)+ \\ a_1\left(\begin{array}{l} 2k^2T^2\left(5v+v_r\right)+M^2v_r^2\left(-3vv'^2-2v'^2v_r+vv_r^2\right)+ \\ kTM\left(-2v\left(v^2+9v'^2\right)-2\left(v^2+6v'^2\right)v_r+4vv_r^2+v_r^3\right)\end{array}\right)\end{array}\right)+ \\
A^3\left(\begin{array}{l} a_0M\left(kT\left(7v+5v_r\right)+M\left(v+v_r\right)\left(v_r^2-v'^2\right)\right)+ \\ a_1\left(\begin{array}{l} 2k^2T^2\left(25v+14v_r\right)+M^2v_r^2\left(v+v_r\right)\left(v_r^2-v'^2\right)+ \\ kTM\left(2v\left(v^2-7v'^2\right)+2\left(v^2-6v'^2\right)v_r+11vv_r^2+7v_r^3\right)\end{array}\right)\end{array}\right)
\end{array}\right],$$

$$Int1pt2 = -\frac{(A+1)^2}{8AM^2v^2} erf\left[\sqrt{\frac{M}{2kT}}(v_r - v)\right] \times$$

$$\begin{bmatrix} 24A^3a_1k^2T^2 - M\left(a_0M + 3a_1kT + a_1Mv^2\right)\left(v^2 + v'^2\right) + \\ AM\left(v^2\left(a_0M + 3a_1kT + a_1Mv^2\right) - \left(a_0M + 7a_1kT + a_1Mv^2\right)v'^2\right) + \\ 4A^2kT\left(5a_1kT + M\left(a_0 + 2a_1v^2 - a_1v'^2\right)\right) \end{bmatrix}$$

$$Int1pt3 = \sqrt{\frac{A+1}{A}} Exp\left[\frac{M}{2A(A+1)kT}\left((A+1)v^2 - Av_r^2\right)\right]\left\{Erf\left[\sqrt{\frac{M}{2A(A+1)kT}}\left((A+1)v - Av_r\right)\right] - 1\right\} \times$$

$$\begin{bmatrix} \frac{(A+1)}{16A^2M^2v^2kT}\left(2(A+1)a_1kT + M\left(a_0 + a_1v_r^2\right)\right)\begin{pmatrix} AkT\left(AkT + (A+1)Mv^2\right) - \\ M(A+1)\left(-AkT + (A+1)Mv^2\right)v'^2 \end{pmatrix} + \\ \frac{\left(-2AkT + Mv^2 + AMv^2 + (A+1)Mv'^2\right)}{16M^2v^2kT}\begin{pmatrix} 2(A+1)kT\left(a_0M + 4(A+1)a_1kT\right) + \\ M\left(a_0M + 4(A+1)a_1kT\right)v_r^2 + a_1M^2v_r^4 \end{pmatrix} \end{bmatrix},$$

$$Int1pt4 = \sqrt{\frac{A+1}{A}} Exp\left[\frac{M}{2A(A+1)kT}\left((A+1)v^2 - Av_r^2\right)\right]\left\{1 - Erf\left[\sqrt{\frac{M}{2A(A+1)kT}}\left((A+1)v - Av_r\right)\right]\right\} \times$$

$$\begin{bmatrix} \frac{A^2a_0}{16(A+1)Mv^2kT}\left(8(A+1)^2k^2T^2 + 4(A+1)kTMv_r^2 + M^2v_r^4\right) + \\ \frac{A^2a_1}{16(A+1)M^2v^2kT}\left(48(A+1)^3k^3T^3 + 24(A+1)^2k^2T^2Mv_r^2 + 6(A+1)kTM^2v_r^4 + M^3v_r^6\right) \end{bmatrix}.$$

4.4.4.2 Solution for second integral for downscattering case

The solution for the second indefinite integral for downscattering in Eq. (4.20) consists of three parts,

$$Integral\_2\_down = \left[Int2pt1 + Int2pt2 + Int2pt3 \right]_{\frac{h^2(v+v')}{2B^2}}^{v_{\max}=v+4\sqrt{\frac{2kT}{Am}}} \tag{4.23}$$

The three terms are:

$$Int2pt1 = -\frac{1}{8A^2M^{3/2}v^2\sqrt{2\pi kT}}\exp\left[-\frac{M}{2AkT}\left(-v^2+(A+1)v'^2-2Av_rv'+Av_r^2\right)\right]\times$$

$$\left[\begin{array}{l}
24A^5a_1k^2T^2(v'+v_r)-Mv^2v'\left(a_0M+2a_1kT+a_1Mv_r^2\right)+ \\
2A^4kT\left(2a_0M(v'+v_r)+a_1\left(kT(31v'+25v_r)+M(v'+v_r)\left(-2v^2+v'^2+3v_r^2\right)\right)\right)+ \\
A^2\left(\begin{array}{l} a_0M\left(kT(2v'+v_r)+M\left(v'v_r^2-v^2(3v'+2v_r)\right)\right)+ \\ a_1\left(\begin{array}{l} 2k^2T^2(5v'+v_r)+kTM\left(-2v'^3-2v'^2v_r+4v'v_r^2+v_r^3-6v^2(3v'+2v_r)\right)+ \\ M^2v_r^2\left(v'v_r^2-v^2(3v'+2v_r)\right)\end{array}\right)\end{array}\right)+ \\
A^3\left(\begin{array}{l} a_0M\left(kT(7v'+5v_r)+M(v'+v_r)\left(v_r^2-v^2\right)\right)+ \\ a_1\left(\begin{array}{l} 2k^2T^2(25v'+14v_r)+M^2v_r^2(v'+v_r)\left(v_r^2-v^2\right)+ \\ kTM\left(2v'^3+2v'^2v_r+11v'v_r^2+7v_r^3-2v^2(7v'+6v_r)\right)\end{array}\right)\end{array}\right)- \\
A\left(\begin{array}{l} a_0M\left(kTv'+Mv^2(3v'+v_r)\right)+ \\ a_1\left(2k^2T^2v'+M^2v^2v_r^2(3v'+v_r)+kTM\left(2v^2(5v'+2v_r)+v'\left(2v'^2+2v'v_r+v_r^2\right)\right)\right)\end{array}\right)
\end{array}\right],$$

$$Int2pt2 = \frac{(A+1)^2}{8AM^2v^2}\exp\left[\frac{M}{2AkT}\left(v^2 - v'^2\right)\right] erf\left[\sqrt{\frac{M}{2kT}}\left(v_r - v'\right)\right]\times$$

$$\left[\begin{array}{l} 24A^3a_1k^2T^2 - M\left(v^2+v'^2\right)\left(a_0M + 3a_1kT + a_1Mv'^2\right) + \\ AM\left(-\left(a_0M+7a_1kT\right)v^2 + \left(a_0M + 3a_1kT - a_1Mv^2\right)v'^2 + a_1Mv'^4\right) + \\ 4A^2kT\left(5a_1kT + M\left(a_0 - a_1v^2 + 2a_1v'^2\right)\right) \end{array}\right],$$

$$Int2pt3 = \frac{1}{16A^{5/2}(A+1)^{1/2}M^2v^2kT}\exp\left[\frac{M}{2A(A+1)kT}\left[(A+1)v^2 - Av_r^2\right]\right]\times$$

$$\left\{1 + erf\left[\sqrt{\frac{M}{2A(A+1)kT}}\left((A+1)v' - Av_r\right)\right]\right\}\times$$

$$\left[\begin{array}{l} -(A+1)^2\left(AkT\left(AkT + (A+1)Mv^2\right) - (A+1)M\left(-AkT + (A+1)Mv^2\right)v'^2\right)\times \\ \quad\left(a_0M + 2(A+1)a_1kT + a_1Mv_r^2\right) + \\ A^4a_0M\left(8(A+1)^2k^2T^2 + 4(A+1)kTMv_r^2 + M^2v_r^4\right) - \\ A^2(A+1)\left(-2AkT + Mv^2 + AMv^2 + (A+1)Mv'^2\right)\left(\begin{array}{l} 2(A+1)kT\left(a_0M + 4(A+1)a_1kT\right) + \\ M\left(a_0M + 4(A+1)a_1kT\right)v_r^2 + a_1M^2v_r^4 \end{array}\right) + \\ A^4a_1\left(48(A+1)^3k^3T^3 + 24(A+1)^2k^2MT^2v_r^2 + 6(A+1)kM^2Tv_r^4 + M^3v_r^6\right) \end{array}\right].$$

4.4.4.3 Solution for first integral for upscattering case

The solution for the first indefinite integral for upscattering in Eq. (4.21) consists of three parts,

$$Integral\_1\_up = \left[Int1pt1 + Int1pt2 + Int1pt3 \right]_{v_{\min}=v-4\sqrt{\frac{2kT}{Am}}}^{\frac{h^2(v+v')}{2B^2}} \tag{4.24}$$

The three terms are:

$$Int1pt1 = \frac{1}{8A^2M^{3/2}v^2\sqrt{2\pi kT}}\exp\left[-\frac{M}{2AkT}\left(-v^2+(A+1)v'^2-2Av_rv'+Av_r^2\right)\right]\times$$

$$\left[\begin{array}{l}
24A^5a_1k^2T^2(v'+v_r)-Mv^2v'\left(a_0M+2a_1kT+a_1Mv_r^2\right)+ \\
2A^4kT\left(2a_0M(v'+v_r)+a_1\left(kT(31v'+25v_r)+M(v'+v_r)\left(-2v^2+v'^2+3v_r^2\right)\right)\right)+ \\
A^2\left(\begin{array}{l} a_0M\left(kT(2v'+v_r)+M\left(v'v_r^2-v^2(3v'+2v_r)\right)\right)+ \\ a_1\left(\begin{array}{l} 2k^2T^2(5v'+v_r)+kTM\left(-2v'^3-2v'^2v_r+4v'v_r^2+v_r^3-6v^2(3v'+2v_r)\right)+ \\ M^2v_r^2\left(v'v_r^2-v^2(3v'+2v_r)\right)\end{array}\right)\end{array}\right)+ \\
A^3\left(\begin{array}{l} a_0M\left(kT(7v'+5v_r)+M(v'+v_r)\left(v_r^2-v^2\right)\right)+ \\ a_1\left(\begin{array}{l} 2k^2T^2(25v'+14v_r)+M^2v_r^2(v'+v_r)\left(v_r^2-v^2\right)+ \\ kTM\left(2v'^3+2v'^2v_r+11v'v_r^2+7v_r^3-2v^2(7v'+6v_r)\right)\end{array}\right)\end{array}\right)- \\
A\left(\begin{array}{l} a_0M\left(kTv'+Mv^2(3v'+v_r)\right)+ \\ a_1\left(2k^2T^2v'+M^2v^2v_r^2(3v'+v_r)+kTM\left(2v^2(5v'+2v_r)+v'\left(2v'^2+2v'v_r+v_r^2\right)\right)\right)\end{array}\right)
\end{array}\right],$$

$$Int1pt2 = -\frac{(A+1)^2}{8AM^2v^2}\exp\left[\frac{M}{2AkT}\left(v^2 - v'^2\right)\right] erf\left[\sqrt{\frac{M}{2kT}}\left(v_r - v'\right)\right]\times$$

$$\left[\begin{array}{l} 24A^3a_1k^2T^2 - M\left(v^2+v'^2\right)\left(a_0M + 3a_1kT + a_1Mv'^2\right) + \\ AM\left(-\left(a_0M+7a_1kT\right)v^2 + \left(a_0M + 3a_1kT - a_1Mv^2\right)v'^2 + a_1Mv'^4\right) + \\ 4A^2kT\left(5a_1kT + M\left(a_0 - a_1v^2 + 2a_1v'^2\right)\right) \end{array}\right],$$

$$Int1pt3 = \frac{1}{16A^{5/2}(A+1)^{1/2}M^2v^2kT}\exp\left[\frac{M}{2A(A+1)kT}\left[(A+1)v^2 - Av_r^2\right]\right]\times$$

$$\left\{erf\left[\sqrt{\frac{M}{2A(A+1)kT}}\left((A+1)v' - Av_r\right)\right] - 1\right\}\times$$

$$\left[\begin{array}{l} (A+1)^2\left(AkT\left(AkT + (A+1)Mv^2\right) - (A+1)M\left(-AkT + (A+1)Mv^2\right)v'^2\right)\times \\ \quad\left(a_0M + 2(A+1)a_1kT + a_1Mv_r^2\right) - \\ A^4a_0M\left(8(A+1)^2k^2T^2 + 4(A+1)kTMv_r^2 + M^2v_r^4\right) - \\ A^2(A+1)\left(-M\left(v^2+v'^2\right) + A\left(2kT - M\left(v^2+v'^2\right)\right)\right)\left(\begin{array}{l} 2(A+1)kT\left(a_0M + 4(A+1)a_1kT\right) + \\ M\left(a_0M + 4(A+1)a_1kT\right)v_r^2 + a_1M^2v_r^4 \end{array}\right) - \\ A^4a_1\left(48(A+1)^3k^3T^3 + 24(A+1)^2k^2MT^2v_r^2 + 6(A+1)kM^2Tv_r^4 + M^3v_r^6\right) \end{array}\right].$$

4.4.4.4 Solution for second integral for upscattering case

The solution for the second indefinite integral for upscattering in Eq. (4.21) consists of three parts,

$$Integral\_2\_up = \left[Int2pt1 + Int2pt2 + Int2pt3 \right]_{\frac{h^2(v+v')}{2B^2}}^{v_{\max}=v+4\sqrt{\frac{2kT}{Am}}} \tag{4.25}$$

The three terms are:

$$Int2pt1 = \frac{1}{8A^2M^{3/2}v^2\sqrt{2\pi kT}}\exp\left[-\frac{M}{2kT}\left(v-v_r\right)^2\right]\times$$

$$\left[\begin{array}{l}
-24A^5a_1k^2T^2\left(v+v_r\right)+Mvv'^2\left(a_0M+2a_1kT+a_1Mv_r^2\right)- \\
2A^4kT\left(2a_0M\left(v+v_r\right)+a_1\left(kT\left(31v+25v_r\right)+M\left(v+v_r\right)\left(v^2-2v'^2+3v_r^2\right)\right)\right)+ \\
A\left(\begin{array}{l} a_0M\left(kTv+Mv'^2\left(3v+v_r\right)\right)+ \\ a_1\left(\begin{array}{l} 2k^2T^2v+M^2v'^2v_r^2\left(3v+v_r\right)+ \\ kTM\left(2v^3+10vv'^2+2v^2v_r+4v'^2v_r+vv_r^2\right)\end{array}\right)\end{array}\right)- \\
A^2\left(\begin{array}{l} a_0M\left(kT\left(2v+v_r\right)+M\left(-3vv'^2-2v'^2v_r+vv_r^2\right)\right)+ \\ a_1\left(\begin{array}{l} 2k^2T^2\left(5v+v_r\right)+M^2v_r^2\left(-3vv'^2-2v'^2v_r+vv_r^2\right)+ \\ kTM\left(-2v\left(v^2+9v'^2\right)-2\left(v^2+6v'^2\right)v_r+4vv_r^2+v_r^3\right)\end{array}\right)\end{array}\right)- \\
A^3\left(\begin{array}{l} a_0M\left(kT\left(7v+5v_r\right)+M\left(v+v_r\right)\left(v_r^2-v'^2\right)\right)+ \\ a_1\left(\begin{array}{l} 2k^2T^2\left(25v+14v_r\right)+M^2v_r^2\left(v+v_r\right)\left(v_r^2-v'^2\right)+ \\ kTM\left(2v\left(v^2-7v'^2\right)+2\left(v^2-6v'^2\right)v_r+11vv_r^2+7v_r^3\right)\end{array}\right)\end{array}\right)
\end{array}\right],$$

$$Int2pt2 = \frac{1}{16A(A+1)M^2v^2kT} \times$$

$$\left[\begin{array}{l} -A^3a_1\begin{pmatrix} 3(19+22A+8A^2)k^3T^3+3(35+4A(7+2A))k^2MT^2v^2+ \\ 3(7+2A)kM^2Tv^4+M^3v^6 \end{pmatrix}+ \\ 2(A+1)^3kT\begin{pmatrix} 24A^3a_1k^2T^2-M(a_0M+3a_1kT+a_1Mv^2)(v^2+v'^2)+ \\ AM\begin{pmatrix} v^2(a_0M+3a_1kT+a_1Mv^2)- \\ (a_0M+7a_1kT+a_1Mv^2)v'^2 \end{pmatrix}+ \\ 4A^2kT(5a_1kT+M(a_0+2a_1v^2-a_1v'^2)) \end{pmatrix} erf\left[\sqrt{\frac{M}{2kT}}(v_r-v)\right] \end{array}\right],$$

$$Int2pt3 = \frac{1}{16A^{5/2}(A+1)^{1/2}M^2v^2kT}\exp\left[\frac{M}{2A(A+1)kT}\left((A+1)v^2-Av_r^2\right)\right]\times$$

$$\left\{1+erf\left[\sqrt{\frac{M}{2A(A+1)kT}}\left((A+1)v-Av_r\right)\right]\right\}\times$$

$$\left[\begin{array}{l} -(A+1)^2\left(AkT(AkT+(A+1)Mv^2)-(A+1)M(-AkT+(A+1)Mv^2)v'^2\right)\times \\ \quad (a_0M+2(A+1)a_1kT+a_1Mv_r^2)+ \\ A^4a_0M\left(8(A+1)^2k^2T^2+4(A+1)kTMv_r^2+M^2v_r^4\right)- \\ A^2(A+1)\left(-2AkT+Mv^2+AMv^2+(A+1)Mv'^2\right)\begin{pmatrix} 2(A+1)kT(a_0M+4(A+1)a_1kT)+ \\ M(a_0M+4(A+1)a_1kT)v_r^2+a_1M^2v_r^4 \end{pmatrix}+ \\ A^4a_1\left(48(A+1)^3k^3T^3+24(A+1)^2k^2MT^2v_r^2+6(A+1)kM^2Tv_r^4+M^3v_r^6\right) \end{array}\right].$$

4.4.5 Results

The P_1 moment generated on-the-fly with the second order approximation applied to the scattering cross section with 41 piecewise regions was compared to the reference P_1 moment obtained from a research Monte Carlo code with DBRC. These coefficients for the scattering cross sections were generated using least squares fitting and are provided in Appendix C, Section C.3. It must be noted that it may be possible to reduce these equations into a simpler form. In this dissertation, the simplifications were kept to a minimum in order to preserve the accuracy. Future studies may focus on further simplification of these equations and their optimization.

Figure 4.11 shows a comparison of the results for P_1 moment obtained from Monte Carlo with DBRC, and to the moment generated on-the-fly using the 2nd order approximation.

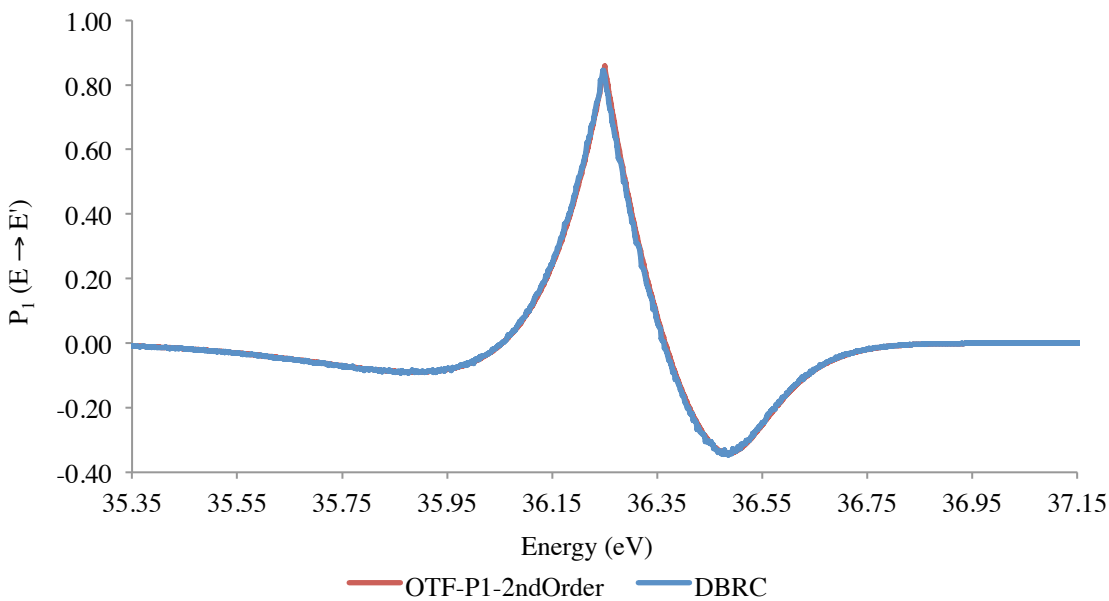

Figure 4.11: Comparison of P_1 moment of differential scattering PDF for ^{238}U at 1000 K and incident neutron energy of 36.25 eV

In Figure 4.11, the red line is the P_1 moment generated on-the-fly using the 2nd order approximation for the cross section. The blue line represents the P_1 moment of the scattering PDF obtained from Monte Carlo with DBRC. The results in the figure indicate that the P_1 moment generated on-the-fly compares very well with the P_1 moment obtained

from DBRC. Using the P_0 and P_1 moments, it is possible to develop an alternative method that can be implemented to calculate k_{eff} in criticality calculations. The exiting energy of the neutron can be determined by the P_0 moment and the angle can be determined by the PDF formed from the P_0 and P_1 moments of the differential scattering PDF. However, this truncated PDF, which uses only two moments, can lead to some difficulties. These issues are discussed in the next section.

4.4.6 Truncated PDFs using Legendre moments

Once the P_0 and P_1 moments were generated on-the-fly, a problem arose because the PDF represented by these moments could at times become negative, and therefore, unphysical. This behavior is explained in more detail in this section and ways to overcome this issue are also described.

The Legendre expansion is given by [9], [10],

$$f(\mu) = \sum_{n=0}^{N} \frac{2n+1}{2} a_n P_n(\mu). \qquad (-1 \le \mu \le 1)$$

It is possible to obtain a negative PDF over part of the range of μ when the PDF is a truncated Legendre expansion of the true (always positive) PDF. The PDF to sample μ can be built from the P_0 and P_1 moments as shown [9], [10]:

$$f(\mu) = \frac{1}{2} P_0 + \frac{3}{2} \mu P_1, \qquad (-1 \le \mu \le 1)$$

$$f(\mu) = \frac{1}{2} + \frac{3}{2} \mu \bar{\mu}. \tag{4.26}$$

Figure 4.1, reintroduced in this section as Figure 4.12, clearly shows why it is possible to obtain negative probabilities when forming PDFs from truncated Legendre expansions.

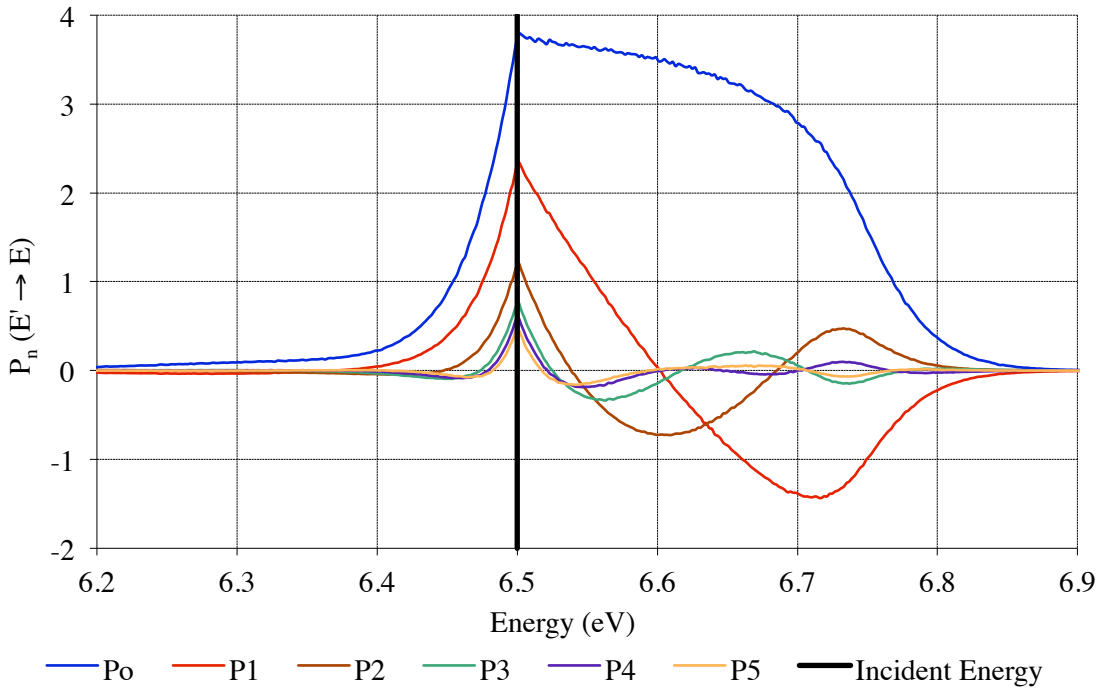

Figure 4.12: Legendre moments of differential scattering PDFs generated with DBRC for incident neutron energy of 6.5 eV scattering in ^{238}U at 1000 K

If $|\bar{\mu}| \leq \frac{1}{3}$, then $f(\mu) > 0$ where $\mu \in [-1,1]$, otherwise, $f(\mu) < 0$. An example of this behavior is shown in Figure 4.13.

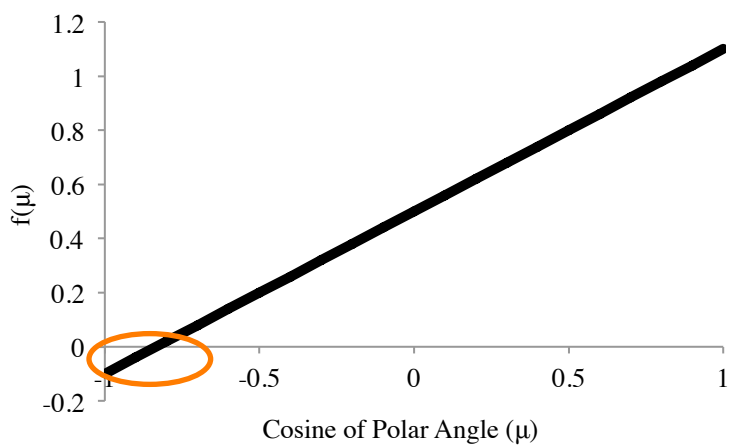

Figure 4.13: $f(\mu) = \frac{1}{2} + \frac{3}{2}\mu\bar{\mu}$ for $\bar{\mu} = 0.4$

There are different ways to take into account this unphysical behavior. In [9], F. Brown *et. al.* recommend using a step function to represent the unphysical values. If $|\bar{\mu}| > 1/3$, then $f(\mu)$ can be replaced by a PDF, $g(\mu)$, that will preserve $\bar{\mu}$. The PDF $g(\mu)$ can be represented by a step function, as shown in Figure 4.14, where $g(\mu) > 0$.

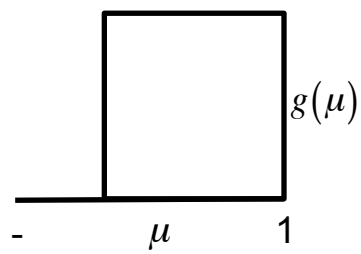

Figure 4.14: New PDF, $g(\mu)$, representing a step function

Since we are trying to preserve, $\bar{\mu} = \int_{-1}^{1} \mu g(\mu)\, d\mu$, we can sample for the angle in the following [9] [10]:

- If $\bar{\mu} > 1/3$, then choose the exiting neutron angle after a collision from $[2\bar{\mu} - 1, 1]$.
- If $\bar{\mu} < -1/3$, then choose the exiting neutron angle after a collision from $[-1, 2\bar{\mu} + 1]$.
- Otherwise, choose angle from $f(\mu) = 1/2 + 3/2\, \mu\bar{\mu}$.

We are able to avoid the issue of having to sample a cosine from a negative PDF by following these steps.

4.5 Conclusion

In summary, the even-ordered approximations for the cross sections are sufficient to approximate the moments of the differential scattering PDF well. Studies done in this chapter showed that there is no need to use an expensive method that takes into account resonance scattering effects for the entire epithermal range. It is sufficient to just account for resonance scattering effects around very specific energies, for resonances with high scattering to absorption ratios in the lower epithermal region. Also, the integration limits

for the equations used in this chapter were modified to represent the bounds used to perform the second rejection test in DBRC. We learned that it is possible to obtain negative PDFs when using only the first two moments. So, we discussed a method where a second function is chosen to preserve the average angle, which is used to develop an algorithm to sample for the angle from the PDF. All this information was applied, and an algorithm will be outlined in Chapter 5 that will look at the generation of the moments on-the-fly. In Chapter 5, results obtained from a research Monte Carlo code on neutron escape probabilities will also be presented. Finally, these scattering models were inserted into MCNP to determine k_{eff} from criticality calculations for a fuel pin and a 2D assembly problem.

4.6 References

[1] T. Högberg, *Monte Carlo calculations of neutron thermalization in a heterogeneous system*, J. Nucl. Energy, Part A: Reactor Science, **12** pp. 145-150 (1960).

[2] G. Arbanas, M. E. Dunn, N. M. Larson, L. C. Leal, M. L. Williams, B. Becker, and R. Dagan, *Computation of Temperature-Dependent Legendre Moments of A Differential Elastic Cross Section*, International Conference on Mathematics and Computational Methods Applied to Nuclear Science and Engineering Conference Proceeding, Brazil (2011).

[3] M. Ouisloumen and R. Sanchez, *A Model for Neutron Scattering Off Heavy Isotopes That Accounts for Thermal Agitation Effects*, Nuclear Science and Engineering, **107**, pp. 189-200 (1991).

[4] G. L. Blackshaw and R. L. Murray, *Scattering Functions for Low-Energy Neutron Collisions in a Maxwellian Monatomic Gas*, Nuclear Science and Engineering, **27** pp. 520-532 (1967).

[5] G. L. Blackshaw, *Scattering of Low-Energy Neutrons In a Monatomic Gas Model Of A Multiplying System*, North Carolina State University, Raleigh, Ph.D. Thesis (1966).

[6] B. Becker, *On the Influence of the Resonance Scattering Treatment in Monte Carlo Codes on High Temperature Reactor Characteristics*, Institut für Kernenergetik und Energiesysteme, Universitât Stuttgart, Thesis (2010).

[7] R. D. Mosteller, *Computational Benchmarks for the Doppler Reactivity Defect*, LA-UR-06-2968, Los Alamos National Laboratory.

[8] Wolfram Research, Inc. *Mathematica Edition: Version 8.0*, Champaign Illinois (2008).

[9] F. Brown and N. Barnett, *One-group MCNP5 Criticality Calculations with Anisotropic Scattering*, LA-UR-08-0567, Los Alamos National Laboratory (2008).

[10] F. Brown and N. Barnett, *A tutorial on Using MCNP for 1-group Transport Calculations*, LA-UR-07-4594, Los Alamos National Laboratory.

[11] B. Becker, R. Dagan & G. Lohnert, *Proof and implementation of the stochastic formula for ideal gas, energy dependent scattering kernel*, Annals of Nuclear Energy, **36**, pp. 470 – 474 (2009).

[12] X-5 Monte Carlo Team, *MCNP – A General Monte Carlo N-Particle Transport Code, Version 5, Volume I: Overview and Theory*, LA-UR-03-1987, Los Alamos National Laboratory (2003).

[13] R. D. Mosteller, *ENDF/B-V, ENDF/B-VI, and ENDF/B-VII.0 Results for the Doppler-defect Benchmark*, Proceedings from M&C+SNA, Monterey, CA (2007).

CHAPTER 5

Results And Analysis of the On-The-Fly Resonance Scattering Method

5.1 Introduction

Chapter 4 presented the equations to generate P_0 and P_1 moments of the differential scattering probability distribution function (PDF) on-the-fly. Moments of the PDFs were shown to be very accurate even with the even-order approximations made to the scattering cross sections. This chapter will discuss the applications of these moments, along with stringent test problems that were set up in a research Monte Carlo code with different scattering models to assess the sensitivity and accuracy of the resonance scattering methodology. This chapter will also discuss the implementation of the new scattering models that were implemented into MCNP5 [1], allowing for the analysis of more complex geometries, i.e. a light water reactor (LWR) fuel pin cell and a Westinghouse 17x17 fuel assembly, with the new and existing scattering models in MCNP5. Before launching into the analysis of the results, a brief discussion of on-the-fly generation of PDFs will be discussed.

5.2 Generating Probability Distribution Functions On-The-Fly

To generate the PDF, the incoming neutron energy was registered and the energy grid for the PDF was produced. This energy grid was based on the bounds used for the rejection technique in DBRC, which significantly sped up the PDF generation. The integration of the energies outside these bounds did not change the PDF significantly, because the scattering probability was expected to be close to zero beyond those points, as discussed in Chapter 4.

Once the incident neutron energy was registered and the bounds were determined for the PDF, the grid was constructed starting at the incident energy and was built

outwards until the bounds were reached. The PDF was constructed on a uniform grid for work in this dissertation. The bounds were modified to extend beyond the original bounds to preserve the uniform energy grid. It is necessary to construct the grid from the incident neutron energy towards the tails of the PDF because it is important to preserve the peak of the PDF, which occurs in the bin with the incident neutron energy. A visual interpretation of this PDF construction is shown in Figure 5.1, below.

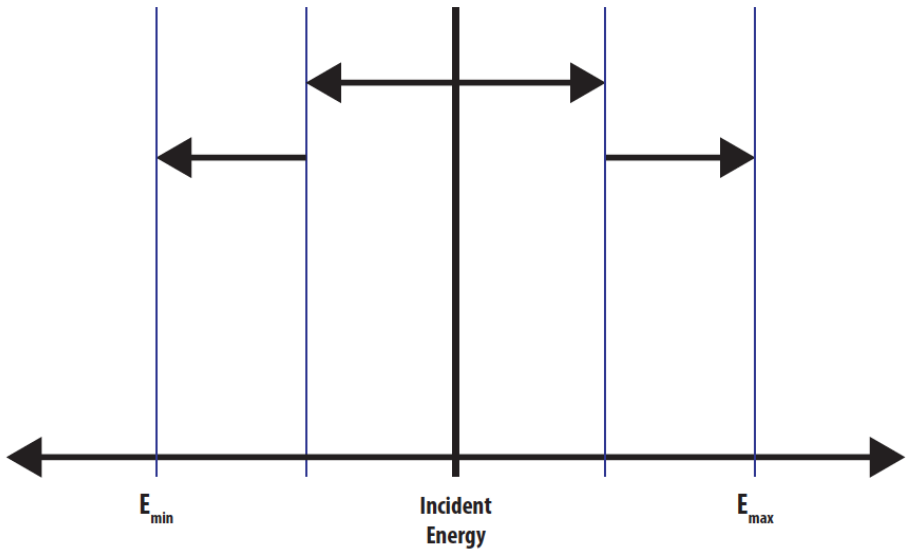

Figure 5.1: Grid for PDF generation

This energy grid now represents the outgoing neutron energies, which was used to generate the PDF. If the grid was not constructed from the incident neutron energy, then the peak was shifted. Examples of this are shown in Figure 5.2 for a differential scattering PDF with energy widths from 0.002 eV to 0.1 eV. When the grid was constructed from the incident neutron energy to the tails of the PDF, the peak of the PDF was preserved and this is shown in Figure 5.3. The various colored lines represent the different energy widths used to generate the grid. In Figures 5.2 and 5.3, each colored line represents the corresponding energy widths of the grid, as shown in the legend.

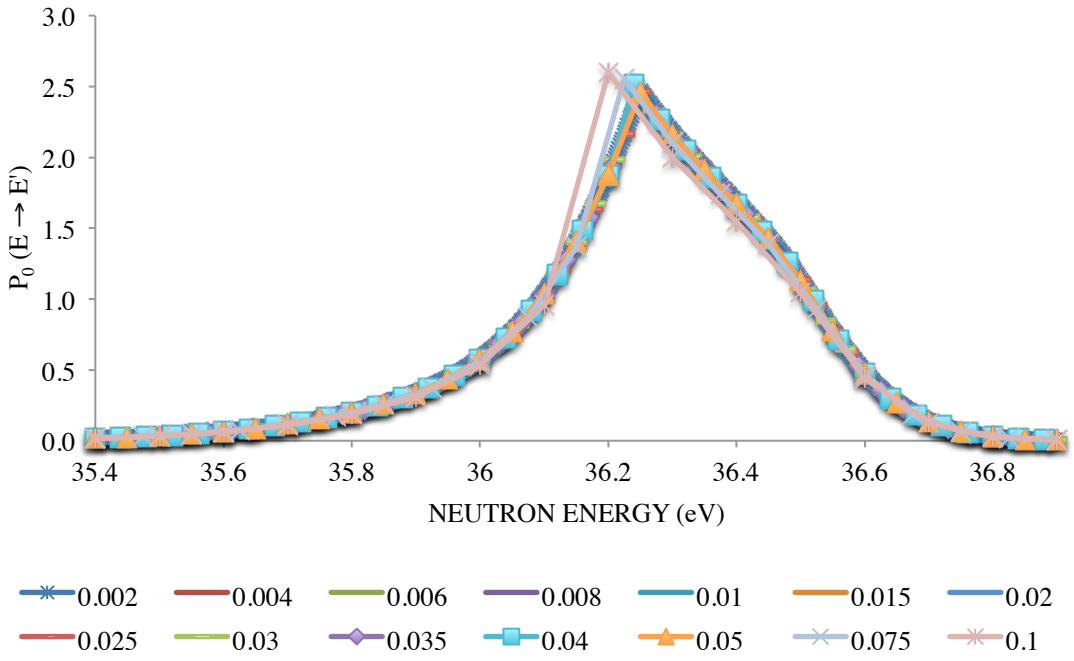

Figure 5.2: Differential scattering PDF (for incident neutron energy of 36.25 eV and ^{238}U at 1000 K) constructed on a grid not preserving the peak at the incident neutron energy

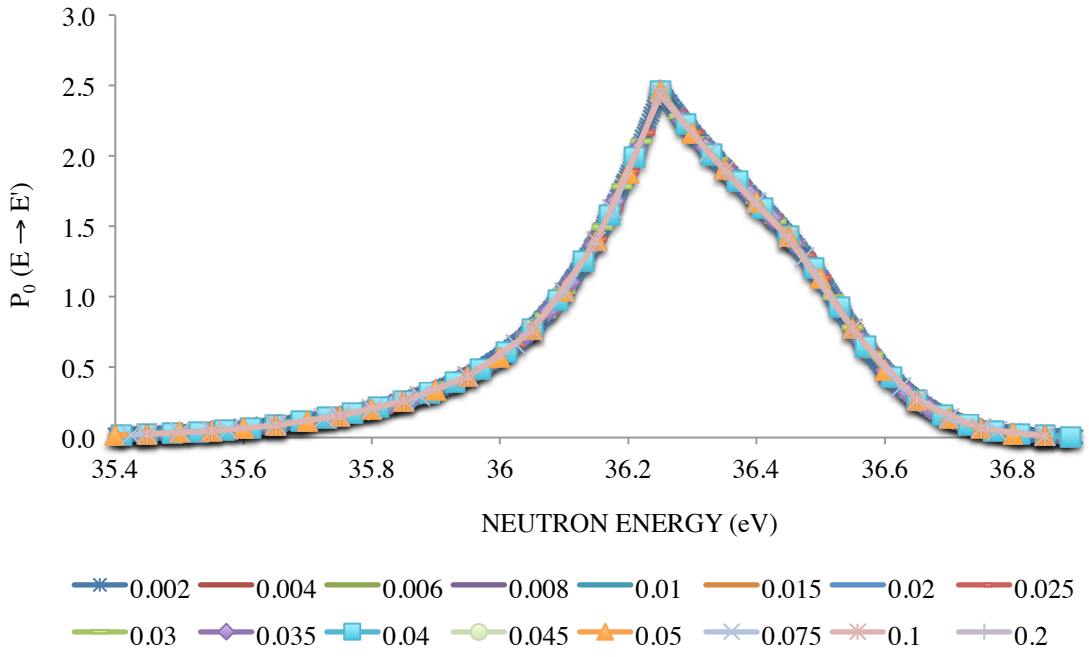

Figure 5.3: Differential scattering PDF (for incident neutron energy of 36.25 eV and ^{238}U at 1000K) constructed on a grid preserving the peak at the incident neutron energy

Once the energy grid was generated, the next step was to convert the energy grid from units of eV to units of m/s since the cross section fits were done as a function of neutron speed in units of m/s. Next, loops were set up to determine the differential scattering PDF. Since the equations presented in Chapter 4 have to be calculated for outgoing speeds, as determined by the energy grid, the newly constructed grid formed the outermost loop. The analytical solutions to the equations in Chapter 4 using the 2nd order and 4th order fits were shown to be solutions to the indefinite integrals, and they were computed at each point on the grid. The bounds must be inserted into those equations to determine the solution of the integrals in order to calculate the scattering distribution, as discussed in Chapter 4. Values defining these integral bounds formed the inner loop in the algorithm that generated the PDF. Since the equations are dependent on the bounds for v_r and the outgoing neutron speed, v', they utilized these parameters within the inner loop to perform the integration. Note that these equations vary for both upscattering and downscattering cases and must be set up appropriately within the loops. An outline of this algorithm is given below:

Given: Incident neutron energy and energy grid for outgoing energies.

Outgoing and incident neutron energies are converted to units of speed (m/s), $v'(i)$ and v respectively, where, $v'(i)$, is determined for each grid point from interval v_{min} to v_{max}.

Upper bound of Integral 2 for downscattering and upscattering equations was set to v_{max} (Eq. (3.9)). Lower Bound of Integral 1 for downscattering and upscattering was set to v_{min} (Eq. (3.10)).

Coefficients in the form of a_0, a_1, a_2 for the cross sections are provided in an array.

Step 1: Do $i = 1$, *Energy_Grid_Points* (Begin Loop 1)

Step 2: Determine the upper bound of Integral 1 and lower bound of Integral 2, which are equivalent to each other for every point on the grid.

$$\textit{Integral 1 Upper Bound} = \textit{Integral 2 Lower Bound} = \frac{h^2\left(v+v'\right)}{2B^2}$$

Step 3: Determine the bin to start and stop the integration based on the bounds of the integrals.

Step 4: If ($v' < v$) then downscatter, else upscatter and use corresponding equations.

Step 5: Do k = *Integral_1_lower_bound_bin*, *Integral_1_upper_bound_bin* (Begin Loop 2).

Step 6: If (k == *Integral_1_lower_bound_bin*) then

*Lower_Bound_*v_r = *Integral_1_lower_bound*

*Upper_Bound_* v_r = *Energy_Grid(k+1)* (m/s)

Else if (*k* == *Integral_1_upper_bound_bin*) then

*Lower_Bound_*v_r = *Energy_Grid(k)* (m/s)

*Upper_Bound_* v_r = *Integral_1_upper_bound*

Else

*Lower_Bound_*v_r = *Energy_Grid(k)* (m/s)

*Upper_Bound_* v_r = *Energy_Grid(k+1)* (m/s)

Step 7: Initialize P_0 and P_1 moment terms for first integral.

Step 8: Do p = 1, 2 (Begin Loop 3) → only two steps in loop because 1 represents upper bound and 2 represents lower bound

Insert the bounds obtained in Step 6 and the energy grid for v' into the equations for Integral 1 for both P_0 and P_1 moments. Use coefficients, a_0, a_1, a_2 within each region in the equations.

Step 9: (End Loop 3) Determine the value from the integration.

P0_Integral_1(i) = P0_Integral_1(i) + …
[P0_terms_in_loop(Upper_bound) – …
P0_terms_in_loop(Lower_bound)]

P1_Integral_1(i) = P1_Integral_1(i) + …
[P1_terms_in_loop(Upper_bound) – …
P1_terms_in_loop(Lower_bound)]

Step 10: (End Loop 2) Determine the bounds again for Integral 2 for the moments.

Step 11: Do k = *Integral_2_lower_bound_bin*, *Integral_2_upper_bound_bin* (Begin Loop 4).

Step 12: If (k == *Integral_2_lower_bound_bin*) then

*Lower_Bound_*v_r = *Integral_2_lower_bound*

*Upper_Bound_* v_r = *Energy_Grid(k+1)* (m/s)

Else if (*k* == *Integral_2_upper_bound_bin*) then

*Lower_Bound_*v_r = *Energy_Grid(k)* (m/s)

*Upper_Bound_* v_r = *Integral_2_upper_bound*

Else

*Lower_Bound_*v_r = *Energy_Grid(k)* (m/s)

*Upper_Bound_* v_r = *Energy_Grid(k+1)* (m/s)

Step 13: Initialize P_0 and P_1 moment terms for second integral.

Step 14: Do p = 1, 2 (Begin Loop 5)

Insert the bounds obtained in Step 12 and the energy grid for *v'* into the equations for Integral 2 for both P_0 and P_1 moments. Use coefficients, a_0, a_1, a_2 within each region in the equations.

Step 15: (End Loop 5) Determine the value from the integration.

P0_Integral_2(i) = P0_Integral_2(i) + …
[P0_terms_in_loop(Upper_bound) – …
P0_terms_in_loop(Lower_bound)]

P1_Integral_2(i) = P1_Integral_2(i) + …
[P1_terms_in_loop(Upper_bound) – …
P1_terms_in_loop(Lower_bound)]

Step 16: (End Loop 4)

Step 17: (End Loop 1)

Step 18: P_0 and P_1 moments for the differential scattering distribution are stored on grid *i* for both Integrals 1 and 2. They need to be renormalized to obtain the moments of the differential scattering PDF, which is an easy step performed in another loop.

```
Do i = 1, Energy_Grid_Points
    P0_Diff_Scat_PDF = P0_Integral_1[i] + P0_Integral_2[i] / …
                        [(sum(P0_Integral_1[i] + …
                              sum(P0_Integral_2))*Energy_width_of_bin]

    P1_Diff_Scat_PDF = P1_Integral_1[i] + P1_Integral_2[i] / …
                        [(sum(P1_Integral_1[i] + …
                              sum(P1_Integral_2))*Energy_width_of_bin]
*Sum function in Fortran adds up all the elements in the array
```

This is an outline of the algorithm used to generate the PDFs on-the-fly. For all the test problems conducted in this chapter, the coarse grid was kept at 0.05 eV.

5.3 Algorithm for Sampling Exiting Conditions

Once the PDF was set up, it was easy to sample for the exiting conditions of the neutron using the moments. For the P_0 moment, an outline is shown below:

Step 1. Generate P_0 moment of the differential scattering kernel on-the-fly given an incident neutron energy.

Step 2. Generate CDF and sample for the outgoing neutron energy.

Step 3. Sample for outgoing neutron cosine angle uniformly from -1 and +1 (isotropic scattering).

Step 4. Once the angle was determined, rotate the angle with respect to the incident neutron velocity as discussed in Chapter 1, Eq. (1.8).

The advantages of this method are that it is very simple to implement and it avoids having to sample for the target speed and cosine of polar angle between the target and neutron. There are no extra rejections and, therefore, no running the risk of

surpassing the random stride in the random number generator for large-scale problems, i.e. a full reactor core. We are able to go directly from laboratory-to-laboratory frame before and after the scattering collision without having to first perform scattering in the center-of-mass frame. The disadvantage of this method is that setting up the PDF can be time consuming. But, this method can be efficient with a coarse energy grid for PDF generation or if there are fewer piecewise intervals to approximate the cross section.

Similarly, when the P_1 moment was generated on-the-fly, it was used to determine the exiting angle of the neutron from a collision. In this case, it is possible to obtain a negative PDF as discussed in Chapter 4. It was possible for $f(\mu)$ to become negative when $|\bar{\mu}| > 1/3$. To avoid this problem, a new PDF, $g(\mu)$, representing a step function was determined [2], [3]. This step function preserved the average angle, $\bar{\mu}$. It was also possible in some cases that the absolute value of P_1 was greater than P_0, which meant that $\bar{\mu}$ yielded unphysical results where $|\bar{\mu}| > 1$ since $|\bar{\mu}| > \left| P_1 / P_0 \right|$. This generally occurred at the outer edge of the PDF where the neutron scattering probability was lower. When this happened, $\bar{\mu}$ was set to one if $\bar{\mu} > 1$, otherwise $\bar{\mu}$ was set to -1 if $\bar{\mu} < -1$. The following outlines the new algorithm incorporating the P_1 moment:

Step 1. Generate P_0 and P_1 moments of the differential scattering kernel on-the-fly given an incident neutron energy.

Step 2. Generate CDF using P_0 moment and sample for the outgoing neutron energy using histogram or linear-linear sampling.

Step 3. Given the outgoing energy sampled from P_0 moment, determine the P_1 moment.

Step 4. Determine $\bar{\mu}$ given P_0 and P_1 moments for the outgoing neutron energy sampled [2], [3].

- **a.** If $\bar{\mu} > 1$, set $\bar{\mu}$ equal to 1 else if $\bar{\mu} < -1$ set $\bar{\mu}$ equal to -1.
- **b.** If $\bar{\mu} > 1/3$, then choose the exiting neutron angle after a collision from $[2\bar{\mu} - 1, 1]$.

c. If $\bar{\mu} < -\frac{1}{3}$, then choose the exiting neutron angle after a collision from $\left[-1, 2\bar{\mu}+1\right]$.

d. Otherwise, choose angle from $f(\mu) = \frac{1}{2} + \frac{3}{2}\mu\bar{\mu}$.

Step 5. Once the angle has been determined, rotate the angle with respect to the incident neutron velocity as discussed in Chapter 1, Eq. (1.8).

In the next few sections, we will look at some test problems involving neutron escape probabilities and criticality calculations using this new scattering model.

5.3.1 Sampling for the outgoing energy

There are different methods that can be implemented to sample the exiting energy of the neutron. Two such cases will be discussed in this section. The first is sampling uniformly between two grid points for the outgoing energy. In uniform sampling, the grid points forming the PDF are represented by a series of histograms. The CDF can be constructed from the PDF, which is then used to sample for the outgoing energy bin, from [1],

$$CDF(i) < \xi < CDF(i+1),$$

where ξ, is a random number sampled uniformly between 0 and 1. The outgoing energy is sampled from,

$$E_{outgoing} = E(i) + \left[E(i+1) - E(i)\right]\left\{\frac{\xi - CDF(i)}{CDF(i+1) - CDF(i)}\right\}.$$

The histogram is being sampled uniformly for the outgoing energy. However, in order to perform linear-linear interpolation between two grid points to sample for the outgoing energy, the following equation must be used [1],

$$E_{outgoing} = E(i) + \left\{ \frac{\sqrt{PDF^2(i) + 2\left[\frac{PDF(i+1) - PDF(i)}{E(i+1) - E(i)}\right]\left(\xi - CDF(i)\right)} - PDF(i)}{\left(\frac{PDF(i+1) - PDF(i)}{E(i+1) - E(i)}\right)} \right\}.$$

This equation is presented as ENDF Law 4 in the MCNP manual [1]. There are other sampling methods, which can be utilized to perform linear-linear interpolation. These other methods will not be discussed here, but can be found in [4]. Figure 5.4 shows an example of the P_0 moment obtained from histogram and linear-linear sampling of the outgoing energies.

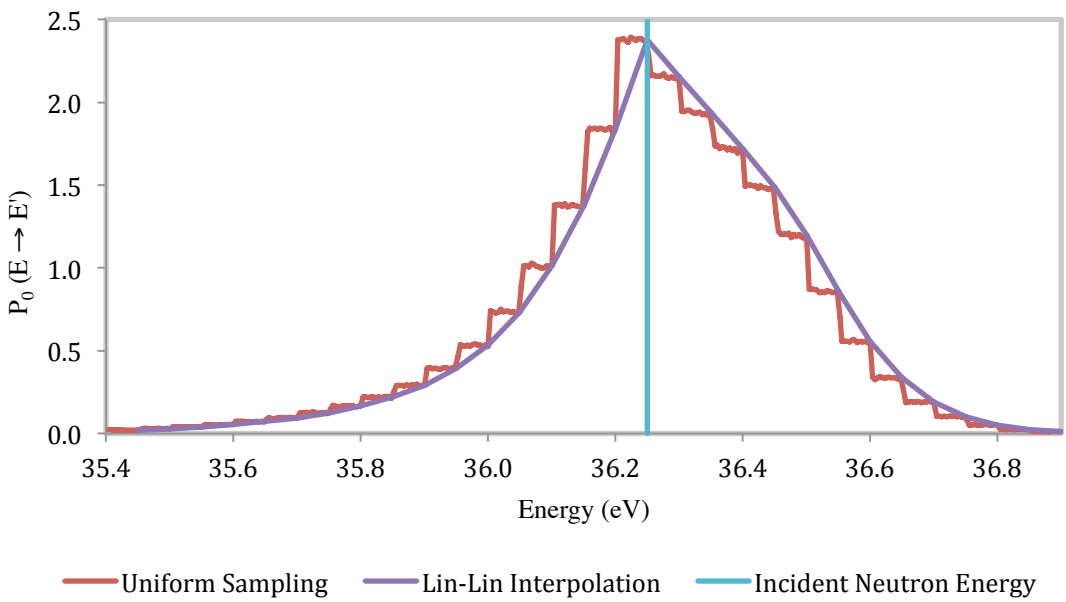

Figure 5.4: Comparison of the results for histogram and linear-linear sampling

The red line represents histogram sampling and the purple line represents linear-linear interpolation. The blue line indicates the incident neutron energy of the neutron, 36.25 eV. This plot was generated for ^{238}U at 1000 K.

5.4 Results from Scattering Models for Neutron Escape Probability

A research Monte Carlo code was set up for a very sensitive problem for neutron resonance scattering in ^{238}U. The problem consisted of an infinite cylinder of ^{238}U at

1000 K with a radius of 0.2 cm and 36.25 eV neutrons incident uniformly (cosine current) on the boundary of this cylinder. This is a stringent test of the efficacy of the resonance scattering model because the 36.67 eV resonance in ^{238}U is the principal contributor to the resonance scattering effect, and the choice of 36.25 eV neutrons focuses on those neutrons which will have the maximum chance of being upscattered, hence contributing to the additional absorption of neutrons due to resonance upscattering. The purpose of the two tests was to determine the neutron escape probability using just the P_0 moment, and then using P_0 and P_1 moments of the differential scattering PDF.

5.4.1 Test for P_0 moment

For this case, the neutron escape probability was calculated using only the P_0 moment of the differential scattering PDF with the 4th order approximation for the cross sections using 17 piecewise regions for the 36.67 eV resonance. Three cases were considered for this test. Case I employed the original free gas algorithm for all incident energies. Case II turned on the Doppler Broadened Rejection Correction (DBRC) method for incident neutron energies between 35.4 eV and 36.6 eV, and the original free gas algorithm was turned on for all other incident neutron energies. In Case III, the new method with only P_0 moment was implemented for the same energy range as DBRC, 35.4 – 36.6 eV, and the free gas algorithm was invoked for all other incident neutron energies. It must be noted that for this problem, the energy width for the grids was 0.05 eV because the resulting P_0 moment of the differential scattering PDF was found to be sufficiently accurate with prior calculations. For this case, the 4th order coefficients generated using least squares fitting are presented in Appendix B, Section B.2. Table 5-1 shows the results from the first test.

Table 5-1: Neutron Escape Probabilities Using P_0 Moment

Case	Neutron Escape Probabilities	Error (%)
I	0.37895 ± 0.00006	69.1
II (Benchmark)	0.22411 ± 0.00007	-
IIIa (Histogram sampling)	0.24547 ± 0.00007	9.5
IIIb (Linear sampling)	0.22750 ± 0.00007	1.5

There were two types of sampling performed to determine the exiting speed of the neutron. The first was uniform or histogram sampling where the speed of the neutron

was a constant within a given bin, and the second was linear sampling where the speed of the neutron was determined linearly between two points on the grid.

The results show that for this very sensitive problem, the neutron escape probability estimated by the free gas scattering model differs by nearly 70% from the benchmark case with DBRC scattering model. Case II results with the DBRC method represents the benchmark case, taking into account resonance scattering effects. Case IIIb results, using the P_0 moment and linear sampling, agreed to within 2% with the DBRC results. Case IIIa shows the advantage of linear sampling versus histogram sampling – the results with histogram sampling are substantially worse, on the order of 10% error. The neutron escape probabilities were in very good agreement with the DBRC results using a 4th order approximation for the cross section. Case III results were generated faster than Case II results for this test.

5.4.2 Test for P_0 and P_1 moments

The neutron escape probabilities were determined once again in this second test problem. This time, the exiting neutron speed was sampled from the P_0 moment and the exiting neutron angle was sampled using the P_1 moment as outlined in the algorithm in the previous section. In this case, the 2nd order approximation for the cross section was used in order to keep the results consistent for P_0 and P_1. This is because the equations used to generate P_1 moment presented in Chapter 4 are based on the 2nd order approximation for the cross section. For this problem, there were 41 piecewise regions representing the 36.67 eV resonance and the coefficients generated using least squares fitting are presented in Appendix C, Section C.3.

As indicated in the previous section, Case I employed the original free gas algorithm for all incident energies. Case II invoked DBRC for incident neutron energies between 35.4 eV and 36.6 eV, and the original free gas algorithm was turned on for all other incident neutron energies. In Case III, the new method with only P_0 moment using 2nd order cross section fits was implemented for the same energy range as DBRC, 35.4 – 36.6 eV, and the free gas algorithm was invoked for all other incident neutron energies. Case IV also employed the new method using $P_0 + P_1$ for the same energy range, 35.4 – 36.6 eV outside of which the free gas scattering model was used.

Table 5-2 shows a comparison of all the scattering models with the new results for neutron escape probabilities.

Table 5-2: Neutron Escape Probabilities From Different Scattering Models

Case	Neutron Escape Probabilities	Error (%)
Case I	0.37895 ± 0.00006	69.1
Case II (Benchmark)	0.22411 ± 0.00007	-
Case IIIa (Histogram sampling)	0.2490 ± 0.0002	11.1
Case IIIb (Linear sampling)	0.2313 ± 0.0002	3.2
Case IVa (Histogram sampling)	0.2411 ± 0.0002	7.6
Case IVb (Linear sampling)	0.2238 ± 0.0002	-0.14

As discussed earlier, Case I results are significantly different from the results for Cases II – IV that uses resonance scattering models. The result from Case IVb shows that linear sampling is essentially exact in comparison to Case II for this highly sensitive problem. Case IIIb is less accurate than Case IVb, showing the increased accuracy in estimating neutron escape probability when going to higher moments. However, histogram sampling introduces a significant error for both Cases IIIa and IIIb, showing that using linear sampling techniques between two grid points is important.

5.4.3 Summary of the neutron escape probability tests

The first two sets of results showed that with a 2nd or 4th order approximation to the cross section, the exiting conditions of a neutron from a collision were predicted with improved accuracy. The test for the 4th order case using only the P_0 moment was faster; however, as more piecewise functions and moments were added, the method became slower for P_0 + P_1 cases. The results also indicated that it is important to use linear sampling between two energy grid points for better accuracy. The research code was not optimized and may be part of future work on this method. This method holds promise, and the next few sections will focus on tests conducted on more complicated geometries.

5.5 MCNP5 results with new scattering models

In order to conduct tests on more complicated geometries, the research code was transformed into a module, which was then attached to MCNP5-1.60. As discussed in Chapter 3, a prototype version of MCNP5-1.60 was created with DBRC for benchmarking purposes. In this new research version with the moments, the final

neutron energies from the free gas scattering module, tgtvel.F90, and angles from rotas.F90 were overwritten by the new outgoing neutron energies and angles sampled on-the-fly. The outgoing cosine of polar angle was rotated using the existing module, rotas.F90, in MCNP5. The scattering moments were implemented in this manner in MCNP5 because the current version requires the calculation of relative neutron energy for certain applications. For this new scattering method using moments, it is unnecessary to calculate relative neutron energy during the collision process since collisions are not performed in the center-of-mass frame. In order to avoid breaking the existing code in MCNP5, the new module was designed to overwrite the final neutron energies and angle after each scattering event in colidn.F90, while keeping the original free gas module, tgtvel.F90, intact. Therefore, this version of MCNP5 was created just for testing purposes for this dissertation work.

The k_{eff} results from studies involving LWR fuel pins and assembly will be presented in the following subsections. For all tests described in the following subsections, DBRC was turned on continuously below 90 eV. The new method was turned on between the energy ranges of 6.35 to 6.90 eV, 20.0 to 21.4 eV, 35.4 to 36.6 eV, and 64.6 and 66.7 eV. The four resonances within these energy ranges in the lower epithermal range are expected to contribute to the biggest bias in k_{eff}. Chapter 3 showed that the Fuel Temperature Coefficient (FTC) does not change much beyond 90 eV. For this reason, the four main resonances in the lower epithermal region for ^{238}U were included to perform this analysis. The 2nd and 4th order coefficients used for these resonances were generated using least squares fitting and are presented in Appendix C. The four resonances at 300 K obtained from [5] are shown in Figure 5.5.

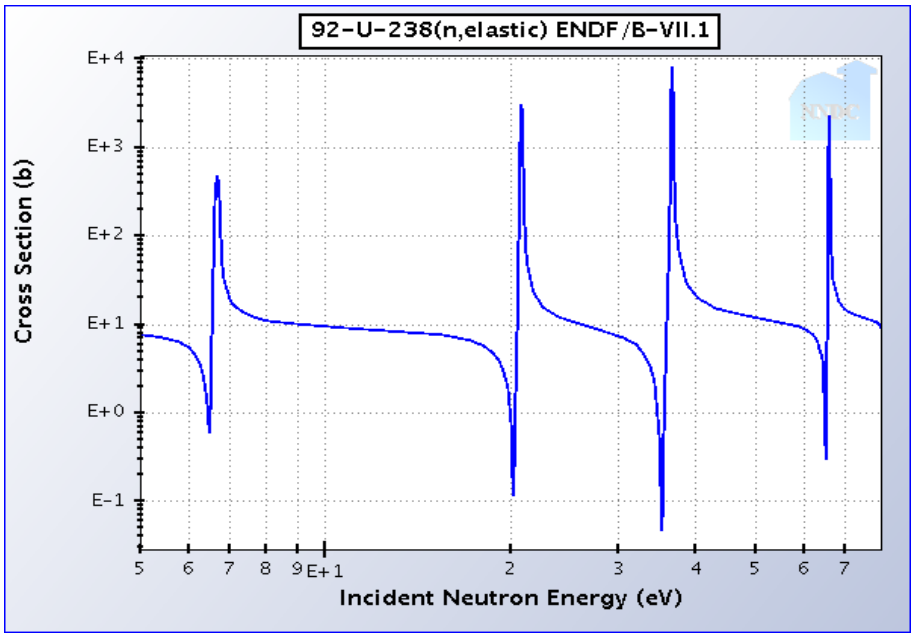

Figure 5.5: Four resonances in low-lying epithermal range in ^{238}U

For all the problems presented in the following subsections, the energy grid width was set to 0.05 eV and the exiting energy and angle were determined using linear sampling.

5.5.1 LWR fuel pin results for hot full power conditions

The specifications for the UO_2 LWR pin cell were taken from the Mosteller Benchmark [6] problem set. Figure 5.6 illustrates a pin cell containing fuel surrounded by a small gap, which is enclosed by the cladding. The moderator surrounds the fuel and cladding. Selected cases for various enrichments were run at Hot Full Power (HFP) conditions using different scattering models. Recall, at HFP conditions, the fuel is at 900 K and the moderator and cladding are at 600 K.

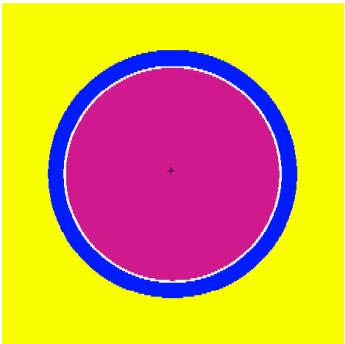

Figure 5.6: LWR pin cell in Mosteller benchmark [6]

Tables 5-3 – 5-5 show the results from different scattering models for the sensitivity study done on varying uranium enriched fuel.

Table 5-3: k_{eff} comparisons for various scattering models for natural U

Case	0.711 wt%			Difference (pcm)		
Free Gas	0.66036	±	0.00016	140	±	24
DBRC (Benchmark)	0.65896	±	0.00018	-		-
P_0 (2nd Order)	0.65825	±	0.00021	-71	±	28
$P_0 + P_1$ (2nd Order)	0.65870	±	0.00019	-26	±	26
P_0 (4th Order)	0.65840	±	0.00013	-56	±	22

Table 5-4: k_{eff} comparisons for various scattering models for 3.1% enriched U

Case	3.1 wt%			Difference (pcm)		
Free Gas	1.16777	±	0.00028	232	±	40
DBRC (Benchmark)	1.16545	±	0.00028	-		-
P_0 (2nd Order)	1.16541	±	0.00030	-4	±	41
$P_0 + P_1$ (2nd Order)	1.16512	±	0.00027	-33	±	39
P_0 (4th Order)	1.16491	±	0.00021	-54	±	35

Table 5-5: k_{eff} comparisons for various scattering models for 5.0% enriched U

Case	5.0 wt%			Difference (pcm)		
Free Gas	1.28990	±	0.00022	249	±	30
DBRC (Benchmark)	1.28741	±	0.00021	-		-
P_0 (2nd Order)	1.28678	±	0.00020	-63	±	29
$P_0 + P_1$ (2nd Order)	1.28626	±	0.00015	-98	±	26
P_0 (4th Order)	1.28653	±	0.00018	-88	±	28

The results show that the P_0 moment is sufficient to estimate k_{eff} in criticality calculations with a reasonable degree of accuracy when linear sampling is employed to determine the exiting conditions of a neutron. Results from the $P_0 + P_1$ case does not provide any more accuracy than what the P_0 results already provide. Therefore, it seems reasonable to generate the P_0 moment of the differential scattering kernel on-the-fly around resonances to sample for the outgoing speed of the neutron. It is also advantageous to go up to 4th order approximation for the scattering cross section because fewer piecewise functions are required to estimate the cross section with reasonable accuracy. The results also suggest that the computational time decreases when a higher

order fit is used because fewer cross section intervals are needed. Also going to P_1 moment does not seem to gain much accuracy, but it costs more computational time.

5.5.2 2-D Westinghouse 17×17 fuel assembly results

Following the study on the fuel pin cell, it was imperative to check the consistency of the results for assembly problems. For this study, CASL benchmark specifications [7] were used for 17×17 Westinghouse fuel assembly. A 2-D problem for the fuel assembly was set up in MCNP5 for HFP conditions.

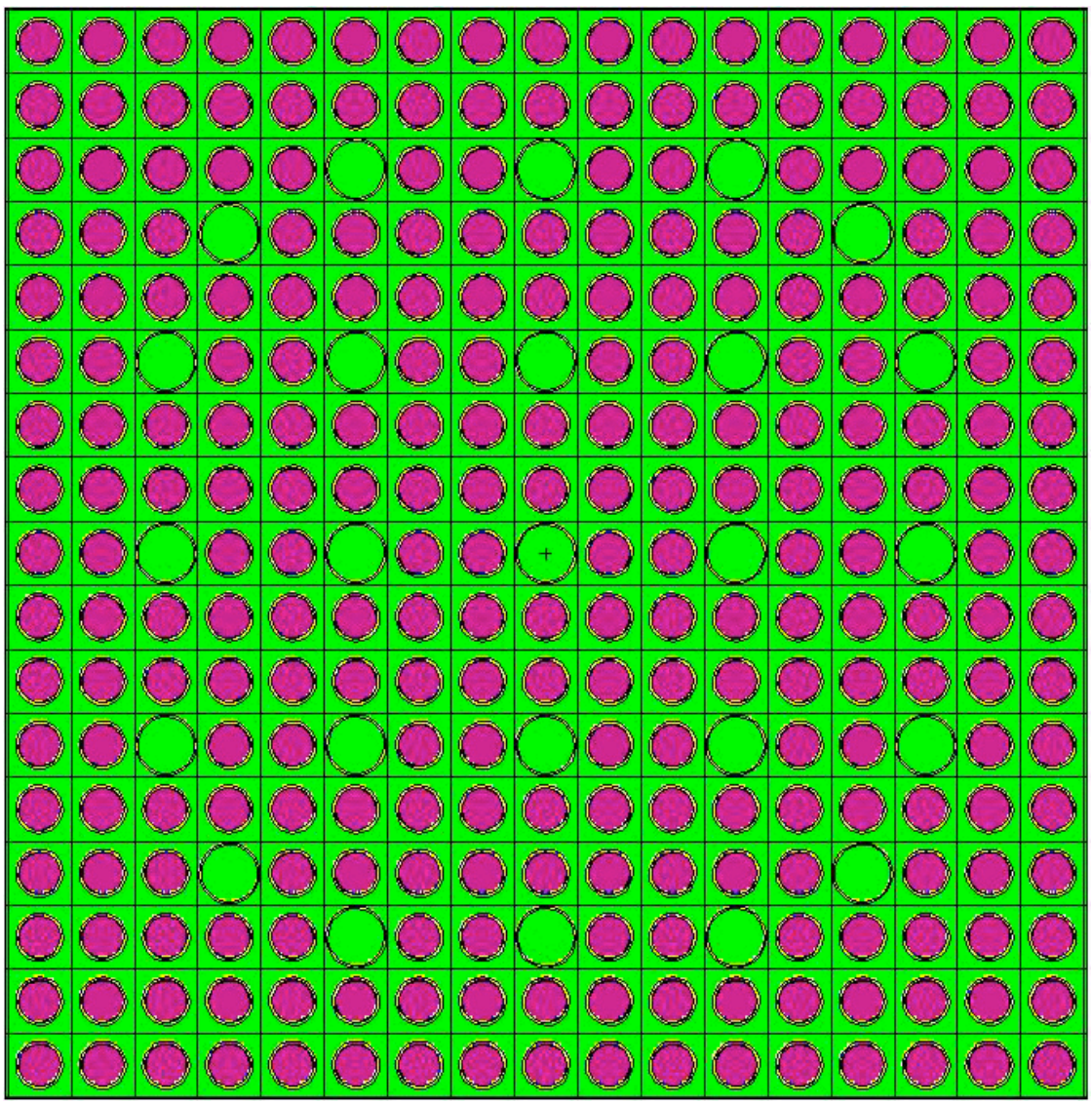

Figure 5.7: 2-D Westinghouse 17×17 fuel assembly

The 17×17 fuel assembly was at beginning-of-life (BOL) and the fuel is composed of UO_2 with Zircaloy-4 cladding [7]. The water is borated and the guide tubes and instrument tube are made out of Zircaloy-4 [7]. In this configuration, there were no control rods in the assembly and the empty tubes were filled with borated water. The results for this configuration using various scattering models are presented in Table 5-6.

Table 5-6: k_{eff} comparisons for various scattering models for 2D 17×17 assembly

Case	k_{eff}			Difference (pcm)		
Free Gas	1.17578	±	0.00016	255	±	25
DBRC (Benchmark)	1.17323	±	0.00019	-	±	-
P_0 (2nd order)	1.17263	±	0.00017	-60	±	25
$P_0 + P_1$ (2nd order)	1.17252	±	0.00017	-71	±	25
P_0 (4th order)	1.17260	±	0.00018	-63	±	26

Table 5-6 shows that the results are consistent with the results obtained for the fuel pin cell problem at HFP conditions. It is sufficient to use the P_0 moment to sample for the exiting energy of the neutron. Going up to higher moments is unnecessary and time consuming when sufficiently accurate results can be obtained with P_0 moments. The difference in the results from the models using the 2nd and 4th order fits for the cross sections is negligible. Therefore, it can be concluded that the 4th order fit with fewer piecewise regions is sufficient to perform criticality calculations.

5.5.3 Reactor-recycle MOX results

It was also important to look at the impact of these scattering models on different types of fuel typically used in a thermal nuclear reactor. Reactor-Recycle Mixed Oxide (MOX) fuel is used in LWRs. MOX fuel contains mixed oxides; uranium dioxide, UO_2, and plutonium dioxide, PuO_2. A fuel pin cell problem from the Mosteller Benchmark [6] for 8 wt% PuO_2 was used to set up this study. This was the highest enrichment available with PuO_2 for Reactor-Recycle MOX in the Mosteller Benchmark problem. Therefore, the impact for this extreme case for MOX fuel would give us an idea of whether resonance scattering is important in MOX. The fuel pin cell problem was run at HFP conditions using the free gas scattering model and DBRC below 90 eV, and the results from this study is presented in Table 5-7.

Table 5-7: Difference in k_{eff} for 8 wt% PuO_2 MOX Fuel at HFP Conditions

Case	k_{eff}			Difference (pcm)		
FG (Benchmark)	1.11703	±	0.00021			
DBRC - ^{239}Pu	1.11635	±	0.00022	-68	±	30
DBRC - ^{238}U	1.11466	±	0.00022	-237	±	30

The results, in Table 5-7, show that it is not essential to turn on resonance scattering in ^{239}Pu because the number density of ^{238}U is far greater than ^{239}Pu in MOX fuel by a factor of approximately 25. Also, the scattering to absorption cross section ratio for the resonances in the lower epithermal range below 90 eV is lower in ^{239}Pu than it is in ^{238}U. Therefore, it is important to turn on resonance scattering in ^{238}U below 90 eV for MOX fuel due to the significant bias in k_{eff} at HFP conditions. Figure 5.8 shows one of many cross sections found in the lower epithermal regions in ^{239}Pu.

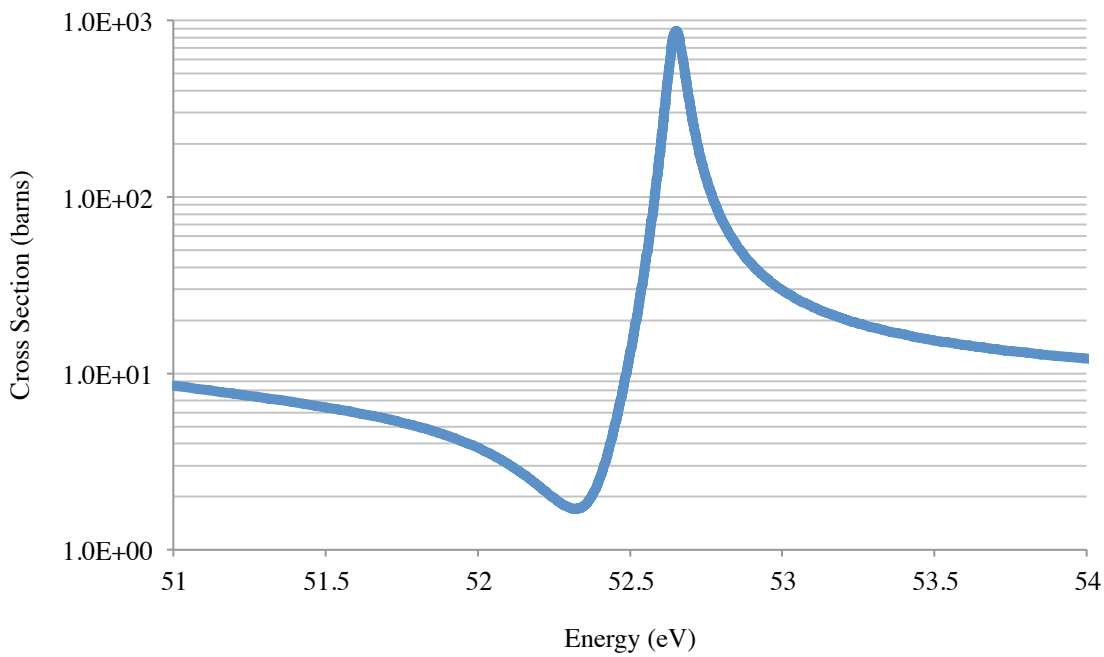

Figure 5.8: 52.6 eV scattering resonance in ^{239}Pu at zero Kelvin [8]

Figure 5.9 shows the differential scattering PDF obtained from DBRC for neutrons with 52.35 eV incident neutron energy, scattering in the vicinity of this resonance.

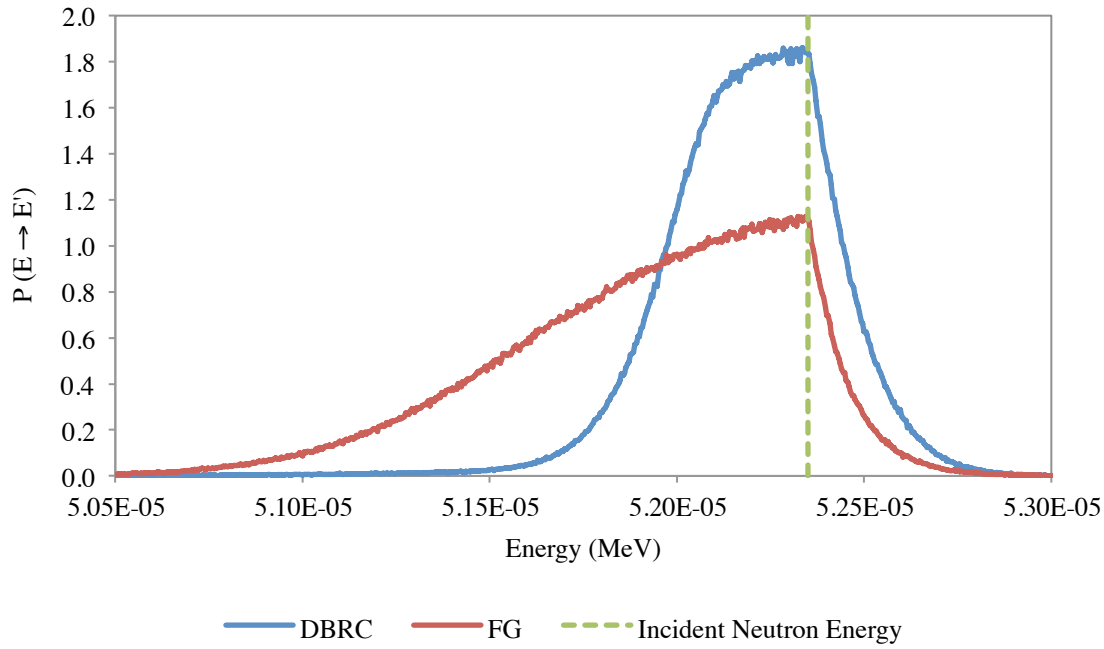

Figure 5.9: Differential scattering PDF for ^{239}Pu at 1200 K and incident neutron energy of 52.35 eV

There are some upscattering effects when the resonance is accounted. But, again, the lower scattering to absorption ratio and lower number density of ^{239}Pu makes resonance scattering effects negligible in MOX for ^{239}Pu below 90 eV, where it is significant for ^{238}U.

5.6 Conclusion

In this chapter, the algorithm used to set up the moments of the scattering PDF were explained in detail. It is important to preserve the peak of the P_0 moment of the scattering kernel when generating the PDF, and to generate the grid towards the tails of the PDF, starting from the incident neutron energy. The algorithms set up for this dissertation work were not optimized, and there are probably several ways in which this work can be optimized in the future.

It has been found that it is sufficient to use the P_0 moment of the differential scattering kernel to determine the exiting conditions of the neutron. It is also sufficient to use the 4th order approximation with fewer piecewise functions for the cross sections to get k_{eff} results with a reasonable degree of accuracy. There is no need to go to higher

moments to determine k_{eff} in criticality calculations. In the lower epithermal region below 90 eV, it was important to invoke the resonance scattering model for ^{238}U in MOX fuel, but not necessary to turn on an expensive resonance scattering model for ^{239}Pu. The bias in k_{eff} was very minimal for the benchmark problem with the highest concentration of PuO_2 (8 wt%) for Reactor-Recycle MOX.

5.7 References

[1] X-5 Monte Carlo Team, *MCNP – A General Monte Carlo N-Particle Transport Code, Version 5, Volume I: Overview and Theory*, LA-UR-03-1987, Los Alamos National Laboratory (2003).

[2] F. Brown and N. Barnett, *One-group MCNP5 Criticality Calculations with Anisotropic Scattering*, LA-UR-08-0567, Los Alamos National Laboratory.

[3] F. Brown and N. Barnett, *A tutorial on Using MCNP for 1-group Transport Calculations*, LA-UR-07-4594, Los Alamos National Laboratory.

[4] M. H. Kalos and P. A. Whitlock, *Monte Carlo Methods*, John Wiley & Sons, Inc. (1986).

[5] National Nuclear Data Center, *Evaluated Nuclear Data File (ENDF)*, Brookhaven National Laboratory <http://www.nndc.bnl.gov/sigma/index.jsp> (2012).

[6] R. D. Mosteller, *Computational Benchmarks for the Doppler Reactivity Defect*, LA-UR-06-2968, Los Alamos National Laboratory.

[7] CASL, *VERA Core Physics Benchmark Progression Problems,* CASL-U-2012-0131-000 (2012).

[8] R. E. MacFarlane and D. W. Muir, *The NJOY Nuclear Data Process System Version 91*, LA-12740-M, Los Alamos National Laboratory (1994).

[9] B. Becker, R. Dagan and G. Lohnert, *Proof and implementation of the stochastic formula for ideal gas, energy dependent scattering kernel*, Annals of Nuclear Energy, **36**, pp. 470 – 474 (2009).

[10] G. L. Blackshaw and R. L. Murray, *Scattering Functions for Low-Energy Neutron Collisions in a Maxwellian Monatomic Gas*, Nuclear Science and Engineering, **27**, pp. 520-532 (1967).

[11] B. Becker, *On the Influence of the Resonance Scattering Treatment in Monte Carlo Codes on High Temperature Reactor Characteristics*, Thesis, Institut fur Kernenergetik und Energiesysteme, *Germany*, 2010.

[12] R. D. Mosteller, *ENDF/B-V, ENDF/B-VI, and ENDF/B-VII.0 Results for the Doppler-defect Benchmark*, Proceedings from M&C+SNA, Monterey, CA (2007).

[13] National Institute of Standards and Technology, *Atomic Data for Zirconium (Zr)*, Handbook of Basic Atomic Spectroscopic Data – online version (2011).

CHAPTER 6

Summary And Future Work

6.1 Summary

During the course of this dissertation, there were several lessons learned on the effects of using various scattering models in Monte Carlo codes. In Chapter 1, a brief introduction to Monte Carlo methods for reactor analysis was presented. In Chapter 2, we explored different nuclear reactions and resonances a neutron would encounter when it slows down from fission energies to thermal energies. In Chapter 3, the algorithms for different existing resonance scattering models were discussed in detail. Discretizing the bivariate scattering PDF and studying it showed that the scattering probability is very close to zero for most of the range of the polar angle cosines and target speeds, except for a very narrow, peaked region where the scattering probability is high. This study indicated why the modified free gas algorithm, the Doppler Broadened Rejection Correction (DBRC) [1] method, could be inefficient for incident neutron energies around a resonance. In a rejection technique, such as the one utilized in the DBRC scheme, this results in a small probability to pass the rejection tests for the selection of the scattering parameters, target nuclide speed, and cosine of polar angle between the target and neutron.

In all existing Monte Carlo methods, collision mechanics are performed in the center-of-mass frame and the scattering parameters are converted to the laboratory frame after passing the rejection tests. For the purposes of this dissertation work, the goal was to avoid having to perform collision mechanics in the center-of-mass frame and, instead, go directly from incident neutron velocities in the laboratory frame to outgoing velocities in the laboratory frame. In Chapter 3, we also saw the importance of taking into account the resonances in the epithermal region. The differences in k_{eff} for criticality calculations were on the order of several hundred pcm for hot full power conditions in standard LWR

fuel pin calculations. These differences were temperature dependent, which means that for high temperature reactors, it is even more important to take into account the low-lying resonances in the epithermal region. In Chapter 4, we looked at equations developed for the Legendre moments of the differential scattering PDF. The moments of the differential scattering PDF were studied to predict the exiting conditions of the neutron, i.e., energy and angle. Blackshaw [2] developed Legendre moments of the differential scattering PDF for his dissertation work in the 1960s. His single-integral representation of the distribution was very appealing for this dissertation work. All the equations developed thus far have involved double integrals, and Blackshaw transformed these double integrals into single integrals, which meant that any method developed using these equations had the potential to be more efficient. However, Blackshaw did not provide any numerical results for the moments using the exact scattering cross sections in his dissertation. His equations were subsequently verified, and the moments of the differential scattering PDF were predicted correctly in this dissertation. It must be noted that the equations that Blackshaw derived were not moments of the scattering PDF, but rather, the moments of a differential scattering distribution. The terms must be normalized to obtain the moments of the differential scattering PDF. Parameter studies showed there is no need to employ true resonance scattering for the entire epithermal region, but it is sufficient to turn on resonance scattering models for incident neutron energies very close to the energy corresponding to the peak of the resonance. In addition to correcting an error in the Blackshaw equations, the integral bounds prescribed by Blackshaw can be approximated such that the minimum and maximum bounds used to perform the second rejection test in DBRC are sufficient to obtain accurate moments. This modification to the integral bounds consequently decreased the computational time of the calculations.

The next step was to approximate the cross section such that an analytical result for the equations could be found without using the exact, tabulated scattering cross sections, eliminating the need to store zero Kelvin cross sections to implement the resonance scattering model. Even-ordered polynomial approximations were found to provide an analytical solution for the moments. Blackshaw mentioned this possibility in his dissertation but did not derive the moments using an even-ordered cross section

model. This was a key contribution of this dissertation research, because it enabled efficient and accurate integration of the moments using sufficiently accurate cross section data. Once the new equations were proven to be correct, they were applied to several test problems. A cylindrical escape probability test problem was developed for comparison with the benchmark DBRC method. This problem was a stringent test of our methodology because it focused on those neutrons that were most likely to be upscattered back into the resonance. The results showed excellent agreement with DBRC. This method was then implemented into MCNP5 [3] where the outgoing neutron energies and angles were sampled using the P_0 and P_1 results showed great improvement over the conventional free gas method and were far better than the asymptotic scattering model. The on-the-fly scheme was turned on for very specific energy ranges, and the k_{eff} calculations for P_0 and P_1 results did not differ from each other significantly. With the simple fits and energy ranges used, the improved scattering model developed in this research agreed well with DBRC. The study also indicated that it is sufficient to use P_0 scattering with fewer piecewise functions and the 4th order approximation for the scattering cross section to obtain good results. There is no need to go to P_1 or higher to calculate k_{eff} for realistic reactor configurations such as a pin cell or an assembly. While the results with the cylindrical escape probability test problem indicated that using P_1 scattering was important to get predictions close to the DBRC results, real reactor configurations involve a spectrum of neutron energies and the overall effect is reasonably predicted with P_0 scattering as long as the scattering cross section is sufficiently accurate.

A brief study conducted on MOX fuel showed that it is not necessary to turn on the improved resonance scattering model in ^{239}Pu for the worst case scenario (8 wt% PuO_2), outlined in the Mosteller Benchmark problem set. The bias in k_{eff} as a result of turning on resonance scattering is negligible in ^{239}Pu due to the lower ^{239}Pu number density (versus ^{238}U) and the lower scattering to absorption ratio of the resonances in the lower epithermal energy range. However, it is still important to invoke the improved resonance scattering model in ^{238}U for MOX for the same reason it is needed for conventional UO_2 fuel.

In summary, the work in this dissertation shows that resonance scattering in ^{238}U can be predicted well using moments of the differential scattering kernel, and that it is sufficient to use only the P_0 moment to predict k_{eff} in realistic reactor configurations.

6.2 Future work

There is certainly more work that can be done on this method. Reducing the equations further and coding them in a more optimal manner, especially the sampling techniques, can further optimize the method. The impact of using the improved resonance scattering on isotopics has not been explored, as this research focused on the effect of k_{eff}. It would be useful to have a metric for deciding when this effect is important enough to be modeled, such as determining a combination of resonance magnitude, resonance scatter-to-total ratio, neutron energy range, and number density that warrant using the improved resonance scattering model. Pin power and flux should also be studied in more detail to determine if the P_0 and P_1 moments are sufficient to predict those parameters accurately. Also, resonance scattering in other isotopes such as Hafnium and Erbium relevant to reactor applications should be explored. For example, Figure 6.1 shows resonances in ^{178}Hf that might affect k_{eff} calculations if resonance scattering models are used.

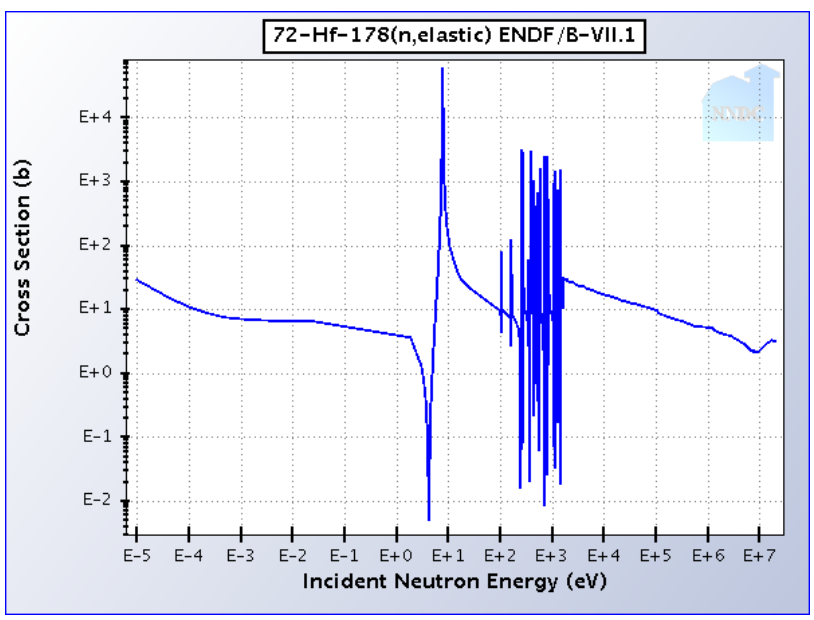

Figure 6.1: ^{178}Hf Resonances at 300 K [4]

The goal in this dissertation was to provide an alternative method for on-the-fly resonance scattering that is not based on a rejection technique. This work should lead to more research in the area of resonance scattering using moments.

6.3 References

[1] B. Becker, R. Dagan and G. Lohnert, *Proof and implementation of the stochastic formula for ideal gas, energy dependent scattering kernel*, Annals of Nuclear Energy, **36**, pp. 470 – 474 (2009).

[2] G. L. Blackshaw, *Scattering of Low-Energy Neutrons In a Monatomic Gas Model Of A Multiplying System*, North Carolina State University, Raleigh, Ph.D. Thesis (1966).

[3] X-5 Monte Carlo Team, *MCNP – A General Monte Carlo N-Particle Transport Code, Version 5, Volume I: Overview and Theory*, LA-UR-03-1987, Los Alamos National Laboratory (2003).

[4] National Nuclear Data Center, *Evaluated Nuclear Data File (ENDF) Retrieval and Plotting*, Brookhaven National Laboratory, <http://www.nndc.bnl.gov/sigma/index.jsp?as=167&lib=endfb7.1&nsub=10> (2012).

[5] G. L. Blackshaw and R. L. Murray, *Scattering Functions for Low-Energy Neutron Collisions in a Maxwellian Monatomic Gas*, Nuclear Science and Engineering, **27**, pp. 520-532 (1967).

[6] B. Becker, R. Dagan and G. Lohnert, *Proof and implementation of the stochastic formula for ideal gas, energy dependent scattering kernel*, Annals of Nuclear Energy, **36**, pp. 470 – 474 (2009).

[7] B. Becker, *On the Influence of the Resonance Scattering Treatment in Monte Carlo Codes on High Temperature Reactor Characteristics*, Thesis, Institut fur Kernenergetik und Energiesysteme, *Germany*, 2010.

APPENDIX A

Relationship between Initial and Final Neutron Velocities in the Laboratory Frame

The relationship between the initial and final neutron velocities in the laboratory frame is represented by the cosine of polar angle, μ_{lab}, determined by,

$$\mu_{lab} = \cos\theta = \cos\alpha \cos\beta + \sin\alpha \sin\beta \cos\varphi. \tag{A.1}$$

The relationships between θ, α, β and φ are shown in Figure A.1. Eq. (A.1) has been presented in [1] and [2], and we can derive it by using the spherical law of cosines. The vectors $\mathbf{v}$, $\mathbf{v'}$ and $\mathbf{v_{CM}}$, are all assumed to originate from the center of the sphere, and are moving outwards.

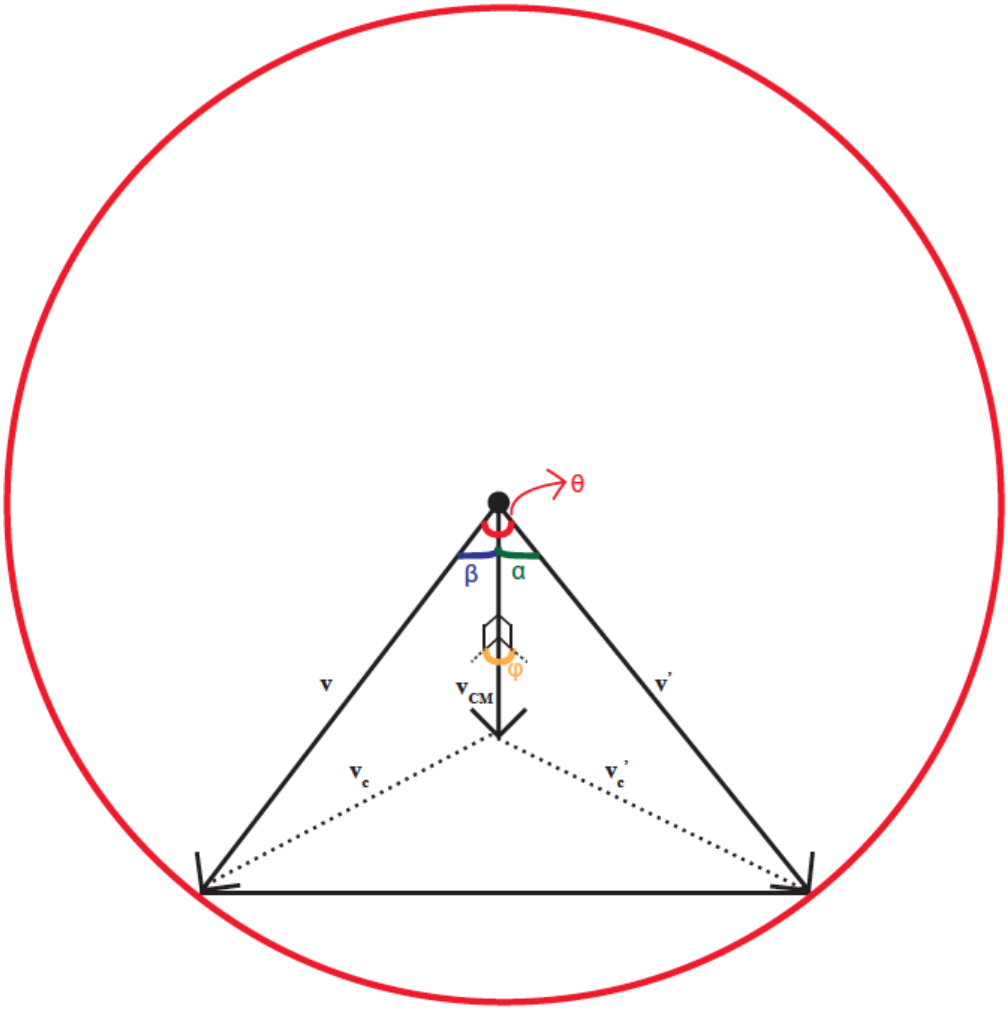

Figure A.1: Neutron scattering angles and directions in laboratory and center-of-mass frames

In Figure A.1, **v** and **v'** are incoming and outgoing neutron velocities in laboratory frame, $\mathbf{v_c}$ and $\mathbf{v_c'}$ are the incoming and outgoing neutron velocities in the center-of-mass frame, and $\mathbf{v_{CM}}$ is the velocity of the center-of-mass in the laboratory frame. θ is the angle between the incoming and outgoing neutron velocities in the laboratory frame. β is the angle between the center-of-mass velocity and the incident neutron velocity in laboratory frame and α is the angle between the center-of-mass velocity and the outgoing neutron velocity in the laboratory frame. The azimuthal angle is represented by φ.

Figure A.1 can be transformed into Figure A.2, shown below, using the relationships between the vectors, $\mathbf{v_{CM}}$, $\mathbf{v}$ and $\mathbf{v'}$, to determine the cosine of θ using the spherical cosine law.

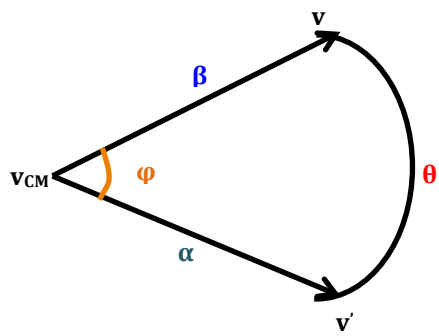

Figure A.2: Neutron scattering angles

$\mathbf{v_{CM}}$, $\mathbf{v}$ and $\mathbf{v'}$ are now depicted as points in Figure A.2 but they are unit vectors coming out of the sphere. Relationships between the unit vectors, $\mathbf{v_{CM}}$, $\mathbf{v}$ and $\mathbf{v'}$, are formed by θ, β, and α, as shown below.

$$\cos\alpha = \mathbf{v_{CM}} \bullet \mathbf{v}',$$
$$\cos\beta = \mathbf{v_{CM}} \bullet \mathbf{v},$$
$$\cos\theta = \mathbf{v} \bullet \mathbf{v}'.$$

The angle, φ, is found by taking the dot product of the normal to the planes forming it. To find the normal to the planes, take the cross product of the vectors, $\mathbf{v_{CM}}$, $\mathbf{v}$ and $\mathbf{v'}$,

$$\left(\mathbf{v_{CM}} \times \mathbf{v}'\right) \bullet \left(\mathbf{v_{CM}} \times \mathbf{v}\right) = \left(\left|\mathbf{v_{CM}}\right|\left|\mathbf{v}'\right|\sin\alpha\right)\left(\left|\mathbf{v_{CM}}\right|\left|\mathbf{v}\right|\sin\beta\right)\cos\varphi. \tag{A.2}$$

Since, $\mathbf{v_{CM}}$, $\mathbf{v}$ and $\mathbf{v'}$, were assumed to be unit vectors, Eq. (A.2) becomes,

$$\left(\mathbf{v_{CM}} \times \mathbf{v}'\right) \bullet \left(\mathbf{v_{CM}} \times \mathbf{v}\right) = \sin\alpha\sin\beta\cos\varphi. \tag{A.3}$$

We can formulate Eq. (A.3) using another vector identity.

$$\begin{aligned}(\mathbf{v}_{\mathbf{CM}} \times \mathbf{v}') \bullet (\mathbf{v}_{\mathbf{CM}} \times \mathbf{v}) &= (\mathbf{v}_{\mathbf{CM}} \bullet \mathbf{v}_{\mathbf{CM}})(\mathbf{v}' \bullet \mathbf{v}) - (\mathbf{v}' \bullet \mathbf{v}_{\mathbf{CM}})(\mathbf{v}_{\mathbf{CM}} \bullet \mathbf{v}) \\ &= (\mathbf{v}' \bullet \mathbf{v}) - (\mathbf{v}' \bullet \mathbf{v}_{\mathbf{CM}})(\mathbf{v}_{\mathbf{CM}} \bullet \mathbf{v}) \\ &= \cos\theta - \cos\alpha\cos\beta\end{aligned}$$

Therefore,

$$(\mathbf{v}_{\mathbf{CM}} \times \mathbf{v}') \bullet (\mathbf{v}_{\mathbf{CM}} \times \mathbf{v}) = \cos\theta - \cos\alpha\cos\beta. \tag{A.4}$$

We can now equate Eqs. (A.3) and (A.4),

$$(\mathbf{v}_{\mathbf{CM}} \times \mathbf{v}') \bullet (\mathbf{v}_{\mathbf{CM}} \times \mathbf{v}) = \sin\alpha\sin\beta\cos\varphi = \cos\theta - \cos\alpha\cos\beta.$$

It is now clear that $\mu_{lab} = \cos\theta = \cos\alpha\cos\beta + \sin\alpha\sin\beta\cos\varphi$.

A.1 References

[1] S. A. Dupree and S. K. Fraley, *A Monte Carlo Primer: A Practical Approach to Radiation Transport,* Kluwer Academic/Plenum Publishers, New York (2002).

[2] T. Högberg, *Monte Carlo Calculations of Neutron Thermalization In a Heterogeneous System,* Journal of Nuclear Energy, Part A: Reactor Science, **12**, pp. 145-150 (1960).

APPENDIX B

Coefficients for 36.67 eV Resonance

The piecewise regions in Tables B-1 and B-4 present the range of speeds defined by each piecewise region. These tables are followed by their corresponding coefficients. The coefficients in Tables B-2 and B-3 were generated using linear interpolation as shown in Section 4.4.1 in Chapter 4. The coefficients listed in Tables B-5 to B-7 for the fourth order polynomial were generated using least squares fits in Mathematica 8.0.

B.1 Second order fit with only 24 piecewise regions around 36.67 eV resonance

Table B-1: Piecewise regions around 36.67 eV resonance

Fit	v_{min} (m/s)	v_{max} (m/s)	Fit	v_{min} (m/s)	v_{max} (m/s)
1	7.964697E+04	8.167405E+04	**13**	8.347810E+04	8.359773E+04
2	8.167405E+04	8.200703E+04	**14**	8.359773E+04	8.367103E+04
3	8.200703E+04	8.212879E+04	**15**	8.367103E+04	8.373208E+04
4	8.212879E+04	8.218131E+04	**16**	8.373208E+04	8.377196E+04
5	8.218131E+04	8.222827E+04	**17**	8.377196E+04	8.381426E+04
6	8.222827E+04	8.234968E+04	**18**	8.381426E+04	8.386014E+04
7	8.234968E+04	8.251497E+04	**19**	8.386014E+04	8.395180E+04
8	8.251497E+04	8.272389E+04	**20**	8.395180E+04	8.407631E+04
9	8.272389E+04	8.296511E+04	**21**	8.407631E+04	8.425907E+04
10	8.296511E+04	8.310731E+04	**22**	8.425907E+04	8.453612E+04
11	8.310731E+04	8.330381E+04	**23**	8.453612E+04	8.497173E+04
12	8.330381E+04	8.347810E+04	**24**	8.497173E+04	8.549152E+04

Table B-2: a_0 for the range in Table B-1 around 36.67 eV resonance

Fit	a_0	Fit	a_0
1	7.327659E+01	**13**	-1.670706E+05
2	6.574523E+01	**14**	-8.168471E+05
3	3.202155E+01	**15**	-5.223203E+06
4	8.603693E+00	**16**	-1.667356E+07
5	-8.903187E+00	**17**	1.546437E+07
6	-4.820046E+01	**18**	6.062479E+06
7	-1.522586E+02	**19**	1.109004E+06
8	-4.207782E+02	**20**	2.017793E+05
9	-1.244791E+03	**21**	5.025375E+04
10	-3.116292E+03	**22**	1.425484E+04
11	-8.592913E+03	**23**	4.329662E+03
12	-3.466312E+04	**24**	1.545231E+03

Table B-3: a_1 for the range in Table B-1 around 36.67 eV resonance

Fit	a_1	Fit	a_1
1	-1.088920E-08	**13**	2.400453E-05
2	-9.760168E-09	**14**	1.169814E-04
3	-4.745609E-09	**15**	7.463852E-04
4	-1.273797E-09	**16**	2.379570E-03
5	1.318368E-09	**17**	-2.199956E-03
6	7.130294E-09	**18**	-8.615762E-04
7	2.247477E-08	**19**	-1.572094E-04
8	6.191237E-08	**20**	-2.848684E-05
9	1.823251E-07	**21**	-7.051098E-06
10	4.542187E-07	**22**	-1.980537E-06
11	1.247148E-06	**23**	-5.916928E-07
12	5.003918E-06	**24**	-2.060479E-07

B.2 Fourth order fit with only 17 piecewise regions around 36.67 eV resonance

Table B-4: Piecewise regions around 36.67 eV resonance

Fit	v_{min} (m/s)	v_{max} (m/s)	Fit	v_{min} (m/s)	v_{max} (m/s)
1	7.964697E+04	8.145131E+04	**10**	8.360316E+04	8.368732E+04
2	8.145131E+04	8.189618E+04	**11**	8.368732E+04	8.375748E+04
3	8.189618E+04	8.213984E+04	**12**	8.375748E+04	8.378852E+04
4	8.213984E+04	8.222827E+04	**13**	8.378852E+04	8.386380E+04
5	8.222827E+04	8.236072E+04	**14**	8.386380E+04	8.401041E+04
6	8.236072E+04	8.272389E+04	**15**	8.401041E+04	8.421524E+04
7	8.272389E+04	8.310731E+04	**16**	8.421524E+04	8.456523E+04
8	8.310731E+04	8.342914E+04	**17**	8.456523E+04	8.549152E+04
9	8.342914E+04	8.360316E+04			

Table B-5: a_0 for the range in Table B-4 around 36.67 eV resonance

Fit	a_0	Fit	a_0
1	-2.86529176111E+02	**10**	4.98272690126E+08
2	1.06506186974E+03	**11**	6.95811254601E+09
3	4.04299610315E+03	**12**	-3.50065505657E+10
4	7.34088922881E+03	**13**	5.90874450887E+09
5	1.11378448276E+04	**14**	2.42508917519E+08
6	3.06696374331E+04	**15**	1.37875370049E+07
7	1.81299386694E+05	**16**	1.40638549110E+06
8	2.06285451306E+06	**17**	1.14714537839E+05
9	3.37406457421E+07		

Table B-6: a_1 for the range in Table B-4 around 36.67 eV resonance

Fit	a_1	Fit	a_1
1	9.99373073049E-08	**10**	-1.42580774909E-01
2	-3.07609776667E-07	**11**	-1.98681520577E+00
3	-1.19578485193E-06	**12**	9.97640668909E+00
4	-2.17391796171E-06	**13**	-1.68046681642E+00
5	-3.29671253642E-06	**14**	-6.87497920176E-02
6	-9.04630465944E-06	**15**	-3.88670099950E-03
7	-5.30067122025E-05	**16**	-3.92858875335E-04
8	-5.97075429111E-04	**17**	-3.13833027426E-05
9	-9.69337723169E-03		

Table B-7: a_2 for the range in Table B-4 around 36.67 eV resonance

Fit	a_2	Fit	a_2
1	-8.52934293597E-18	**10**	1.01998919383E-11
2	2.21929728199E-17	**11**	1.41828570418E-10
3	8.84181089092E-17	**12**	-7.10785668102E-10
4	1.60945072053E-16	**13**	1.19482679753E-10
5	2.43950246974E-16	**14**	4.87255057687E-12
6	6.67078442063E-16	**15**	2.73919501280E-13
7	3.87447890104E-15	**16**	2.74371349546E-14
8	4.32051025731E-14	**17**	2.14721123794E-15
9	6.96207852051E-13		

APPENDIX C

Coefficients For Four Resonances In ^{238}U

The coefficients generated using second order and fourth order least squares fits for the four low-lying resonances around 6.67 eV, 20.67 eV, 36.67 eV and 66.0 eV are presented in this appendix. The piecewise regions generated using the second order fits for these resonances are listed in Tables C-1, C-4, C-7 and C-10. These tables are followed by their corresponding coefficients. Piecewise regions generated using fourth order fits are listed in Tables C-13, C-17, C-21 and C-25, which are also followed by their related coefficients. All the coefficients here were generated using Mathematica 8.0.

C.1 Second order fit around 6.67 eV resonance

Table C-1: Piecewise regions around 6.67 eV resonance

Fit	v_{min} (m/s)	v_{max} (m/s)	Fit	v_{min} (m/s)	v_{max} (m/s)
1	3.332505E+04	3.464066E+04	**14**	3.554747E+04	3.559111E+04
2	3.464066E+04	3.510363E+04	**15**	3.559111E+04	3.563034E+04
3	3.510363E+04	3.524045E+04	**16**	3.563034E+04	3.566300E+04
4	3.524045E+04	3.528667E+04	**17**	3.566300E+04	3.568911E+04
5	3.528667E+04	3.530427E+04	**18**	3.568911E+04	3.571632E+04
6	3.530427E+04	3.531526E+04	**19**	3.571632E+04	3.573470E+04
7	3.531526E+04	3.532625E+04	**20**	3.573470E+04	3.578379E+04
8	3.532625E+04	3.534821E+04	**21**	3.578379E+04	3.582337E+04
9	3.534821E+04	3.537455E+04	**22**	3.582337E+04	3.587607E+04
10	3.537455E+04	3.540964E+04	**23**	3.587607E+04	3.598125E+04
11	3.540964E+04	3.545126E+04	**24**	3.598125E+04	3.618546E+04
12	3.545126E+04	3.549940E+04	**25**	3.618546E+04	3.668329E+04
13	3.549940E+04	3.554747E+04	**26**	3.668329E+04	3.789928E+04

Table C-2: a_0 for the range in Table C-1 around 6.67 eV resonance

Fit	a_0	Fit	a_0
1	4.08003113730E+01	**14**	-7.66192275488E+03
2	9.54242889138E+01	**15**	-2.01701844946E+04
3	1.05255607830E+02	**16**	-5.72688272230E+04
4	6.43972235301E+01	**17**	-1.62436777351E+05
5	3.00683702653E+01	**18**	-4.29052589003E+05
6	8.21176609831E+00	**19**	-3.91262329286E+05
7	-1.20000609196E+01	**20**	3.84256462444E+05
8	-4.84164447117E+01	**21**	1.27736201102E+05
9	-1.22448440865E+02	**22**	4.06136099124E+04
10	-2.62671561534E+02	**23**	1.12260235645E+04
11	-5.55426427891E+02	**24**	2.71001933448E+03
12	-1.26167016148E+03	**25**	5.36616461332E+02
13	-3.02476188850E+03	**26**	1.01478466824E+02

Table C-3: a_1 for the range in Table C-1 around 6.67 eV resonance

Fit	a_1	Fit	a_1
1	-3.08342351762E-08	**14**	6.07339366185E-06
2	-7.65031938032E-08	**15**	1.59464467395E-05
3	-8.45637522226E-08	**16**	4.51660347620E-05
4	-5.16561053176E-08	**17**	1.27849510633E-04
5	-2.40812241293E-08	**18**	3.37156208552E-04
6	-6.54456038021E-09	**19**	3.07595651401E-04
7	9.66152814038E-09	**20**	-2.99703526941E-04
8	3.88395368010E-08	**21**	-9.93580206793E-05
9	9.80857586858E-08	**22**	-3.14603624309E-05
10	2.10127854922E-07	**23**	-8.62648993980E-06
11	4.43584310328E-07	**24**	-2.04673534044E-06
12	1.00543639927E-06	**25**	-3.86185834949E-07
13	2.40426458659E-06	**26**	-6.22602360623E-08

C.2 Second order fit around 20.67 eV resonance

Table C-4: Piecewise regions around 20.67 eV resonance

Fit	v_{min} (m/s)	v_{max} (m/s)	Fit	v_{min} (m/s)	v_{max} (m/s)
1	6.034672E+04	6.130478E+04	**18**	6.288514E+04	6.296628E+04
2	6.130478E+04	6.209362E+04	**19**	6.296628E+04	6.302706E+04
3	6.209362E+04	6.217579E+04	**20**	6.302706E+04	6.307261E+04
4	6.217579E+04	6.221683E+04	**21**	6.307261E+04	6.311056E+04
5	6.221683E+04	6.224249E+04	**22**	6.311056E+04	6.313835E+04
6	6.224249E+04	6.225786E+04	**23**	6.313835E+04	6.315983E+04
7	6.225786E+04	6.226555E+04	**24**	6.315983E+04	6.319016E+04
8	6.226555E+04	6.227836E+04	**25**	6.319016E+04	6.321627E+04
9	6.227836E+04	6.229374E+04	**26**	6.321627E+04	6.323884E+04
10	6.229374E+04	6.232446E+04	**27**	6.323884E+04	6.326970E+04
11	6.232446E+04	6.236028E+04	**28**	6.326970E+04	6.331006E+04
12	6.236028E+04	6.241655E+04	**29**	6.331006E+04	6.337172E+04
13	6.241655E+04	6.249318E+04	**30**	6.337172E+04	6.347119E+04
14	6.249318E+04	6.258503E+04	**31**	6.347119E+04	6.364135E+04
15	6.258503E+04	6.268692E+04	**32**	6.364135E+04	6.395215E+04
16	6.268692E+04	6.278865E+04	**33**	6.395215E+04	6.449476E+04
17	6.278865E+04	6.288514E+04	**34**	6.449476E+04	6.552986E+04

Table C-5: a_0 for the range in Table C-4 around 20.67 eV resonance

Fit	a_0	Fit	a_0
1	6.35703277946E+01	**18**	-1.90269195000E+04
2	8.56974198613E+01	**19**	-5.32543759232E+04
3	5.68487172705E+01	**20**	-1.49051566493E+05
4	3.60804407467E+01	**21**	-4.24583601037E+05
5	2.05452701727E+01	**22**	-1.31771675767E+06
6	9.18445400471E+00	**23**	-3.81847737138E+06
7	2.22330223072E+00	**24**	-8.31355725680E+06
8	-4.72190726974E+00	**25**	8.00390293518E+06
9	-1.47805320642E+01	**26**	4.42018379734E+06
10	-3.35147116222E+01	**27**	1.47640122283E+06
11	-6.59148074778E+01	**28**	4.82125809704E+05
12	-1.24605372463E+02	**29**	1.62847391885E+05
13	-2.49204718174E+02	**30**	5.08798375211E+04
14	-5.19898620487E+02	**31**	1.44487502589E+04
15	-1.14784332331E+03	**32**	3.99061944813E+03
16	-2.73384229254E+03	**33**	1.05321936672E+03
17	-6.89738750435E+03	**34**	2.90939644336E+02

Table C-6: a_1 for the range in Table C-4 around 20.67 eV resonance

Fit	a_1	Fit	a_1
1	-1.62822108212E-08	**18**	4.81980959161E-06
2	-2.21726850321E-08	**19**	1.34520665360E-05
3	-1.46877720327E-08	**20**	3.75653888491E-05
4	-9.31478267113E-09	**21**	1.06821131014E-04
5	-5.30124653843E-09	**22**	3.31050056411E-04
6	-2.36863611438E-09	**23**	9.58342640832E-04
7	-5.72635063573E-10	**24**	2.08520742865E-03
8	1.21872046789E-09	**25**	-2.00132503954E-03
9	3.81205293665E-09	**26**	-1.10465401723E-03
10	8.63943223179E-09	**27**	-3.68530899399E-04
11	1.69803187625E-08	**28**	-1.20138379840E-04
12	3.20705183176E-08	**29**	-4.04764937455E-05
13	6.40479727543E-08	**30**	-1.25935846104E-05
14	1.33347930877E-07	**31**	-3.54885848795E-06
15	2.93634853770E-07	**32**	-9.66109208112E-07
16	6.97149261438E-07	**33**	-2.47489280810E-07
17	1.75300652475E-06	**34**	-6.40580507282E-08

C.3 Second order fit around 36.67 eV resonance

Table C-7: Piecewise regions around 36.67 eV resonance

Fit	v_{min} (m/s)	v_{max} (m/s)	Fit	v_{min} (m/s)	v_{max} (m/s)
1	7.964697E+04	8.064435E+04	**22**	8.330381E+04	8.342914E+04
2	8.064435E+04	8.154048E+04	**23**	8.342914E+04	8.352706E+04
3	8.154048E+04	8.191837E+04	**24**	8.352706E+04	8.359773E+04
4	8.191837E+04	8.204026E+04	**25**	8.359773E+04	8.364932E+04
5	8.204026E+04	8.210667E+04	**26**	8.364932E+04	8.368732E+04
6	8.210667E+04	8.213984E+04	**27**	8.368732E+04	8.371987E+04
7	8.213984E+04	8.215644E+00	**28**	8.371987E+04	8.374506E+04
8	8.215644E+00	8.217025E+04	**29**	8.374506E+04	8.376783E+04
9	8.217025E+04	8.218131E+04	**30**	8.376783E+04	8.377300E+04
10	8.218131E+04	8.219237E+04	**31**	8.377300E+04	8.378024E+04
11	8.219237E+04	8.220617E+04	**32**	8.378024E+04	8.381426E+04
12	8.220617E+04	8.222827E+04	**33**	8.381426E+04	8.384363E+04
13	8.222827E+04	8.226140E+04	**34**	8.384363E+04	8.387848E+04
14	8.226140E+04	8.231658E+04	**35**	8.387848E+04	8.392982E+04
15	8.231658E+04	8.239380E+04	**36**	8.392982E+04	8.401041E+04
16	8.239380E+04	8.249296E+04	**37**	8.401041E+04	8.413484E+04
17	8.249296E+04	8.263599E+04	**38**	8.413484E+04	8.434667E+04
18	8.263599E+04	8.280071E+04	**39**	8.434667E+04	8.463797E+04
19	8.280071E+04	8.297605E+04	**40**	8.463797E+04	8.505858E+04
20	8.297605E+04	8.315102E+04	**41**	8.505858E+04	8.549152E+04
21	8.315102E+04	8.330381E+04	**42**	8.549152E+04	8.617971E+04

Table C-8: a_0 for the range in Table C-7 around 36.67 eV resonance

Fit	a_0	Fit	a_0
1	6.52031927356E+01	**22**	-2.63133474313E+04
2	8.19689391307E+01	**23**	-7.41139795827E+04
3	7.45804259992E+01	**24**	-2.12964388954E+05
4	4.93425875436E+01	**25**	-6.07085350340E+05
5	3.11284664408E+01	**26**	-1.64908634141E+06
6	1.82973070900E+01	**27**	-4.76345394861E+06
7	1.10314644827E+01	**28**	-1.32470909717E+07
8	6.05092902915E+00	**29**	-1.98051776438E+07
9	1.82795295936E+00	**30**	-4.48071888385E+06
10	-2.07957354615E+00	**31**	7.58580927448E+06
11	-6.69283450089E+00	**32**	1.83449170418E+07
12	-1.38667865610E+01	**33**	7.40613916067E+06
13	-2.55229186259E+01	**34**	2.75384814921E+06
14	-4.72050896568E+01	**35**	9.87258063376E+05
15	-8.73707009299E+01	**36**	3.33716249012E+05
16	-1.59699257389E+02	**37**	1.02955233694E+05
17	-3.12277145552E+02	**38**	3.11394716495E+04
18	-6.60770265550E+02	**39**	9.39703354031E+03
19	-1.48161634332E+03	**40**	3.32562922102E+03
20	-3.61051507416E+03	**41**	1.39869882067E+03
21	-9.46082533461E+03	**42**	6.67917785986E+02

Table C-9: a_1 for the range in Table C-7 around 36.67 eV resonance

Fit	a_1	Fit	a_1
1	-9.61126167211E-09	**22**	3.79986189556E-06
2	-1.21912369455E-08	**23**	1.06663709449E-05
3	-1.10836902419E-08	**24**	3.05668642540E-05
4	-7.32094344785E-09	**25**	8.69577629335E-05
5	-4.61437069524E-09	**26**	2.35868518276E-04
6	-2.71085971482E-09	**27**	6.80530191159E-04
7	-1.63389698625E-09	**28**	1.89088810968E-03
8	-8.96001039226E-10	**29**	2.82609433737E-03
9	-2.70553368680E-10	**30**	6.42136294396E-04
10	3.08016147354E-10	**31**	-1.07724711663E-03
11	9.90893736451E-10	**32**	-2.61010032565E-03
12	2.05243446288E-09	**33**	-1.05291307624E-03
13	3.77626849757E-09	**34**	-3.91085887058E-04
14	6.98011807771E-09	**35**	-1.39984785803E-04
15	1.29070986823E-08	**36**	-4.72040032214E-05
16	2.35599235973E-08	**37**	-1.45043648423E-05
17	4.59752195689E-08	**38**	-4.35768890839E-06
18	9.69963276906E-08	**39**	-1.30049155178E-06
19	2.16692761973E-07	**40**	-4.52642436890E-07
20	5.25817128269E-07	**41**	-1.86097231801E-07
21	1.37179060006E-06	**42**	-8.61003211899E-08

C.4 Second order fit around 66.0 eV resonance

Table C-10: Piecewise regions around 66.0 eV resonance

Fit	v_{min} (m/s)	v_{max} (m/s)	Fit	v_{min} (m/s)	v_{max} (m/s)
1	1.097575E+05	1.104161E+05	**18**	1.120885E+05	1.121551E+05
2	1.104161E+05	1.112743E+05	**19**	1.121551E+05	1.122132E+05
3	1.112743E+05	1.116341E+05	**20**	1.122132E+05	1.122631E+05
4	1.116341E+05	1.117009E+05	**21**	1.122631E+05	1.123005E+05
5	1.117009E+05	1.117260E+05	**22**	1.123005E+05	1.123295E+05
6	1.117260E+05	1.117427E+05	**23**	1.123295E+05	1.123513E+05
7	1.117427E+05	1.117531E+05	**24**	1.123513E+05	1.123690E+05
8	1.117531E+05	1.117614E+05	**25**	1.123690E+05	1.123969E+05
9	1.117614E+05	1.117698E+05	**26**	1.123969E+05	1.124256E+05
10	1.117698E+05	1.117802E+05	**27**	1.124256E+05	1.124470E+05
11	1.117802E+05	1.117927E+05	**28**	1.124470E+05	1.124779E+05
12	1.117927E+05	1.118136E+05	**29**	1.124779E+05	1.125207E+05
13	1.118136E+05	1.118469E+05	**30**	1.125207E+05	1.125968E+05
14	1.118469E+05	1.118928E+05	**31**	1.125968E+05	1.127203E+05
15	1.118928E+05	1.119511E+05	**32**	1.127203E+05	1.129479E+05
16	1.119511E+05	1.120178E+05	**33**	1.129479E+05	1.134772E+05
17	1.120178E+05	1.120885E+05	**34**	1.134772E+05	1.144100E+05

Table C-11: a_0 for the range in Table C-10 around 66.0 eV resonance

Fit	a_0	Fit	a_0
1	1.16726057689E+02	**18**	-1.37662184855E+04
2	1.98082828833E+02	**19**	-3.50293435049E+04
3	2.77865992459E+02	**20**	-9.51382859413E+04
4	1.87912604054E+02	**21**	-2.70538279715E+05
5	1.17721161792E+02	**22**	-7.56265787716E+05
6	7.44566347919E+01	**23**	-2.19020744470E+06
7	4.02457346622E+01	**24**	-6.15159617105E+06
8	1.40691639930E+01	**25**	-1.57028582859E+07
9	-1.11502500553E+01	**26**	1.47736424036E+07
10	-4.24723198747E+01	**27**	5.07914339071E+06
11	-8.38007851696E+01	**28**	1.62632565689E+06
12	-1.53308043592E+02	**29**	4.94251443258E+05
13	-2.93775825917E+02	**30**	1.46423029665E+05
14	-5.77389287272E+02	**31**	4.09353640036E+04
15	-1.17451900038E+03	**32**	1.07800986559E+04
16	-2.50296010216E+03	**33**	2.32708065730E+03
17	-5.69017697529E+03	**34**	5.35281502549E+02

Table C-12: a_1 for the range in Table C-10 around 66.0 eV resonance

Fit	a_1	Fit	a_1
1	-9.14961407888E-09	**18**	1.09659315855E-06
2	-1.58155748611E-08	**19**	2.78689985264E-06
3	-2.22738221035E-08	**20**	7.56030927654E-06
4	-1.50542291441E-08	**21**	2.14770532368E-05
5	-9.42809390550E-09	**22**	5.99909518153E-05
6	-5.96208005513E-09	**23**	1.73631958432E-04
7	-3.22219445438E-09	**24**	4.87453653256E-04
8	-1.12617849224E-09	**25**	1.24387853278E-03
9	8.92889329083E-10	**26**	-1.16858615998E-03
10	3.40015361355E-09	**27**	-4.01573666282E-04
11	6.70777865806E-09	**28**	-1.28495192822E-04
12	1.22692884327E-08	**29**	-3.90092075992E-05
13	2.35041830968E-08	**30**	-1.15361379605E-05
14	4.61743987350E-08	**31**	-3.21505357170E-06
15	9.38652625533E-08	**32**	-8.41470735962E-07
16	1.99852493845E-07	**33**	-1.78797067806E-07
17	4.53834855988E-07	**34**	-3.95576263783E-08

C.5 Fourth order fit around 6.67 eV resonance

Table C-13: Piecewise regions around 6.67 eV resonance

Fit	v_{min} (m/s)	v_{max} (m/s)	Fit	v_{min} (m/s)	v_{max} (m/s)
1	3.332505E+04	3.503280E+04	**8**	3.566083E+04	3.572857E+04
2	3.503280E+04	3.525806E+04	**9**	3.572857E+04	3.577058E+04
3	3.525806E+04	3.535699E+04	**10**	3.577058E+04	3.583919E+04
4	3.535699E+04	3.543155E+04	**11**	3.583919E+04	3.598125E+04
5	3.543155E+04	3.552126E+04	**12**	3.598125E+04	3.634176E+04
6	3.552126E+04	3.559983E+04	**13**	3.634176E+04	3.699103E+04
7	3.559983E+04	3.566083E+04	**14**	3.699103E+04	3.789928E+04

Table C-14: a_0 for the range in Table C-13 around 6.67 eV resonance

Fit	a_0	Fit	a_0
1	-3.59386503924E+02	**8**	8.14427195463E+07
2	1.39713721648E+03	**9**	-1.32420801640E+08
3	1.54066274056E+04	**10**	3.49295607221E+07
4	5.24310116181E+04	**11**	2.18690260638E+06
5	2.06458812089E+05	**12**	9.99287219800E+04
6	1.26002330622E+06	**13**	6.46514518348E+03
7	9.58160801475E+06	**14**	8.80001442776E+02

Table C-15: a_1 for the range in Table C-13 around 6.67 eV resonance

Fit	a_1	Fit	a_1
1	6.61739128213E-07	**8**	-1.28106993356E-01
2	-2.17470108651E-06	**9**	2.07493251804E-01
3	-2.47120400363E-05	**10**	-5.43880124716E-02
4	-8.39324329195E-05	**11**	-3.37940343058E-03
5	-3.29154570825E-04	**12**	-1.51452408697E-04
6	-1.99808418286E-03	**13**	-9.39833609807E-06
7	-1.51239594093E-02	**14**	-1.18942728352E-06

Table C-16: a_2 for the range in Table C-13 around 6.67 eV resonance

Fit	a_2	Fit	a_2
1	-2.99499788691E-16	**8**	5.03772424094E-11
2	8.45403484299E-16	**9**	-8.12805970376E-11
3	9.90948422530E-15	**10**	2.11717103681E-11
4	3.35902108088E-14	**11**	1.30558244875E-12
5	1.31192583285E-13	**12**	5.74010065659E-14
6	7.92121996684E-13	**13**	3.42414163165E-15
7	5.96807840551E-12	**14**	4.07760219694E-16

C.6 Fourth order fit around 20.67 eV resonance

Table C-17: Piecewise regions around 20.67 eV resonance

Fit	v_{min} (m/s)	v_{max} (m/s)	Fit	v_{min} (m/s)	v_{max} (m/s)
1	6.034672E+04	6.198046E+04	**10**	6.313962E+04	6.318453E+04
2	6.198046E+04	6.219632E+04	**11**	6.318453E+04	6.321186E+04
3	6.219632E+04	6.235004E+04	**12**	6.321186E+04	6.325546E+04
4	6.235004E+04	6.249318E+04	**13**	6.325546E+04	6.332429E+04
5	6.249318E+04	6.269710E+04	**14**	6.332429E+04	6.346172E+04
6	6.269710E+04	6.287499E+04	**15**	6.346172E+04	6.382047E+04
7	6.287499E+04	6.300173E+04	**16**	6.382047E+04	6.442019E+04
8	6.300173E+04	6.308526E+04	**17**	6.442019E+04	6.552986E+04
9	6.308526E+04	6.313962E+04			

Table C-18: a_0 for the range in Table C-16 around 20.67 eV resonance

Fit	a_0	Fit	a_0
1	-4.28971329567E+02	**10**	3.44062439059E+09
2	3.41954766708E+03	**11**	-9.07522000888E+09
3	1.09034153869E+04	**12**	2.47305295577E+09
4	2.89651061422E+04	**13**	2.27151057274E+08
5	1.04522614313E+05	**14**	1.73428490503E+07
6	6.57091359256E+05	**15**	9.45415987503E+05
7	5.00634124243E+06	**16**	6.23098137098E+04
8	4.73871631538E+07	**17**	6.52366842426E+03
9	5.16608405053E+08		

Table C-19: a_1 for the range in Table C-16 around 20.67 eV resonance

Fit	a_1	Fit	a_1
1	2.49167388537E-07	**10**	-1.72655960490E+00
2	-1.75675023769E-06	**11**	4.54590770227E+00
3	-5.62543098774E-06	**12**	-1.23608576609E+00
4	-1.49147904056E-05	**13**	-1.13286607610E-01
5	-5.35740170710E-05	**14**	-8.61197336317E-03
6	-3.34493425804E-04	**15**	-4.64528144837E-04
7	-2.53366556859E-03	**16**	-2.99672351481E-05
8	-2.38801835074E-02	**17**	-3.01481849188E-06
9	-2.59621959614E-01		

Table C-20: a_2 for the range in Table C-16 around 20.67 eV resonance

Fit	a_2	Fit	a_2
1	-3.57613303385E-17	**10**	2.16603834893E-10
2	2.25620872277E-16	**11**	-5.69276823069E-10
3	7.25586418792E-16	**12**	1.54455768184E-10
4	1.91999634217E-15	**13**	1.41248379550E-11
5	6.86502604859E-15	**14**	1.06912742405E-12
6	4.25690761993E-14	**15**	5.70647301963E-14
7	3.20568735982E-13	**16**	3.60468908663E-15
8	3.00854104252E-12	**17**	3.49217085194E-16
9	3.26183409167E-11		

C.7 Fourth order fit around 36.67 eV resonance

Table C-21: Piecewise regions around 36.67 eV resonance

Fit	v_{min} (m/s)	v_{max} (m/s)	Fit	v_{min} (m/s)	v_{max} (m/s)
1	7.964697E+04	8.145131E+04	**10**	8.360316E+04	8.368732E+04
2	8.145131E+04	8.189618E+04	**11**	8.368732E+04	8.375748E+04
3	8.189618E+04	8.213984E+04	**12**	8.375748E+04	8.378852E+04
4	8.213984E+04	8.222827E+04	**13**	8.378852E+04	8.386380E+04
5	8.222827E+04	8.236072E+04	**14**	8.386380E+04	8.401041E+04
6	8.236072E+04	8.272389E+04	**15**	8.401041E+04	8.421524E+04
7	8.272389E+04	8.310731E+04	**16**	8.421524E+04	8.456523E+04
8	8.310731E+04	8.342914E+04	**17**	8.456523E+04	8.549152E+04
9	8.342914E+04	8.360316E+04	**18**	8.549152E+04	8.617971E+04

Table C-22: a_0 for the range in Table C-21 around 36.67 eV resonance

Fit	a_0	Fit	a_0
1	-2.86529176111E+02	**10**	4.98272690126E+08
2	1.06506186974E+03	**11**	6.95811254601E+09
3	4.04299610315E+03	**12**	-3.50065505657E+10
4	7.34088922881E+03	**13**	5.90874450887E+09
5	1.11378448276E+04	**14**	2.42508917519E+08
6	3.06696374331E+04	**15**	1.37875370049E+07
7	1.81299386694E+05	**16**	1.40638549110E+06
8	2.06285451306E+06	**17**	1.14714537839E+05
9	3.37406457421E+07	**18**	1.69806597394E+04

Table C-23: a_1 for the range in Table C-21 around 36.67 eV resonance

Fit	a_1	Fit	a_1
1	9.99373073049E-08	**10**	-1.42580774909E-01
2	-3.07609776667E-07	**11**	-1.98681520577E+00
3	-1.19578485193E-06	**12**	9.97640668909E+00
4	-2.17391796171E-06	**13**	-1.68046681642E+00
5	-3.29671253642E-06	**14**	-6.87497920176E-02
6	-9.04630465944E-06	**15**	-3.88670099950E-03
7	-5.30067122025E-05	**16**	-3.92858875335E-04
8	-5.97075429111E-04	**17**	-3.13833027426E-05
9	-9.69337723169E-03	**18**	-4.51529032532E-06

Table C-24: a_2 for the range in Table C-21 around 36.67 eV resonance

Fit	a_2	Fit	a_2
1	-8.52934293597E-18	**10**	1.01998919383E-11
2	2.21929728199E-17	**11**	1.41828570418E-10
3	8.84181089092E-17	**12**	-7.10785668102E-10
4	1.60945072053E-16	**13**	1.19482679753E-10
5	2.43950246974E-16	**14**	4.87255057687E-12
6	6.67078442063E-16	**15**	2.73919501280E-13
7	3.87447890104E-15	**16**	2.74371349546E-14
8	4.32051025731E-14	**17**	2.14721123794E-15
9	6.96207852051E-13	**18**	3.00642542046E-16

C.8 Fourth order fit around 66.0 eV resonance

Table C-25: Piecewise regions around 66.0 eV resonance

Fit	v_{min} (m/s)	v_{max} (m/s)	Fit	v_{min} (m/s)	v_{max} (m/s)
1	1.097575E+05	1.116258E+05	**10**	1.123617E+05	1.123931E+05
2	1.116258E+05	1.117260E+05	**11**	1.123931E+05	1.124172E+05
3	1.117260E+05	1.118136E+05	**12**	1.124172E+05	1.124541E+05
4	1.118136E+05	1.119053E+05	**13**	1.124541E+05	1.125184E+05
5	1.119053E+05	1.120386E+05	**14**	1.125184E+05	1.126538E+05
6	1.120386E+05	1.121675E+05	**15**	1.126538E+05	1.130047E+05
7	1.121675E+05	1.122631E+05	**16**	1.130047E+05	1.136257E+05
8	1.122631E+05	1.123233E+05	**17**	1.136257E+05	1.144100E+05
9	1.123233E+05	1.123617E+05			

Table C-26: a_0 for the range in Table C-25 around 66.0 eV resonance

Fit	a_0	Fit	a_0
1	-3.29181121727E+03	**10**	1.23219393291E+10
2	3.82055268702E+04	**11**	-2.49684921845E+10
3	9.25190901142E+04	**12**	8.19217706940E+09
4	2.19297942742E+05	**13**	6.58551813052E+08
5	7.36145007987E+05	**14**	4.42110337530E+07
6	4.17279319334E+06	**15**	2.20601941407E+06
7	3.42031438089E+07	**16**	1.29745827994E+05
8	3.41307930299E+08	**17**	1.94638933125E+04
9	3.68669785750E+09		

Table C-27: a_1 for the range in Table C-25 around 66.0 eV resonance

Fit	a_1	Fit	a_1
1	5.52507203761E-07	**10**	-1.95258791805E+00
2	-6.11280429232E-06	**11**	3.95334243185E+00
3	-1.48144120839E-05	**12**	-1.29560397387E+00
4	-3.50928573711E-05	**13**	-1.04031570555E-01
5	-1.17609087169E-04	**14**	-6.96747217513E-03
6	-6.64988153442E-04	**15**	-3.45620930227E-04
7	-5.43756825212E-03	**16**	-2.00678035198E-05
8	-5.41653209882E-02	**17**	-2.95720257281E-06
9	-5.84428803104E-01		

Table C-28: a_2 for the range in Table C-25 around 66.0 eV resonance

Fit	a_2	Fit	a_2
1	-2.31372666321E-17	**10**	7.73538934650E-11
2	2.44508702832E-16	**11**	-1.56486318873E-10
3	5.93031151423E-16	**12**	5.12253929486E-11
4	1.40392224582E-15	**13**	4.10847502334E-12
5	4.69741515968E-15	**14**	2.74511897813E-13
6	2.64936431187E-14	**15**	1.35375559102E-14
7	2.16114491100E-13	**16**	7.76119727810E-16
8	2.14900032454E-12	**17**	1.12428232480E-16
9	2.31614510010E-11		

APPENDIX D

Derivation of P_1 Moment

D.1 P_1 Moment

We begin the derivation with a general equation for the P_1 moment of the differential scattering kernel,

$$K_1(v,v') = \frac{B^3}{\sqrt{\pi}} \frac{(A+1)}{A} v' \int_{\mu} \int_{V} \frac{(S\cos\alpha)\sigma_s(v_r)V^2 \exp\left(-B^2V^2\right)}{v_c} dV\, d\mu, \tag{D.1}$$

where, $S = \dfrac{v'^2 - \left(\dfrac{A}{A+1}\right)^2 v_r^2 + v_c^2}{2v'v_c}$ and $\cos\alpha = \dfrac{v + AV\mu}{(A+1)v_c}$.

Substitute S and $\cos\alpha$ into Eq. (D.1):

$$K_1(v,v') = \frac{B^3}{\sqrt{\pi}} \frac{(A+1)}{A} v' \int_{\mu} \int_{V} \left\{ \begin{array}{l} \left(\dfrac{v'^2 - \left(\dfrac{A}{A+1}\right)^2 v_r^2 + v_c^2}{2v'v_c} \right) \left(\dfrac{\sigma_s(v_r)V^2 \exp\left(-B^2V^2\right)}{v_c} \right) \times \\ \left(\dfrac{v + AV\mu}{(A+1)v_c} \right) \end{array} \right\} dV\, d\mu,$$

$$K_1(v,v') = \frac{B^3}{2A\sqrt{\pi}} \int_{\mu}\int_{V} \left(v'^2 - \left(\frac{A}{A+1}\right)^2 v_r^2 + v_c^2 \right) \left(v + AV\mu \right) \left(\frac{\sigma_s(v_r) V^2 \exp\left(-B^2 V^2\right)}{v_c^3} \right) dV\, d\mu.$$

The following terms provided in [1] are restated below:

$$AV\mu = \frac{(A+1)^2 v_c^2 - v^2 - A^2 V^2}{2v} \text{ and } d\mu = \frac{(A+1)^2 v_c dv_c}{AvV},$$

$$V^2 = \frac{v_r^2}{A+1} + \frac{(A+1)}{A} v_c^2 - \frac{v^2}{A} \text{ and } dV = \frac{v_r}{(A+1)V} dv_r.$$

Substitute these values into $K_1(v,v')$:

$$K_1(v,v') = \frac{B^3}{2A\sqrt{\pi}} \times$$

$$\int_{v_c}\int_{v_r} \left\{ \begin{array}{l} \left(v'^2 - \left(\frac{A}{A+1}\right)^2 v_r^2 + v_c^2 \right) \\ \left(v + \frac{(A+1)^2 v_c^2 - v^2 - A^2 \left(\frac{v_r^2}{A+1} + \frac{(A+1)}{A} v_c^2 - \frac{v^2}{A} \right)}{2v} \right) \times \\ \left(\frac{\sigma_s(v_r)}{v_c^3} V^2 \exp\left(-B^2 \left(\frac{v_r^2}{A+1} + \frac{(A+1)}{A} v_c^2 - \frac{v^2}{A} \right) \right) \right) \end{array} \right\} \frac{v_r}{(A+1)V} dv_r \frac{(A+1)^2 v_c dv_c}{AvV},$$

$$K_1(v,v') = \frac{B^3}{2A\sqrt{\pi}} \times$$

$$\int_{v_c}\int_{v_r} \left\{ \begin{array}{l} \left(v'^2 - \left(\frac{A}{A+1}\right)^2 v_r^2 + v_c^2 \right) \\ \left(v + \frac{(A+1)^2 v_c^2 - v^2 - A^2\left(\frac{v_r^2}{A+1} + \frac{(A+1)}{A} v_c^2 - \frac{v^2}{A}\right)}{2v} \right) \times \\ \left(\frac{\sigma_s(v_r)}{v_c^2} \exp\left(-\frac{B^2 v_r^2}{A+1}\right) \exp\left(-\frac{B^2(A+1)}{A} v_c^2\right) \exp\left(\frac{B^2 v^2}{A}\right) \right) \end{array} \right\} \frac{(A+1)v_r}{Av} dv_r\, dv_c.$$

Move constants, $\frac{(A+1)}{Av}$, and $\exp\left(\frac{B^2 v^2}{A}\right)$ outside the integral,

$$K_1(v,v') = \frac{B^3(A+1)}{2A^2\sqrt{\pi}v} \exp\left(\frac{B^2 v^2}{A}\right) \times$$

$$\int_{v_c}\int_{v_r} \left\{ \begin{array}{l} \left(v'^2 - \left(\frac{A}{A+1}\right)^2 v_r^2 + v_c^2 \right) \\ \left(\frac{2v^2 + (A+1)^2 v_c^2 - v^2 - A^2\left(\frac{v_r^2}{A+1} + \frac{(A+1)}{A} v_c^2 - \frac{v^2}{A}\right)}{2v} \right) \times \\ \left(\frac{\sigma_s(v_r)}{v_c^2} \exp\left(-\frac{B^2 v_r^2}{A+1}\right) \exp\left(-\frac{B^2(A+1)}{A} v_c^2\right) \right) \end{array} \right\} v_r\, dv_r\, dv_c.$$

Simplify terms within the second set of brackets, and move v_r into the third set of brackets within the integral,

$$K_1(v,v') = \frac{B^3(A+1)}{4\sqrt{\pi}A^2v^2}\exp\left(\frac{B^2v^2}{A}\right)\int_{v_c}\int_{v_r}\left\{\begin{array}{l}\left(v'^2 - \left(\frac{A}{A+1}\right)^2 v_r^2 + v_c^2\right) \\ \left(v^2 + (A+1)^2 v_c^2 - \frac{A^2v_r^2}{A+1} - A(A+1)v_c^2 + Av^2\right)\times \\ \left(\frac{\sigma_s(v_r)}{v_c^2}v_r\exp\left(-\frac{B^2v_r^2}{A+1}\right)\exp\left(-\frac{B^2(A+1)}{A}v_c^2\right)\right)\end{array}\right\}dv_r\,dv_c.$$

Multiply terms in the second set of brackets by $\left(\frac{A+1}{A+1}\right)$,

$$K_1(v,v') = \frac{B^3(A+1)}{4\sqrt{\pi}A^2v^2}\exp\left(\frac{B^2v^2}{A}\right)\int_{v_c}\int_{v_r}\left\{\begin{array}{l}\left(v'^2 - \left(\frac{A}{A+1}\right)^2 v_r^2 + v_c^2\right) \\ \left(\frac{A+1}{A+1}\right)\left(v^2 + (A+1)^2 v_c^2 - \frac{A^2v_r^2}{A+1} - A(A+1)v_c^2 + Av^2\right)\times \\ \left(\frac{\sigma_s(v_r)}{v_c^2}v_r\exp\left(-\frac{B^2v_r^2}{A+1}\right)\exp\left(-\frac{B^2(A+1)}{A}v_c^2\right)\right)\end{array}\right\}dv_r\,dv_c.$$

Move (A+1) in the numerator outside the integral and keep the denominator with (A+1) within the integral and simplify terms in the second set of brackets,

$$K_1(v,v') = \frac{B^3(A+1)^2}{4\sqrt{\pi}A^2v^2}\exp\left(\frac{B^2v^2}{A}\right)\int_{v_c}\int_{v_r}\left\{\begin{array}{l}\left(v'^2 - \left(\frac{A}{A+1}\right)^2 v_r^2 + v_c^2\right) \\ \left(\frac{1}{A+1}\right)\left((A+1)v^2 + (A+1)v_c^2 - \frac{A^2v_r^2}{A+1}\right)\times \\ \left(\frac{\sigma_s(v_r)}{v_c^2}v_r\exp\left(-\frac{B^2v_r^2}{A+1}\right)\exp\left(-\frac{B^2(A+1)}{A}v_c^2\right)\right)\end{array}\right\}dv_r\,dv_c,$$

$$K_1(v,v') = \frac{B^3(A+1)^2}{4\sqrt{\pi}A^2v^2}\exp\left(\frac{B^2v^2}{A}\right)\int_{v_c}\int_{v_r}\left\{\begin{array}{l}\left(v'^2 - \left(\frac{A}{A+1}\right)^2 v_r^2 + v_c^2\right)\left(v^2 + v_c^2 - \frac{A^2v_r^2}{(A+1)^2}\right)\times \\ \left(\frac{\sigma_s(v_r)}{v_c^2}v_r\exp\left(-\frac{B^2v_r^2}{A+1}\right)\exp\left(-\frac{B^2(A+1)}{A}v_c^2\right)\right)\end{array}\right\}dv_r\,dv_c.$$

Multiply the terms in the first and second set of brackets above,

$$K_1(v,v') = \frac{B^3(A+1)^2}{4\sqrt{\pi}A^2v^2}\exp\left(\frac{B^2v^2}{A}\right)\int_{v_c}\int_{v_r}\left\{\begin{array}{l}\left(\begin{array}{l}v'^2v^2 + v'^2v_c^2 - \frac{A^2}{(A+1)^2}v'^2v_r^2 - \left(\frac{A}{A+1}\right)^2 v^2v_r^2 - \\ \left(\frac{A}{A+1}\right)^2 v_c^2v_r^2 + \left(\frac{A}{A+1}\right)^4 v_r^4 + v^2v_c^2 + v_c^4 - \frac{A^2v_c^2v_r^2}{(A+1)^2}\end{array}\right) \\ \left(\frac{\sigma_s(v_r)}{v_c^2}v_r\exp\left(-\frac{B^2v_r^2}{A+1}\right)\exp\left(-\frac{B^2(A+1)}{A}v_c^2\right)\right)\end{array}\right\}dv_r\,dv_c.$$

Group all the terms without v_c^2 or v_c^4 in the first set of brackets and the rest in the second set,

$$K_1(v,v') = \frac{B^3(A+1)^2}{4\sqrt{\pi}A^2v^2}\exp\left(\frac{B^2v^2}{A}\right)\times$$
$$\int_{v_c}\int_{v_r}\left\{\begin{array}{l}\left[\begin{array}{l}\left(v'^2v^2 - \frac{A^2}{(A+1)^2}v'^2v_r^2 - \left(\frac{A}{A+1}\right)^2 v^2v_r^2 + \left(\frac{A}{A+1}\right)^4 v_r^4\right)\frac{1}{v_c^2} + \\ \left(v'^2v_c^2 - 2\left(\frac{A}{A+1}\right)^2 v_c^2v_r^2 + v^2v_c^2 + v_c^4\right)\frac{1}{v_c^2}\end{array}\right]\times \\ \left(\sigma_s(v_r)v_r\exp\left(-\frac{B^2v_r^2}{A+1}\right)\exp\left(-\frac{B^2(A+1)}{A}v_c^2\right)\right)\end{array}\right\}dv_r\,dv_c.$$

Simplify the terms the second set of brackets,

$$K_1(v,v') = \frac{B^3(A+1)^2}{4\sqrt{\pi}A^2v^2}\exp\left(\frac{B^2v^2}{A}\right)\times$$

$$\int_{v_c}\int_{v_r}\left\{\begin{array}{l}\left[\begin{array}{l}\left(v'^2v^2 - \frac{A^2}{(A+1)^2}v'^2v_r^2 - \left(\frac{A}{A+1}\right)^2 v^2v_r^2 + \left(\frac{A}{A+1}\right)^4 v_r^4\right)\frac{1}{v_c^2} + \\ \left(v'^2 - 2\left(\frac{A}{A+1}\right)^2 v_r^2 + v^2 + v_c^2\right)\end{array}\right]\times \\ \left(\sigma_s(v_r)v_r\exp\left(-\frac{B^2v_r^2}{A+1}\right)\exp\left(-\frac{B^2(A+1)}{A}v_c^2\right)\right)\end{array}\right\}dv_r\,dv_c. \tag{D.2}$$

We will now use this equation to derive the upscattering and downscattering cases for P_1 moment.

D.1.1 Downscattering Case (v' < v)

We start off the derivation for the downscattering case for P_1 moment from Eq. (D.2),

$$K_1(v,v') = \frac{B^3(A+1)^2}{4\sqrt{\pi}A^2v^2}\exp\left(\frac{B^2v^2}{A}\right)\times$$

$$\int_{v_c}\int_{v_r}\left\{\begin{array}{l}\left[\begin{array}{l}\left(v'^2v^2 - \frac{A^2}{(A+1)^2}v'^2v_r^2 - \left(\frac{A}{A+1}\right)^2 v^2v_r^2 + \left(\frac{A}{A+1}\right)^4 v_r^4\right)\frac{1}{v_c^2} + \\ \left(v'^2 - 2\left(\frac{A}{A+1}\right)^2 v_r^2 + v^2 + v_c^2\right)\end{array}\right]\times \\ \left(\sigma_s(v_r)v_r\exp\left(-\frac{B^2v_r^2}{A+1}\right)\exp\left(-\frac{B^2(A+1)}{A}v_c^2\right)\right)\end{array}\right\}dv_r\,dv_c.$$

We will generalize the previous equation and restate it in the following form:

$$K_1(v,v') = \frac{B^3(A+1)^2}{4\sqrt{\pi}A^2v^2}\exp\left(\frac{B^2v^2}{A}\right)\times$$
$$\left\{\int_{v_{r\_11}}^{v_{r\_12}} f(v_r)dv_r \int_{v_{c\_11}}^{v_{c\_12}} g(v_c)dv_c + \int_{v_{r\_21}}^{\infty} f(v_r)dv_r \int_{v_{c\_21}}^{v_{c\_22}} g(v_c)dv_c\right\}, \tag{D.3}$$

where,

$$g(v_c) = \left[\begin{array}{l}\left(v'^2v^2 - \frac{A^2}{(A+1)^2}v'^2v_r^2 - \left(\frac{A}{A+1}\right)^2 v^2v_r^2 + \left(\frac{A}{A+1}\right)^4 v_r^4\right)\frac{1}{v_c^2} + \\ \left(v'^2 - 2\left(\frac{A}{A+1}\right)^2 v_r^2 + v^2 + v_c^2\right)\end{array}\right]\exp\left(-\frac{B^2(A+1)}{A}v_c^2\right),$$

and $f(v_r) = \sigma_s(v_r)v_r\exp\left(-\frac{B^2v_r^2}{A+1}\right)$.

We will now begin the integration of the first part of the integral in Eq. (D.3),

$$K_1(v,v') = \frac{B^3(A+1)^2}{4\sqrt{\pi}A^2v^2}\exp\left(\frac{B^2v^2}{A}\right)\int_{v_{r\_11}}^{v_{r\_12}} f(v_r)dv_r \int_{v_{c\_11}}^{v_{c\_12}} g(v_c)dv_c.$$

Integrate $\int_{v_{c\_11}}^{v_{c\_12}} g(v_c)dv_c$ where $v_{c\_12} = v' + \frac{Av_r}{A+1}$ and $v_{c\_31} = v - \frac{Av_r}{A+1}$,

$$\int_{v-\frac{Av_r}{A+1}}^{v'+\frac{Av_r}{A+1}} \left[\begin{array}{l}\left(v'^2v^2 - \frac{A^2}{(A+1)^2}v'^2v_r^2 - \left(\frac{A}{A+1}\right)^2 v^2v_r^2 + \left(\frac{A}{A+1}\right)^4 v_r^4\right)\frac{1}{v_c^2} + \\ \left(v'^2 - 2\left(\frac{A}{A+1}\right)^2 v_r^2 + v^2 + v_c^2\right)\end{array}\right]\exp\left(-\frac{B^2(A+1)}{A}v_c^2\right)dv_c.$$

Split the previous integral into three integrals,

$$\int_{v-\frac{Av_r}{A+1}}^{v'+\frac{Av_r}{A+1}} \left(v'^2 v^2 - \frac{A^2}{(A+1)^2} v'^2 v_r^2 - \left(\frac{A}{A+1}\right)^2 v^2 v_r^2 + \left(\frac{A}{A+1}\right)^4 v_r^4 \right) \frac{1}{v_c^2} \exp\left(-\frac{B^2(A+1)}{A} v_c^2 \right) dv_c +$$

$$\int_{v-\frac{Av_r}{A+1}}^{v'+\frac{Av_r}{A+1}} \left(v'^2 - 2\left(\frac{A}{A+1}\right)^2 v_r^2 + v^2 \right) \exp\left(-\frac{B^2(A+1)}{A} v_c^2 \right) dv_c + \tag{D.4}$$

$$\int_{v-\frac{Av_r}{A+1}}^{v'+\frac{Av_r}{A+1}} v_c^2 \exp\left(-\frac{B^2(A+1)}{A} v_c^2 \right) dv_c .$$

Solution for the first integral in Eq. (D.4):

$$\int_{v'-\frac{Av_r}{A+1}}^{v+\frac{Av_r}{A+1}} \left(v'^2 v^2 - \frac{A^2}{(A+1)^2} v'^2 v_r^2 - \left(\frac{A}{A+1}\right)^2 v^2 v_r^2 + \left(\frac{A}{A+1}\right)^4 v_r^4 \right) \frac{1}{v_c^2} \exp\left(-\frac{B^2(A+1)}{A} v_c^2 \right) dv_c ,$$

$$= \left(v'^2 v^2 - \frac{A^2}{(A+1)^2} v'^2 v_r^2 - \left(\frac{A}{A+1}\right)^2 v^2 v_r^2 + \left(\frac{A}{A+1}\right)^4 v_r^4 \right) \times$$

$$\left. \left\{ \begin{array}{l} -\sqrt{\pi}\sqrt{\dfrac{B^2(A+1)}{A}}\, erf\left[\sqrt{\dfrac{B^2(A+1)}{A}}\; v_c \right] - \\ \dfrac{1}{v_c} \exp\left[-\dfrac{B^2(A+1)v_c^2}{A} \right] \end{array} \right\} \right|_{v-\frac{Av_r}{A+1}}^{v'+\frac{Av_r}{A+1}} .$$

Substitute the bounds of the integral,

$$\left(v'^2v^2-\frac{A^2}{(A+1)^2}v'^2v_r^2-\left(\frac{A}{A+1}\right)^2v^2v_r^2+\left(\frac{A}{A+1}\right)^4v_r^4\right)\times$$

$$\left[\begin{array}{l}\left\{-\sqrt{\pi}\sqrt{\frac{B^2(A+1)}{A}}erf\left[\sqrt{\frac{B^2(A+1)}{A}}\left(v'+\frac{Av_r}{A+1}\right)\right]-\frac{1}{\left(v'+\frac{Av_r}{A+1}\right)}\exp\left[-\frac{B^2(A+1)\left(v'+\frac{Av_r}{A+1}\right)^2}{A}\right]\right\}- \\ \left\{-\sqrt{\pi}\sqrt{\frac{B^2(A+1)}{A}}erf\left[\sqrt{\frac{B^2(A+1)}{A}}\left(v-\frac{Av_r}{A+1}\right)\right]-\frac{1}{\left(v-\frac{Av_r}{A+1}\right)}\exp\left[-\frac{B^2(A+1)\left(v-\frac{Av_r}{A+1}\right)^2}{A}\right]\right\}\end{array}\right].$$

Substitute $h^2=\frac{B^2(A+1)}{A}$ into the equation above,

$$\left(v'^2v^2-\frac{A^2}{(A+1)^2}\left(v'^2+v^2\right)v_r^2+\left(\frac{A}{A+1}\right)^4v_r^4\right)\times$$

$$\left[\begin{array}{l}-\sqrt{\pi}\,h\,erf\left[\left(hv'+h\frac{Av_r}{A+1}\right)\right]-\frac{1}{\left(v'+\frac{Av_r}{A+1}\right)}\exp\left[-h^2\left(v'+\frac{Av_r}{A+1}\right)^2\right]+ \\ \sqrt{\pi}\,h\,erf\left[\left(hv-h\frac{Av_r}{A+1}\right)\right]+\frac{1}{\left(v-\frac{Av_r}{A+1}\right)}\exp\left[-h^2\left(v-\frac{Av_r}{A+1}\right)^2\right]\end{array}\right].$$

Also, from $h^2=\frac{B^2(A+1)}{A}$, we know that $\frac{A}{(A+1)}=\frac{B^2}{h^2}$. As a result, $\left(\frac{A}{A+1}\right)^2=\frac{B^4}{h^4}$ and $\left(\frac{A}{A+1}\right)^4=\frac{B^8}{h^8}$, and substituting these terms in the previous equation gives,

$$\left(v'^2v^2-\frac{B^4}{h^4}\left(v'^2+v^2\right)v_r^2+\frac{B^8}{h^8}v_r^4\right)\times$$
$$\left[\begin{array}{l}-\sqrt{\pi}\,h\,erf\left[\left(hv'+\frac{B^2}{h}v_r\right)\right]-\frac{1}{\left(v'+\frac{Av_r}{A+1}\right)}\exp\left[-h^2\left(v'+\frac{Av_r}{A+1}\right)^2\right]+\\ \sqrt{\pi}\,h\,erf\left[\left(hv-\frac{B^2}{h}v_r\right)\right]+\frac{1}{\left(v-\frac{Av_r}{A+1}\right)}\exp\left[-h^2\left(v-\frac{Av_r}{A+1}\right)^2\right]\end{array}\right].$$

After the simplifications, the solution for the first integral is,

$$\left(v'^2v^2-\frac{B^4}{h^4}\left(v'^2+v^2\right)v_r^2+\frac{B^8}{h^8}v_r^4\right)\times$$
$$\left[\begin{array}{l}-\sqrt{\pi}\,h\left\{erf\left[\left(hv'+\frac{B^2}{h}v_r\right)\right]-erf\left[\left(hv-\frac{B^2}{h}v_r\right)\right]\right\}-\\ \frac{1}{\left(v'+\frac{B^2}{h^2}v_r\right)}\exp\left[-h^2\left(v'+\frac{B^2}{h^2}v_r\right)^2\right]+\frac{1}{\left(v-\frac{B^2}{h^2}v_r\right)}\exp\left[-h^2\left(v-\frac{B^2}{h^2}v_r\right)^2\right]\end{array}\right]. \tag{D.5}$$

Solution for the second integral in Eq. (D.4):

$$\int_{v-\frac{Av_r}{A+1}}^{v'+\frac{Av_r}{A+1}}\left(v'^2-2\left(\frac{A}{A+1}\right)^2v_r^2+v^2\right)\exp\left(-\frac{B^2\left(A+1\right)}{A}v_c^2\right)dv_c,$$

$$=\left(v'^2-2\left(\frac{A}{A+1}\right)^2v_r^2+v^2\right)\frac{\sqrt{\pi}}{2}\sqrt{\frac{A}{B^2\left(A+1\right)}}\left\{erf\left[\sqrt{\frac{B^2\left(A+1\right)}{A}}v_c\right]\right\}\Bigg|_{v-\frac{Av_r}{A+1}}^{v'+\frac{Av_r}{A+1}},$$

$$=\left(v'^2-2\left(\frac{A}{A+1}\right)^2 v_r^2+v^2\right)\frac{\sqrt{\pi}}{2}\sqrt{\frac{A}{B^2\left(A+1\right)}}\times$$
$$\left\{erf\left[\sqrt{\frac{B^2\left(A+1\right)}{A}}\left(v'+\frac{Av_r}{A+1}\right)\right]-erf\left[\sqrt{\frac{B^2\left(A+1\right)}{A}}\left(v-\frac{Av_r}{A+1}\right)\right]\right\}.$$

Substitute $h^2=\frac{B^2\left(A+1\right)}{A}$ into the equation above,

$$\left(v'^2-2\left(\frac{A}{A+1}\right)^2 v_r^2+v^2\right)\frac{\sqrt{\pi}}{2h}\left\{erf\left[h\left(v'+\frac{Av_r}{A+1}\right)\right]-erf\left[h\left(v-\frac{Av_r}{A+1}\right)\right]\right\}.$$

Also, from $h^2=\frac{B^2\left(A+1\right)}{A}$, we know that $\frac{A}{\left(A+1\right)}=\frac{B^2}{h^2}$. Subsequently, $\left(\frac{A}{A+1}\right)^2=\frac{B^4}{h^4}$ and $\left(\frac{A}{A+1}\right)^4=\frac{B^8}{h^8}$,

$$\left(v'^2-2\frac{B^4}{h^4}v_r^2+v^2\right)\frac{\sqrt{\pi}}{2h}\left\{erf\left[\left(hv'+\frac{B^2}{h}v_r\right)\right]-erf\left[\left(hv-\frac{B^2}{h}v_r\right)\right]\right\}. \tag{D.6}$$

Solution for the third integral in Eq. (D.4):

$$\int_{v-\frac{Av_r}{A+1}}^{v'+\frac{Av_r}{A+1}} v_c^2\exp\left(-\frac{B^2\left(A+1\right)}{A}v_c^2\right)dv_c,$$

$$=\left\{\frac{\sqrt{\pi}}{4}\left(\frac{A}{B^2\left(A+1\right)}\right)^{3/2}erf\left[\sqrt{\frac{B^2\left(A+1\right)}{A}}v_c\right]-\frac{v_c\exp\left(-\frac{B^2\left(A+1\right)}{A}v_c^2\right)}{2\left(\frac{B^2\left(A+1\right)}{A}\right)}\right\}\Bigg|_{v-\frac{Av_r}{A+1}}^{v'+\frac{Av_r}{A+1}},$$

$$
=\left\{\begin{array}{l}
\dfrac{\sqrt{\pi}}{4}\left(\dfrac{A}{B^2(A+1)}\right)^{3/2} erf\left[\sqrt{\dfrac{B^2(A+1)}{A}}\left(v'+\dfrac{Av_r}{A+1}\right)\right]-\dfrac{\left(v'+\dfrac{Av_r}{A+1}\right)\exp\left(-\dfrac{B^2(A+1)}{A}\left(v'+\dfrac{Av_r}{A+1}\right)^2\right)}{2\left(\dfrac{B^2(A+1)}{A}\right)}- \\
\dfrac{\sqrt{\pi}}{4}\left(\dfrac{A}{B^2(A+1)}\right)^{3/2} erf\left[\sqrt{\dfrac{B^2(A+1)}{A}}\left(v-\dfrac{Av_r}{A+1}\right)\right]+\dfrac{\left(v-\dfrac{Av_r}{A+1}\right)\exp\left(-\dfrac{B^2(A+1)}{A}\left(v-\dfrac{Av_r}{A+1}\right)^2\right)}{2\left(\dfrac{B^2(A+1)}{A}\right)}
\end{array}\right\}.
$$

Substitute $h^2=\dfrac{B^2(A+1)}{A}$ into the equation above,

$$
\left\{\begin{array}{l}
\dfrac{\sqrt{\pi}}{4}\left(h^{-2}\right)^{3/2} erf\left[h\left(v'+\dfrac{Av_r}{A+1}\right)\right]-\dfrac{\left(v'+\dfrac{Av_r}{A+1}\right)\exp\left(-h^2\left(v'+\dfrac{Av_r}{A+1}\right)^2\right)}{2h^2}- \\
\dfrac{\sqrt{\pi}}{4}\left(h^{-2}\right)^{3/2} erf\left[h\left(v-\dfrac{Av_r}{A+1}\right)\right]+\dfrac{\left(v-\dfrac{Av_r}{A+1}\right)\exp\left(-h^2\left(v-\dfrac{Av_r}{A+1}\right)^2\right)}{2h^2}
\end{array}\right\}.
$$

Also, from $h^2=\dfrac{B^2(A+1)}{A}$, we know that $\dfrac{A}{(A+1)}=\dfrac{B^2}{h^2}$. So, $\left(\dfrac{A}{A+1}\right)^2=\dfrac{B^4}{h^4}$ and $\left(\dfrac{A}{A+1}\right)^4=\dfrac{B^8}{h^8}$,

$$
\left\{\begin{array}{l}
\dfrac{\sqrt{\pi}}{4}\dfrac{1}{h^3}\left\{erf\left[\left(hv'+\dfrac{B^2}{h}v_r\right)\right]-erf\left[\left(hv-\dfrac{B^2}{h}v_r\right)\right]\right\}- \\
\dfrac{\left(v'+\dfrac{B^2}{h^2}v_r\right)\exp\left(-h^2\left(v'+\dfrac{B^2}{h^2}v_r\right)^2\right)}{2h^2}+\dfrac{\left(v-\dfrac{B^2}{h^2}v_r\right)\exp\left(-h^2\left(v-\dfrac{B^2}{h^2}v_r\right)^2\right)}{2h^2}
\end{array}\right\}. \qquad \text{(D.7)}
$$

Combine solutions from all three integrals, Eq. (D.5) – Eq. (D.7),

$$\left(v'^2v^2-\frac{B^4}{h^4}\left(v'^2+v^2\right)v_r^2+\frac{B^8}{h^8}v_r^4\right)\times$$

$$\left[\begin{array}{l}-\sqrt{\pi}\,h\left\{erf\left[\left(hv'+\frac{B^2}{h}v_r\right)\right]-erf\left[\left(hv-\frac{B^2}{h}v_r\right)\right]\right\}-\\ \frac{1}{\left(v'+\frac{B^2}{h^2}v_r\right)}\exp\left[-h^2\left(v'+\frac{B^2}{h^2}v_r\right)^2\right]+\frac{1}{\left(v-\frac{B^2}{h^2}v_r\right)}\exp\left[-h^2\left(v-\frac{B^2}{h^2}v_r\right)^2\right]\end{array}\right]+$$

$$\left(v'^2-2\frac{B^4}{h^4}v_r^2+v^2\right)\frac{\sqrt{\pi}}{2h}\left\{erf\left[\left(hv'+\frac{B^2}{h}v_r\right)\right]-erf\left[\left(hv-\frac{B^2}{h}v_r\right)\right]\right\}+ \tag{D.8}$$

$$\left\{\begin{array}{l}\frac{\sqrt{\pi}}{4}\frac{1}{h^3}\left\{erf\left[\left(hv'+\frac{B^2}{h}v_r\right)\right]-erf\left[\left(hv-\frac{B^2}{h}v_r\right)\right]\right\}-\\ \frac{\left(v'+\frac{B^2}{h^2}v_r\right)\exp\left(-h^2\left(v'+\frac{B^2}{h^2}v_r\right)^2\right)}{2h^2}+\frac{\left(v-\frac{B^2}{h^2}v_r\right)\exp\left(-h^2\left(v-\frac{B^2}{h^2}v_r\right)^2\right)}{2h^2}\end{array}\right\}.$$

Group and simplify terms with $\exp\left[-h^2\left(v-\frac{B^2}{h^2}v_r\right)^2\right]$ from Eq. (D.8),

$$\left\{\left(v'^2v^2-\frac{B^4}{h^4}\left(v'^2+v^2\right)v_r^2+\frac{B^8}{h^8}v_r^4\right)\frac{1}{\left(v-\frac{B^2}{h^2}v_r\right)}+\frac{\left(v-\frac{B^2}{h^2}v_r\right)}{2h^2}\right\}\exp\left[-h^2\left(v-\frac{B^2}{h^2}v_r\right)^2\right],$$

$$=\left\{\frac{\left(v^2-\frac{B^4}{h^4}v_r^2\right)\left(v'^2-\frac{B^4}{h^4}v_r^2\right)}{\left(v-\frac{B^2}{h^2}v_r\right)}+\frac{\left(v-\frac{B^2}{h^2}v_r\right)}{2h^2}\right\}\exp\left[-h^2\left(v-\frac{B^2}{h^2}v_r\right)^2\right],$$

$$=\left\{\frac{\left(v-\frac{B^2}{h^2}v_r\right)\left(v+\frac{B^2}{h^2}v_r\right)\left(v'^2-\frac{B^4}{h^4}v_r^2\right)}{\left(v-\frac{B^2}{h^2}v_r\right)}+\frac{\left(v-\frac{B^2}{h^2}v_r\right)}{2h^2}\right\}\exp\left[-h^2\left(v-\frac{B^2}{h^2}v_r\right)^2\right],$$

$$=\left\{\left(v+\frac{B^2}{h^2}v_r\right)\left(v'^2-\frac{B^4}{h^4}v_r^2\right)+\frac{\left(v-\frac{B^2}{h^2}v_r\right)}{2h^2}\right\}\exp\left[-h^2\left(v-\frac{B^2}{h^2}v_r\right)^2\right],$$

$$=\left\{vv'^2-\frac{B^4}{h^4}vv_r^2+\frac{B^2}{h^2}v_rv'^2-\frac{B^6}{h^6}v_r^3+\frac{v}{2h^2}-\frac{1}{2h^2}\frac{B^2}{h^2}v_r\right\}\exp\left[-h^2\left(v-\frac{B^2}{h^2}v_r\right)^2\right].$$

After all the simplifications, the terms with $\exp\left[-h^2\left(v-\frac{B^2}{h^2}v_r\right)^2\right]$ are,

$$\left\{v\left(v'^2+\frac{1}{2h^2}\right)+\frac{B^2}{h^2}\left(v'^2-\frac{1}{2h^2}\right)v_r-\frac{B^4}{h^4}vv_r^2-\frac{B^6}{h^6}v_r^3\right\}\exp\left[-h^2\left(v-\frac{B^2}{h^2}v_r\right)^2\right]. \qquad \text{(D.9)}$$

Group and simplify terms with, $\exp\left[-h^2\left(v'+\frac{B^2}{h^2}v_r\right)^2\right]$, from Eq. (D.8),

$$\left\{\left(v'^2v^2-\frac{B^4}{h^4}\left(v'^2+v^2\right)v_r^2+\frac{B^8}{h^8}v_r^4\right)\left(-\frac{1}{\left(v'+\frac{B^2}{h^2}v_r\right)}\right)-\frac{\left(v'+\frac{B^2}{h^2}v_r\right)}{2h^2}\right\}\exp\left[-h^2\left(v'+\frac{B^2}{h^2}v_r\right)^2\right],$$

$$= -\left\{ \frac{\left(v^2 - \frac{B^4}{h^4} v_r^2\right)\left(v'^2 - \frac{B^4}{h^4} v_r^2\right)}{\left(v' + \frac{B^2}{h^2} v_r\right)} + \frac{\left(v' + \frac{B^2}{h^2} v_r\right)}{2h^2} \right\} \exp\left[-h^2 \left(v' + \frac{B^2}{h^2} v_r \right)^2 \right],$$

$$= -\left\{ \frac{\left(v^2 - \frac{B^4}{h^4} v_r^2\right)\left(v' - \frac{B^2}{h^2} v_r\right)\left(v' + \frac{B^2}{h^2} v_r\right)}{\left(v' + \frac{B^2}{h^2} v_r\right)} + \frac{\left(v' + \frac{B^2}{h^2} v_r\right)}{2h^2} \right\} \exp\left[-h^2 \left(v' + \frac{B^2}{h^2} v_r \right)^2 \right],$$

$$= -\left\{ \left(v^2 - \frac{B^4}{h^4} v_r^2\right)\left(v' - \frac{B^2}{h^2} v_r\right) + \frac{\left(v' + \frac{B^2}{h^2} v_r\right)}{2h^2} \right\} \exp\left[-h^2 \left(v' + \frac{B^2}{h^2} v_r \right)^2 \right],$$

$$= -\left\{ v'v^2 - \frac{B^2}{h^2} v_r v^2 - \frac{B^4}{h^4} v_r^2 v' + \frac{B^6}{h^6} v_r^3 + \frac{v'}{2h^2} + \frac{1}{2h^2} \frac{B^2}{h^2} v_r \right\} \exp\left[-h^2 \left(v' + \frac{B^2}{h^2} v_r \right)^2 \right].$$

After the simplifications, the terms with $\exp\left[-h^2 \left(v' + \frac{B^2}{h^2} v_r \right)^2 \right]$ are,

$$-\left\{ v'\left(v^2 + \frac{1}{2h^2}\right) + \frac{B^2}{h^2}\left(\frac{1}{2h^2} - v^2\right) v_r - \frac{B^4}{h^4} v_r^2 v' + \frac{B^6}{h^6} v_r^3 \right\} \exp\left[-h^2 \left(v' + \frac{B^2}{h^2} v_r \right)^2 \right]. \qquad \text{(D.10)}$$

Group all the error functions from Eq. (D.8),

$$-\sqrt{\pi}\,h\left(v'^2v^2-\frac{B^4}{h^4}\left(v'^2+v^2\right)v_r^2+\frac{B^8}{h^8}v_r^4\right)\left\{erf\left[\left(hv'+\frac{B^2}{h}v_r\right)\right]-erf\left[\left(hv-\frac{B^2}{h}v_r\right)\right]\right\}+\ldots$$

$$\left(v'^2-2\frac{B^4}{h^4}v_r^2+v^2\right)\frac{\sqrt{\pi}}{2h}\left\{erf\left[\left(hv'+\frac{B^2}{h}v_r\right)\right]-erf\left[\left(hv-\frac{B^2}{h}v_r\right)\right]\right\}+\ldots$$

$$\frac{\sqrt{\pi}}{4}\frac{1}{h^3}\left\{erf\left[\left(hv'+\frac{B^2}{h}v_r\right)\right]-erf\left[\left(hv-\frac{B^2}{h}v_r\right)\right]\right\},$$

$$=\left\{-\sqrt{\pi}\,h\left(v'^2v^2-\frac{B^4}{h^4}\left(v'^2+v^2\right)v_r^2+\frac{B^8}{h^8}v_r^4\right)+\frac{\sqrt{\pi}}{2h}\left(v'^2-2\frac{B^4}{h^4}v_r^2+v^2\right)+\frac{\sqrt{\pi}}{4}\frac{1}{h^3}\right\}\times$$
$$\left\{erf\left[\left(hv'+\frac{B^2}{h}v_r\right)\right]-erf\left[\left(hv-\frac{B^2}{h}v_r\right)\right]\right\},$$

$$=\left\{-\sqrt{\pi}\,h\left(v'^2v^2-\frac{B^4}{h^4}\left(v'^2+v^2\right)v_r^2+\frac{B^8}{h^8}v_r^4\right)+\frac{\sqrt{\pi}}{2h}\frac{h}{h}\left(v'^2-2\frac{B^4}{h^4}v_r^2+v^2\right)+\frac{\sqrt{\pi}}{4}\frac{1}{h^3}\frac{h}{h}\right\}\times$$
$$\left\{erf\left[\left(hv'+\frac{B^2}{h}v_r\right)\right]-erf\left[\left(hv-\frac{B^2}{h}v_r\right)\right]\right\},$$

$$=\sqrt{\pi}\,h\left\{-v'^2v^2+\frac{B^4}{h^4}v'^2v_r^2+\frac{B^4}{h^4}v^2v_r^2-\frac{B^8}{h^8}v_r^4+\frac{1}{2h^2}v'^2-\frac{2}{2h^2}\frac{B^4}{h^4}v_r^2+\frac{v^2}{2h^2}+\frac{1}{4h^4}\right\}\times$$
$$\left\{erf\left[\left(hv'+\frac{B^2}{h}v_r\right)\right]-erf\left[\left(hv-\frac{B^2}{h}v_r\right)\right]\right\}.$$

Rearrange the previous equation and after the simplifications, the terms with the error functions are,

$$\sqrt{\pi}\,h\left\{-v'^2\left(v^2-\frac{1}{2h^2}\right)+\frac{1}{2h^2}\left(v^2+\frac{1}{2h^2}\right)+\frac{B^4}{h^4}v_r^2\left(v'^2+v^2-\frac{1}{h^2}\right)-\frac{B^8}{h^8}v_r^4\right\}\times$$
$$\left\{erf\left[\left(hv'+\frac{B^2}{h}v_r\right)\right]-erf\left[\left(hv-\frac{B^2}{h}v_r\right)\right]\right\}. \tag{D.11}$$

Combine the solutions from the three integrals, Eq. (D.9) – Eq. (D.11),

$$\left\{v\left(v'^2+\frac{1}{2h^2}\right)+\frac{B^2}{h^2}\left(v'^2-\frac{1}{2h^2}\right)v_r-\frac{B^4}{h^4}vv_r^2-\frac{B^6}{h^6}v_r^3\right\}\exp\left[-h^2\left(v-\frac{B^2}{h^2}v_r\right)^2\right]-$$
$$\left\{v'\left(v^2+\frac{1}{2h^2}\right)+\frac{B^2}{h^2}\left(\frac{1}{2h^2}-v^2\right)v_r-\frac{B^4}{h^4}v'v_r^2+\frac{B^6}{h^6}v_r^3\right\}\exp\left[-h^2\left(v'+\frac{B^2}{h^2}v_r\right)^2\right]+$$
$$\sqrt{\pi}\,h\left\{-v'^2\left(v^2-\frac{1}{2h^2}\right)+\frac{1}{2h^2}\left(v^2+\frac{1}{2h^2}\right)+\frac{B^4}{h^4}v_r^2\left(v'^2+v^2-\frac{1}{h^2}\right)-\frac{B^8}{h^8}v_r^4\right\}\times$$
$$\left\{erf\left[\left(hv'+\frac{B^2}{h}v_r\right)\right]-erf\left[\left(hv-\frac{B^2}{h}v_r\right)\right]\right\}. \tag{D.12}$$

We continue on to the second integral in P_1 upscattering equation from Eq. (D.3):

$$K_1(v,v')=\frac{B^3(A+1)^2}{4\sqrt{\pi}A^2v^2}\exp\left(\frac{B^2v^2}{A}\right)\int_{v_{r\_21}}^{\infty}f(v_r)\,dv_r\int_{v_{c\_21}}^{v_{c\_22}}g(v_c)\,dv_c,$$

where $v_{c\_22}=v'+\frac{Av_r}{A+1}=v'+\frac{B^2}{h^2}v_r$ and $v_{c\_21}=\frac{Av_r}{A+1}-v'=\frac{B^2}{h^2}v_r-v'$.

After making the substitutions for the bounds, we solve for $\int_{v_{c\_21}}^{v_{c\_22}}g(v_c)\,dv_c$, ,

$$\int_{\frac{B^2}{h^2}v_r - v'}^{v' + \frac{B^2}{h^2}v_r} \left[\begin{array}{l} \left(v'^2 v^2 - \frac{A^2}{(A+1)^2} v'^2 v_r^2 - \left(\frac{A}{A+1}\right)^2 v^2 v_r^2 + \left(\frac{A}{A+1}\right)^4 v_r^4 \right) \frac{1}{v_c^2} + \\ \left(v'^2 - 2\left(\frac{A}{A+1}\right)^2 v_r^2 + v^2 + v_c^2 \right) \end{array} \right] \exp\left(-\frac{B^2(A+1)}{A} v_c^2 \right) dv_c .$$

We now split this integral into three integrals,

$$\begin{aligned} &\int_{\frac{B^2}{h^2}v_r - v'}^{v' + \frac{B^2}{h^2}v_r} \left(v'^2 v^2 - \frac{A^2}{(A+1)^2} v'^2 v_r^2 - \left(\frac{A}{A+1}\right)^2 v^2 v_r^2 + \left(\frac{A}{A+1}\right)^4 v_r^4 \right) \frac{1}{v_c^2} \exp\left(-\frac{B^2(A+1)}{A} v_c^2 \right) dv_c + \\ &\int_{\frac{B^2}{h^2}v_r - v'}^{v' + \frac{B^2}{h^2}v_r} \left(v'^2 - 2\left(\frac{A}{A+1}\right)^2 v_r^2 + v^2 \right) \exp\left(-\frac{B^2(A+1)}{A} v_c^2 \right) dv_c + \\ &\int_{\frac{B^2}{h^2}v_r - v'}^{v' + \frac{B^2}{h^2}v_r} v_c^2 \exp\left(-\frac{B^2(A+1)}{A} v_c^2 \right) dv_c . \end{aligned} \tag{D.13}$$

Solution for the first integral from Eq. (D.13):

$$\int_{\frac{B^2}{h^2}v_r - v'}^{v' + \frac{B^2}{h^2}v_r} \left(v'^2 v^2 - \frac{A^2}{(A+1)^2} v'^2 v_r^2 - \left(\frac{A}{A+1}\right)^2 v^2 v_r^2 + \left(\frac{A}{A+1}\right)^4 v_r^4 \right) \frac{1}{v_c^2} \exp\left(-\frac{B^2(A+1)}{A} v_c^2 \right) dv_c ,$$

$$=\left(v'^2v^2-\frac{A^2}{(A+1)^2}v'^2v_r^2-\left(\frac{A}{A+1}\right)^2v^2v_r^2+\left(\frac{A}{A+1}\right)^4v_r^4\right)\times$$

$$\left\{\begin{array}{l}-\sqrt{\pi}\sqrt{\frac{B^2(A+1)}{A}}erf\left[\sqrt{\frac{B^2(A+1)}{A}}\,v_c\right]-\\ \frac{1}{v_c}\exp\left[-\frac{B^2(A+1)v_c^2}{A}\right]\end{array}\right\}\Bigg|_{\frac{B^2}{h^2}v_r-v'}^{v'+\frac{B^2}{h^2}v_r}.$$

Substitute the integral bounds, and $h^2=\frac{B^2(A+1)}{A}$ into the equation above. Also, from $h^2=\frac{B^2(A+1)}{A}$, we know that $\frac{A}{(A+1)}=\frac{B^2}{h^2}$. Subsequently, $\left(\frac{A}{A+1}\right)^2=\frac{B^4}{h^4}$ and $\left(\frac{A}{A+1}\right)^4=\frac{B^8}{h^8}$ which are also substituted into the equation,

$$\left(v'^2v^2-\frac{B^4}{h^4}\left(v'^2+v^2\right)v_r^2+\frac{B^8}{h^8}v_r^4\right)\times$$

$$\left[\begin{array}{l}-\sqrt{\pi}h\,erf\left[\left(hv'+\frac{B^2}{h}v_r\right)\right]-\frac{1}{\left(v'+\frac{B^2}{h^2}v_r\right)}\exp\left[-h^2\left(v'+\frac{B^2}{h^2}v_r\right)^2\right]+\\ \sqrt{\pi}h\,erf\left[\left(\frac{B^2}{h}v_r-hv'\right)\right]+\frac{1}{\left(\frac{B^2}{h^2}v_r-v'\right)}\exp\left[-h^2\left(\frac{B^2}{h^2}v_r-v'\right)^2\right]\end{array}\right].$$

After the simplifications, the solution for the first integral is,

$$\left(v'^2 v^2 - \frac{B^4}{h^4}\left(v'^2 + v^2\right)v_r^2 + \frac{B^8}{h^8}v_r^4\right)\times$$

$$\left[\begin{array}{l} -\sqrt{\pi}h\left(erf\left[\left(hv' + \frac{B^2}{h}v_r\right)\right] - erf\left[\left(\frac{B^2}{h}v_r - hv'\right)\right]\right) - \\ \frac{1}{\left(v' + \frac{B^2}{h^2}v_r\right)}\exp\left[-h^2\left(v' + \frac{B^2}{h^2}v_r\right)^2\right] + \frac{1}{\left(\frac{B^2}{h^2}v_r - v'\right)}\exp\left[-h^2\left(\frac{B^2}{h^2}v_r - v'\right)^2\right] \end{array}\right]. \tag{D.14}$$

Solution for the second integral term from Eq. (D.13):

$$\int_{\frac{B^2}{h^2}v_r - v'}^{v' + \frac{B^2}{h^2}v_r}\left(v'^2 - 2\left(\frac{A}{A+1}\right)^2 v_r^2 + v^2\right)\exp\left(-\frac{B^2\left(A+1\right)}{A}v_c^2\right)dv_c,$$

$$= \left(v'^2 - 2\left(\frac{A}{A+1}\right)^2 v_r^2 + v^2\right)\frac{\sqrt{\pi}}{2}\sqrt{\frac{A}{B^2\left(A+1\right)}}\left\{erf\left[\sqrt{\frac{B^2\left(A+1\right)}{A}}\,v_c\right]\right\}\Bigg|_{\frac{B^2}{h^2}v_r - v'}^{v' + \frac{B^2}{h^2}v_r}.$$

Substitute the integral bounds, and $h^2 = \frac{B^2\left(A+1\right)}{A}$ into the equation above. Also, from $h^2 = \frac{B^2\left(A+1\right)}{A}$, we know that $\frac{A}{\left(A+1\right)} = \frac{B^2}{h^2}$. So, $\left(\frac{A}{A+1}\right)^2 = \frac{B^4}{h^4}$ and $\left(\frac{A}{A+1}\right)^4 = \frac{B^8}{h^8}$, and after the substitutions, the equation becomes,

$$\left(v'^2 - 2\frac{B^4}{h^4}v_r^2 + v^2\right)\frac{\sqrt{\pi}}{2h}\left\{erf\left[h\left(v' + \frac{B^2}{h^2}v_r\right)\right] - erf\left[h\left(\frac{B^2}{h^2}v_r - v'\right)\right]\right\}.$$

After the simplifications, the solution for the second integral is,

$$\left(v'^2 - 2\frac{B^4}{h^4}v_r^2 + v^2\right)\frac{\sqrt{\pi}}{2h}\left\{erf\left[\left(hv' + \frac{B^2}{h}v_r\right)\right] - erf\left[\left(\frac{B^2}{h}v_r - hv'\right)\right]\right\} \tag{D.15}$$

Solution for the third integral from Eq. (D.13):

$$\int_{\frac{B^2}{h^2}v_r - v'}^{v' + \frac{B^2}{h^2}v_r} v_c^2 \exp\left(-\frac{B^2(A+1)}{A}v_c^2\right)dv_c,$$

$$= \left\{\frac{\sqrt{\pi}}{4}\left(\frac{A}{B^2(A+1)}\right)^{3/2} erf\left[\sqrt{\frac{B^2(A+1)}{A}}v_c\right] - \frac{v_c \exp\left(-\frac{B^2(A+1)}{A}v_c^2\right)}{2\left(\frac{B^2(A+1)}{A}\right)}\right\}\Bigg|_{\frac{B^2}{h^2}v_r - v'}^{v' + \frac{B^2}{h^2}v_r}.$$

Substitute the integral bounds, and $h^2 = \frac{B^2(A+1)}{A}$ into the equation above. Also, from $h^2 = \frac{B^2(A+1)}{A}$, we know that $\frac{A}{(A+1)} = \frac{B^2}{h^2}$. So, $\left(\frac{A}{A+1}\right)^2 = \frac{B^4}{h^4}$ and $\left(\frac{A}{A+1}\right)^4 = \frac{B^8}{h^8}$. After these substitutions, the solution for the third integral is,

$$\left\{\begin{array}{l}\frac{\sqrt{\pi}}{4h^3}\left(erf\left[\left(hv' + \frac{B^2}{h}v_r\right)\right] - erf\left[\left(\frac{B^2}{h}v_r - hv'\right)\right]\right) - \\ \frac{\left(v' + \frac{B^2}{h^2}v_r\right)\exp\left(-h^2\left(v' + \frac{B^2}{h^2}v_r\right)^2\right)}{2h^2} + \frac{\left(\frac{B^2}{h^2}v_r - v'\right)\exp\left(-h^2\left(\frac{B^2}{h^2}v_r - v'\right)^2\right)}{2h^2}\end{array}\right\}. \tag{D.16}$$

Combine the solutions for the three integrals, Eq. (D.14) – Eq. (D.16),

$$\left(v'^2v^2-\frac{B^4}{h^4}\left(v'^2+v^2\right)v_r^2+\frac{B^8}{h^8}v_r^4\right)\times$$

$$\left[\begin{array}{l}-\sqrt{\pi}h\left(erf\left[\left(hv'+\frac{B^2}{h}v_r\right)\right]-erf\left[\left(\frac{B^2}{h}v_r-hv'\right)\right]\right)-\\ \frac{1}{\left(v'+\frac{B^2}{h^2}v_r\right)}\exp\left[-h^2\left(v'+\frac{B^2}{h^2}v_r\right)^2\right]+\frac{1}{\left(\frac{B^2}{h^2}v_r-v'\right)}\exp\left[-h^2\left(\frac{B^2}{h^2}v_r-v'\right)^2\right]\end{array}\right]+$$

$$\left(v'^2-2\frac{B^4}{h^4}v_r^2+v^2\right)\frac{\sqrt{\pi}}{2h}\left\{erf\left[\left(hv'+\frac{B^2}{h}v_r\right)\right]-erf\left[\left(\frac{B^2}{h}v_r-hv'\right)\right]\right\}+ \tag{D.17}$$

$$\left\{\begin{array}{l}\frac{\sqrt{\pi}}{4h^3}\left(erf\left[\left(hv'+\frac{B^2}{h}v_r\right)\right]-erf\left[\left(\frac{B^2}{h}v_r-hv'\right)\right]\right)-\\ \frac{\left(v'+\frac{B^2}{h^2}v_r\right)\exp\left(-h^2\left(v'+\frac{B^2}{h^2}v_r\right)^2\right)}{2h^2}+\frac{\left(\frac{B^2}{h^2}v_r-v'\right)\exp\left(-h^2\left(\frac{B^2}{h^2}v_r-v'\right)^2\right)}{2h^2}\end{array}\right\}.$$

Simplify and group the terms with $\exp\left[-h^2\left(\frac{B^2}{h^2}v_r-v'\right)^2\right]$ from Eq. (D.17),

$$=\left[\left(v'^2v^2-\frac{B^4}{h^4}\left(v'^2+v^2\right)v_r^2+\frac{B^8}{h^8}v_r^4\right)\left(\frac{1}{\left(\frac{B^2}{h^2}v_r-v'\right)}\right)+\frac{\left(\frac{B^2}{h^2}v_r-v'\right)}{2h^2}\right]\exp\left[-h^2\left(\frac{B^2}{h^2}v_r-v'\right)^2\right],$$

$$=\left[\frac{\left(\frac{B^4}{h^4}v_r^2-v^2\right)\left(\frac{B^4}{h^4}v_r^2-v'^2\right)}{\left(\frac{B^2}{h^2}v_r-v'\right)}+\frac{1}{2h^2}\frac{B^2}{h^2}v_r-\frac{v'}{2h^2}\right]\exp\left[-h^2\left(\frac{B^2}{h^2}v_r-v'\right)^2\right],$$

$$=\left[\frac{\left(\frac{B^4}{h^4}v_r^2-v^2\right)\left(\frac{B^2}{h^2}v_r-v'\right)\left(\frac{B^2}{h^2}v_r+v'\right)}{\left(\frac{B^2}{h^2}v_r-v'\right)}+\frac{1}{2h^2}\frac{B^2}{h^2}v_r-\frac{v'}{2h^2}\right]\exp\left[-h^2\left(\frac{B^2}{h^2}v_r-v'\right)^2\right],$$

$$=\left[\left(\frac{B^4}{h^4}v_r^2-v^2\right)\left(\frac{B^2}{h^2}v_r+v'\right)+\frac{1}{2h^2}\frac{B^2}{h^2}v_r-\frac{v'}{2h^2}\right]\exp\left[-h^2\left(\frac{B^2}{h^2}v_r-v'\right)^2\right],$$

$$=\left[\frac{B^4}{h^4}v_r^2\frac{B^2}{h^2}v_r+\frac{B^4}{h^4}v'v_r^2-\frac{B^2}{h^2}v_rv^2-v'v^2+\frac{1}{2h^2}\frac{B^2}{h^2}v_r-\frac{v'}{2h^2}\right]\exp\left[-h^2\left(\frac{B^2}{h^2}v_r-v'\right)^2\right].$$

After the simplifications, the terms with $\exp\left[-h^2\left(\frac{B^2}{h^2}v_r-v'\right)^2\right]$ becomes,

$$\left[-v'\left(v^2+\frac{1}{2h^2}\right)+\frac{B^2}{h^2}\left(\frac{1}{2h^2}-v^2\right)v_r+\frac{B^4}{h^4}v'v_r^2+\frac{B^6}{h^6}v_r^3\right]\exp\left[-h^2\left(\frac{B^2}{h^2}v_r-v'\right)^2\right]. \qquad \text{(D.18)}$$

Simplify and group the terms with $\exp\left[-h^2\left(v'+\frac{B^2}{h^2}v_r\right)^2\right]$ from Eq. (D.17),

$$=\left[-\frac{\left(v'^2v^2-\frac{B^4}{h^4}\left(v'^2+v^2\right)v_r^2+\frac{B^8}{h^8}v_r^4\right)}{\left(v'+\frac{B^2}{h^2}v_r\right)}-\frac{\left(v'+\frac{B^2}{h^2}v_r\right)}{2h^2}\right]\exp\left[-h^2\left(v'+\frac{B^2}{h^2}v_r\right)^2\right],$$

$$=-\left[\frac{\left(v'^2v^2-\frac{B^4}{h^4}v'^2v_r^2-\frac{B^4}{h^4}v^2v_r^2+\frac{B^8}{h^8}v_r^4\right)}{\left(v'+\frac{B^2}{h^2}v_r\right)}+\frac{\left(v'+\frac{B^2}{h^2}v_r\right)}{2h^2}\right]\exp\left[-h^2\left(v'+\frac{B^2}{h^2}v_r\right)^2\right],$$

$$= -\left[\frac{\left(v^2 - \frac{B^4}{h^4}v_r^2\right)\left(v'^2 - \frac{B^4}{h^4}v_r^2\right)}{\left(v' + \frac{B^2}{h^2}v_r\right)} + \frac{\left(v' + \frac{B^2}{h^2}v_r\right)}{2h^2}\right]\exp\left[-h^2\left(v' + \frac{B^2}{h^2}v_r\right)^2\right],$$

$$= -\left[\frac{\left(v^2 - \frac{B^4}{h^4}v_r^2\right)\left(v' + \frac{B^2}{h^2}v_r\right)\left(v' - \frac{B^2}{h^2}v_r\right)}{\left(v' + \frac{B^2}{h^2}v_r\right)} + \frac{\left(v' + \frac{B^2}{h^2}v_r\right)}{2h^2}\right]\exp\left[-h^2\left(v' + \frac{B^2}{h^2}v_r\right)^2\right],$$

$$= -\left[\left(v^2 - \frac{B^4}{h^4}v_r^2\right)\left(v' - \frac{B^2}{h^2}v_r\right) + \frac{\left(v' + \frac{B^2}{h^2}v_r\right)}{2h^2}\right]\exp\left[-h^2\left(v' + \frac{B^2}{h^2}v_r\right)^2\right],$$

$$= -\left[v'v^2 - \frac{B^2}{h^2}v_r v^2 - \frac{B^4}{h^4}v'v_r^2 + \frac{B^4}{h^4}v_r^2\frac{B^2}{h^2}v_r + \frac{v'}{2h^2} + \frac{1}{2h^2}\frac{B^2}{h^2}v_r\right]\exp\left[-h^2\left(v' + \frac{B^2}{h^2}v_r\right)^2\right],$$

After the simplifications, the terms with $\exp\left[-h^2\left(v' + \frac{B^2}{h^2}v_r\right)^2\right]$ become,

$$-\left[v'\left(v^2 + \frac{1}{2h^2}\right) + \frac{B^2}{h^2}\left(\frac{1}{2h^2} - v^2\right)v_r - \frac{B^4}{h^4}v'v_r^2 + \frac{B^6}{h^6}v_r^3\right]\exp\left[-h^2\left(v' + \frac{B^2}{h^2}v_r\right)^2\right]. \qquad \text{(D.19)}$$

Simplify and group together the error functions from Eq. (D.17):

$$= \left[-\sqrt{\pi}h\left(v'^2v^2 - \frac{B^4}{h^4}\left(v'^2 + v^2\right)v_r^2 + \frac{B^8}{h^8}v_r^4\right) + \frac{\sqrt{\pi}}{2h}\left(v'^2 - 2\frac{B^4}{h^4}v_r^2 + v^2\right) + \frac{\sqrt{\pi}}{4h^3}\right]\times$$
$$\left(erf\left[\left(hv' + \frac{B^2}{h}v_r\right)\right] - erf\left[\left(\frac{B^2}{h}v_r - hv'\right)\right]\right),$$

$$= \left[-\sqrt{\pi} h \left(v'^2 v^2 - \frac{B^4}{h^4} \left(v'^2 + v^2 \right) v_r^2 + \frac{B^8}{h^8} v_r^4 \right) + \frac{\sqrt{\pi}}{2h} \frac{h}{h} \left(v'^2 - 2 \frac{B^4}{h^4} v_r^2 + v^2 \right) + \frac{\sqrt{\pi}}{4h^3} \frac{h}{h} \right] \times$$

$$\left(erf\left[\left(hv' + \frac{B^2}{h} v_r \right) \right] - erf\left[\left(\frac{B^2}{h} v_r - hv' \right) \right] \right),$$

$$= \sqrt{\pi} h \left[-v'^2 v^2 + \frac{B^4}{h^4} v'^2 v_r^2 + \frac{B^4}{h^4} v^2 v_r^2 - \frac{B^8}{h^8} v_r^4 + \frac{1}{2h^2} v'^2 - \frac{1}{2h^2} 2 \frac{B^4}{h^4} v_r^2 + \frac{1}{2h^2} v^2 + \frac{1}{4h^4} \right] \times$$

$$\left(erf\left[\left(hv' + \frac{B^2}{h} v_r \right) \right] - erf\left[\left(\frac{B^2}{h} v_r - hv' \right) \right] \right).$$

After the simplifications, the terms with the error functions become,

$$\sqrt{\pi} h \left[-v'^2 \left(v^2 - \frac{1}{2h^2} \right) + \frac{1}{2h^2} \left(v^2 + \frac{1}{2h^2} \right) + \frac{B^4}{h^4} \left(v'^2 + v^2 - \frac{1}{h^2} \right) v_r^2 - \frac{B^8}{h^8} v_r^4 \right] \times$$

$$\left(erf\left[\left(hv' + \frac{B^2}{h} v_r \right) \right] - erf\left[\left(\frac{B^2}{h} v_r - hv' \right) \right] \right). \tag{D.20}$$

Combine solutions from the three integrals, Eqs. (D.18) – (D.20),

$$\left[-v' \left(v^2 + \frac{1}{2h^2} \right) + \frac{B^2}{h^2} \left(\frac{1}{2h^2} - v^2 \right) v_r + \frac{B^4}{h^4} v' v_r^2 + \frac{B^6}{h^6} v_r^3 \right] \exp\left[-h^2 \left(\frac{B^2}{h^2} v_r - v' \right)^2 \right] -$$

$$\left[v' \left(v^2 + \frac{1}{2h^2} \right) + \frac{B^2}{h^2} \left(\frac{1}{2h^2} - v^2 \right) v_r - \frac{B^4}{h^4} v_r^2 v' + \frac{B^6}{h^6} v_r^3 \right] \exp\left[-h^2 \left(v' + \frac{B^2}{h^2} v_r \right)^2 \right] +$$

$$\sqrt{\pi} h \left[-v'^2 \left(v^2 - \frac{1}{2h^2} \right) + \frac{1}{2h^2} \left(v^2 + \frac{1}{2h^2} \right) + \frac{B^4}{h^4} \left(v^2 + v'^2 - \frac{1}{h^2} \right) v_r^2 - \frac{B^8}{h^8} v_r^4 \right] \times \tag{D.21}$$

$$\left(erf\left[\left(hv' + \frac{B^2}{h} v_r \right) \right] - erf\left[\left(\frac{B^2}{h} v_r - hv' \right) \right] \right).$$

Final form of $K_1(v,v')$ for ($v' < v$), downscattering case:

$$K_1(v,v') = \frac{B^3(A+1)^2}{4\sqrt{\pi}A^2v^2}\exp\left(\frac{B^2v^2}{A}\right)\left\{\int_{v_{r\_11}}^{v_{r\_12}} f(v_r)\,dv_r \int_{v_{c\_11}}^{v_{c\_12}} g(v_c)\,dv_c + \int_{v_{r\_21}}^{\infty} f(v_r)\,dv_r \int_{v_{c\_21}}^{v_{c\_22}} g(v_c)\,dv_c\right\}$$

Substitute $f(v_r) = \sigma_s(v_r)v_r\exp\left(-\frac{B^2v_r^2}{A+1}\right)$, Eqs. (D.12) and (D.21), and simplify the constants to obtain the final form of the equation for downscatter,

$$K_1(v,v') = \frac{h^4}{4\sqrt{\pi}Bv^2}\exp\left(\frac{B^2v^2}{A}\right)\times$$

$$\left\{\begin{array}{l}
\displaystyle\int_{\frac{h^2}{B^2}\left(\frac{v-v'}{2}\right)}^{\frac{h^2}{B^2}\left(\frac{v+v'}{2}\right)} \sigma_s(v_r)v_r\exp\left(-\frac{B^2v_r^2}{A+1}\right)\times \\
\left[\begin{array}{l}
\left\{v\left(v'^2+\frac{1}{2h^2}\right)+\frac{B^2}{h^2}\left(v'^2-\frac{1}{2h^2}\right)v_r-\frac{B^4}{h^4}vv_r^2-\frac{B^6}{h^6}v_r^3\right\}\exp\left[-h^2\left(v-\frac{B^2}{h^2}v_r\right)^2\right] \\
-\left\{v'\left(v^2+\frac{1}{2h^2}\right)+\frac{B^2}{h^2}\left(\frac{1}{2h^2}-v^2\right)v_r-\frac{B^4}{h^4}v'v_r^2+\frac{B^6}{h^6}v_r^3\right\}\exp\left[-h^2\left(v'+\frac{B^2}{h^2}v_r\right)^2\right] \\
+\sqrt{\pi}\,h\left\{-v'^2\left(v^2-\frac{1}{2h^2}\right)+\frac{1}{2h^2}\left(v^2+\frac{1}{2h^2}\right)+\frac{B^4}{h^4}v_r^2\left(v'^2+v^2-\frac{1}{h^2}\right)-\frac{B^8}{h^8}v_r^4\right\}\times \\
\left\{erf\left[\left(hv'+\frac{B^2}{h}v_r\right)\right]-erf\left[\left(hv-\frac{B^2}{h}v_r\right)\right]\right\}
\end{array}\right]dv_r \\
+ \\
\displaystyle\int_{\frac{h^2}{B^2}\left(\frac{v+v'}{2}\right)}^{\infty} \sigma_s(v_r)v_r\exp\left(-\frac{B^2v_r^2}{A+1}\right)\times \\
\left[\begin{array}{l}
\left[-v'\left(v^2+\frac{1}{2h^2}\right)+\frac{B^2}{h^2}\left(\frac{1}{2h^2}-v^2\right)v_r+\frac{B^4}{h^4}v'v_r^2+\frac{B^6}{h^6}v_r^3\right]\exp\left[-h^2\left(\frac{B^2}{h^2}v_r-v'\right)^2\right] \\
-\left[v'\left(v^2+\frac{1}{2h^2}\right)+\frac{B^2}{h^2}\left(\frac{1}{2h^2}-v^2\right)v_r-\frac{B^4}{h^4}v_r^2v'+\frac{B^6}{h^6}v_r^3\right]\exp\left[-h^2\left(v'+\frac{B^2}{h^2}v_r\right)^2\right] \\
+\sqrt{\pi}h\left[-v'^2\left(v^2-\frac{1}{2h^2}\right)+\frac{1}{2h^2}\left(v^2+\frac{1}{2h^2}\right)+\frac{B^4}{h^4}\left(v^2+v'^2-\frac{1}{h^2}\right)v_r^2-\frac{B^8}{h^8}v_r^4\right]\times \\
\left(erf\left[\left(hv'+\frac{B^2}{h}v_r\right)\right]-erf\left[\left(\frac{B^2}{h}v_r-hv'\right)\right]\right)
\end{array}\right]dv_r
\end{array}\right\}$$

D.1.2 *Upscattering Case*

Again, we begin with the equation derived in the first part of Section D.1,

$$K_1(v,v') = \frac{B^3(A+1)^2}{4\sqrt{\pi}A^2v^2}\exp\left(\frac{B^2v^2}{A}\right)\times$$
$$\int_{v_c}\int_{v_r}\left\{\begin{array}{l}\left[\begin{array}{l}\left(v'^2v^2 - \frac{A^2}{(A+1)^2}v'^2v_r^2 - \left(\frac{A}{A+1}\right)^2 v^2v_r^2 + \left(\frac{A}{A+1}\right)^4 v_r^4\right)\frac{1}{v_c^2} + \\ \left(v'^2 - 2\left(\frac{A}{A+1}\right)^2 v_r^2 + v^2 + v_c^2\right)\end{array}\right]\times \\ \left(\sigma_s(v_r)v_r\exp\left(-\frac{B^2v_r^2}{A+1}\right)\exp\left(-\frac{B^2(A+1)}{A}v_c^2\right)\right)\end{array}\right\}dv_r\,dv_c.$$

We can restate this equation as,

$$K_1(v,v') = \frac{B^3(A+1)^2}{4\sqrt{\pi}A^2v^2}\exp\left(\frac{B^2v^2}{A}\right)\times$$
$$\left\{\int_{v_{r\_31}}^{v_{r\_32}} f(v_r)dv_r\int_{v_{c\_31}}^{v_{c\_32}} g(v_c)dv_c + \int_{v_{r\_41}}^{\infty} f(v_r)dv_r\int_{v_{c\_41}}^{v_{c\_42}} g(v_c)dv_c\right\}, \tag{D.22}$$

where,

$$g(v_c) = \left[\begin{array}{l}\left(v'^2v^2 - \frac{A^2}{(A+1)^2}v'^2v_r^2 - \left(\frac{A}{A+1}\right)^2 v^2v_r^2 + \left(\frac{A}{A+1}\right)^4 v_r^4\right)\frac{1}{v_c^2} + \\ \left(v'^2 - 2\left(\frac{A}{A+1}\right)^2 v_r^2 + v^2 + v_c^2\right)\end{array}\right]\exp\left(-\frac{B^2(A+1)}{A}v_c^2\right).$$

and, $f(v_r) = \sigma_s(v_r)v_r\exp\left(-\frac{B^2v_r^2}{A+1}\right)$.

We begin with the integration of the first integral in Eq. (D.22) containing $\int_{v_{c\_31}}^{v_{c\_32}} g(v_c)\,dv_c$,

$$K_1(v,v') = \frac{B^3(A+1)^2}{4\sqrt{\pi}A^2v^2}\exp\left(\frac{B^2v^2}{A}\right)\int_{v_{r\_31}}^{v_{r\_32}} f(v_r)\,dv_r \int_{v_{c\_31}}^{v_{c\_32}} g(v_c)\,dv_c.$$

Substitute $v_{c\_32} = v + \frac{Av_r}{A+1}$ and $v_{c\_31} = v' - \frac{Av_r}{A+1}$ into the integral bounds to obtain,

$$\int_{v'-\frac{Av_r}{A+1}}^{v+\frac{Av_r}{A+1}} \left[\begin{array}{l}\left(v'^2v^2 - \frac{A^2}{(A+1)^2}v'^2v_r^2 - \left(\frac{A}{A+1}\right)^2 v^2v_r^2 + \left(\frac{A}{A+1}\right)^4 v_r^4\right)\frac{1}{v_c^2} + \\ \left(v'^2 - 2\left(\frac{A}{A+1}\right)^2 v_r^2 + v^2 + v_c^2\right)\end{array}\right]\exp\left(-\frac{B^2(A+1)}{A}v_c^2\right)dv_c.$$

Split the integral into three terms,

$$\begin{aligned}&\int_{v'-\frac{Av_r}{A+1}}^{v+\frac{Av_r}{A+1}} \left(v'^2v^2 - \frac{A^2}{(A+1)^2}v'^2v_r^2 - \left(\frac{A}{A+1}\right)^2 v^2v_r^2 + \left(\frac{A}{A+1}\right)^4 v_r^4\right)\frac{1}{v_c^2}\exp\left(-\frac{B^2(A+1)}{A}v_c^2\right)dv_c + \\ &\int_{v'-\frac{Av_r}{A+1}}^{v+\frac{Av_r}{A+1}} \left(v'^2 - 2\left(\frac{A}{A+1}\right)^2 v_r^2 + v^2\right)\exp\left(-\frac{B^2(A+1)}{A}v_c^2\right)dv_c + \\ &\int_{v'-\frac{Av_r}{A+1}}^{v+\frac{Av_r}{A+1}} v_c^2\exp\left(-\frac{B^2(A+1)}{A}v_c^2\right)dv_c.\end{aligned} \tag{D.23}$$

Solution for the first integral in Eq. (D.23):

$$\int_{v'-\frac{Av_r}{A+1}}^{v+\frac{Av_r}{A+1}} \left(v'^2 v^2 - \frac{A^2}{(A+1)^2} v'^2 v_r^2 - \left(\frac{A}{A+1}\right)^2 v^2 v_r^2 + \left(\frac{A}{A+1}\right)^4 v_r^4 \right) \frac{1}{v_c^2} \exp\left(-\frac{B^2(A+1)}{A} v_c^2 \right) dv_c,$$

$$= \left(v'^2 v^2 - \frac{A^2}{(A+1)^2} v'^2 v_r^2 - \left(\frac{A}{A+1}\right)^2 v^2 v_r^2 + \left(\frac{A}{A+1}\right)^4 v_r^4 \right) \times$$

$$\left\{ -\sqrt{\pi} \sqrt{\frac{B^2(A+1)}{A}} erf\left[\sqrt{\frac{B^2(A+1)}{A}}\ v_c \right] - \frac{1}{v_c} \exp\left[-\frac{B^2(A+1) v_c^2}{A} \right] \right\} \Bigg|_{v'-\frac{Av_r}{A+1}}^{v+\frac{Av_r}{A+1}}.$$

$$= \left(v'^2 v^2 - \frac{A^2}{(A+1)^2} v'^2 v_r^2 - \left(\frac{A}{A+1}\right)^2 v^2 v_r^2 + \left(\frac{A}{A+1}\right)^4 v_r^4 \right) \times$$

$$\left[\begin{array}{l} \left\{ -\sqrt{\pi} \sqrt{\frac{B^2(A+1)}{A}} erf\left[\sqrt{\frac{B^2(A+1)}{A}} \left(v + \frac{Av_r}{A+1} \right) \right] - \frac{1}{\left(v + \frac{Av_r}{A+1} \right)} \exp\left[-\frac{B^2(A+1)\left(v + \frac{Av_r}{A+1} \right)^2}{A} \right] \right\} - \\ \left\{ -\sqrt{\pi} \sqrt{\frac{B^2(A+1)}{A}} erf\left[\sqrt{\frac{B^2(A+1)}{A}} \left(v' - \frac{Av_r}{A+1} \right) \right] - \frac{1}{\left(v' - \frac{Av_r}{A+1} \right)} \exp\left[-\frac{B^2(A+1)\left(v' - \frac{Av_r}{A+1} \right)^2}{A} \right] \right\} \end{array} \right].$$

Substitute $h^2 = \dfrac{B^2(A+1)}{A}$ into the equation above,

$$\left(v'^2v^2-\frac{A^2}{(A+1)^2}\left(v'^2+v^2\right)v_r^2+\left(\frac{A}{A+1}\right)^4 v_r^4\right)\times$$

$$\left[\begin{array}{l}-\sqrt{\pi}\,h\,erf\left[\left(hv+h\frac{Av_r}{A+1}\right)\right]-\frac{1}{\left(v+\frac{Av_r}{A+1}\right)}\exp\left[-h^2\left(v+\frac{Av_r}{A+1}\right)^2\right]+\\ \sqrt{\pi}\,h\,erf\left[\left(hv'-h\frac{Av_r}{A+1}\right)\right]+\frac{1}{\left(v'-\frac{Av_r}{A+1}\right)}\exp\left[-h^2\left(v'-\frac{Av_r}{A+1}\right)^2\right]\end{array}\right].$$

Also, from $h^2=\frac{B^2(A+1)}{A}$, we know that $\frac{A}{(A+1)}=\frac{B^2}{h^2}$. So, $\left(\frac{A}{A+1}\right)^2=\frac{B^4}{h^4}$ and $\left(\frac{A}{A+1}\right)^4=\frac{B^8}{h^8}$. Substituting these terms into the equation above gives,

$$\left(v'^2v^2-\frac{B^4}{h^4}\left(v'^2+v^2\right)v_r^2+\frac{B^8}{h^8}v_r^4\right)\times$$

$$\left[\begin{array}{l}-\sqrt{\pi}\,h\,erf\left[\left(hv+h\frac{B^2}{h^2}v_r\right)\right]-\frac{1}{\left(v+\frac{Av_r}{A+1}\right)}\exp\left[-h^2\left(v+\frac{Av_r}{A+1}\right)^2\right]+\\ \sqrt{\pi}\,h\,erf\left[\left(hv'-h\frac{B^2}{h^2}v_r\right)\right]+\frac{1}{\left(v'-\frac{Av_r}{A+1}\right)}\exp\left[-h^2\left(v'-\frac{Av_r}{A+1}\right)^2\right]\end{array}\right].$$

After the simplifications, we obtain the solution for the first integral,

$$\left(v'^2 v^2 - \frac{B^4}{h^4}\left(v'^2 + v^2\right)v_r^2 + \frac{B^8}{h^8}v_r^4\right)\times$$
$$\left[\begin{array}{l}\sqrt{\pi}\,h\left\{erf\left[\left(hv' - \frac{B^2}{h}v_r\right)\right] - erf\left[\left(hv + \frac{B^2}{h}v_r\right)\right]\right\} - \\ \frac{1}{\left(v + \frac{B^2}{h^2}v_r\right)}\exp\left[-h^2\left(v + \frac{B^2}{h^2}v_r\right)^2\right] + \frac{1}{\left(v' - \frac{B^2}{h^2}v_r\right)}\exp\left[-h^2\left(v' - \frac{B^2}{h^2}v_r\right)^2\right]\end{array}\right]. \tag{D.24}$$

Solution for the second integral in Eq. (D.23):

$$\int_{v'-\frac{Av_r}{A+1}}^{v+\frac{Av_r}{A+1}}\left(v'^2 - 2\left(\frac{A}{A+1}\right)^2 v_r^2 + v^2\right)\exp\left(-\frac{B^2\left(A+1\right)}{A}v_c^2\right)dv_c,$$

$$= \left(v'^2 - 2\left(\frac{A}{A+1}\right)^2 v_r^2 + v^2\right)\frac{\sqrt{\pi}}{2}\sqrt{\frac{A}{B^2\left(A+1\right)}}\left\{erf\left[\sqrt{\frac{B^2\left(A+1\right)}{A}}\,v_c\right]\right\}\Bigg|_{v'-\frac{Av_r}{A+1}}^{v+\frac{Av_r}{A+1}},$$

$$= \left(v'^2 - 2\left(\frac{A}{A+1}\right)^2 v_r^2 + v^2\right)\frac{\sqrt{\pi}}{2}\sqrt{\frac{A}{B^2\left(A+1\right)}}\times$$
$$\left\{erf\left[\sqrt{\frac{B^2\left(A+1\right)}{A}}\left(v + \frac{Av_r}{A+1}\right)\right] - erf\left[\sqrt{\frac{B^2\left(A+1\right)}{A}}\left(v' - \frac{Av_r}{A+1}\right)\right]\right\}.$$

Substitute $h^2 = \frac{B^2\left(A+1\right)}{A}$ into the equation above.

$$\left(v'^2 - 2\left(\frac{A}{A+1}\right)^2 v_r^2 + v^2\right)\frac{\sqrt{\pi}}{2h}\left\{erf\left[h\left(v + \frac{Av_r}{A+1}\right)\right] - erf\left[h\left(v' - \frac{Av_r}{A+1}\right)\right]\right\}.$$

Also, from $h^2 = \frac{B^2(A+1)}{A}$, we know that $\frac{A}{(A+1)} = \frac{B^2}{h^2}$. So, $\left(\frac{A}{A+1}\right)^2 = \frac{B^4}{h^4}$ and $\left(\frac{A}{A+1}\right)^4 = \frac{B^8}{h^8}$. Substituting these terms into the previous equation produces the simplified solution for the second integral,

$$\left(v'^2 - 2\frac{B^4}{h^4}v_r^2 + v^2\right)\frac{\sqrt{\pi}}{2h}\left\{erf\left[\left(hv + \frac{B^2}{h}v_r\right)\right] - erf\left[\left(hv' - \frac{B^2}{h}v_r\right)\right]\right\}. \tag{D.25}$$

Solution for the third integral in Eq. (D.23):

$$\int_{v'-\frac{Av_r}{A+1}}^{v+\frac{Av_r}{A+1}} v_c^2 \exp\left(-\frac{B^2(A+1)}{A}v_c^2\right)dv_c,$$

$$= \left\{\frac{\sqrt{\pi}}{4}\left(\frac{A}{B^2(A+1)}\right)^{3/2} erf\left[\sqrt{\frac{B^2(A+1)}{A}}\,v_c\right] - \frac{v_c \exp\left(-\frac{B^2(A+1)}{A}v_c^2\right)}{2\left(\frac{B^2(A+1)}{A}\right)}\right\}\Bigg|_{v'-\frac{Av_r}{A+1}}^{v+\frac{Av_r}{A+1}},$$

$$= \left\{\begin{array}{l} \frac{\sqrt{\pi}}{4}\left(\frac{A}{B^2(A+1)}\right)^{3/2} erf\left[\sqrt{\frac{B^2(A+1)}{A}}\left(v + \frac{Av_r}{A+1}\right)\right] - \frac{\left(v + \frac{Av_r}{A+1}\right)\exp\left(-\frac{B^2(A+1)}{A}\left(v + \frac{Av_r}{A+1}\right)^2\right)}{2\left(\frac{B^2(A+1)}{A}\right)} - \\ \frac{\sqrt{\pi}}{4}\left(\frac{A}{B^2(A+1)}\right)^{3/2} erf\left[\sqrt{\frac{B^2(A+1)}{A}}\left(v' - \frac{Av_r}{A+1}\right)\right] + \frac{\left(v' - \frac{Av_r}{A+1}\right)\exp\left(-\frac{B^2(A+1)}{A}\left(v' - \frac{Av_r}{A+1}\right)^2\right)}{2\left(\frac{B^2(A+1)}{A}\right)} \end{array}\right\}.$$

Substituting $h^2 = \frac{B^2(A+1)}{A}$ into the equation above gives,

$$\left\{\begin{array}{l}\frac{\sqrt{\pi}}{4}\left(h^{-2}\right)^{3/2} erf\left[h\left(v+\frac{Av_r}{A+1}\right)\right]-\frac{\left(v+\frac{Av_r}{A+1}\right)\exp\left(-h^2\left(v+\frac{Av_r}{A+1}\right)^2\right)}{2h^2}- \\ \frac{\sqrt{\pi}}{4}\left(h^{-2}\right)^{3/2} erf\left[h\left(v'-\frac{Av_r}{A+1}\right)\right]+\frac{\left(v'-\frac{Av_r}{A+1}\right)\exp\left(-h^2\left(v'-\frac{Av_r}{A+1}\right)^2\right)}{2h^2}\end{array}\right\}.$$

Also, from $h^2=\frac{B^2\left(A+1\right)}{A}$, we know that $\frac{A}{\left(A+1\right)}=\frac{B^2}{h^2}$. So, $\left(\frac{A}{A+1}\right)^2=\frac{B^4}{h^4}$ and $\left(\frac{A}{A+1}\right)^4=\frac{B^8}{h^8}$. Substituting these terms into the previous equation gives,

$$\left\{\begin{array}{l}\frac{\sqrt{\pi}}{4}\frac{1}{h^3} erf\left[\left(hv+h\frac{B^2}{h^2}v_r\right)\right]-\frac{\left(v+\frac{B^2}{h^2}v_r\right)\exp\left(-h^2\left(v+\frac{Av_r}{A+1}\right)^2\right)}{2h^2}- \\ \frac{\sqrt{\pi}}{4}\frac{1}{h^3} erf\left[\left(hv'-h\frac{B^2}{h^2}v_r\right)\right]+\frac{\left(v'-\frac{B^2}{h^2}v_r\right)\exp\left(-h^2\left(v'-\frac{Av_r}{A+1}\right)^2\right)}{2h^2}\end{array}\right\}.$$

The simplified solution for the third integral is,

$$\left\{\begin{array}{l}\frac{\sqrt{\pi}}{4}\frac{1}{h^3}\left\{erf\left[\left(hv+\frac{B^2}{h}v_r\right)\right]-erf\left[\left(hv'-\frac{B^2}{h}v_r\right)\right]\right\}- \\ \frac{\left(v+\frac{B^2}{h^2}v_r\right)\exp\left(-h^2\left(v+\frac{B^2}{h^2}v_r\right)^2\right)}{2h^2}+\frac{\left(v'-\frac{B^2}{h^2}v_r\right)\exp\left(-h^2\left(v'-\frac{B^2}{h^2}v_r\right)^2\right)}{2h^2}\end{array}\right\}. \qquad \text{(D.26)}$$

Combine solutions, Eqs (D.24) – (D.26) from all three integrals,

$$\left(v'^2v^2-\frac{B^4}{h^4}\left(v'^2+v^2\right)v_r^2+\frac{B^8}{h^8}v_r^4\right)\times$$

$$\left[\begin{array}{l}\sqrt{\pi}\,h\left\{erf\left[\left(hv'-\frac{B^2}{h}v_r\right)\right]-erf\left[\left(hv+\frac{B^2}{h}v_r\right)\right]\right\}-\\ \frac{1}{\left(v+\frac{B^2}{h^2}v_r\right)}\exp\left[-h^2\left(v+\frac{B^2}{h^2}v_r\right)^2\right]+\frac{1}{\left(v'-\frac{B^2}{h^2}v_r\right)}\exp\left[-h^2\left(v'-\frac{B^2}{h^2}v_r\right)^2\right]\end{array}\right]+$$

$$\left(v'^2-2\frac{B^4}{h^4}v_r^2+v^2\right)\frac{\sqrt{\pi}}{2h}\left\{erf\left[\left(hv+\frac{B^2}{h}v_r\right)\right]-erf\left[\left(hv'-\frac{B^2}{h}v_r\right)\right]\right\}+ \tag{D.27}$$

$$\left\{\begin{array}{l}\frac{\sqrt{\pi}}{4}\frac{1}{h^3}\left\{erf\left[\left(hv+\frac{B^2}{h}v_r\right)\right]-erf\left[\left(hv'-\frac{B^2}{h}v_r\right)\right]\right\}-\\ \frac{\left(v+\frac{B^2}{h^2}v_r\right)\exp\left(-h^2\left(v+\frac{B^2}{h^2}v_r\right)^2\right)}{2h^2}+\frac{\left(v'-\frac{B^2}{h^2}v_r\right)\exp\left(-h^2\left(v'-\frac{B^2}{h^2}v_r\right)^2\right)}{2h^2}\end{array}\right\}$$

Group and simplify the terms with $\exp\left[-h^2\left(v'-\frac{B^2}{h^2}v_r\right)^2\right]$ from Eq. (D.27),

$$\left\{\left(v'^2v^2-\frac{B^4}{h^4}\left(v'^2+v^2\right)v_r^2+\frac{B^8}{h^8}v_r^4\right)\frac{1}{\left(v'-\frac{B^2}{h^2}v_r\right)}+\frac{\left(v'-\frac{B^2}{h^2}v_r\right)}{2h^2}\right\}\exp\left[-h^2\left(v'-\frac{B^2}{h^2}v_r\right)^2\right],$$

$$=\left\{\frac{v'^2\left(v^2-\frac{B^4}{h^4}v_r^2\right)-\frac{B^4}{h^4}v_r^2\left(v^2-\frac{B^4}{h^4}v_r^2\right)}{\left(v'-\frac{B^2}{h^2}v_r\right)}+\frac{\left(v'-\frac{B^2}{h^2}v_r\right)}{2h^2}\right\}\exp\left[-h^2\left(v'-\frac{B^2}{h^2}v_r\right)^2\right],$$

$$=\left\{\frac{\left(v^2-\frac{B^4}{h^4}v_r^2\right)\left(v'^2-\frac{B^4}{h^4}v_r^2\right)}{\left(v'-\frac{B^2}{h^2}v_r\right)}+\frac{\left(v'-\frac{B^2}{h^2}v_r\right)}{2h^2}\right\}\exp\left[-h^2\left(v'-\frac{B^2}{h^2}v_r\right)^2\right],$$

$$=\left\{\frac{\left(v^2-\frac{B^4}{h^4}v_r^2\right)\left(v'-\frac{B^2}{h^2}v_r\right)\left(v'+\frac{B^2}{h^2}v_r\right)}{\left(v'-\frac{B^2}{h^2}v_r\right)}+\frac{\left(v'-\frac{B^2}{h^2}v_r\right)}{2h^2}\right\}\exp\left[-h^2\left(v'-\frac{B^2}{h^2}v_r\right)^2\right],$$

$$=\left\{v'v^2-v'\frac{B^4}{h^4}v_r^2+v^2\frac{B^2}{h^2}v_r-\frac{B^6}{h^6}v_r^3+\frac{v'}{2h^2}-\frac{1}{2h^2}\frac{B^2}{h^2}v_r\right\}\exp\left[-h^2\left(v'-\frac{B^2}{h^2}v_r\right)^2\right],$$

After the simplifications, the terms with $\exp\left[-h^2\left(v'-\frac{B^2}{h^2}v_r\right)^2\right]$ are,

$$\left\{v'\left(v^2+\frac{1}{2h^2}\right)+\frac{B^2}{h^2}\left(v^2-\frac{1}{2h^2}\right)v_r-\frac{B^4}{h^4}v'v_r^2-\frac{B^6}{h^6}v_r^3\right\}\exp\left[-h^2\left(v'-\frac{B^2}{h^2}v_r\right)^2\right]. \qquad \text{(D.28)}$$

Group and simplify the terms with $\exp\left[-h^2\left(v+\frac{B^2}{h^2}v_r\right)^2\right]$ from Eq. (D.27),

$$\left\{\left(v'^2v^2-\frac{B^4}{h^4}\left(v'^2+v^2\right)v_r^2+\frac{B^8}{h^8}v_r^4\right)\left(-\frac{1}{\left(v+\frac{B^2}{h^2}v_r\right)}\right)-\frac{\left(v+\frac{B^2}{h^2}v_r\right)}{2h^2}\right\}\exp\left[-h^2\left(v+\frac{B^2}{h^2}v_r\right)^2\right],$$

$$= -\left\{ \frac{\left(v'^2 \left(v^2 - \frac{B^4}{h^4} v_r^2 \right) - \frac{B^4}{h^4} v_r^2 \left(v^2 - \frac{B^4}{h^4} v_r^2 \right) \right)}{\left(v + \frac{B^2}{h^2} v_r \right)} + \frac{\left(v + \frac{B^2}{h^2} v_r \right)}{2h^2} \right\} \exp\left[-h^2 \left(v + \frac{B^2}{h^2} v_r \right)^2 \right],$$

$$= -\left\{ \frac{\left(v^2 - \frac{B^4}{h^4} v_r^2 \right)\left(v'^2 - \frac{B^4}{h^4} v_r^2 \right)}{\left(v + \frac{B^2}{h^2} v_r \right)} + \frac{\left(v + \frac{B^2}{h^2} v_r \right)}{2h^2} \right\} \exp\left[-h^2 \left(v + \frac{B^2}{h^2} v_r \right)^2 \right],$$

$$= -\left\{ \frac{\left(v - \frac{B^2}{h^2} v_r \right)\left(v + \frac{B^2}{h^2} v_r \right)\left(v'^2 - \frac{B^4}{h^4} v_r^2 \right)}{\left(v + \frac{B^2}{h^2} v_r \right)} + \frac{\left(v + \frac{B^2}{h^2} v_r \right)}{2h^2} \right\} \exp\left[-h^2 \left(v + \frac{B^2}{h^2} v_r \right)^2 \right],$$

$$= -\left\{ vv'^2 - \frac{B^2}{h^2} v'^2 v_r - \frac{B^4}{h^4} vv_r^2 + \frac{B^6}{h^6} v_r^3 + \frac{v}{2h^2} + \frac{1}{2h^2} \frac{B^2}{h^2} v_r \right\} \exp\left[-h^2 \left(v + \frac{B^2}{h^2} v_r \right)^2 \right],$$

After the simplifications, terms with $\exp\left[-h^2 \left(v + \frac{B^2}{h^2} v_r \right)^2 \right]$ are,

$$-\left\{ v\left(v'^2 + \frac{1}{2h^2} \right) + \frac{B^2}{h^2}\left(\frac{1}{2h^2} - v'^2 \right) v_r - \frac{B^4}{h^4} vv_r^2 + \frac{B^6}{h^6} v_r^3 \right\} \exp\left[-h^2 \left(v + \frac{B^2}{h^2} v_r \right)^2 \right]. \qquad \text{(D.29)}$$

Group all the error functions from Eq. (D.27),

$$\left(v'^2v^2-\frac{B^4}{h^4}\left(v'^2+v^2\right)v_r^2+\frac{B^8}{h^8}v_r^4\right)\sqrt{\pi}\,h\left\{erf\left[\left(hv'-\frac{B^2}{h}v_r\right)\right]-erf\left[\left(hv+\frac{B^2}{h}v_r\right)\right]\right\}+$$
$$\left(v'^2-2\frac{B^4}{h^4}v_r^2+v^2\right)\frac{\sqrt{\pi}}{2h}\left\{erf\left[\left(hv+\frac{B^2}{h}v_r\right)\right]-erf\left[\left(hv'-\frac{B^2}{h}v_r\right)\right]\right\}+$$
$$\frac{\sqrt{\pi}}{4}\frac{1}{h^3}\left\{erf\left[\left(hv+\frac{B^2}{h}v_r\right)\right]-erf\left[\left(hv'-\frac{B^2}{h}v_r\right)\right]\right\},$$

$$=\left\{-\sqrt{\pi}\,h\left(v'^2v^2-\frac{B^4}{h^4}\left(v'^2+v^2\right)v_r^2+\frac{B^8}{h^8}v_r^4\right)+\frac{\sqrt{\pi}}{2h}\left(v'^2-2\frac{B^4}{h^4}v_r^2+v^2\right)+\frac{\sqrt{\pi}}{4}\frac{1}{h^3}\right\}\times$$
$$\left\{erf\left[\left(hv+\frac{B^2}{h}v_r\right)\right]-erf\left[\left(hv'-\frac{B^2}{h}v_r\right)\right]\right\},$$

$$=\left\{-\sqrt{\pi}\,h\left(v'^2v^2-\frac{B^4}{h^4}\left(v'^2+v^2\right)v_r^2+\frac{B^8}{h^8}v_r^4\right)+\frac{\sqrt{\pi}}{2h}\frac{h}{h}\left(v'^2-2\frac{B^4}{h^4}v_r^2+v^2\right)+\frac{\sqrt{\pi}}{4}\frac{1}{h^3}\frac{h}{h}\right\}\times$$
$$\left\{erf\left[\left(hv+\frac{B^2}{h}v_r\right)\right]-erf\left[\left(hv'-\frac{B^2}{h}v_r\right)\right]\right\},$$

$$=\sqrt{\pi}\,h\left\{-v'^2v^2+\frac{B^4}{h^4}v'^2v_r^2+\frac{B^4}{h^4}v^2v_r^2-\frac{B^8}{h^8}v_r^4+\frac{1}{2h^2}v'^2-\frac{2}{2h^2}\frac{B^4}{h^4}v_r^2+\frac{v^2}{2h^2}+\frac{1}{4h^4}\right\}\times$$
$$\left\{erf\left[\left(hv+\frac{B^2}{h}v_r\right)\right]-erf\left[\left(hv'-\frac{B^2}{h}v_r\right)\right]\right\}.$$

Rearrange the terms and simplify to obtain,

$$=\sqrt{\pi}\,h\left\{-v^2\left(v'^2-\frac{1}{2h^2}\right)+\frac{1}{2h^2}\left(v'^2+\frac{1}{2h^2}\right)+\frac{B^4}{h^4}v_r^2\left(v'^2+v^2-\frac{1}{h^2}\right)-\frac{B^8}{h^8}v_r^4\right\}\times$$
$$\left\{erf\left[\left(hv+\frac{B^2}{h}v_r\right)\right]-erf\left[\left(hv'-\frac{B^2}{h}v_r\right)\right]\right\}. \tag{D.30}$$

Combine the solutions, Eqs. (D.28) – (D.30), from all three integrals,

$$\left\{v'\left(v^2+\frac{1}{2h^2}\right)+\frac{B^2}{h^2}\left(v^2-\frac{1}{2h^2}\right)v_r-\frac{B^4}{h^4}v'v_r^2-\frac{B^6}{h^6}v_r^3\right\}\exp\left[-h^2\left(v'-\frac{B^2}{h^2}v_r\right)^2\right]-$$
$$\left\{v\left(v'^2+\frac{1}{2h^2}\right)+\frac{B^2}{h^2}\left(\frac{1}{2h^2}-v'^2\right)v_r-\frac{B^4}{h^4}vv_r^2+\frac{B^6}{h^6}v_r^3\right\}\exp\left[-h^2\left(v+\frac{B^2}{h^2}v_r\right)^2\right]+$$
$$\sqrt{\pi}\,h\left\{-v^2\left(v'^2-\frac{1}{2h^2}\right)+\frac{1}{2h^2}\left(v'^2+\frac{1}{2h^2}\right)+\frac{B^4}{h^4}v_r^2\left(v'^2+v^2-\frac{1}{h^2}\right)-\frac{B^8}{h^8}v_r^4\right\}\times \tag{D.31}$$
$$\left\{erf\left[\left(hv+\frac{B^2}{h}v_r\right)\right]-erf\left[\left(hv'-\frac{B^2}{h}v_r\right)\right]\right\},$$

Next, we begin the integration of the second integral in Eq. (C.22) with $\int_{v_{c\_41}}^{v_{c\_42}} g(v_c)\,dv_c$,

$$K_1(v,v')=\frac{B^3(A+1)^2}{4\sqrt{\pi}A^2v^2}\exp\left(\frac{B^2v^2}{A}\right)\int_{v_{r\_41}}^{\infty} f(v_r)\,dv_r\int_{v_{c\_41}}^{v_{c\_42}} g(v_c)\,dv_c.$$

Here, $v_{c\_42}=v+\frac{Av_r}{A+1}=v+\frac{B^2}{h^2}v_r$ and $v_{c\_41}=\frac{Av_r}{A+1}-v=\frac{B^2}{h^2}v_r-v$.

After the bounds have been substituted into the previous equation, we obtain,

$$\int_{\frac{B^2}{h^2}v_r-v}^{v+\frac{B^2}{h^2}v_r}\left[\begin{array}{l}\left(v'^2v^2-\frac{A^2}{(A+1)^2}v'^2v_r^2-\left(\frac{A}{A+1}\right)^2v^2v_r^2+\left(\frac{A}{A+1}\right)^4v_r^4\right)\frac{1}{v_c^2}+\\ \left(v'^2-2\left(\frac{A}{A+1}\right)^2v_r^2+v^2+v_c^2\right)\end{array}\right]\exp\left(-\frac{B^2(A+1)}{A}v_c^2\right)dv_c.$$

Split the integral above into three integrals,

$$\int_{\frac{B^2}{h^2}v_r-v}^{v+\frac{B^2}{h^2}v_r}\left(v'^2v^2-\frac{A^2}{(A+1)^2}v'^2v_r^2-\left(\frac{A}{A+1}\right)^2v^2v_r^2+\left(\frac{A}{A+1}\right)^4v_r^4\right)\frac{1}{v_c^2}\exp\left(-\frac{B^2(A+1)}{A}v_c^2\right)dv_c+$$

$$\int_{\frac{B^2}{h^2}v_r-v}^{v+\frac{B^2}{h^2}v_r}\left(v'^2-2\left(\frac{A}{A+1}\right)^2v_r^2+v^2\right)\exp\left(-\frac{B^2(A+1)}{A}v_c^2\right)dv_c+ \tag{D.32}$$

$$\int_{\frac{B^2}{h^2}v_r-v}^{v+\frac{B^2}{h^2}v_r}v_c^2\exp\left(-\frac{B^2(A+1)}{A}v_c^2\right)dv_c.$$

Solution for the first integral in Eq. (D.32):

$$\int_{\frac{B^2}{h^2}v_r-v}^{v+\frac{B^2}{h^2}v_r}\left(v'^2v^2-\frac{A^2}{(A+1)^2}v'^2v_r^2-\left(\frac{A}{A+1}\right)^2v^2v_r^2+\left(\frac{A}{A+1}\right)^4v_r^4\right)\frac{1}{v_c^2}\exp\left(-\frac{B^2(A+1)}{A}v_c^2\right)dv_c,$$

$$=\left(v'^2v^2-\frac{A^2}{(A+1)^2}v'^2v_r^2-\left(\frac{A}{A+1}\right)^2v^2v_r^2+\left(\frac{A}{A+1}\right)^4v_r^4\right)\times$$

$$\left\{-\sqrt{\pi}\sqrt{\frac{B^2(A+1)}{A}}erf\left[\sqrt{\frac{B^2(A+1)}{A}}\,v_c\right]-\frac{1}{v_c}\exp\left[-\frac{B^2(A+1)v_c^2}{A}\right]\right\}\Bigg|_{\frac{B^2}{h^2}v_r-v}^{v+\frac{B^2}{h^2}v_r}.$$

Substitute the integral bounds and $h^2=\frac{B^2(A+1)}{A}$ into the equation above. Also, from $h^2=\frac{B^2(A+1)}{A}$, we know that $\frac{A}{(A+1)}=\frac{B^2}{h^2}$. So, $\left(\frac{A}{A+1}\right)^2=\frac{B^4}{h^4}$ and $\left(\frac{A}{A+1}\right)^4=\frac{B^8}{h^8}$. Substituting these terms gives,

$$\left(v'^2 v^2 - \frac{B^4}{h^4}\left(v'^2 + v^2\right)v_r^2 + \frac{B^8}{h^8}v_r^4\right)\times$$

$$\left[\begin{array}{l} -\sqrt{\pi}h\left(erf\left[\left(hv + \frac{B^2}{h}v_r\right)\right] - erf\left[\left(\frac{B^2}{h}v_r - hv\right)\right]\right) - \\ \frac{1}{\left(v + \frac{B^2}{h^2}v_r\right)}\exp\left[-h^2\left(v + \frac{B^2}{h^2}v_r\right)^2\right] + \frac{1}{\left(\frac{B^2}{h^2}v_r - v\right)}\exp\left[-h^2\left(\frac{B^2}{h^2}v_r - v\right)^2\right] \end{array}\right]. \tag{D.33}$$

Solution for the second integral in Eq. (D.32):

$$\int_{\frac{B^2}{h^2}v_r - v}^{v + \frac{B^2}{h^2}v_r}\left(v'^2 - 2\left(\frac{A}{A+1}\right)^2 v_r^2 + v^2\right)\exp\left(-\frac{B^2\left(A+1\right)}{A}v_c^2\right)dv_c,$$

$$= \left(v'^2 - 2\left(\frac{A}{A+1}\right)^2 v_r^2 + v^2\right)\frac{\sqrt{\pi}}{2}\sqrt{\frac{A}{B^2\left(A+1\right)}}\left\{erf\left[\sqrt{\frac{B^2\left(A+1\right)}{A}}v_c\right]\right\}\Bigg|_{\frac{B^2}{h^2}v_r - v}^{v + \frac{B^2}{h^2}v_r},$$

Substitute the integral bounds and $h^2 = \frac{B^2\left(A+1\right)}{A}$ into the equation above. Also, from $h^2 = \frac{B^2\left(A+1\right)}{A}$, we know that $\frac{A}{\left(A+1\right)} = \frac{B^2}{h^2}$. Subsequently, $\left(\frac{A}{A+1}\right)^2 = \frac{B^4}{h^4}$ and $\left(\frac{A}{A+1}\right)^4 = \frac{B^8}{h^8}$, and when substituted in the previous equation gives,

$$\left(v'^2 - 2\frac{B^4}{h^4}v_r^2 + v^2\right)\frac{\sqrt{\pi}}{2h}\left\{erf\left[h\left(v + \frac{B^2}{h^2}v_r\right)\right] - erf\left[h\left(\frac{B^2}{h^2}v_r - v\right)\right]\right\}.$$

After the simplifications, the solution of the second integral is,

$$\left(v'^2 - 2\frac{B^4}{h^4}v_r^2 + v^2\right)\frac{\sqrt{\pi}}{2h}\left\{erf\left[\left(hv + \frac{B^2}{h}v_r\right)\right] - erf\left[\left(\frac{B^2}{h}v_r - hv\right)\right]\right\}. \tag{D.34}$$

Solution for the third integral in Eq. (D.32):

$$\int_{\frac{B^2}{h^2}v_r - v}^{v+\frac{B^2}{h^2}v_r} v_c^2 \exp\left(-\frac{B^2(A+1)}{A}v_c^2\right)dv_c,$$

$$= \left\{\frac{\sqrt{\pi}}{4}\left(\frac{A}{B^2(A+1)}\right)^{3/2} erf\left[\sqrt{\frac{B^2(A+1)}{A}}v_c\right] - \frac{v_c \exp\left(-\frac{B^2(A+1)}{A}v_c^2\right)}{2\left(\frac{B^2(A+1)}{A}\right)}\right\}\Bigg|_{\frac{B^2}{h^2}v_r - v}^{v+\frac{B^2}{h^2}v_r}.$$

Substitute the integral bounds and $h^2 = \frac{B^2(A+1)}{A}$ into the equation above. Also, from $h^2 = \frac{B^2(A+1)}{A}$, we know that $\frac{A}{(A+1)} = \frac{B^2}{h^2}$. So, $\left(\frac{A}{A+1}\right)^2 = \frac{B^4}{h^4}$ and $\left(\frac{A}{A+1}\right)^4 = \frac{B^8}{h^8}$, and after applying the substitutions for these terms, we obtain,

$$\left\{\begin{array}{l} \frac{\sqrt{\pi}}{4}\left(h^{-2}\right)^{3/2} erf\left[h\left(v + \frac{B^2}{h^2}v_r\right)\right] - \frac{\left(v + \frac{B^2}{h^2}v_r\right)\exp\left(-h^2\left(v + \frac{B^2}{h^2}v_r\right)^2\right)}{2h^2} - \\ \frac{\sqrt{\pi}}{4}\left(h^{-2}\right)^{3/2} erf\left[h\left(\frac{B^2}{h^2}v_r - v\right)\right] + \frac{\left(\frac{B^2}{h^2}v_r - v\right)\exp\left(-h^2\left(\frac{B^2}{h^2}v_r - v\right)^2\right)}{2h^2} \end{array}\right\}.$$

After the simplifications, the solution for the third integral is,

$$\left\{\begin{array}{l}\frac{\sqrt{\pi}}{4h^3}\left(erf\left[\left(hv+\frac{B^2}{h}v_r\right)\right]-erf\left[\left(\frac{B^2}{h}v_r-hv\right)\right]\right)- \\ \frac{\left(v+\frac{B^2}{h^2}v_r\right)\exp\left(-h^2\left(v+\frac{B^2}{h^2}v_r\right)^2\right)}{2h^2}+\frac{\left(\frac{B^2}{h^2}v_r-v\right)\exp\left(-h^2\left(\frac{B^2}{h^2}v_r-v\right)^2\right)}{2h^2}\end{array}\right\}. \tag{D.35}$$

Combine the solutions, Eqs. (D.33) – (D.35), for the three integrals,

$$\begin{array}{l}\left(v'^2v^2-\frac{B^4}{h^4}\left(v'^2+v^2\right)v_r^2+\frac{B^8}{h^8}v_r^4\right)\times \\ \left[\begin{array}{l}-\sqrt{\pi}h\left(erf\left[\left(hv+\frac{B^2}{h}v_r\right)\right]-erf\left[\left(\frac{B^2}{h}v_r-hv\right)\right]\right)- \\ \frac{\exp\left[-h^2\left(v+\frac{B^2}{h^2}v_r\right)^2\right]}{\left(v+\frac{B^2}{h^2}v_r\right)}+\frac{\exp\left[-h^2\left(\frac{B^2}{h^2}v_r-v\right)^2\right]}{\left(\frac{B^2}{h^2}v_r-v\right)}\end{array}\right]+ \\ \left(v'^2-2\frac{B^4}{h^4}v_r^2+v^2\right)\frac{\sqrt{\pi}}{2h}\left\{erf\left[\left(hv+\frac{B^2}{h}v_r\right)\right]-erf\left[\left(\frac{B^2}{h}v_r-hv\right)\right]\right\}+ \\ \left\{\begin{array}{l}\frac{\sqrt{\pi}}{4h^3}\left(erf\left[\left(hv+\frac{B^2}{h}v_r\right)\right]-erf\left[\left(\frac{B^2}{h}v_r-hv\right)\right]\right)- \\ \frac{\left(v+\frac{B^2}{h^2}v_r\right)\exp\left(-h^2\left(v+\frac{B^2}{h^2}v_r\right)^2\right)}{2h^2}+\frac{\left(\frac{B^2}{h^2}v_r-v\right)\exp\left(-h^2\left(\frac{B^2}{h^2}v_r-v\right)^2\right)}{2h^2}\end{array}\right\}.\end{array} \tag{D.36}$$

Simplify and group the terms with $\exp\left[-h^2\left(\frac{B^2}{h^2}v_r-v\right)^2\right]$ from Eq. (D.36),

$$\left[\left(v'^2v^2-\frac{B^4}{h^4}\left(v'^2+v^2\right)v_r^2+\frac{B^8}{h^8}v_r^4\right)\left(\frac{1}{\left(\frac{B^2}{h^2}v_r-v\right)}\right)+\frac{\left(\frac{B^2}{h^2}v_r-v\right)}{2h^2}\right]\exp\left[-h^2\left(\frac{B^2}{h^2}v_r-v\right)^2\right],$$

$$=\left[\frac{v'^2v^2-\frac{B^4}{h^4}v'^2v_r^2-\frac{B^4}{h^4}v^2v_r^2+\frac{B^8}{h^8}v_r^4}{\left(\frac{B^2}{h^2}v_r-v\right)}+\frac{1}{2h^2}\frac{B^2}{h^2}v_r-\frac{v}{2h^2}\right]\exp\left[-h^2\left(\frac{B^2}{h^2}v_r-v\right)^2\right],$$

$$=\left[\frac{\left(\frac{B^4}{h^4}v_r^2-v^2\right)\left(\frac{B^4}{h^4}v_r^2-v'^2\right)}{\left(\frac{B^2}{h^2}v_r-v\right)}+\frac{1}{2h^2}\frac{B^2}{h^2}v_r-\frac{v}{2h^2}\right]\exp\left[-h^2\left(\frac{B^2}{h^2}v_r-v\right)^2\right],$$

$$=\left[\frac{\left(\frac{B^2}{h^2}v_r-v\right)\left(\frac{B^2}{h^2}v_r+v\right)\left(\frac{B^4}{h^4}v_r^2-v'^2\right)}{\left(\frac{B^2}{h^2}v_r-v\right)}+\frac{1}{2h^2}\frac{B^2}{h^2}v_r-\frac{v}{2h^2}\right]\exp\left[-h^2\left(\frac{B^2}{h^2}v_r-v\right)^2\right],$$

$$=\left[\frac{B^6}{h^6}v_r^3-\frac{B^2}{h^2}v_rv'^2+\frac{B^4}{h^4}vv_r^2-vv'^2+\frac{1}{2h^2}\frac{B^2}{h^2}v_r-\frac{v}{2h^2}\right]\exp\left[-h^2\left(\frac{B^2}{h^2}v_r-v\right)^2\right].$$

After the simplifications, the terms with $\exp\left[-h^2\left(\frac{B^2}{h^2}v_r-v\right)^2\right]$ are,

$$\left[-v\left(v'^2+\frac{1}{2h^2}\right)+\frac{B^2}{h^2}\left(\frac{1}{2h^2}-v'^2\right)v_r+\frac{B^4}{h^4}vv_r^2+\frac{B^6}{h^6}v_r^3\right]\exp\left[-h^2\left(\frac{B^2}{h^2}v_r-v\right)^2\right] \qquad \text{(D.37)}$$

Simplify and group the terms with $\exp\left[-h^2\left(v+\frac{B^2}{h^2}v_r\right)^2\right]$ from Eq. (D.36),

$$\left[-\frac{\left(v'^2v^2-\frac{B^4}{h^4}\left(v'^2+v^2\right)v_r^2+\frac{B^8}{h^8}v_r^4\right)}{\left(v+\frac{B^2}{h^2}v_r\right)}-\frac{\left(v+\frac{B^2}{h^2}v_r\right)}{2h^2}\right]\exp\left[-h^2\left(v+\frac{B^2}{h^2}v_r\right)^2\right],$$

$$=-\left[\frac{\left(v'^2\left(v^2-\frac{B^4}{h^4}v_r^2\right)-\frac{B^4}{h^4}v_r^2\left(v^2-\frac{B^4}{h^4}v_r^2\right)\right)}{\left(v+\frac{B^2}{h^2}v_r\right)}+\frac{\left(v+\frac{B^2}{h^2}v_r\right)}{2h^2}\right]\exp\left[-h^2\left(v+\frac{B^2}{h^2}v_r\right)^2\right],$$

$$=-\left[\frac{\left(v-\frac{B^2}{h^2}v_r\right)\left(v+\frac{B^2}{h^2}v_r\right)\left(v'^2-\frac{B^4}{h^4}v_r^2\right)}{\left(v+\frac{B^2}{h^2}v_r\right)}+\frac{\left(v+\frac{B^2}{h^2}v_r\right)}{2h^2}\right]\exp\left[-h^2\left(v+\frac{B^2}{h^2}v_r\right)^2\right],$$

$$=-\left[vv'^2-\frac{B^2}{h^2}v_rv'^2-\frac{B^4}{h^4}v_r^2v+\frac{B^6}{h^6}v_r^3+\frac{v}{2h^2}+\frac{1}{2h^2}\frac{B^2}{h^2}v_r\right]\exp\left[-h^2\left(v+\frac{B^2}{h^2}v_r\right)^2\right].$$

After the simplifications, the terms with $\exp\left[-h^2\left(\frac{B^2}{h^2}v_r-v\right)^2\right]$ are,

$$-\left[v\left(v'^2+\frac{1}{2h^2}\right)+\frac{B^2}{h^2}\left(\frac{1}{2h^2}-v'^2\right)v_r-\frac{B^4}{h^4}v_r^2v+\frac{B^6}{h^6}v_r^3\right]\exp\left[-h^2\left(v+\frac{B^2}{h^2}v_r\right)^2\right]. \qquad \text{(D.38)}$$

Simplify and group together the error functions from Eq. (D.36),

$$\left[-\sqrt{\pi}h\left(v'^2v^2-\frac{B^4}{h^4}\left(v'^2+v^2\right)v_r^2+\frac{B^8}{h^8}v_r^4\right)+\frac{\sqrt{\pi}}{2h}\left(v'^2-2\frac{B^4}{h^4}v_r^2+v^2\right)+\frac{\sqrt{\pi}}{4h^3}\right]\times$$
$$\left(erf\left[\left(hv+\frac{B^2}{h}v_r\right)\right]-erf\left[\left(\frac{B^2}{h}v_r-hv\right)\right]\right),$$

$$=\sqrt{\pi}h\left[-v'^2v^2+\frac{B^4}{h^4}v'^2v_r^2+\frac{B^4}{h^4}v^2v_r^2-\frac{B^8}{h^8}v_r^4+\frac{1}{2h^2}v'^2-\frac{1}{2h^2}2\frac{B^4}{h^4}v_r^2+\frac{1}{2h^2}v^2+\frac{1}{4h^4}\right]\times$$
$$\left(erf\left[\left(hv+\frac{B^2}{h}v_r\right)\right]-erf\left[\left(\frac{B^2}{h}v_r-hv\right)\right]\right).$$

After the simplifications, terms with the error functions are,

$$\sqrt{\pi}h\left[-v^2\left(v'^2-\frac{1}{2h^2}\right)+\frac{1}{2h^2}\left(v'^2+\frac{1}{2h^2}\right)+\frac{B^4}{h^4}\left(v^2+v'^2-\frac{1}{h^2}\right)v_r^2-\frac{B^8}{h^8}v_r^4\right]\times$$
$$\left(erf\left[\left(hv+\frac{B^2}{h}v_r\right)\right]-erf\left[\left(\frac{B^2}{h}v_r-hv\right)\right]\right). \tag{D.39}$$

Combine the solutions, Eqs. (D.37) – (D.39), from the three integrals,

$$\left[-v\left(v'^2+\frac{1}{2h^2}\right)+\frac{B^2}{h^2}\left(\frac{1}{2h^2}-v'^2\right)v_r+\frac{B^4}{h^4}vv_r^2+\frac{B^6}{h^6}v_r^3\right]\exp\left[-h^2\left(\frac{B^2}{h^2}v_r-v\right)^2\right]-$$
$$\left[v\left(v'^2+\frac{1}{2h^2}\right)+\frac{B^2}{h^2}\left(\frac{1}{2h^2}-v'^2\right)v_r-\frac{B^4}{h^4}v_r^2v+\frac{B^6}{h^6}v_r^3\right]\exp\left[-h^2\left(v+\frac{B^2}{h^2}v_r\right)^2\right]+$$
$$\sqrt{\pi}h\left[-v^2\left(v'^2-\frac{1}{2h^2}\right)+\frac{1}{2h^2}\left(v'^2+\frac{1}{2h^2}\right)+\frac{B^4}{h^4}\left(v^2+v'^2-\frac{1}{h^2}\right)v_r^2-\frac{B^8}{h^8}v_r^4\right]\times$$
$$\left(erf\left[\left(hv+\frac{B^2}{h}v_r\right)\right]-erf\left[\left(\frac{B^2}{h}v_r-hv\right)\right]\right). \tag{D.40}$$

Final form of $K_1(v,v')$ for ($v < v'$), upscattering case:

$$K_1(v,v') = \frac{B^3(A+1)^2}{4\sqrt{\pi}A^2v^2}\exp\left(\frac{B^2v^2}{A}\right)\left\{\int_{v_{r\_31}}^{v_{r\_32}} f(v_r)\,dv_r \int_{v_{c\_31}}^{v_{c\_32}} g(v_c)\,dv_c + \int_{v_{r\_41}}^{\infty} f(v_r)\,dv_r \int_{v_{c\_41}}^{v_{c\_42}} g(v_c)\,dv_c\right\}$$

Substitute $f(v_r) = \sigma_s(v_r)v_r\exp\left(-\frac{B^2v_r^2}{A+1}\right)$, Eqs. (D.31) and (D.40), and simplify the constants to obtain the final form of the equation for upscatter,

$$K_1(v,v') = \frac{h^4}{4\sqrt{\pi B}v^2}\exp\left(\frac{B^2v^2}{A}\right)\times$$

$$\left\{\begin{array}{l}
\displaystyle\int_{\frac{h^2}{B^2}\left(\frac{v'-v}{2}\right)}^{\frac{h^2}{B^2}\left(\frac{v+v'}{2}\right)} \sigma_s(v_r)v_r\exp\left(-\frac{B^2v_r^2}{A+1}\right)\times \\
\left[\begin{array}{l}
\left\{v'\left(v^2+\frac{1}{2h^2}\right)+\frac{B^2}{h^2}\left(v^2-\frac{1}{2h^2}\right)v_r-\frac{B^4}{h^4}v'v_r^2-\frac{B^6}{h^6}v_r^3\right\}\exp\left[-h^2\left(v'-\frac{B^2}{h^2}v_r\right)^2\right] \\
-\left\{v\left(v'^2+\frac{1}{2h^2}\right)+\frac{B^2}{h^2}\left(\frac{1}{2h^2}-v'^2\right)v_r-\frac{B^4}{h^4}vv_r^2+\frac{B^6}{h^6}v_r^3\right\}\exp\left[-h^2\left(v+\frac{B^2}{h^2}v_r\right)^2\right] \\
+\sqrt{\pi}\,h\left\{-v^2\left(v'^2-\frac{1}{2h^2}\right)+\frac{1}{2h^2}\left(v'^2+\frac{1}{2h^2}\right)+\frac{B^4}{h^4}v_r^2\left(v'^2+v^2-\frac{1}{h^2}\right)-\frac{B^8}{h^8}v_r^4\right\}\times \\
\left\{erf\left[\left(hv+\frac{B^2}{h}v_r\right)\right]-erf\left[\left(hv'-\frac{B^2}{h}v_r\right)\right]\right\}
\end{array}\right]dv_r \\
+ \\
\displaystyle\int_{\frac{h^2}{B^2}\left(\frac{v+v'}{2}\right)}^{\infty} \sigma_s(v_r)v_r\exp\left(-\frac{B^2v_r^2}{A+1}\right)\times \\
\left[\begin{array}{l}
\left[-v\left(v'^2+\frac{1}{2h^2}\right)+\frac{B^2}{h^2}\left(\frac{1}{2h^2}-v'^2\right)v_r+\frac{B^4}{h^4}vv_r^2+\frac{B^6}{h^6}v_r^3\right]\exp\left[-h^2\left(\frac{B^2}{h^2}v_r-v\right)^2\right] \\
-\left[v\left(v'^2+\frac{1}{2h^2}\right)+\frac{B^2}{h^2}\left(\frac{1}{2h^2}-v'^2\right)v_r-\frac{B^4}{h^4}v_r^2v+\frac{B^6}{h^6}v_r^3\right]\exp\left[-h^2\left(v+\frac{B^2}{h^2}v_r\right)^2\right] \\
+\sqrt{\pi}h\left[-v^2\left(v'^2-\frac{1}{2h^2}\right)+\frac{1}{2h^2}\left(v'^2+\frac{1}{2h^2}\right)+\frac{B^4}{h^4}\left(v^2+v'^2-\frac{1}{h^2}\right)v_r^2-\frac{B^8}{h^8}v_r^4\right]\times \\
\left(erf\left[\left(hv+\frac{B^2}{h}v_r\right)\right]-erf\left[\left(\frac{B^2}{h}v_r-hv\right)\right]\right)
\end{array}\right]dv_r
\end{array}\right\}$$

D.2 References

[1] G. L. Blackshaw, *Scattering of Low-Energy Neutrons In a Monatomic Gas Model Of A Multiplying System*, North Carolina State University, Raleigh, Ph.D. Thesis (1966).

[2] G. L. Blackshaw and R. L. Murray, *Scattering Functions for Low-Energy Neutron Collisions in a Maxwellian Monatomic Gas*, Nuclear Science and Engineering, **27** pp. 520-532 (1967).